JACC
Basic to Translational Science

A Journal of the American College of Cardiology

JACC
Basic to Translational Science
A Journal of the American College of Cardiology

CORRESPONDENCE FOR AMERICAN COLLEGE OF CARDIOLOGY

All correspondence for the College, other than that related to *JACC: Basic to Translational Science* should be sent to Resource Center, American College of Cardiology, 2400 N Street, NW, Washington, DC 20037

JACC: BASIC TO TRANSLATIONAL SCIENCE VOL. 4, NO. 5, 2019

CLINICAL RESEARCH

Comparative Transcriptomics of *Ex Vivo*, Patient-Derived Endothelial Cells Reveals Novel Pathways Associated With Type 2 Diabetes Mellitus

Joshua A. Beckman, MD,[a] Sean P. Doherty, BA,[a] Zachary B. Feldman, BA,[a] Emily S. Banks, BS,[a] Javid Moslehi, MD,[a] Iris Z. Jaffe, MD, PhD,[b] Naomi M. Hamburg, MD,[c] Quanhu Sheng, PhD,[d] Jonathan D. Brown, MD[a]

VISUAL ABSTRACT

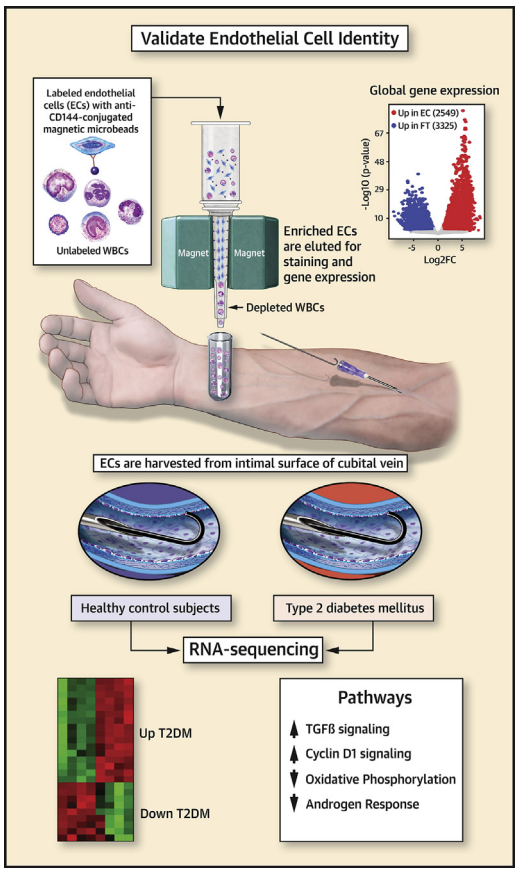

Beckman, J.A. et al. J Am Coll Cardiol Basic Trans Science. 2019;4(5):567–74.

HIGHLIGHTS

- **Endothelial cells can be harvested directly from humans, rapidly sorted and subjected to RNA-sequencing to study global gene expression.**
- **In endothelial cells isolated from patients with type 2 diabetes mellitus, pathways involved in TGF-β and Cyclin-D1 signaling were positively enriched while androgen signaling and oxidative phosphorylation were negatively enriched compared to healthy individuals.**
- **Patient-derived endothelial cells can be used to discover and validate disease-associated pathways.**

ISSN 2452-302X https://doi.org/10.1016/j.jacbts.2019.05.012

JACC: BASIC TO TRANSLATIONAL SCIENCE VOL. 4, NO. 5, 2019
SEPTEMBER 2019:567–74

ABBREVIATIONS AND ACRONYMS

BSA = bovine serum albumin

ddCt = delta-delta cycle threshold

EC = endothelial cell

EDTA = ethylenediamine tetra-acetic acid

FACS = fluorescence activated cell sorting

FDR = false discovery rate

GSEA = gene set enrichment analysis

HUVEC = human umbilical vein endothelial cell

IV = intravenous

PBS = phosphate buffered saline

qPCR = quantitative polymerase chain reaction

Seq = sequencing

T2DM = type 2 diabetes mellitus

TGFβ = transforming growth factor beta

VEGF = vascular endothelial growth factor

VUMC = Vanderbilt University Medical Center

WBC = white blood cell

SUMMARY

In this study low-input RNA-sequencing was used to annotate the molecular identity of endothelial cells isolated and immunopurified with CD144 microbeads. Using this technique, comparative gene expression profiling from healthy subjects and patients with type 2 diabetes mellitus identified both known and novel pathways linked with EC dysfunction. Modeling of diabetes by treating cultured ECs with high glucose identified shared changes in gene expression in diabetic cells. Overall, the data demonstrate how purified ECs from patients can be used to generate new hypotheses about mechanisms of human vascular disease.
(J Am Coll Cardiol Basic Trans Science 2019;4:567–74)

The vascular endothelium—a single-cell thick layer situated at the interface of flowing blood and the vessel wall—plays a central role in cardiovascular homeostasis by regulating blood pressure, thrombosis, leukocyte trafficking, and metabolism (1). The ability to culture endothelial cells (ECs), including human umbilical vein ECs (HUVECs), in vitro revolutionized vascular biology by providing a renewable source of cells to study human EC structure and function. These model systems have generated key insights into EC biology involved in the pathophysiology of cardiovascular disease. However, the culture of ECs outside the context of the blood vessel alters function and cell differentiation in fundamental ways. For example, the nonphysiological static microenvironment of cell culture affects biochemical signaling and gene expression in ECs (2). Thus, acquiring ECs directly from patient vessels may facilitate the discovery of new mechanisms of EC dysfunction that arise from genetic mutations, chronic disease states, or drug toxicities, all of which are known to modulate vascular disease risk *in vivo* in humans. In addition, the inability to study patient-specific effects of drugs on EC signaling and gene regulation in vivo remains a significant obstacle for successful translation of potential vascular disease treatments. Accordingly, complementary methods for studying EC biology more directly in humans are needed.

Multiple groups have reported using wire biopsy of ECs from peripheral vein or artery to study the activity of specific signaling pathways implicated in EC dysfunction (3–5). These targeted approaches identify ECs on the basis of staining for known EC markers. Other blood cells, especially leukocytes, contaminate these preparations, thereby complicating analysis using conventional microscopy. To overcome these issues, fluorescence-activated cell sorting (FACS) (6) or magnetic microbeads (7) have been used to enrich for ECs during the procedure. However, FACS is time intensive and can damage fragile cells. In addition, the molecular identity of cells retrieved during biopsy and purification has not been determined using unbiased analysis. These issues raise questions about the utility of the EC biopsy technique in discovery-based investigation of vascular disease in humans.

In this study, we used a positive selection step with anti-CD144 microbeads to enrich for ECs rapidly and deplete non-ECs (i.e., circulating leukocytes). We then annotated the molecular identity of both selected and nonselected fractions of cells using unbiased, low-input RNA sequencing. Differential gene expression identified 2,549 up-regulated transcripts in the CD144-selected cell fraction. Gene ontology analysis of these

From the [a]Division of Cardiovascular Medicine, Vanderbilt University Medical Center, Nashville, Tennessee; [b]Molecular Cardiology Research Institute, Tufts Medical Center, Boston, Massachusetts; [c]Evans Department of Medicine and Whitaker Cardiovascular Institute, Boston University School of Medicine, Boston, Massachusetts; and the [d]Center for Quantitative Sciences, Department of Biostatistics, Vanderbilt University School of Medicine, Nashville, Tennessee. This work was supported by grants HL131977 (to Dr. Beckman) and the Vanderbilt-Ingram Cancer Center Young Ambassador Award (to Dr. Brown). All other authors have reported that they have no relationships relevant to the contents of this paper to disclose.
The authors attest they are in compliance with human studies committees and animal welfare regulations of the authors' institutions and Food and Drug Administration guidelines, including patient consent where appropriate. For more information, visit the *JACC: Basic to Translational Science* author instructions page.

Manuscript received November 7, 2018; revised manuscript received May 23, 2019, accepted May 23, 2019.

transcripts revealed highly significant enrichment for pathways related to EC development and function. Furthermore, expression of classic EC markers clustered perfectly with selected cells, whereas leukocyte markers clustered in nonselected cells. We then used this approach to uncover novel gene expression pathways that are differentially regulated in ECs from patients with type 2 diabetes mellitus (T2DM) compared with healthy control patients. Comparison of genes induced by high glucose in HUVEC, a model of diabetic hyperglycemia, revealed a partial, but statistically significant overlap with genes identified in T2DM ECs. Collectively, these results demonstrate that immunopurification of cells isolated with wire biopsy strongly enriches for ECs, and comparative transcriptomic analysis can be used in conjunction with established EC culture models to discover clinically relevant disease-related pathways for future investigation.

METHODS

EC HARVEST AND ENRICHMENT. The protocol was approved by the Vanderbilt University Medical Center Human Research Committee, and all subjects provided written informed consent. A total of 5 healthy subjects (n = 3 men, 2 women, self-identified Caucasian = 4; self-identified African American = 1, average hemoglobin A1C = 5.1 ± 0.3) and 5 patients with diabetes (n = 4 men, 1 woman; self-identified Caucasian = 5, average hemoglobin A1C = 8.2 ± 1.2) were recruited. A 20-gauge intravenous (IV) catheter was inserted into a patient's cubital vein under sterile conditions. ECs were gently scraped from the intimal surface of the cubital vein with a J-wire (Arrow International, Reading, Pennsylvania). The wire and cells were centrifuged (400 x g for 7 min at room temperature with no brake) in dissociation buffer (phosphate-buffered saline [PBS], 2 mM ethylenediamine tetra-acetic acid [EDTA], heparin 0.1 mg/ml, pH 7.4). After centrifugation, dissociation buffer was aspirated ,and cells were resuspended in 80 μl of labeling buffer (PBS supplemented with 0.5% bovine serum albumin [BSA], 2mM EDTA, pH 7.2) along with 20 μl of CD144 microbeads (Cat# 130-097-857 Miltenyi Biotec, Bergisch Gladbach, Germany). Cells were incubated for 15 min at 4°C. After incubation, cells were sorted through a magnetic column in a magnetic field (QuadraMACS, Miltenyi). Cells were washed 3 times with labeling buffer. Labeled ECs were recovered by gravity flow with 4 ml of cold labeling buffer after removing the column from the magnet.

CELL FIXATION AND STAINING. Cells were fixed and stained as previously described (5). Cells were plated on poly-L-lysine-coated chamber slides. Slides were centrifuged at 400 revolutions/min for 5 s with no break, then rotated 180° for a second spin. Buffer was aspirated, and cells were stained with 4% paraformaldehyde for 10 min at room temperature. After second wash, slides were air dried then frozen at −80°C. For staining, slides were rehydrated with PBS/glycine 50 mM then incubated with anti-Von Willebrand factor antibody (Dako, Clone F8/86, Carpinteria, California) at 1:300 for 1 h at 37°C followed by secondary goat anti-mouse antibody conjugated to Alexa Fluor 488 dye (Invitrogen, Thermo Fisher Scientific, Waltham, Massachusetts) at 1:800 for 45 min at 37°C. Cells were mounted with ProLong Gold Antifade with DAPI (Invitrogen) and imaged with an immunofluorescence microscope (OIympus IX81, Olympus, Shinjuku, Tokyo, Japan).

RNA ISOLATION AND SEQUENCING. For RNA isolation, isolated cells were quickly pelleted by centrifugation and immediately placed in RNA lysis buffer per protocol (Qiagen, RNeasy Plus Micro, Venlo, the Netherlands). Isolated RNA was quantified and sequencing libraries generated using low-input, mRNA sequencing DNA preparation kit per company protocol (Illumina, San Diego, California). Paired End-75 sequencing was performed on an Illumina HiSeq3000. Reads were trimmed to remove adapter sequences using Cutadapt v1.16 (8) and aligned to the GENCODE GRCm38.p5/human b37 genome using STAR v2.5.3a (9). GENCODE vM12/Ensembl v75 gene annotations were provided to STAR to improve the accuracy of mapping. Quality control on both raw reads and adaptor-trimmed reads was performed using FastQC. FeatureCounts v1.15.2 (10) was used to count the number of mapped reads to each gene. Differentially expressed, protein-coding genes were detected by DESeq2 (v1.18.1) (11). Heatmap3 was used for cluster analysis and visualization (12). Genome ontology analysis was performed on differentially expressed genes using the ToppGene suite. Gene set enrichment analysis (GSEA) was performed using the GSEA package (13). The gene set for the EC-restricted gene list (n = 151) was obtained from a previously published curated dataset (14).

EC CULTURE. Pooled HUVEC were purchased from Lonza (Lonza Inc, Walkersville, Maryland) and maintained in growth media (ATCC VEGF bullet kit) on 0.1% gelatin-coated plates. Cells for gene expression were used at passage 3 or less. For glucose stimulation, media was supplemented with

FIGURE 1 Ex Vivo CD144-Selection Enriches Vascular ECs in Patient-Derived Samples

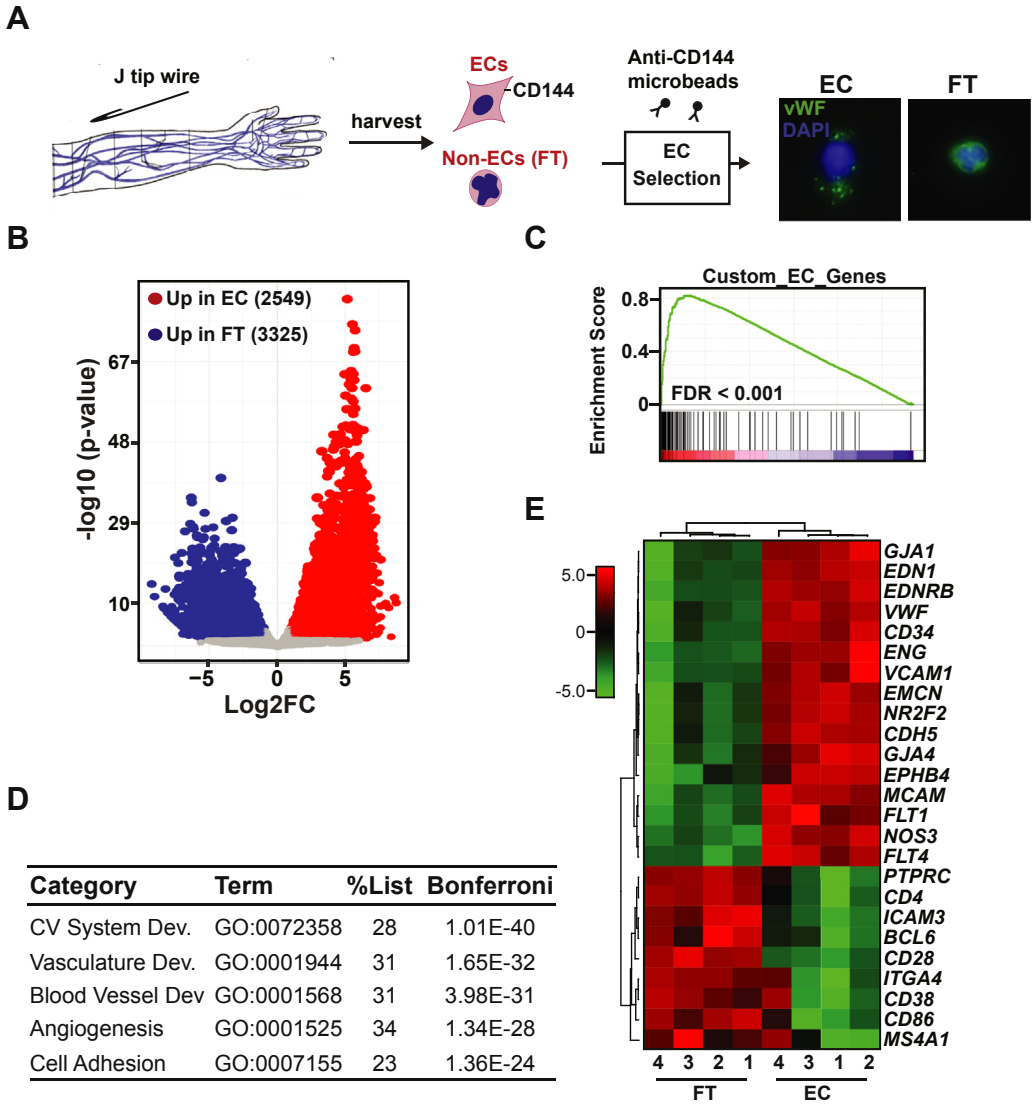

D

Category	Term	%List	Bonferroni
CV System Dev.	GO:0072358	28	1.01E-40
Vasculature Dev.	GO:0001944	31	1.65E-32
Blood Vessel Dev	GO:0001568	31	3.98E-31
Angiogenesis	GO:0001525	34	1.34E-28
Cell Adhesion	GO:0007155	23	1.36E-24

(A) Schematic of endothelial cell (EC) isolation procedure, selection of ECs using anti-CD144 magnetic microbeads and photomicrographs of immunofluorescence for von Willebrand factor (VWF) **(green)** in CD144 selected ECs and flow through cells (FT = nonselected). Nuclei were counterstained with DAPI **(blue)**. Results shown at 40x magnification. **(B)** Volcano plot showing Log2 fold change (Log2FC) expression vs. log10 (p value) of differentially expressed genes in CD144-selected cells vs. FT. For significance cutoff, false discovery rate (FDR) adjusted p value <0.05 and 2-fold change was used. **(C)** Gene set enrichment plot showing positive enrichment of genes expressed in CD144-selected cells in a curated EC gene set. **(D)** Table showing results of gene ontology analysis (ToppGene suite) of differentially expressed genes from CD144-selected cells vs. FT cells. Bonferroni adjusted p value is shown. All statistically significantly upregulated genes in CD144 selected cells vs. FT cells from Figure 1B were included in the analysis using a cutoff of 2-fold; FDR <0.05. GO: Biological Processes are listed. **(E)** Heat map showing expression data of specific EC-restricted and leukocyte-restricted marker genes in EC and FT samples. Samples were clustered using Pearson correlation. For each EC and FT patient-derived sample, pairwise analysis was performed. Numbers below the heat map indicate paired samples.

additional glucose to a final concentration of 25 mM. Cells were treated for 24 h with high glucose (25 mM) vs. standard glucose (5 mM). After treatment, cells were washed, trypsinized, counted on a hemocytometer, and 1,000 cells were used for RNA sequencing to mimic the low cell counts from the human EC harvests. Separate kinetic experiments compared high glucose and mannitol with a final

FIGURE 2 Comparative Transcriptomics Identifies Changes in Pathways of Proliferation, Metabolism, and Androgen Signaling in ECs From Patients With T2DM

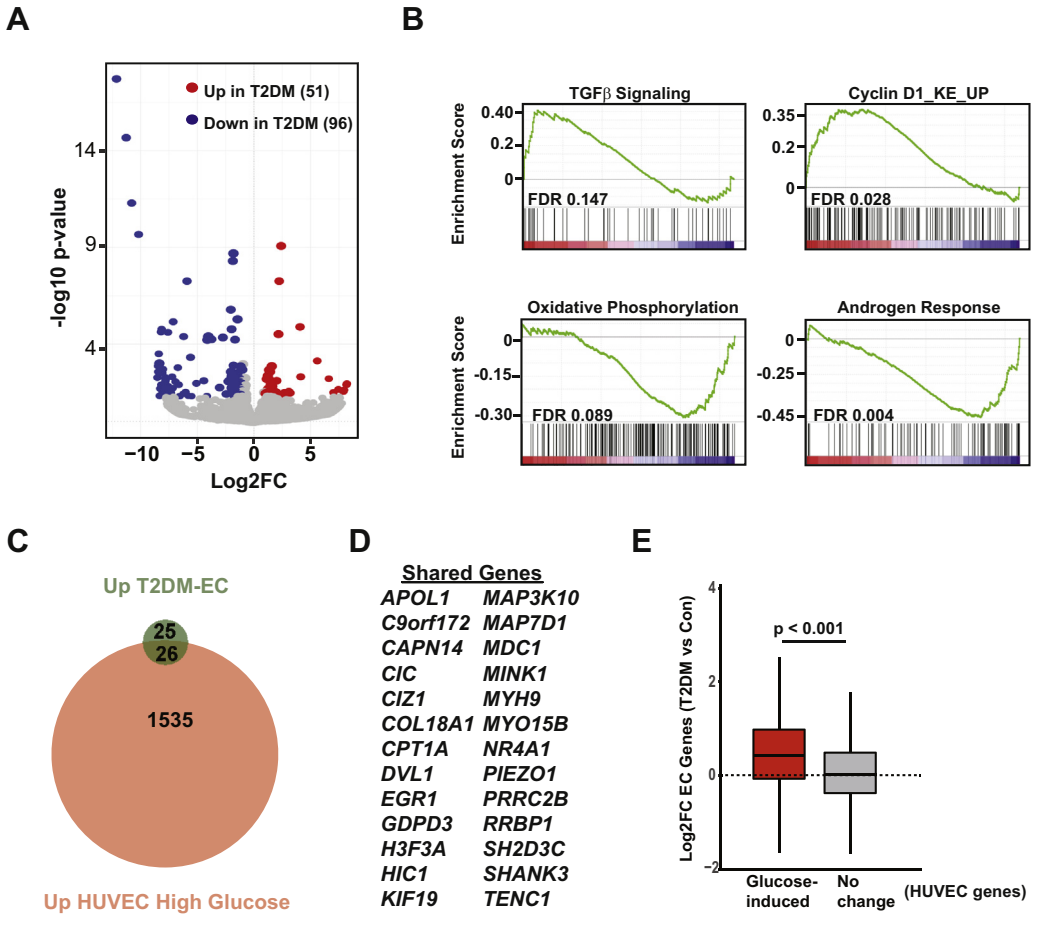

(A) Volcano plot showing Log2 fold change (Log2FC) in expression of protein coding genes vs. log10 (p value) in T2DM (endothelial cells) ECs compared with EC-Con (Same RNA-seq data from Figure 1). False discovery rate (FDR adjusted p value cutoff <0.05. **(B)** Gene set enrichment plots in T2DM ECs vs. EC-Con. Genes were ranked using the "stat" parameter generated in the DESeq2 pipeline. For each plot, FDR is included. **(C)** Venn diagram showing overlap in genes induced in T2DM-ECs **(green)** and HUVEC treated with 25 mM glucose for 24 h **(red)**. **(D)** List of shared genes from panel C. **(E)** Boxplot showing median Log2FC (T2DM ECs vs. EC-Con) of all HUVEC genes induced by high glucose (2-fold, FDR <0.05) or HUVEC genes that did not change with glucose stimulation. For **E**, p value was determined by Wilcoxon rank sum test.

concentration of 25 mM (n = 4). For the mannitol experiment, RNA was extracted by column purification after 6-h, 24-h, or 36-h treatment, then 100 ng was reverse transcribed (iScript, BioRad, Philadelphia, Pennsylvania), and real time-qPCR was performed using standard protocol (2-step amplification, Bio-Rad CFX96 cycler). All qPCR data are normalized to internal control gene 36B4. Primers available upon request.

STATISTICS. For RNA-sequencing data, differentially expressed protein-coding genes were identified with DESeq2 using false discovery rate (FDR)-adjusted p value <0.05 and absolute fold change >2.0 as the threshold for statistical significance (v1.18.1) (11). All the differential expression data are presented as volcano plots (Figures 1B and 2A). For GSEA, each individual gene set was tested against the entire experimental gene list, using the "stat" result generated by the DESeq2 analysis. The enrichment plots for GSEA and the FDR adjusted p values were generated using the GSEA package, as described in the original publication, without modification (Figures 1C and 2B) (13). For gene ontology analysis, we used the

Bonferroni method to adjust for multiple hypothesis testing because it was the most stringent method in the ToppGene Suite (**Figure 1D**). To generate the heatmap comparing EC and FT samples, the gene-expression data were transformed using variance-stabilizing transformation in DESeq2 (**Figure 1E**). Samples were then clustered by Pearson correlation using the specified leukocyte and EC genes. In HUVEC stimulated with mannitol or glucose, the heatmap displays row normalized mean fold change compared with Time 0 (Supplemental Figure 1). Mean fold change from real-time qPCR data was calculated using the delta-delta cycle threshold (ddCt) method. We used 2-way analysis of variance (ANOVA) with Dunnett's multiple comparisons test to determine significant changes in expression in mannitol- or glucose-treated HUVEC vs. Time 0 cells. The threshold for statistical significance was a p value <0.05. For comparison of fold changes in HUVEC vs. T2DM ECs gene expression, a standard box plot was drawn using ggplot2. The plot shows the minimum, first quartile, median, third quartile, and maximum values (**Figure 2E**). The p value was determined by Wilcoxon rank sum test.

RESULTS

Cells collected via venous cannulation and wire abrasion were immediately labeled with anti-CD144-conjugated magnetic microbeads, which recognize the EC surface marker VE-Cadherin (aka CD144). This method reproducibly recovers 1,000 ECs from 1 arm of a human donor within 45 min. CD144- selected cells stained positive for the EC protein Von Willebrand factor and possess characteristic nuclear morphology that distinguishes them from non-ECs, as previously described (**Figure 1A**) (5). To evaluate the molecular identity of these cells more comprehensively, we performed unbiased gene-expression profiling by paired-end RNA sequencing of EC ($n = 4$, EC-Con) and flow-through fractions ($n = 4$, FT-Con) from healthy control subjects. One pair of EC-FT was left out of this analysis because of low quality in the FT fraction. Pairwise analysis of differential expression identified 2,549 genes more highly expressed in the CD144-selected cell fraction and 3,325 genes in the FT fraction (**Figure 1B**) (adjusted p value <0.05; $\log_2$ fold change ≥ 1). We next used a curated list of genes previously identified as highly restricted to ECs to perform gene set enrichment analysis on the RNA-seq data from isolated cells (14). This approach identified striking positive enrichment for EC genes in the human CD144-selected cells (**Figure 1C**). To address the molecular identity of the EC fraction in an orthogonal manner, we evaluated the gene ontology of differentially up-regulated genes in CD144-selected cells. Pathways related to the cardiovascular system, blood vessel development, angiogenesis, and cellular adhesion were strongly over-represented, revealing excellent enrichment for ECs and depletion of white blood cells (WBCs) in these cell fractions (**Figure 1D**). Finally, we extracted expression data for well-known EC-specific and WBC-specific genes and detected a clear clustering of gene expression by cell fraction (**Figure 1E**). Overall, these unbiased data demonstrate that CD144 selection of extracted cells enriches for ECs, as defined by global gene-expression patterns and known markers of EC identity.

We next exploited this EC-enrichment method to examine how T2DM alters global gene expression by comparing transcriptomic profiles of ECs isolated from patients with T2DM ($n = 4$) with data from healthy controls ($n = 5$, EC-Con) (15). In T2DM ECs, 51 genes were significantly up-regulated and 101 genes significantly down-regulated compared with EC-Con (**Figure 2A**). GSEA identified that pathways of metabolism and growth, including TGFβ and oxidative phosphorylation, were positively and negatively enriched in T2DM ECs, respectively (**Figure 2B**). Significant positive enrichment occurred in Cyclin D1 signaling, a pathway that has not yet been implicated in vascular disease in T2DM. Notably, androgen signaling was negatively enriched in T2DM ECs, consistent with emerging links between androgen deficiency, T2DM, and cardiovascular disease (16). Finally, we modeled the hyperglycemia associated with T2DM in vitro by treating HUVEC with high glucose (25 mM, 24 h). Although many more genes are modulated by glucose in vitro, of the 51 genes induced in T2DM, a significant number of genes ($p < 4.32e\text{-}13$ for probability of overlap) were shared in glucose-stimulated HUVEC (**Figures 2C and 2D**). Independent validation of these targets in a separate experiment of HUVEC treated with high glucose or mannitol (as an osmolarity control) identified up-regulation of a subset of genes (Supplemental Figure 1). Based on these results, we considered the possibility that the trends in gene up-regulation may be similar in T2DM ECs and glucose-treated HUVEC. For this analysis, we derived 2 gene lists from the HUVEC RNA-seq dataset: glucose-induced genes and genes that did not change expression. We then compared the composite fold change of these 2 gene lists in the T2DM EC RNA-seq dataset. With this approach, we detected a significant global shift in expression of glucose-induced genes in T2DM ECs (**Figure 2E**).

DISCUSSION

Vascular ECs play a central role in cardiovascular homeostasis and disease. Tools to study ECs in an unbiased manner directly in humans are limited but are critical to improve discovery-based research in human vascular biology. We address this limitation by developing a reproducible method for isolating, enriching, and then profiling global gene-expression programs in ECs from human subjects. Previous reports demonstrate rapid dedifferentiation of ECs and macrophages following their removal from resident tissue microenvironments (17,18). The method presented here enables the study of context-dependent gene regulation in human ECs without supervening effects of cell culture. As a result, ECs isolated from patients can be used to broaden our insights into molecular mechanisms governing blood-vessel function in humans.

Previous work with freshly isolated ECs studied differences in candidate signaling pathways in ECs using targeted immunofluorescence (3,5,19,20). A key goal of our study was to demonstrate that global differences in gene expression between 2 different patient groups could be measured with isolated ECs. We chose to study patients with T2DM, given the strong links between T2DM, EC dysfunction, and vascular disease (21). Notably, androgen signaling was negatively enriched in T2DM ECs, providing validation for our experimental system, given established associations between androgen deprivation—both physiologic and cancer treatment-induced—with metabolic and cardiovascular disease (16,22,23). This is also the first study to implicate impaired androgen signaling in *ex vivo* diabetic ECs. Down-regulation of oxidative phosphorylation observed here in isolated ECs is consistent with known changes in mitochondrial and EC function provoked by hyperglycemia and insulin resistance (24). In contrast to the androgen pathway, the role of cyclin D1 signaling in diabetic vascular disease is unknown and merits further study. Cyclin D2, a closely related homologue involved in cell-cycle control, is induced by glucose in rat ECs and promotes EC proliferation (25). Connections between cyclin D1 and EC dysfunction in diabetes mellitus may be particularly relevant now, given ongoing trials of new cancer therapies that inhibit the cyclin D1 axis. These therapies could be deployed to disrupt cyclin D1 signaling in ECs and test whether this intervention affects EC function under diabetic states in humans (26). Finally, the positive enrichment for TGF-β signaling may be relevant to the anticorrelation of diabetes mellitus and aneurysm disease that has been described, given that loss of function mutations in the TGF-β pathway are causally linked to genetic aneurysm syndromes such as Loeys-Dietz syndrome (27,28).

Despite known differences in homeostatic gene-expression programs of cultured ECs vs. ECs immediately after isolation from organ depots, we detected a partially shared gene regulatory response between glucose-treated HUVECs and T2DM ECs (17). In addition, some genes were also up-regulated by mannitol in HUVEC, suggesting hyperosmolarity itself controls EC gene expression in vitro and may be relevant to gene regulation in vivo in patients with diabetes mellitus. Notably, this experiment compares stress responses in vitro and in vivo, unlike previous work examining baseline transcriptional profiles in ECs. Although the number of patients studied was small, the data presented herein suggest that stress signaling can lead to some convergences in gene expression in vitro and in vivo.

STUDY LIMITATIONS. We cannot exclude the possibility that our CD144 cell-sorting method might bias these results if EC differentiation state and CD144 expression is down-regulated during progression of diabetes, as has been shown in other contexts (29). Orthogonal methods, such as multimarker sorting and single-cell RNA-sequencing could be used to overcome these potential limitations. Another limitation of this study is the relatively small number of patients included in this first study of diabetes. In the future, increasing sample size will improve statistical power to discern subtle changes in gene expression between disease or treatment groups.

CONCLUSIONS

These results illustrate how a multimodal experimental platform that couples data from primary human samples with data from established *in vitro* model systems could prioritize pathways for further exploration as mediators of EC dysfunction in human disease. We anticipate that this approach, which couples immunopurification with unbiased gene expression, can be applied to study mechanisms of chronic cardiovascular diseases in humans as well as vascular effects and toxicities of drugs in clinical use or preclinical development.

ADDRESS FOR CORRESPONDENCE: Dr. Jonathan D. Brown, Vanderbilt University Medical Center, 2220 Pierce Avenue, Preston Research Building, Suite 383, Nashville, Tennessee 37232. E-mail: jonathan.d.brown@vumc.org.

PERSPECTIVES

COMPETENCY IN MEDICAL KNOWLEDGE: Endothelial function is an important clinical feature of diabetes mellitus. However, tools to study endothelial molecular biology directly in patients are limited. The current study provides validation of a method to study gene regulation in endothelial cells from humans. This tool can be used to probe how endothelial function changes in systemic diseases including diabetes mellitus.

TRANSLATIONAL OUTLOOK: Patient-derived endothelial cells can be used to discover new biological pathways in systemic diseases that feature vascular dysfunction.

REFERENCES

1. Gimbrone MA Jr., Garcia-Cardena G. Endothelial cell dysfunction and the pathobiology of atherosclerosis. Circ Res 2016;118:620–36.

2. Nagel T, Resnick N, Dewey CF Jr., Gimbrone MA Jr. Vascular endothelial cells respond to spatial gradients in fluid shear stress by enhanced activation of transcription factors. Arterioscler Thromb Vasc Biol 1999;19:1825–34.

3. Colombo PC, Ashton AW, Celaj S, et al. Biopsy coupled to quantitative immunofluorescence: a new method to study the human vascular endothelium. J Appl Physiol 2002;92:1331–8.

4. Donato AJ, Eskurza I, Silver AE, et al. Direct evidence of endothelial oxidative stress with aging in humans: relation to impaired endothelium-dependent dilation and upregulation of nuclear factor-kappaB. Circ Res 2007;100:1659–66.

5. Tabit CE, Shenouda SM, Holbrook M, et al. Protein kinase C-beta contributes to impaired endothelial insulin signaling in humans with diabetes mellitus. Circulation 2013;127:86–95.

6. Waldo SW, Brenner DA, McCabe JM, et al. A novel minimally-invasive method to sample human endothelial cells for molecular profiling. PLoS One 2015;10:e0118081.

7. Emin M, Wang G, Castagna F, et al. Increased internalization of complement inhibitor CD59 may contribute to endothelial inflammation in obstructive sleep apnea. Sci Transl Med 2016;8:320.

8. Martin M. Cutadapt removes adapter sequences from high-throughput sequencing reads. EMBnet J 2011;17:10–2.

9. Dobin A, Davis CA, Schlesinger F, et al. STAR: ultrafast universal RNA-seq aligner. Bioinformatics 2013;29:15–21.

10. Liao Y, Smyth GK, Shi W. featureCounts: an efficient general purpose program for assigning sequence reads to genomic features. Bioinformatics 2014;30:923–30.

11. Love MI, Huber W, Anders S. Moderated estimation of fold change and dispersion for RNA-seq data with DESeq2. Genome Biol 2014;15:550.

12. Zhao S, Guo Y, Sheng Q, Shyr Y. Advanced heat map and clustering analysis using heatmap3. Biomed Res Int 2014;2014:986048.

13. Subramanian A, Tamayo P, Mootha VK, et al. Gene set enrichment analysis: a knowledge-based approach for interpreting genome-wide expression profiles. Proc Natl Acad Sci USA 2005;102:15545–50.

14. Bhasin M, Yuan L, Keskin DB, Otu HH, Libermann TA, Oettgen P. Bioinformatic identification and characterization of human endothelial cell-restricted genes. BMC Genom 2010;11:342.

15. Luscher TF, Creager MA, Beckman JA, Cosentino F. Diabetes and vascular disease: pathophysiology, clinical consequences, and medical therapy: Part II. Circulation 2003;108:1655–61.

16. Rovira-Llopis S, Banuls C, de Maranon AM, et al. Low testosterone levels are related to oxidative stress, mitochondrial dysfunction and altered subclinical atherosclerotic markers in type 2 diabetic male patients. Free Radic Biol Med 2017;108:155–62.

17. Lacorre DA, Baekkevold ES, Garrido I, et al. Plasticity of endothelial cells: rapid dedifferentiation of freshly isolated high endothelial venule endothelial cells outside the lymphoid tissue microenvironment. Blood 2004;103:4164–72.

18. Gosselin D, Skola D, Coufal NG, et al. An environment-dependent transcriptional network specifies human microglia identity. Science 2017;356.

19. Feng L, Stern DM, Pile-Spellman J. Human endothelium: endovascular biopsy and molecular analysis. Radiology 1999;212:655–64.

20. Silver AE, Christou DD, Donato AJ, et al. Protein expression in vascular endothelial cells obtained from human peripheral arteries and veins. J Vasc Res 2010;47:1–8.

21. Beckman JA, Paneni F, Cosentino F, Creager MA. Diabetes and vascular disease: pathophysiology, clinical consequences, and medical therapy: part II. Eur Heart J 2013;34:2444–52.

22. Bhatia N, Santos M, Jones LW, et al. Cardiovascular effects of androgen deprivation therapy for the treatment of prostate cancer: ABCDE steps to reduce cardiovascular disease in patients with prostate cancer. Circulation 2016;133:537–41.

23. Navarro G, Xu W, Jacobson DA, et al. Extranuclear actions of the androgen receptor enhance glucose-stimulated insulin secretion in the male. Cell Metab 2016;23:837–51.

24. Tang X, Luo YX, Chen HZ, Liu DP. Mitochondria, endothelial cell function, and vascular diseases. Front Physiol 2014;5:175.

25. Li XX, Liu YM, Li YJ, et al. High glucose concentration induces endothelial cell proliferation by regulating cyclin-D2-related miR-98. J Cell Mol Med 2016;20:1159–69.

26. Turner NC, Ro J, Andre F, et al. Palbociclib in hormone-receptor-positive advanced breast cancer. N Engl J Med 2015;373:209–19.

27. Raffort J, Lareyre F, Clement M, Hassen-Khodja R, Chinetti G, Mallat Z. Diabetes and aortic aneurysm: current state of the art. Cardiovasc Res 2018;114:1702–13.

28. Loeys BL, Schwarze U, Holm T, et al. Aneurysm syndromes caused by mutations in the TGF-beta receptor. N Engl J Med 2006;355:788–98.

29. Widyantoro B, Emoto N, Nakayama K, et al. Endothelial cell-derived endothelin-1 promotes cardiac fibrosis in diabetic hearts through stimulation of endothelial-to-mesenchymal transition. Circulation 2010;121:2407–18.

KEY WORDS endothelial cells, gene expression, diabetes mellitus, endothelial cell dysfunction

APPENDIX For a supplemental figure, please see the online version of this paper.

JACC: BASIC TO TRANSLATIONAL SCIENCE VOL. 4, NO. 5, 2019

PRECLINICAL RESEARCH

Cardiac Microvascular Endothelial Enhancement of Cardiomyocyte Function Is Impaired by Inflammation and Restored by Empagliflozin

Rio P. Juni, PhD,[a] Diederik W.D. Kuster, PhD,[a] Max Goebel, MSc,[a] Michiel Helmes, PhD,[a,b] René J.P. Musters, PhD,[a] Jolanda van der Velden, PhD,[a,c] Pieter Koolwijk, PhD,[a] Walter J. Paulus, MD, PhD,[a] Victor W.M. van Hinsbergh, PhD[a,c]

VISUAL ABSTRACT

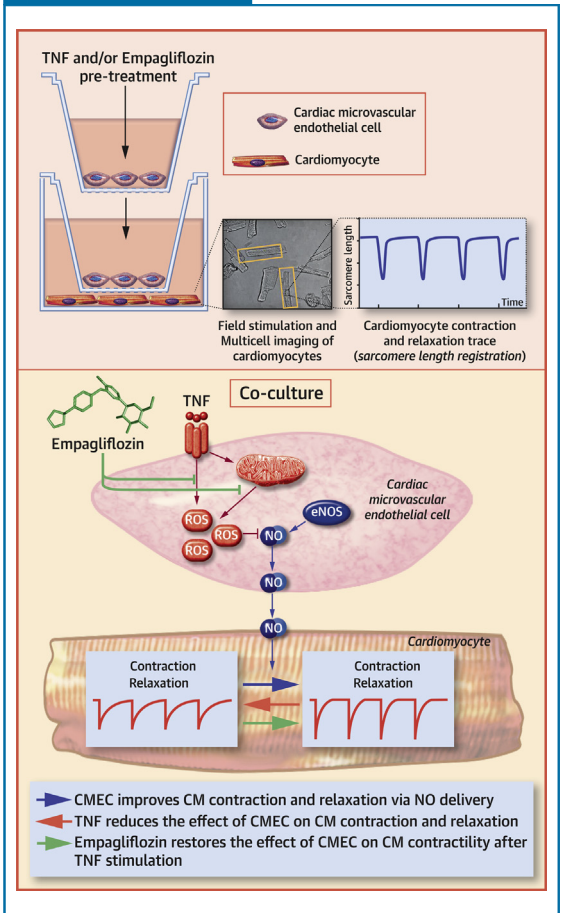

Juni, R.P. et al. J Am Coll Cardiol Basic Trans Science. 2019;4(5):575-91.

HIGHLIGHTS

- **CMECs exert a direct positive effect on cardiomyocyte contraction and relaxation, which is mainly mediated by endothelial-derived NO.**
- **Pro-inflammatory stimulation of CMECs by pre-incubation with TNF-α or interleukin-1β abrogates the positive regulatory function of these cells on cardiomyocyte contractile property.**
- **Mechanistically, pro-inflammatory activation of CMECs leads to mitochondrial and cytoplasmic ROS accumulation that results in the scavenging of NO.**
- **Empagliflozin directly restores the beneficial effect of CMECs on cardiomyocyte contraction and relaxation by reducing TNF-α-induced mitochondrial and cytoplasmic ROS accumulation, which leads to reinstatement of CMEC-derived NO delivery.**

From the [a]Amsterdam Cardiovascular Sciences, Department of Physiology, Amsterdam University Medical Centers, Amsterdam, the Netherlands; [b]CytoCypher B.V., Wageningen, the Netherlands; and the [c]Netherlands Heart Institute, Utrecht, the Netherlands.
This project is funded by the Netherlands Heart Foundation (CVON-RECONNECT consortium, no. 2014-11). The authors have reported that they have no relationships relevant to the contents of this paper to disclose.

ISSN 2452-302X https://doi.org/10.1016/j.jacbts.2019.04.003

ABBREVIATIONS AND ACRONYMS

Ca = calcium

CM = cardiomyocyte

CMEC = cardiac microvascular endothelial cell

DPPH = 1,1-diphenyl-picrylhydrazyl

DM = diabetes mellitus

EC = endothelial cell

eNOS = endothelial nitric oxide synthase

HF = heart failure

HFpEF = heart failure with preserved ejection fraction

HFrEF = heart failure with reduced ejection fraction

JNK = Jun N-terminal kinase

L-NAME = N(ω)-nitro-L-arginine methyl ester

LV = left ventricular

NK-κB = nuclear factor-κB

NO = nitric oxide

ROS = reactive oxygen species

SGLT2 = sodium glucose transporter 2

SUMMARY

The positive findings of the EMPA-REG OUTCOME trial (Randomized, Placebo-Controlled Cardiovascular Outcome Trial of Empagliflozin) on heart failure (HF) outcome in patients with type 2 diabetes mellitus suggest a direct effect of empagliflozin on the heart. These patients frequently have HF with preserved ejection fraction (HFpEF), in which a metabolic risk-related pro-inflammatory state induces cardiac microvascular endothelial cell (CMEC) dysfunction with subsequent cardiomyocyte (CM) contractility impairment. This study showed that CMECs confer a direct positive effect on contraction and relaxation of CMs, an effect that requires nitric oxide, is diminished after CMEC stimulation with tumor necrosis factor-α, and is restored by empagliflozin. Our findings on the effect of empagliflozin on CMEC-mediated preservation of CM function suggests that empagliflozin can be used to treat the cardiac mechanical implications of microvascular dysfunction in HFpEF.

Heart failure with preserved ejection fraction (HFpEF) accounts for 50% of patients with heart failure (HF) (1) and lacks an effective treatment. Therapies that are used in HF patients with reduced EF (HFrEF) have failed to improve primary outcomes in patients with HFpEF (2–5), which suggests different pathomechanisms in HFpEF compared with HFrEF. Recently, the paradigm of HFpEF has shifted from a mere cardiomyocyte (CM) disease to a disorder that initially involves cardiac microvascular endothelial cells (CMECs), which subsequently leads to CM dysfunction (6,7). Comorbidities, such as type 2 diabetes mellitus (DM), obesity, hypertension, and chronic kidney disease, are highly prevalent

SEE PAGE 592

in patients with HFpEF (8–10). These metabolic diseases are accompanied by microvascular endothelial dysfunction, including that of CMECs, which are characterized by impaired nitric oxide (NO) generation, increased reactive oxygen species (ROS) production, inflammatory activation (7,11–13), and rarefaction of the cardiac microvascular bed (14). Recent findings in patients with breast cancer showed that the relative risk of HFpEF increased with increasing cardiac radiation exposure during breast cancer radiotherapy (15,16). In adults, CMs do not or rarely proliferate and thus are highly radioresistant (17–19). Cardiac radiation exposure causes coronary microvascular endothelial cell (EC) damage and inflammation with subsequent coronary microvascular dysfunction and rarefaction that impair myocardial function (19–21). These studies provide proof of concept as they underpin the essential role of the cardiac microvascular endothelium in determining risk of left ventricular (LV) diastolic dysfunction. Interaction between endocardial ECs and CMs has been shown in earlier studies on cardiac papillary muscles (22,23). However, a direct causal effect of cardiac microvascular endothelial dysfunction on cardiac contraction and relaxation, which has been proposed based on clinical associations (11,24), needs to be fundamentally established. If the CMEC-CM axis plays an important role in the pathogenesis of HFpEF, improvement of CMEC function may represent an important target in developing new treatments and prevention strategies for HFpEF.

Empagliflozin, a sodium glucose transporter 2 (SGLT2) inhibitor that is primarily used in patients with type 2 DM to lower blood glucose levels, may represent a novel therapy to treat HFpEF patients. Recent findings of the EMPA-REG OUTCOME trial (Randomized, Placebo-Controlled Cardiovascular Outcome Trial of Empagliflozin) showed an unexpected beneficial effect of empagliflozin on HF outcome in patients with DM and suggested that empagliflozin acts not only on kidney tubular cells but also directly on the heart (25). The significant reduction of cardiovascular mortality and HF hospitalization by empagliflozin treatment (19,25)

The authors attest they are in compliance with human studies committees and animal welfare regulations of the authors' institutions and Food and Drug Administration guidelines, including patient consent where appropriate. For more information, visit the *JACC: Basic to Translational Science* author instructions page.

Manuscript received November 19, 2018; revised manuscript received April 23, 2019, accepted April 27, 2019.

indicated that empagliflozin could be useful as treatment of HFpEF because metabolically compromised patients, such as patients with DM, frequently have HFpEF. This suggestion is currently being investigated in a large clinical trial (EMPEROR-Preserved [Empagliflozin Outcome Trial in Patients With Chronic Heart Failure With Preserved Ejection Fraction]) (26). Apart from a recent study that showed that empagliflozin acts directly on sodium and calcium (Ca^{2+}) exchange in isolated CMs (27), it was recently reported that empagliflozin improved diastolic cardiac function by increasing cyclic guanosine monophosphate (cGMP)-dependent titin phosphorylation in human ventricular trabeculae and in a murine model of HFpEF (28). However, the cardiac mechanisms of action for empagliflozin remain largely unexplored, in particular with respect to interactions between CMECs and CMs, which are especially relevant for cardiac dysfunction in HFpEF.

We report on the effect of CMEC on CM function in a novel co-culture system combined with a novel high-throughput analysis of CM function. We demonstrate that CMECs improve CM contraction and relaxation, an effect that is lost after pre-incubation of CMECs with the inflammatory mediator tumor necrosis factor-α (TNF-α). Moreover, we provide evidence that empagliflozin restored this beneficial effect of CMECs by reducing mitochondrial ROS production and cytoplasmic ROS accumulation, which led to restoration of endothelial NO bioavailability and preservation of CM contraction and relaxation. These data provide a new mechanism underlying the effect of empagliflozin on the heart by modulating CMEC-mediated enhancement of CM function.

METHODS

CMEC CULTURE. Human CMECs (CC-7030, Lonza Europe, Breda, the Netherlands) were cultured and characterized (CD31, vWF, and VE-cadherin) before being used in the experiments. For co-culture experiments (see the following), CMECs (passage 5 to 7) were cultured on 24-well format, 3 μm filter inserts (ThinCert, 662631, Grenier Bio-one, Monroe, North Carolina) coated with 1% gelatin (104070, Merck, Whitehouse Station, New Jersey) in endothelial growth medium-2MV (CC-3203, Lonza) at 37°C in a 5% carbon dioxide-95% air atmosphere. For the assessment of NO production (see the following), CMECs were grown on 8-well format μ-Slide (80826, Ibidi GmbH, Gräfelfing, Bayern, Germany) with the same medium and culture condition.

ADULT RAT VENTRICULAR CM ISOLATION AND CULTURE. The animal experiments were performed in accordance with the guidelines from Directive 2010/63/EU of the European Parliament on the protection of animals used for scientific purposes and were approved by the ethics committees of VU University Medical Center, Amsterdam, the Netherlands.

Adult rat CMs were isolated using liberase digestion of hearts as described previously (29,30). Briefly, adult wild-type Wistar rats weighing 200 to 250 g were anesthetized with isoflurane (45.112.110, Pharmachemie, Haarlem, the Netherlands) inhalation. The chest was opened, and the heart was injected with cold Ethylene glycol tetraacetic acid (EGTA) solution. Afterward, it was quickly removed, cannulated via the aorta, and perfused in a Langendorff setup with a perfusion buffer for 5 min. Next, it was perfused with enzyme solution until the tissue was digested sufficiently. The atria and right ventricle were removed, and the LV was cut into small pieces and triturated with a plastic Pasteur pipette for 3 min. Subsequently, the cell suspension was filtered through a 300-μm stainless steel autoclaveable filter and resuspended in calcium chloride buffers of increasing Ca^{2+} concentrations to reach a final concentration of 0.2 mM Ca^{2+}.

Isolated adult CMs were finally resuspended in plating medium containing Medium 199 (BE12-117F, Lonza), 1% penicillin/streptomycin (DE17-602DE, Lonza), and 5% fetal bovine serum (A15-101, PAA Cell Culture Company, Cambridge, United Kingdom), and seeded on 1% laminin (L2020-1MG, Sigma-Aldrich, St. Louis, Missouri) coated plates (24-well format Costar culture plate, 3524, Corning, Corning, New York). One h after plating, cells that were not attached were removed by replacing the plating medium with culture medium endothelial growth medium-2MV. Subsequently, the cells were co-cultured with CMECs pre-seeded on inserts (see the preceding) at 37°C in humidified air with 5% carbon dioxide. Isolation protocol details can be found in the Supplemental Appendix.

CO-CULTURE MODEL OF CMECs AND CMs. CMECs were seeded overnight on inserts with a seeding density of 2.5×10^4 per insert. Subsequently, the culture medium was renewed, and the cells were either not stimulated or stimulated with 10 ng/ml TNF-α (T6674, Sigma), 10 ng/ml interleukin-1β (200-01B-10 μg, PeproTech, Rocky Hill, New Jersey), 1 μM empagliflozin (HY-15409, MedChem Express, Monmouth Junction, New Jersey), 10 μM butylated hydroxytoluene (PHR1117, Sigma), or a combination thereof, for 6 h before the co-culture procedure. After this pre-stimulation period, the cells were rinsed 3 times, and the medium was renewed to ensure that all treatments were washed away before the co-culture protocol. Co-culture of CMECs was started

FIGURE 1 CMEC-CM Co-Culture and High-Throughput MultiCell CM Detection System

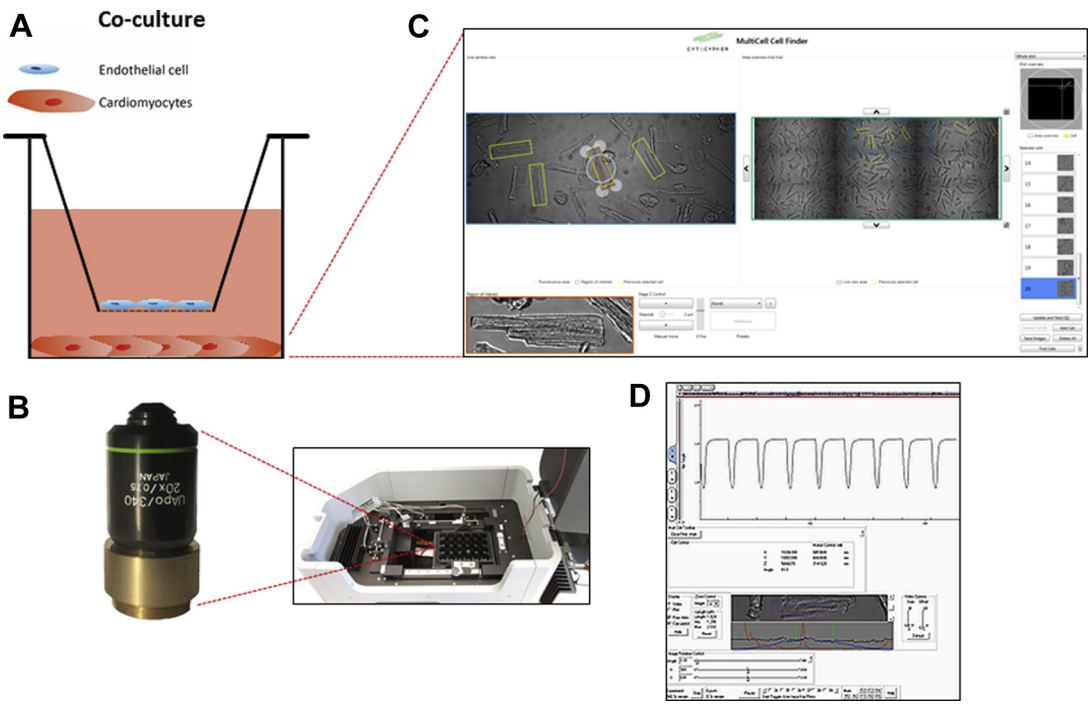

(A) Cardiac microvascular endothelial cells (CMECs) were cultured on an insert placed above the cardiomyocytes (CMs) seeded on a well of a culture plate. **(B, right panel)** After a co-culture procedure, the CMEC compartment was removed, and **(C)** the CM compartment was placed into a temperature-controlled inverted microscope chamber and visualized. **(B, left panel)** The objective lens was positioned directly under the well containing CMs **(A)**. **(D)** CMs were paced, and cell contraction and relaxation profiles were monitored.

by placing the inserts with untreated or treated CMECs closely above the CMs cultured separately in another culture plate (Figure 1, Supplemental Figure 1). After 2 h of co-culture, the inserts containing the CMECs were removed, and CM contractile profiles were assessed as described in the following. To inhibit NO production, CMECs were incubated with 100 μM N(ω)-nitro-L-arginine methyl ester (L-NAME) (N5751, Sigma-Aldrich, St. Louis, Missouri) for 1 h before the co-culture procedure, which was continued subsequently for 2 h during the co-culture period with CMs.

INCUBATION OF CMs WITH ENDOTHELIAL CELL-CONDITIONED MEDIUM WITH AND WITHOUT NO SCAVENGING. CMECs were seeded in 1% gelatin-coated 6-well plates (Costar culture plate, 3506, Corning) until it reached confluency. The cell medium was then refreshed, and after 6 h, the CMEC-conditioned medium was pipetted onto the CMs pre-plated in a separate 24-well plate. The contraction profiles were measured after 30 min, 1 h, 1.5 h, and 2 h incubation of CMs with the conditioned medium. In a separate experiment, 10 μm of the NO scavenger carboxy-PTIO (C221, Sigma) was added to the endothelial-conditioned medium before being administered to the CMs. After 30 min of incubation, the contractility of the CMs was measured.

HIGH-THROUGHPUT MULTICELL CM FUNCTION EVALUATION SYSTEM. To investigate whether CMECs regulated the contractile properties of CMs, we developed an assay in which we assessed CM contraction and relaxation kinetics during a co-culture period with CMECs. After the co-culture procedure, the plate containing CMs was placed in a high-throughput inverted microscope (Olympus 20x 0.75 aperture objective lens, Olympus, Shinjuku, Japan) setup (CytoCypher, Amsterdam, the Netherlands) (Figure 1B), and the cells were visualized (Figure 1C). The camera-based MultiCell microscope system (CytoCypher, Amsterdam, the Netherlands) (Figure 1C) allowed the selection and assay of numerous CMs within a relatively short period of time. Unloaded intact rat CMs were monitored following field stimulation, and sarcomere shortening was measured using the MultiCell CM detection system in combination with the Ionoptix high-speed

sarcomere length measuring software (Ionoptix LLC, Westwood, Massachusetts) (Figure 1D). The contractility profiles were analyzed with the automated, batch analysis software Transient Analysis Tools (CytoCypher). Subsequent to co-culture procedure with CMECs or after direct treatment with 1 μM empagliflozin for 2 h, CMs were placed into a temperature-controlled microscope chamber with platinum electrodes to electrically stimulate the cells. Single CMs were selected based on the following criteria: rod-shaped, no spontaneous contractions, and diastolic sarcomere length of at least 1.6 μm. Upon field stimulation (2 Hz, 4 ms, 25 V), cell contraction and relaxation kinetics were monitored.

NO MEASUREMENT IN ENDOTHELIAL CELLS. NO bioavailability was assessed on confluent CMECs cultured on μ-slides (Ibidi, 80826). A copper-based NO probe (Cu_2FL2E; 96-0396, Strem, Newburyport, Massachusetts) was added in a final concentration of 20 μM and incubated for 45 min to allow cellular uptake. Stimulation with 10 μM acetylcholine (A6625-25G, Sigma) was performed for 45 min, at the same time as the incubation with the Cu_2FL2E probe. For NO measurement after 6 h of TNF-α, empagliflozin, and butylated hydroxytoluene treatment, the probe was added during the final 45 min of the incubation period. For inhibition of NO synthases, CMECs were pre-incubated with 100 μM L-NAME for 1 h before addition of and during incubation with Cu_2FL2E. The cells were then washed 3 times with Hanks' Balanced Salt Solution (HBSS) (BE10-547F, Lonza); subsequently, live-cell imaging was performed at 37°C and in a 5% carbon dioxide environment on a Zeiss Axiovert 200M Marianas inverted fluorescence microscope (Intelligent Imaging Innovations, Denver, Colorado), equipped with a motorized stage, a turret with diamidino-2-phenylindole, fluorescein isothiocyanate (FITC), Cy3, and Cy5 filter cubes, a cooled CCD camera (Cooke Sensicam SVGA, Cooke Co., Tonawanda, New York), and a 63× oil-immersion objective (Zeiss, Breda, the Netherlands). The camera was linear over its full dynamic range (up to intensities of >4,000), whereas dark and/or background currents (measured by the intensity outside the cells) were typically <100. All fluorescent images were corrected for background (including dark current) and negative controls. Quantification of all fluorescent images was performed using dedicated digital cell masking software (Slidebook 6, Intelligent Imaging Innovations).

CYTOPLASMIC AND MITOCHONDRIAL ROS MEASUREMENT IN ENDOTHELIAL CELLS. Cytoplasmic ROS level was assessed on confluent CMECs cultured on Ibidi μ-slides. A fluorescent dye-based ROS probe (CM-H2DCFDA, C6827, ThermoFischer, Waltham, Massachusetts) was added in a final concentration of 5 μM and incubated for 30 min in phosphate-buffered saline (220/12257974/1110, Braun, Kronberg im Taunus, Germany), supplemented with 1 mM calcium chloride, 0.5 mM magnesium chloride, and 5.4 mM D-glucose, to allow cellular uptake. Mitochondrial CMEC ROS level was assessed with 500 nM MitoTracker Red CM-H2Xros (M7513, ThermoFischer). Six h after TNF-α and/or empagliflozin treatment, the cells were washed 1 time with supplemented phosphate buffer saline and subsequently incubated with the probe. The cells were then washed 1 time, followed by live-cell imaging at 37°C and in a 5% carbon dioxide environment on a Zeiss Axiovert 200M Marianas inverted fluorescence microscope (Intelligent Imaging Innovations) with a 63× oil-immersion objective. All fluorescent images were corrected for background and negative controls. Quantification of all fluorescent images was performed using digital cell masking software (Slidebook 6, Intelligent Imaging Innovations).

DETERMINATION OF ANTIOXIDANT CAPACITY. To determine whether empagliflozin possesses direct antioxidant capacity, we performed a 1,1-diphenylpicrylhydrazyl (DPPH) assay. The antioxidant activity was measured in terms of hydrogen donating or radical scavenging ability, using the stable radical DPPH. DPPH (25 μM) (D9132, Sigma) solution in methanol was pipetted into 96-well plate format (Costar, 3599, Corning), and 1 or 10 μM of empagliflozin was added. Butylated hydroxytoluene (0.4 mg/ml) and ascorbic acid (A5960, Sigma) (0.5 mg/ml) served as positive controls, and methanol served as a negative control. The plate was incubated for 30 min in the dark at room temperature. Afterward, the decrease in absorbance was measured at 517 nm with an enzyme-linked immunosorbent assay reader/spectrophotometer (Epoch, Biotek, Winooski, Vermont). The capability of scavenging the DPPH radical, or the direct antioxidant capacity, was calculated by using the following formula: $((A0 - A1)/A0) \times 100)$, where A0 is the absorbance of the negative control reaction, and A1 is the absorbance in the presence of samples or positive control antioxidants.

CELL ADHESION MOLECULE MEASUREMENT. Cell adhesion molecules were assayed by a cell-bound enzyme-linked immunosorbent assay. CMECs were grown in 96-well plates (Costar, 3599, Corning) until confluency was reached. Subsequently, the culture medium endothelial growth medium-2MV was renewed, and the cells were either not stimulated or stimulated with 10 ng/ml TNF-α, or a combination of

FIGURE 2 CMECs Enhance CM Function

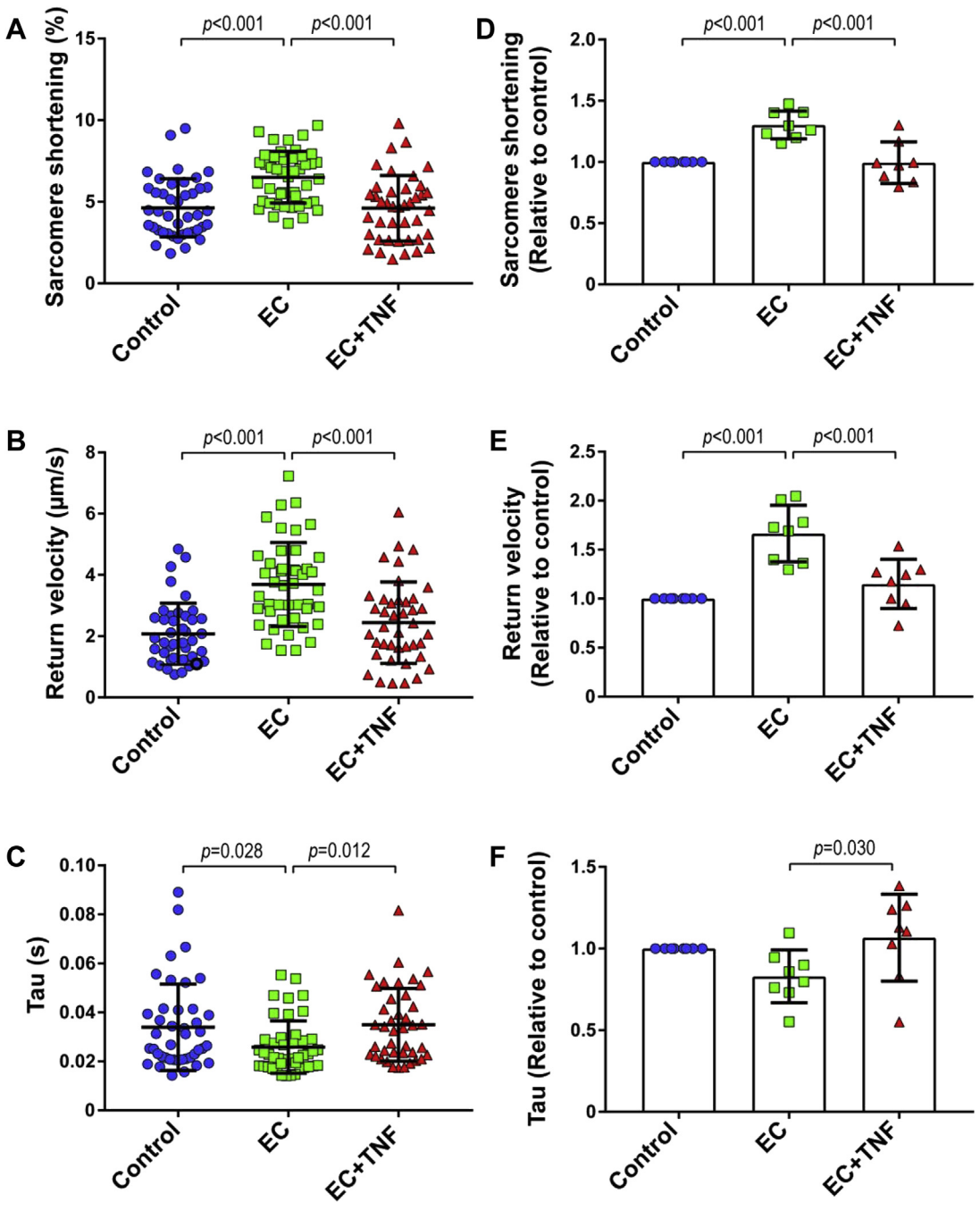

CM contraction and relaxation were evaluated under basal conditions (control) and after co-culture with untreated (endothelial cells [ECs]) or tumor necrosis factor (TNF)-α pre-treated CMEC (EC+TNF). **(A and D)** Co-culture of CMs with ECs increased CM contraction (proportion sarcomere shortening), and **(B and E)** improved CM relaxation as shown by increased speed of relaxation (return velocity) and **(C and F)** shortened time constant of relaxation (tau). **(A and D)** Pre-treatment of CMECs with TNF-α (EC+TNF) abolished the beneficial effect of CMECs on CM contraction and **(B, C, E, and F)** relaxation. **(A to C)** Graphs representing single CMs isolated from 1 individual rat, distributed into the 3 corresponding experimental conditions; 40 to 45 CMs were measured per condition. **(D to F)** Data are representative of 8 independent experiments. **(D to F)** Graphs of combined average values obtained from 8 independent experiments corresponding to 8 individual rats. All data are represented as mean ± SD. Other abbreviations as in Figure 1.

10 ng/ml TNF-α and 1 μM empagliflozin for 6 h. After the 6 h stimulation, CMECs were washed with phosphate-buffered saline and fixated with 0.025% glutaraldehyde (G5882-50mL, Sigma). A cell-bound enzyme-linked immunosorbent assay was performed using either mouse anti-VCAM 1:5,000 (Clone P3C4, MAB2144, Millipore B.V., Amsterdam, the Netherlands) or mouse anti–E-selectin 1:5,000 (CD62E, clone 1.2B6, CBL180, Chemicon) antibody, and peroxidase labeled-goat, anti-mouse immunoglobulin-G 1:2000 (P0447, Dako) as the secondary antibody. The reaction was visualized with a 3',3',5,5'-Tetramethylbenzidine (TMB) (980828, Organon Teknika, Durham, North Carolina) solution and stopped by administration of 2 M sulphuric acid (M205 K17208431 1L, Merck). Adhesion molecules were measured in triplicate with an enzyme-linked immunosorbent assay reader (Epoch, Biotek) at 450 nm.

SODIUM DODECYL SULFATE–POLYACRYLAMIDE GEL ELECTROPHORESIS AND WESTERN BLOTTING. Cell lysates were produced in sample buffer containing 187.5-mM TRIS-hydrochloride, pH 6.8, 6% w/v sodium dodecyl sulfate (SDS), 30% glycerol, 150 mM Dithiothreitol (DTT), and 0.03% w/v bromphenol blue. For endothelial nitric oxide synthase (eNOS) dimer and/or monomer assessment, the SDS was adjusted to 2%, and the DTT was omitted from the sample buffer. Subsequently, samples were boiled for 5 min at 95°C. SDS-polyacrylamide gel electrophoresis (PAGE) was performed in 8% gel at room temperature at 120 V followed by transfer of the protein at 200 mA to a nitrocellulose membrane. Western blotting was performed using the Mini-TransBlot Cell (Bio-Rad, Foster City, California). For eNOS dimer and/or monomer assessment, sodium dodecyl sulfate-polyacrylamide gel electrophoresis was performed in 6% gel at 10 mA followed by membrane blotting at 95 mA at 4°C. The blotted membranes were blocked in 5% bovine serum albumin (A9647, Sigma) or 5% milk (170-6404, Bio-Rad Laboratories B.V., Lunteren, the Netherlands) in Tris-buffered saline-Tween. Primary antibody labeling was performed overnight at 4°C, whereas secondary immunoglobulin-G–horseradish peroxidase-conjugated antibodies were applied for 2 h at room temperature. After each antibody incubation, blots were washed for 3 × 5 min in Tris-buffered saline-Tween. Images were generated using ECL Prime (RPN2232, Amersham, GE Healthcare, Buckinghamshire, United Kingdom) and the LAS-3000 documentation system (Fuji Film Life Science, Stamford, Connecticut). Outputs were normalized for loading, and results were expressed as an n-fold increase over the values of the control group in densitometric arbitrary units. Primary antibodies that were

FIGURE 3 Inhibition of Endothelial NOS Eliminates the Beneficial Effect of CMEC on CM Contraction and Relaxation

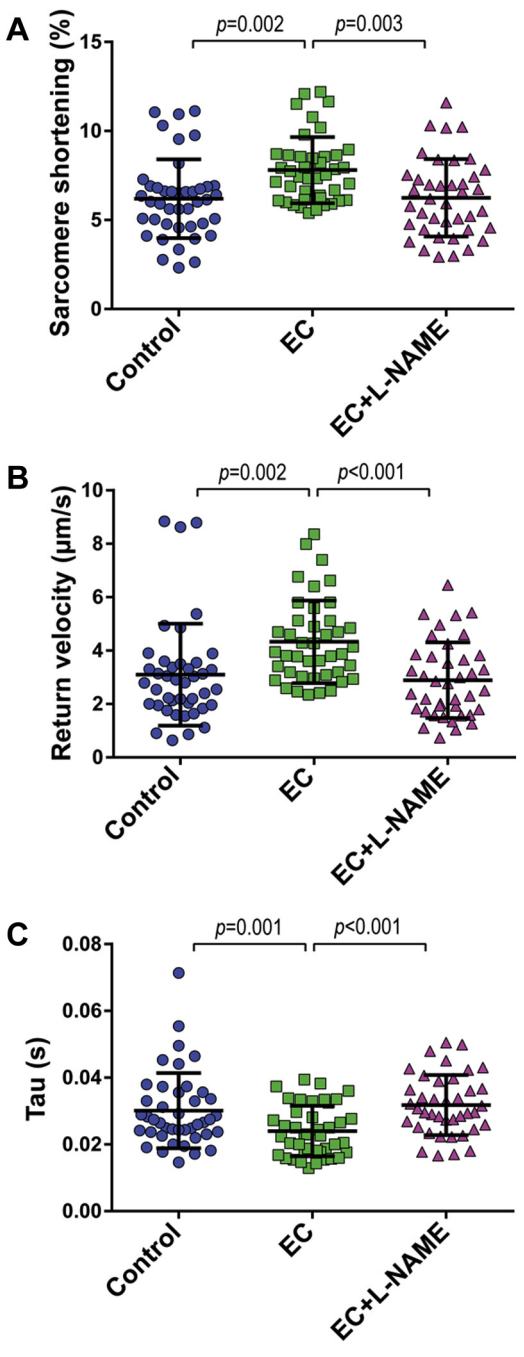

(A) Inhibition of CMEC nitric oxide (NO) generation with N(ω)-nitro-L-arginine methyl ester (L-NAME) abrogated the effect of CMECs on CM sarcomere shortening, **(B)** return velocity, and **(C)** tau. **(A to C)** Graphs representing single CMs isolated from 1 individual rat, distributed into the 3 corresponding experimental conditions; 40 to 45 CMs were measured per condition. Data are representative of 3 independent experiments. Data are represented as mean ± SD. NOS = nitric oxide synthase; other abbreviations as in Figures 1 and 2.

FIGURE 4 TNF-α Reduces NO Bioavailability in CMECs

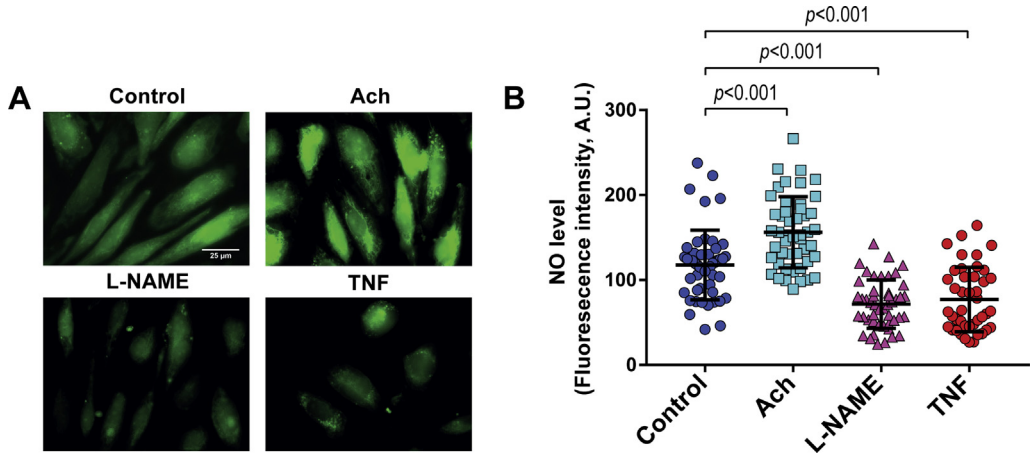

(A and B) NO levels in CMEC. Acetylcholine (Ach)–induced upregulation of NO production in CMECs. Similar to L-NAME treatment, TNF-α reduced CMEC NO levels. (n = 4 to 50, refers to number of cells per group from 3 independent experiments). Data represented as mean ± SD. Other abbreviations as in Figures 1 to 3.

used included rabbit monoclonal phospho–Jun N-terminal kinase (JNK) T185/Y185 (4668T, 1:1,000, Cell Signaling, Danvers, Massachusetts), rabbit total JNK (9252T, 1:1,000, Cell Signaling), rabbit monoclonal phospho-eNOS Ser1177 (9570S, 1:1,000, Cell Signaling), mouse total eNOS (Ab95254, Abcam, Cambridge, United Kingdom), rabbit glyceraldehyde-3-phosphate dehydrogenase (1:100.000, Cell Signaling). Secondary antibodies included goat anti-rabbit (P0448, 1:5,000, Dako) and goat anti-mouse immunoglobulin-G-horseradish peroxidase (P0447, 1:5,000, Dako).

GENE EXPRESSION ASSESSMENT. RNA was isolated with Direct-zol RNA MiniPrep kit (R2052, Zymo Research, Irvine, California), and cDNA was generated with the iScript cDNA Synthesis Kit (1708890, Bio-Rad). Quantitative real-time polymerase chain reaction was performed using IQ SYBR Green Supermix (170-8886, Bio-Rad) in C1000 Touch Thermal Cycler CFX96 Real Time System (Bio-Rad), and data were analyzed with Bio-Rad CFX manager 3.1 software (Bio-Rad). Transcript quantities were compared using the relative Ct (cycle threshold) method, in which the amount of target was normalized to the amount of reference gene, β2 microglobulin, and calculated relative to the control group based on the $2^{-\Delta Ct}$ method. The primers for the genes of interest are listed in Supplemental Table 1.

STATISTICS. The results are presented as mean ± SD. Statistical analyses were performed using Prism software (GraphPad Software Inc., San Diego, California), and consisted of 1-way analysis of variance followed by Tukey's multiple comparison test when comparing >2 experimental groups, or unpaired Student's *t*-test when comparing 2 experimental groups. Differences were considered significant when $p < 0.05$.

RESULTS

CMECs IMPROVE CONTRACTION AND RELAXATION OF CMs. To investigate whether CMECs regulate CM function, we co-cultured both cell types for 2 h (Supplemental Figure 1) and subsequently measured the contraction and relaxation kinetics of individual CMs paced at 2 Hz (Figure 1). The presence of CMECs significantly enhanced CM contraction as shown by an increase in the fractional shortening or the proportion of sarcomere length shortening (Figures 2A and 2D). CMECs also improved CM relaxation as indicated by a higher relaxation velocity (Figures 2B and 2E) and a shorter time constant of relaxation (tau) (Figures 2C and 2F), in comparison to the non-co-incubated control CMs. These contractility improving effects were lost when CMECs were pre-exposed to the pro-inflammatory cytokine TNF-α for 6 h before the co-culture period (Figure 2). In these experiments, TNF-α was washed away and omitted during the 2 h co-culture period. The contractility-improving effect of CMECs was also lost when CMECs were pre-incubated with interleukin-1β (Supplemental Figure 2).

NO MEDIATES CMEC CONTROL OF CARDIOMYOCYTE FUNCTION. To investigate if EC-derived NO is involved in CMEC-mediated improvement of CM function, we inhibited NO synthases in CMECs with

FIGURE 5 Empa Restores CMEC-Mediated CM Function During TNF-α Exposure

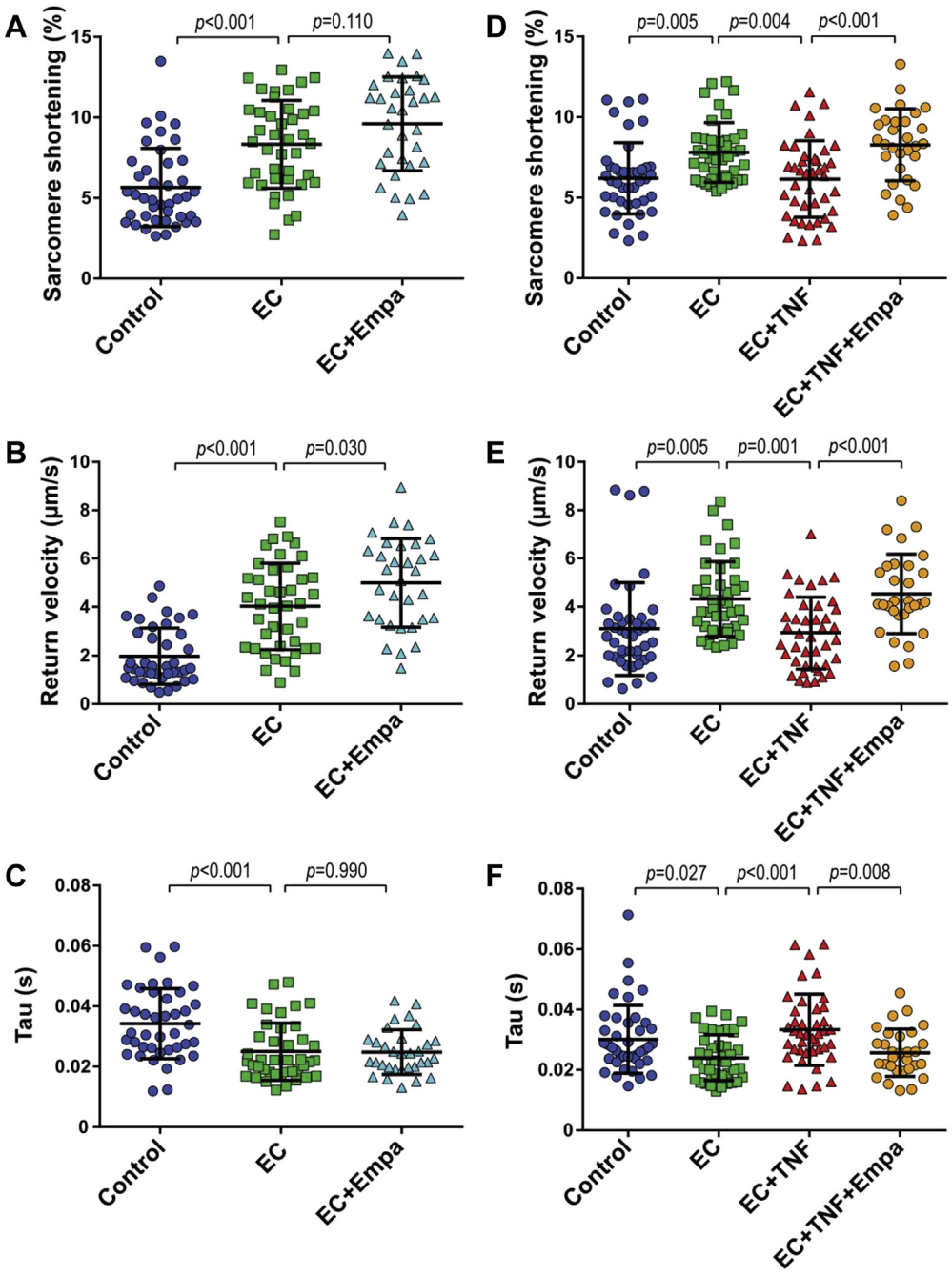

(A) Co-culture of CMEC with CMs increased CM shortening and **(B)** speed of relaxation, and **(C)** shortened tau. **(A)** Pre-treatment of CMECs with empagliflozin (EC+Empa) slightly increased CM contraction compared with CMEC alone (EC). **(B)** Empa pre-treatment increased CM return velocity but did not affect relaxation time, in comparison to CMEC alone. **(D to F)** Pre-incubation of CMEC with either TNF-α or a combination of TNF-α and Empa and subsequent co-culture of CMEC with CMs. **(D)** Co-treatment of TNF-α-stimulated CMEC with Empa prevented reduction of CM contraction in comparison to TNF-α stimulation alone. Co-treatment with Empa also maintained CMEC beneficial effect on **(E)** CM relaxation velocity and **(F)** tau. **(A to C)** Graphs representing single CMs isolated from 1 individual rat, distributed into the 3 corresponding experimental conditions; 30 to 40 CMs were measured per condition. Data are representative of 3 independent experiments. **(D to F)** Graphs representing single CMs isolated from 1 individual rat, distributed into the 4 corresponding experimental conditions; 30 to 40 CMs were measured per condition. Data are representative of 5 independent experiments; all data are represented as mean ± SD. Abbreviations as in Figures 1 to 3.

FIGURE 6 NO Mediates the Beneficial Effect of Empa on CMEC-CM Interaction

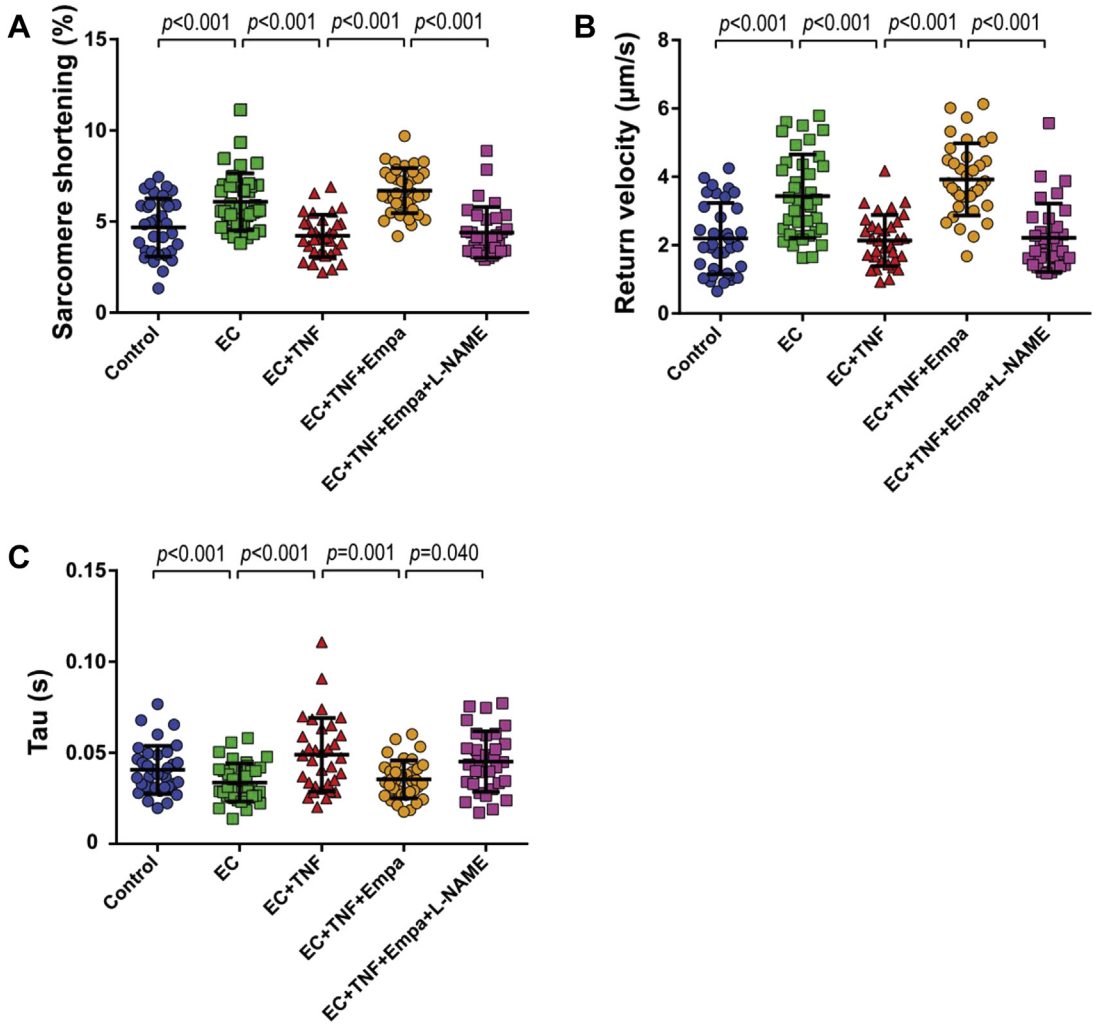

(A) Co-treatment with Empa maintained the beneficial effects of CMEC on CM contraction and **(B and C)** relaxation after TNF-α stimulation. **(A to C)** The beneficial effect of Empa was abolished when CMECs were co-treated with L-NAME. **(A to C)** Graphs representing single CMs isolated from 1 individual rat, distributed into the 4 corresponding experimental conditions; 40 to 45 CMs were measured per condition. Data are representative of 3 independent experiments; data are represented as mean ± SD. Abbreviations as in Figures 1 to 3 and 5.

L-NAME, a NO synthase inhibitor, for 1 h before and during 2 h of CMEC-CM co-culture. Inhibition of endothelial NO production completely abolished the beneficial effect of CMECs on CM contraction (**Figure 3A**, Supplemental Figure 3A) and relaxation parameters (**Figures 3B and 3C**, Supplemental Figures 3B and 3C). Direct incubation of CMs with L-NAME did not affect CM contraction and relaxation, which suggested no contribution of CM-derived NO.

Incubation of CMs with CMEC-conditioned medium also enhanced CM contractility performance, an effect that declined during the 2-h evaluation period (Supplemental Figures 3D to 3F). Furthermore, the stimulatory activity of the CMEC-conditioned medium was fully abolished by the NO scavenger carboxy-PTIO (Supplemental Figures 3G to 3I), which indicated that CMEC-derived NO was a major factor mediating the beneficial effect of CMECs on CM contraction and relaxation.

TNF-α REDUCES CMEC NO BIOAVAILABILITY. The level of NO in CMECs was assayed by live-cell microscopy using a copper-based NO probe. CMECs produced a detectable amount of NO at the basal level (**Figures 4A and 4B**), which increased by exposure to acetylcholine (**Figures 4A and 4B**). In contrast, exposure of CMECs to TNF-α largely reduced the NO

bioavailability to a level nearly similar to that in the presence of L-NAME (**Figures 4A and 4B**).

EMPAGLIFLOZIN RESTORES CMEC CONTROL OF CM FUNCTION DURING EXPOSURE TO TNF-α. We investigated whether empagliflozin could also modulate the effect of CMECs on CM function. CMECs were treated with empagliflozin at a physiological relevant concentration of 1 μM for a 6 h before the co-culture procedure. After several washing steps to ensure elimination of this drug from the CMEC compartment, the cells were co-incubated with CMs. Pre-treatment of CMECs with empagliflozin slightly, but not significantly, enhanced CM sarcomere shortening (**Figure 5A**, Supplemental Figure 4A) compared with the untreated CMEC group. Moreover, there was a small but significant increase in relaxation velocity in comparison to the effect of CMECs alone (**Figure 5B**, Supplemental Figure 4B), although tau did not reach a significant difference after empagliflozin pre-treatment (**Figure 5C**, Supplemental Figure 4C).

Subsequently, we examined whether empagliflozin could modulate the effect of TNF-α-treated CMECs on the contraction and relaxation performance of CMs. We pre-incubated CMECs with either TNF-α or a combination of TNF-α and empagliflozin, and co-incubated the cells with CMs afterward. The presence of empagliflozin during exposure to TNF-α preserved the ability of CMECs to improve CM contraction, which was lost when only TNF-α was added (**Figure 5D**, Supplemental Figure 4D). Moreover, co-treatment with empagliflozin also maintained the enhancing effects of CMECs on CM diastolic function as shown by a higher relaxation velocity and shorter tau (**Figures 5E and 5F**, Supplemental Figures 4E and 4F). In addition, empagliflozin restored the beneficial effect of CMECs on CM function, which was inhibited by pre-treatment of CMEC with interleukin-1β (Supplemental Figure 2). These findings indicated that empagliflozin not only acted in concert with endothelium to positively modulate CM function, but also maintained the CMEC-mediated regulation of CM contraction and relaxation that was lost when CMECs were exposed to pro-inflammatory cytokines (e.g., TNF-α and interleukin-1β). The beneficial effects of empagliflozin were abrogated when CMECs were co-treated with L-NAME (**Figures 6A to 6C**, Supplemental Figures 5A to 5C), which showed that endothelial-derived NO mediates the beneficial effect of empagliflozin on CM function.

EMPAGLIFLOZIN ATTENUATES TNF-α INDUCED LOSS OF NO AVAILABILITY IN CMECs. Empagliflozin has been reported to directly affect CMs (27). We also observed that 1 μM empagliflozin treatment of CMs enhanced CM function (Supplemental Figures 6A and 6D) and relaxation (Supplemental Figures 6B, 6C, 6E, and 6F), which indicated that empagliflozin could directly act on CMs and regulate their contractile profile. However, this direct effect did not explain the results of the co-culture experiments because empagliflozin was only present in the CMEC compartment during the 6 h pre-treatment period and was removed before the onset of co-culture with CMs.

To underscore the effect of empagliflozin on NO production in CMECs, we determined the cellular NO concentration in CMECs. Live-cell microscopy evaluation showed that NO levels in CMECs were reduced by exposure of the cells to TNF-α but was maintained when the cells were incubated with TNF-α and empagliflozin simultaneously (**Figures 7A and 7B**).

EMPAGLIFLOZIN DOES NOT ACT VIA THE NUCLEAR FACTOR–kB PATHWAY AND eNOS DIMERIZATION OR PHOSPHORYLATION. Several pathways have been shown to be activated by TNF-α, in particular, the nuclear factor-κB (NK-κB) pathway, p38 mitogen-activated protein kinase (MAPK), JNK pathways, and ROS generation (31,32), which might be attenuated by empagliflozin. A possible role of the NF-κB pathway as a target for the beneficial effect of empagliflozin on CMECs treated with TNF-α was refuted because empagliflozin did not change the transcription (Supplemental Figures 7A and 7B) nor the protein expression (**Figures 7C and 7D**) of vascular cell adhesion molecule (VCAM)-1 and E-selectin, 2 genes that are commonly induced by TNF-α via NF-κB pathway activation. Similarly, superoxide dismutase 2 (SOD2) mRNA expression, which was strongly enhanced by TNF-α in ECs in an NF-kB dependent manner (33), was not affected by empagliflozin (Supplemental Figure 7C).

Empagliflozin did not change the transcription of eNOS (NOS3), which was attenuated by TNF-α (Supplemental Figure 7D). The eNOS protein in CMECs was mainly encountered as a dimer, which remained stabile after 6 h TNF-α exposure, whereas the small amount of eNOS monomer decreased (Supplemental Figure 8A). Empagliflozin neither affected the amount of eNOS dimer nor altered the eNOS monomer content in control or TNF-α-exposed CMECs (Supplemental Figure 8A). Furthermore, after the 6 h incubation period, empagliflozin did not change the total eNOS protein content or the phosphorylation of eNOS at position Ser1177 in control or TNF-α-treated CMECs (Supplemental Figure 8B).

EMPAGLIFLOZIN RESTORES CMEC NO BIOAVAILABILITY BY ATTENUATION OF MITOCHONDRIAL ROS LEVEL. Subsequently, we evaluated if empagliflozin could preserve NO levels in CMECs by attenuating

FIGURE 7 Empagliflozin Reduced Mitochondrial and Cytoplasmic ROS Level and Restores NO Bioavailability in CMECs After TNF-α Stimulation

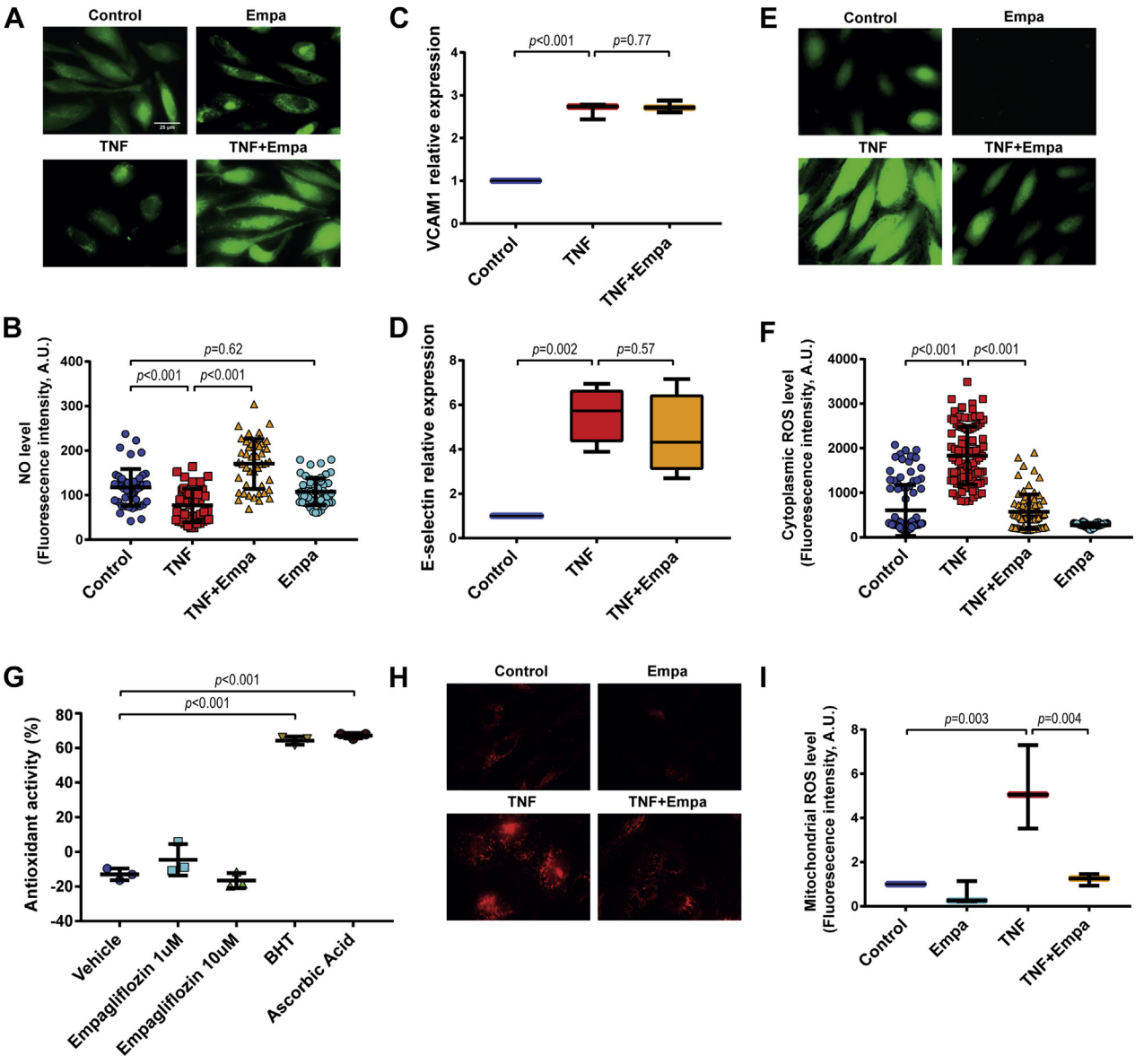

(A and B) TNF-α treatment reduced CMEC NO levels. Co-treatment of CMEC with TNF-α and Empa resulted in higher CMEC NO bioavailability in comparison to TNF-α treatment alone (n = 40 to 50, refers to number of cells per group from 3 independent experiments; data represented as mean ± SD). **(C and D)** TNF-α stimulation led to increased VCAM and E-selectin expression on the cell surface of CMECs, as assayed by a cell-bound enzyme linked immunosorbent assay, and co-treatment with Empa did not change the level of both proteins (n = 4, refers to number of independent experiments; data represented as mean ± SD). **(E and F)** TNF-α treatment increased cytoplasmic reactive oxygen species (ROS) levels in CMECs, which were attenuated by simultaneous treatment of Empa (n = 40 to 50, refers to number of cells per group from 3 independent experiments; data represented as mean ± SD). **(G)** Empa did not possess direct antioxidant activity at 1 and 10 μM concentrations, whereas 2 potent antioxidants, butylated hydroxytoluene (BHT) and ascorbic acid, showed a strong radical scavenging effect (n = 3, refers to number of independent experiments; data represented as mean ± SD). **(H and I)** Empa reduced mitochondrial ROS production after TNF-α stimulation in CMECs (n = 3, refers to number of independent experiments; data represented as mean ± SD). VCAM = vascular cell adhesion molecule; other abbreviations as in Figures 1 to 3 and 5.

TNF-α-induced ROS production. As detected by fluorescent dye-based free radical sensors, TNF-α increased cytoplasmic ROS accumulation in CMECs (Figures 7E and 7F). Because ROS, in particular, as a superoxide, can scavenge NO, we first verified if antioxidants that scavenge ROS could increase the bioavailability of NO in CMECs. Administration of the general antioxidant butylated hydroxytoluene

rescued NO bioavailability, which was diminished by exposure to TNF-α (Supplemental Figure 8C). The induction of ROS production by TNF-α was fully blunted by co-treatment with empagliflozin (**Figures 7E and 7F**). We then examined whether the reduction of ROS with empagliflozin co-treatment was due to a direct antioxidant or radical scavenging capacity of empagliflozin. Using DPPH as a free radical, we observed that empagliflozin at 1 and 10 μM concentration showed no direct antioxidant capability, whereas the antioxidants butylated hydroxytoluene and ascorbic acid displayed a strong direct radical scavenging effect (**Figure 7G**).

TNF-α–induced ROS generation is complex and involves various pathways, resulting in ROS generation, as well as modulation of ROS scavenging enzymes. TNF-α can induce ROS production via NOX4 (31,34). However, we observed no effects of empagliflozin on NADPH oxidase 4 (NOX4) expression (Supplemental Figure 7E). In addition, empagliflozin did not alter the mRNA expression of the radical scavenging enzymes SOD1 and SOD2 after TNF-α stimulation (Supplemental Figures 7C and 7F). NOX1, NOX2, NOX3, NOX5, and SOD3 mRNA in CMECs remained below detection level in these conditions (data not shown).

Mitochondria are a major source of ROS (31). JNK activation is enhanced by TNF-α and can contribute to mitochondrial ROS production (31). However, the TNF-α-induced JNK phosphorylation was not altered by empagliflozin (Supplemental Figure 8D). However, we observed that TNF-α induced mitochondrial ROS generation in CMECs (**Figures 7H and 7I**), and remarkably, empagliflozin significantly reduced the mitochondrial ROS production that was enhanced by TNF-α exposure (**Figures 7H and 7I**). Overall, because empagliflozin showed no direct antioxidant capacity, these data suggested that, in the presence of TNF-α stimulation, empagliflozin could activate intracellular mechanisms that cause a reduction in mitochondrial ROS generation. This resulted in an inhibition of cytoplasmic ROS accumulation, which led to an enhancement of CMEC NO bioavailability.

DISCUSSION

In a co-culture model of CMECs and CMs, we showed that CMECs exerted a direct positive effect on CM contraction and relaxation. These effects were mediated by endothelial-derived NO and lost after pre-exposure of CMECs to TNF-α, predominantly due to NO scavenging by the generation of cytoplasmic and mitochondrial ROS. Moreover, we demonstrated that empagliflozin counteracted the TNF-α-mediated impairment of CMEC-CM interaction. It reduced the mitochondrial ROS level, prevented accumulation of cytoplasmic ROS, and enhanced the bioavailability of NO, both within the CMECs and in its conditioned medium, which resulted in the preservation of both contraction and relaxation of CMs. The latter implied a novel mechanism by which empagliflozin could restore CMEC function in various types of HF with disturbed microvascular function, including HFpEF.

INVOLVEMENT OF ENDOTHELIAL-DERIVED NO IN CMEC REGULATION OF CM CONTRACTION AND RELAXATION. In the present study, we provided evidence that CMECs directly regulated contraction and relaxation of CMs and that intact cardiac EC function was vital to the regulation of CM function. On the basis of dedicated studies on the role of endocardial endothelium in controlling CM contractility, Brutsaert et al. (23,35) postulated that intracardiac microvascular endothelial cells would exert a similar effect. In these studies, myocardial contractility was assessed in a papillary muscle from a rabbit right ventricle, with and without damage of endocardial endothelial cells by perfusion with Triton X-100. Subsequent animal intervention studies confirmed the existence of beneficial effects of tissue NO on cardiac contractility, likely derived from ECs (36). Our study added further evidence by using an in vitro co-culture system, which provided a simple and straightforward approach to study direct effects of human CMECs on both the contraction and relaxation performance of CMs. Our observation that L-NAME administration on CMs did not change their basal contractility was in line with other studies (37,38). It suggests that in isolated CMs, endogenous NO played only a minor role in regulating CM contractile performance and implied that CMEC-derived NO was the more predominant contributor to myocardial contraction and relaxation. How NO exactly modulates CMs warrants further research. Because of the distance between the CMEC and CM compartment in the co-culture setup and the sustained effect of CMEC-derived NO, which spans a 20 min to 30 min interval and is inhibited by carboxy-PTIO, it can be anticipated that NO stabilizes during its transfer from CMECs or that its effect is maintained after reaching the CMs. Further studies are needed to clarify whether stabilization of CMEC-derived NO is due to interaction of NO with sulfhydryl (SH) groups or by protection of NO within vesicles and/or vesicular membranes.

LOSS OF CMEC-MEDIATED REGULATION OF CM FUNCTION AFTER TNF-α STIMULATION IS MEDIATED BY REDUCED CMEC NO BIOAVAILABILITY. The beneficial effect of CMECs on CM contraction and relaxation was

lost after pre-exposure of CMECs to TNF-α or interleukin-1β. This is of interest for the pathogenesis of HF because Paulus and Tschöpe (7) and others (14,16) proposed that inflammatory activation of CMECs might be a pivotal initial mechanism in changing the cardiac mechanical properties in HFpEF. Using an NO copper-based probe with high sensitivity for detecting NO at minute levels (39,40), we confirmed that exposure of CMECs to TNF-α abolished the NO availability in these cells. Most importantly, NO availability in TNF-α-treated CMECs was restored by empagliflozin.

TNF-α causes a reduction in NO bioavailability by 2 major mechanisms: reduction of eNOS mRNA stability and induction of superoxide generation. First, TNF-α reduces eNOS (NOS3) mRNA transcriptionally and post-transcriptionally in ECs (41,42). Although the transcriptional regulation is dependent on NF-κB, the post-transcriptional regulation proceeds via binding of 52- and 57-kD protein(s) (eEF1A1 and PTB1) to the 3′-untranslated region of NOS3 mRNA, which enhances its degradation (41-43). However, empagliflozin did not reverse the drop in NOS3 mRNA. Moreover, empagliflozin did not affect the eNOS total protein level and phosphorylation at serine 1177, and it did not alter the dimerization status of eNOS after TNF-α stimulation in CMECs. In addition, empagliflozin did not change the induction of VCAM or E-selectin or the affected SOD2 mRNA that was upregulated by TNF-α, which further excluded a role of NF-kB in the protective effect of empagliflozin.

Second, TNF-α reduces NO by its ability to enhance ROS generation (44,45), potentially either via an immediate activation of NOX with riboflavin kinase as a connector between the TNF receptor and the p22phox subunit (34), or via impairment of the mitochondrial respiratory chain, which can be achieved via several pathways, including JNK activation (31,34). Excessive ROS production exerts a deleterious effect on the cells. Superoxide can rapidly react with NO forming peroxynitrite, whereas its conversion to hydrogen peroxide allows generation of highly reactive hydroxyl radicals, which together can cause toxic oxidation of proteins, lipids, and DNA (46,47). In addition, superoxide can eventually cause eNOS uncoupling, which results in loss of NO production and additional superoxide formation (48,49). Although empagliflozin completely inhibited the TNF-α–induced production of cytoplasmic and mitochondrial ROS in CMECs, we could not establish a direct ROS scavenging effect of empagliflozin even at a 10-fold higher concentration than used in our experiments. This was in contrast to the observation in a study that used only 1 supra-pharmacological dose of approximately 2 mM of empagliflozin (50). Although several studies, including ours (data not shown), could not demonstrate SGLT2 mRNAs in the whole heart tissue or CMECs (51,52), recent studies reported on the presence of small amounts of SGLT2 protein in ECs (53,54). Nevertheless, the mode of action of empagliflozin seems complex and its effect on ECs and their ROS production needs further elucidation. If the effect of empagliflozin on endothelial NO production is also found in arterial and other types of endothelial cells, the impact of these findings may extend to vessels and tissues beyond the heart (54–56).

EMPAGLIFLOZIN IMPROVES CMEC REGULATION OF CM CONTRACTION AND RELAXATION. After finding reduced HF hospitalization and mortality in patients with diabetes who were treated with the SGLT2 inhibitor empagliflozin (25), recent studies showed a direct effect of empagliflozin on the heart, despite the absence of detectable SGLT2 in the heart (57,58). Baartscheer et al. (27) reported that empagliflozin treatment reduced CM cytoplasmic sodium and Ca^{2+} and increased mitochondrial Ca^{2+} levels by inhibiting the sodium/hydrogen exchanger. It is interesting to note that the sodium/hydrogen exchanger-1 inhibitors decrease myocardial superoxide production via direct mitochondrial action (59). Whether empagliflozin can affect the sodium/hydrogen exchanger in CMECs needs further investigation and is beyond the scope of our present study. Byrne et al. (60) also reported that empagliflozin prevented further loss of cardiac function in mice with pressure-overload–induced HF. Pabel et al. (28) demonstrated beneficial diastolic effects of empagliflozin in contracting human heart trabeculae, which was accompanied by phosphorylation of titin without changing the Ca^{2+} influx pattern. Our data provided further proof of a direct effect of empagliflozin on CM contraction and relaxation. Furthermore, our study demonstrated, for the first time, that empagliflozin could act directly on CMECs and thus enhanced the beneficial effect of CMECs on CM function and, most importantly, could preserve CMEC-mediated enhancement of CM contraction and relaxation during pro-inflammatory stimulation.

The beneficial effect of empagliflozin on HF hospitalization was observed in metabolically compromised patients with DM, who are at risk for developing HFpEF (25). HFpEF is characterized by a disturbance in LV diastolic function. However, strain imaging modality also detects impaired systolic function in patients with HFpEF (61). Our data show that CMECs enhanced both CM contraction and relaxation, an effect that was vastly mediated by CMEC-derived NO. NO increases cGMP levels, which can induce a concentration-dependent biphasic contractile response (62). Although at a low

concentration cGMP triggers a positive inotropic effect, at a higher concentration it leads to a negative inotropic effect (62). Detachment of CMs from their in vivo environment, which we applied in our co-culture setup, may lead to relatively low cGMP level in the CMs. At a higher, more physiological CM cGMP concentration, CMECs may show a more predominant beneficial effect on the diastolic function of CMs.

STUDY LIMITATIONS. Our study shows a beneficial effect of empagliflozin on disturbed endothelial NO delivery to CMs and subsequent improvement of CM contraction and relaxation. Our functional CM measurements were performed in unloaded CMs, which does not reflect the loaded CM as present in the heart. These measurements enable to study diastolic functional parameters such as re-lengthening or relaxation velocity and time constant of relaxation tau. Another limitation regards our co-culture model that combines human CMECs and adult rat CMs. Although this allows the recognition of NO as a major player in mediating the effect of CMEC on CM, it may overlook additional effects of species-specific acting mediators. Future studies using human CMs will clarify this aspect. Finally, most of our studies were performed with TNF-α as an inflammatory mediator and within a limited time period of 6 h. These studies have to be extended with other factors that contribute to heart failure and evaluation of the mutual CMEC-CM interaction over prolonged time periods. Notwithstanding these limitations, the observed mechanism fits with clinical trials on empagliflozin and heart failure.

CONCLUSIONS

Our findings showed that CMECs conferred a direct positive effect on CM contraction and relaxation and that impairment of EC function with the pro-inflammatory cytokine TNF-α abolished this beneficial effect. Moreover, we provided the first evidence of a direct effect of empagliflozin on CMECs and on CMEC-enhanced CM function. Our findings on the effect of empagliflozin on EC-mediated preservation of CM contraction and relaxation suggested that empagliflozin would be especially beneficial for treatment of the cardiac mechanical implications of deranged microvascular function in HF.

ACKNOWLEDGMENTS The authors acknowledge the support for CVON-RECONNECT from the Netherlands CardioVascular Research Initiative, including the Dutch Heart Foundation, Dutch Federation of University Medical Centers, the Netherlands Organization for Health Research and Development, and the Royal Netherlands Academy of Science. The authors also acknowledge Jeroen Kole, BSc, and Michiel van Wijhe, BSc, for the provided technical support and Etto Eringa, PhD, for his critical reading of the manuscript.

ADDRESS FOR CORRESPONDENCE: Dr. Victor W.M. van Hinsbergh, Amsterdam Cardiovascular Sciences, Amsterdam University Medical Centers, Department of Physiology, O|2 Research Building, Room 11W53, De Boelelaan 1117, 1081 HV Amsterdam, the Netherlands. E-mail: v.vanhinsbergh@amsterdamumc.nl.

PERSPECTIVES

COMPETENCY IN MEDICAL KNOWLEDGE: HF is an important and growing clinical problem. HFpEF currently accounts for 50% of patients with HF and is expected to become more prevalent than HFrEF in the future. Unlike HFrEF, there is lack of effective treatments for HFpEF. Therapies that are used in HFrEF failed to improve primary outcomes in patients with HFpEF, suggesting different patho-mechanisms of these diseases. The current paradigm of HFpEF proposes that a metabolic risk-related pro-inflammatory state in these patients induces cardiac microvascular dysfunction with subsequent CM contractility impairment. We showed that CMECs positively regulated CM contraction and relaxation. This effect requires NO, is diminished after stimulation of CMECs with pro-inflammatory cytokines, and is restored by empagliflozin by preventing accumulation of ROS, leading to restoration of endothelial NO bioavailability. This suggests that empagliflozin can be beneficial for treatment of the cardiac mechanical implications of microvascular dysfunction in HF, and potentially in HFpEF.

TRANSLATIONAL OUTLOOK: For the clinical translation, our findings should be first evaluated in vivo in an experimental HF model, in particular, an HFpEF model. ZSF1 rats is one of the HFpEF models that have been shown to recapitulate cardiac microvascular and diastolic dysfunction in patients with HFpEF. Further evaluation in larger HFpEF experimental models, such as the swine model of microvascular dysfunction, may be warranted to test the effect of empagliflozin on improving endothelial dysfunction and the subsequent effect on diastolic function. For other types of HF, these findings should be evaluated in their corresponding models. Nevertheless, the notion of empagliflozin as a potential treatment of HF is currently under investigation in a large clinical trial of EMPEROR-Preserved and EMPEROR-Reduced. The outcome of this trial may show whether empagliflozin can be repurposed from being merely a glucose-lowering drug to an effective therapy for HF and possibly HFpEF.

REFERENCES

1. Dunlay SM, Roger VL, Redfield MM. Epidemiology of heart failure with preserved ejection fraction. Nat Rev Cardiol 2017;65:1–12.

2. Carson PE, Anand IS, Win S, et al. The hospitalization burden and post-hospitalization mortality risk in heart failure with preserved ejection fraction: results from the I-PRESERVE Trial (Irbesartan in Heart Failure and Preserved Ejection Fraction). J Am Coll Cardiol HF 2015;3:429–41.

3. Pitt B, Pfeffer MA, Assmann SF, et al. Spironolactone for heart failure with preserved ejection fraction. N Engl J Med 2014;370:1383–92.

4. Ahmed A, Rich MW, Fleg JL, et al. Effects of digoxin on morbidity and mortality in diastolic heart failure: the Ancillary Digitalis Investigation Group trial. Circulation 2006;114:397–403.

5. Redfield MM, Chen HH, Borlaug BA, et al. Effect of phosphodiesterase-5 inhibition on exercise capacity and clinical status in heart failure with preserved ejection fraction: a randomized clinical trial. JAMA 2013;309:1268–77.

6. Yancy CW, Jessup M, Bozkurt B, et al. 2013 ACCF/AHA guideline for the management of heart failure: a report of the American College of Cardiology Foundation/American Heart Association Task Force on practice guidelines. J Am Coll Cardiol 2013;62:e147–239.

7. Paulus WJ, Tschope C. A novel paradigm for heart failure with preserved ejection fraction: comorbidities drive myocardial dysfunction and remodeling through coronary microvascular endothelial inflammation. J Am Coll Cardiol 2013;62:263–71.

8. Sharma K, Hill T, Grams M, et al. Outcomes and worsening renal function in patients hospitalized with heart failure with preserved ejection fraction. Am J Cardiol 2015;116:1534–40.

9. Ather S, Chan W, Bozkurt B, et al. Impact of noncardiac comorbidities on morbidity and mortality in a predominantly male population with heart failure and preserved versus reduced ejection fraction. J Am Coll Cardiol 2012;59:998–1005.

10. Seferovic PM, Paulus WJ. Clinical diabetic cardiomyopathy: a two-faced disease with restrictive and dilated phenotypes. Eur Heart J 2015;36:1718–27. 1727a–c.

11. Franssen C, Chen S, Unger A, et al. Myocardial microvascular inflammatory endothelial activation in heart failure with preserved ejection fraction. J Am Coll Cardiol HF 2016;4:312–24.

12. Gevaert AB, Shakeri H, Leloup AJ, et al. Endothelial senescence contributes to heart failure with preserved ejection fraction in an aging mouse model. Circ Heart Fail 2017;10:1–10.

13. Westermann D, Lindner D, Kasner M, et al. Cardiac inflammation contributes to changes in the extracellular matrix in patients with heart failure and normal ejection fraction. Circ Heart Fail 2011;4:44–52.

14. Mohammed SF, Hussain S, Mirzoyev SA, Edwards WD, Maleszewski JJ, Redfield MM. Coronary microvascular rarefaction and myocardial fibrosis in heart failure with preserved ejection fraction. Circulation 2015;131:550–9.

15. Saiki H, Moulay G, Guenzel AJ, et al. Experimental cardiac radiation exposure induces ventricular diastolic dysfunction with preserved ejection fraction. Am J Physiol Heart Circ Physiol 2017;313:H392–407.

16. Saiki H, Petersen IA, Scott CG, et al. Risk of heart failure with preserved ejection fraction in older women after contemporary radiotherapy for breast cancer. Circulation 2017;135:1388–96.

17. Wang Y, Boerma M, Zhou D. Ionizing radiation-induced endothelial cell senescence and cardiovascular diseases. Radiat Res 2016;186:153–61.

18. Lee C, Moding E, Cuneo K, et al. p53 functions in endothelial cells to prevent radiation-induced myocardial injury in mice. Science Signalling 2012;5:1–14.

19. Lauk S, Kiszel Z, Buschmann J, Diger Trott K. Radiation induced heart disease in rats. Int J Radiation Oncology Biol Phys 1985;11:801–8.

20. Fajardo L, Stewart J. Experimental radiation-induced heart disease. Am J Pathol 1970;59:299–316.

21. Fajardo L, Stewart J. Capillary injury preceding radiation-induced myocardial fibrosis. Radiology 1971;101:429–33.

22. Li K, Rouleau J, Andries L, Brutsaert D. Effect of dysfunctional vascular endothelium on myocardial performance in isolated papillary muscles. Circ Res 1993:768–77.

23. Brutsaert D. Cardiac Endothelial-myocardial signaling: its role in cardiac growth, contractile performance, and rhythmicity. Physiol Rev 2003:59–115.

24. Shah SJ, Lam CSP, Svedlund S, et al. Prevalence and correlates of coronary microvascular dysfunction in heart failure with preserved ejection fraction: PROMIS-HFpEF. Eur Heart J 2018;39:3439–50.

25. Fitchett D, Zinman B, Wanner C, et al. Heart failure outcomes with empagliflozin in patients with type 2 diabetes at high cardiovascular risk: results of the EMPA-REG OUTCOME(R) trial. Eur Heart J 2016;37:1526–34.

26. U.S. National Library of Medicine CG. Empagliflozin Outcome Trial in Patients With Chronic Heart Failure With Preserved Ejection Fraction (EMPEROR-Preserved). Available at: https://clinicaltrials.gov/ct2/show/NCT03057977. Accessed February 17, 2017.

27. Baartscheer A, Schumacher CA, Wust RC, et al. Empagliflozin decreases myocardial cytoplasmic Na+ through inhibition of the cardiac Na+/H+ exchanger in rats and rabbits. Diabetologia 2017;60:568–73.

28. Pabel S, Wagner S, Bollenberg H, et al. Empagliflozin directly improves diastolic function in human heart failure. Eur J Heart Fail 2018;20:1690–700.

29. Kaestner L, Scholz A, Hammer K, Vecerdea A, Ruppenthal S, Lipp P. Isolation and genetic manipulation of adult cardiac myocytes for confocal imaging. J Vis Exp 2009;31:1–5.

30. van Deel ED, Najafi A, Fontoura D, et al. In vitro model to study the effects of matrix stiffening on Ca(2+) handling and myofilament function in isolated adult rat cardiomyocytes. J Physiol 2017;595:4597–610.

31. Blaser H, Dostert C, Mak TW, Brenner D. TNF and ROS crosstalk in inflammation. Trends Cell Biol 2016;26:249–61.

32. Zhou H, Wang S, Zhu P, Hu S, Chen Y, Ren J. Empagliflozin rescues diabetic myocardial microvascular injury via AMPK-mediated inhibition of mitochondrial fission. Redox Biol 2018;15:335–46.

33. Visner GA, Chesrown SE, Monnier J, Ryan US, Nick HS. Regulation of manganese superoxide dismutase: IL-l and TNF induction in pulmonary artery and microvascular endothelial cells. Biochem Biophys Res Commun 1992;188:453–62.

34. Yazdanpanah B, Wiegmann K, Tchikov V, et al. Riboflavin kinase couples TNF receptor 1 to NADPH oxidase. Nature 2009;460:1159–63.

35. Brutsaert D, Meulemans A, Sipido K, Stanilas U. Effects of damaging the endocardial surface on the mechanical performance of isolated cardiac muscle. Circ Res 1988:358–66.

36. Sorop O, Heinonen I, van Kranenburg M, et al. Multiple common comorbidities produce left ventricular diastolic dysfunction associated with coronary microvascular dysfunction, oxidative stress, and myocardial stiffening. Cardiovasc Res 2018;114:954–64.

37. Jin CL, Wu YN, Jang JH, et al. Negligible effect of eNOS palmitoylation on fatty acid regulation of contraction in ventricular myocytes from healthy and hypertensive rats. Pflugers Arch 2017:1141–9.

38. Smith JM, Sondgeroth KB, Wahler GM. Inhibition of nitric oxide synthase enhances contractile response of ventricular myocytes from streptozotocin-diabetic rats. Mol Cell Biochem 2007;300:129–37.

39. Lim MH, Xu D, Lippard SJ. Visualization of nitric oxide in living cells by a copper-based fluorescent probe. Nat Chem Biol 2006;2:375–80.

40. Ghosh M, van den Akker NM, Wijnands KA, et al. Specific visualization of nitric oxide in the vasculature with two-photon microscopy using a copper based fluorescent probe. PLoS One 2013;8:1–14.

41. Anderson HD, Rahmutula D, Gardner DG. Tumor necrosis factor-alpha inhibits endothelial nitric-oxide synthase gene promoter activity in bovine aortic endothelial cells. J Biol Chem 2004;279:963–9.

42. Yan G, You B, Chen SP, Liao JK, Sun J. Tumor necrosis factor-alpha downregulates endothelial nitric oxide synthase mRNA stability via translation elongation factor 1-alpha 1. Circ Res 2008;103:591–7.

43. Yi B, Ozerova M, Zhang GX, Yan G, Huang S, Sun J. Post-transcriptional regulation of endothelial nitric oxide synthase expression by polypyrimidine tract-binding protein 1. Arterioscler Thromb Vasc Biol 2015;35:2153–60.

44. van Buul J, Fernandez-Borja M, Anthony E, Hordijk P. Expression and localization of NOX2 and

NOX4 in primary human endothelial cells. Antioxidant Redox Signaling 2005;7:308–17.

45. Bedard K, Krause KH. The NOX family of ROS-generating NADPH oxidases: physiology and pathophysiology. Physiol Rev 2007;87:245–313.

46. Zhang H, Park Y, Wu J, et al. Role of TNF-alpha in vascular dysfunction. Clin Sci (Lond) 2009;116:219–30.

47. Zhao Y, Vanhoutte PM, Leung SW. Vascular nitric oxide: beyond eNOS. J Pharmacol Sci 2015;129:83–94.

48. Antoniades C, Shirodaria C, Leeson P, et al. Association of plasma asymmetrical dimethylarginine (ADMA) with elevated vascular superoxide production and endothelial nitric oxide synthase uncoupling: implications for endothelial function in human atherosclerosis. Eur Heart J 2009;30:1142–50.

49. Bendall JK, Alp NJ, Warrick N, et al. Stoichiometric relationships between endothelial tetrahydrobiopterin, endothelial NO synthase (eNOS) activity, and eNOS coupling in vivo: insights from transgenic mice with endothelial-targeted GTP cyclohydrolase 1 and eNOS overexpression. Circ Res 2005;97:864–71.

50. Dhuja DMS, Hiah DNSM, Swari DRR. Comparative efficacy of canagliflozin versus empagliflozin on oxidative stress - in-vitro method. Int J Pharma Bio Sci 2017;8:232–6.

51. Chen J, Williams S, Ho S, et al. Quantitative PCR tissue expression profiling of the human SGLT2 gene and related family members. Diabetes Ther 2010;1:57–92.

52. Van Steenbergen A, Balteau M, Ginion A, et al. Sodium-myoinositol cotransporter-1, SMIT1, mediates the production of reactive oxygen species induced by hyperglycemia in the heart. Sci Rep 2017;7:41166.

53. Mancini SJ, Boyd D, Katwan OJ, et al. Canagliflozin inhibits interleukin-1beta-stimulated cytokine and chemokine secretion in vascular endothelial cells by AMP-activated protein kinase-dependent and -independent mechanisms. Sci Rep 2018;8:5276.

54. El-Daly M, Pulakazhi Venu VK, Saifeddine M, et al. Hyperglycaemic impairment of PAR2-mediated vasodilation: prevention by inhibition of aortic endothelial sodium-glucose-co-transporter-2 and minimizing oxidative stress. Vascul Pharmacol 2018;109:56–71.

55. Uthman L, Baartscheer A, Bleijlevens B, et al. Class effects of SGLT2 inhibitors in mouse cardiomyocytes and hearts: inhibition of Na(+)/H(+) exchanger, lowering of cytosolic Na(+) and vasodilation. Diabetologia 2018;61:722–6.

56. Scognamiglio R, Negut C, De Kreutzenberg SV, Tiengo A, Avogaro A. Postprandial myocardial perfusion in healthy subjects and in type 2 diabetic patients. Circulation 2005;112:179–84.

57. Vrhovac I, Eror D, Klessen D, et al. Localizations of Na+-D-glucose cotransporters SGLT1 and SGLT2 in human kidney and of SGLT1 in human small intestine, liver, lung, and heart. Pflugers Arch Eur J Physiol 2015:1881–98.

58. Van Steenbergen A, Balteau M, Scholasse J. Identification of a glucose sensor in the heart (abstr.). Eur Heart J 2015:381.

59. Garciarena CD, Caldiz CI, Correa MV, et al. Na+/H+ exchanger-1 inhibitors decrease myocardial superoxide production via direct mitochondrial action. J Appl Physiol (1985) 2008;105:1706–13.

60. Byrne NJ, Parajuli N, Levasseur JL, et al. Empagliflozin prevents worsening of cardiac function in an experimental model of pressure overload-induced heart failure. J Am Coll Cardiol Basic Trans Science 2017;2:347–54.

61. Kraigher-Krainer E, Shah AM, Gupta DK, et al. Impaired systolic function by strain imaging in heart failure with preserved ejection fraction. J Am Coll Cardiol 2014;63:447–56.

62. Mohan P, Brutsaert DL, Paulus WJ, Sys SU. Myocardial contractile response to nitric oxide and cGMP. Circulation 1996;93:1223–9.

KEY WORDS contraction and relaxation, endothelial cell-derived nitric oxide, empagliflozin, heart failure, oxidative stress

APPENDIX For an expanded Methods section and supplemental figures, please see the online version of this paper.

JACC: BASIC TO TRANSLATIONAL SCIENCE
PUBLISHED BY ELSEVIER ON BEHALF OF THE AMERICAN COLLEGE OF CARDIOLOGY FOUNDATION.

VOL. 4, NO. 5, 2019

EDITORIAL COMMENT

Empagliflozin and Protecting Microvascular Support of Heart Mechanics

SGLT2 Inhibition or More?*

Chris Sorel Mantsounga, PhD,[a,b] Alan R. Morrison, MD, PhD[a,b]

Approximately 6.5 million adults in the United States have heart failure (HF), representing a major cause of morbidity and mortality (1). HF is traditionally divided into 2 subtypes, HF with preserved ejection (HFpEF) and HF with reduced ejection fraction (HFrEF), with each accounting for about 50% of HF cases. Although HFpEF and HFrEF can display similar clinical presentations during acute HF exacerbations, they are often associated with different risk factors, pathophysiological processes, and responses to therapy (2). Many therapies with unequivocal benefit in HFrEF have failed to show efficacy for HFpEF. This is, in part, why the recent findings of EMPA-REG OUTCOME (Empagliflozin, Cardiovascular Outcomes, and Mortality in Type 2 Diabetes) have generated tremendous enthusiasm. EMPA-REG OUTCOME was a randomized, double-blind, placebo-controlled trial of 7,020 patients with type 2 diabetes mellitus, and it demonstrated that the primary endpoint, a composite of myocardial infarction, stroke, and cardiovascular death, was significantly reduced (hazard ratio [HR]: 0.86; 95% confidence interval [CI]: 0.74 to 0.99) over a median follow-up of 3.1 years (3). The composite outcome was largely driven by a 38% relative risk reduction of cardiovascular death (HR: 0.62; 95% CI: 0.49 to 0.77) and a 32% relative risk reduction in all-cause mortality (HR: 0.68; 95% CI: 0.57 to 0.82). Of interest, there was a 35% relative risk reduction in hospitalization for HF (HR: 0.65; 95% CI: 0.50 to 0.85), supporting favorable hemodynamic effects of the drug. Further analysis revealed that the reduction of hospitalizations for HF and cardiovascular death were observed both in patients with and without HF at baseline (4). HF was not phenotyped at baseline, but 2 ongoing clinical trials, EMPEROR-Preserved (EMPagliflozin outcomE tRial in Patients With chrOnic heaRt Failure With Preserved Ejection Fraction) and EMPEROR-Reduced (EMPagliflozin outcomE tRial in Patients With chrOnic heaRt Failure With Reduced Ejection Fraction), are actively enrolling patients to study the effect of empagliflozin versus placebo on top of guideline-directed medical therapy in patients with each subset of HF (5,6).

Empagliflozin is one of a family of inhibitors that target the sodium (Na^+)-glucose cotransporter-2 (SGLT2). SGLTs are transmembrane proteins that facilitate entry of glucose into cells by making use of the Na^+ gradient maintained by sodium-potassium adenosine triphosphatase (7). SGLT2 inhibitors were developed as a therapeutic treatment for diabetes because of their inhibition of glucose reabsorption in the proximal tubules of the kidneys, increasing glucose excretion. In EMPA-REG OUTCOME, the adjusted mean reduction in glycated hemoglobin

*Editorials published in *JACC: Basic to Translational Science* reflect the views of the authors and do not necessarily represent the views of *JACC: Basic to Translational Science* or the American College of Cardiology.

From the [a]Providence VA Medical Center, Providence, Rhode Island; and the [b]Section of Cardiovascular Medicine, Department of Internal Medicine, Alpert Medical School at Brown University, Providence, Rhode Island. Supported by a Research Project Grant from the National Institutes of Health National Heart, Lung, and Blood Institute (R01HL139795 to Dr. Morrison) and an Institutional Development Award from National Institutes of Health National Institute of General Medical Sciences (P20GM103652 to Dr. Morrison). Dr. Mantsounga has reported that he has no relationships relevant to the contents of this paper to disclose.

The authors attest they are in compliance with human studies committees and animal welfare regulations of the authors' institutions and Food and Drug Administration guidelines, including patient consent where appropriate. For more information, visit the *JACC: Basic to Translational Science* author instructions page.

ISSN 2452-302X https://doi.org/10.1016/j.jacbts.2019.08.003

relative to placebo was modest and gradually shrunk over the course of the study (3). These findings, in part, have led to an increasing recognition of potential pleiotropic effects of SGLT2 inhibitors beyond simply hypoglycemic effects. Although the molecular mechanisms are not fully understood, the effects of SGLT2 inhibitors are postulated to be multifactorial, including hemodynamics involving blood pressure reduction and diuresis, loss of body weight, and reductions in the renin-angiotensin-aldosterone system (7,8). SGLT2 inhibitors have also demonstrated some adverse reactions; canagliflozin is associated with a doubling of the risk for lower-limb amputation and with increased risk of fractures, and empagliflozin is associated with increased genital infections (3,9).

SEE PAGE 575

In the paper by Juni et al. (10) in this issue of *JACC: Basic to Translational Science*, the investigators set out to carefully examine the impact of empagliflozin on the interaction between cardiac microvascular endothelial cells (CMEC) and cardiac myocytes (CM) in a unique coculture model. The investigators established that secreted soluble factors from human CMEC improved advanced measures of primary rat CM contraction and relaxation, including sarcomere length shortening, return velocity, and relaxation time constant (tau). This beneficial effect was abolished by pre-incubation of the CMEC but not CM with nitric oxide (NO) synthase inhibitor, N(ω)-nitro-L-arginine methyl ester (L-NAME), indicating a significant role of endothelial produced NO. CMEC-conditioned medium had similar effects on CM contraction and relaxation that were also abrogated by the NO scavenger, carboxy-PTIO. Inflammatory cytokines, tumor necrosis factor (TNF)-α or interleukin-1β, reduced the availability of NO in endothelial cells and abrogated the effects of CMEC on measures of CM contraction and relaxation. Pretreatment of endothelial cells with empagliflozin had modest effect on the return velocity and no significant effects on sarcomere shortening and tau, but it had a significant impact on preventing the inflammatory cytokines from reducing measures of CM contraction and relaxation. Empagliflozin prevented the TNF-α-mediated reductions in NO, indicating that the protective effects of empagliflozin are mediated, in part, by endothelial NO production.

The downstream effects of TNF-α, including nuclear factor-κB-dependent upregulation of inflammatory adhesion factors, VCAM-1 and E-selectin, and mitochondrial superoxide dismutase 2 (SOD2), were unchanged by empagliflozin treatment. Moreover, empagliflozin had no effect on endothelial NO synthase expression or phosphorylation. However, empagliflozin did significantly blunt TNF-α-induced production of reactive oxygen species (ROS) in both the cytoplasm and in the mitochondria of the CMEC. This effect did not seem to be mediated by JNK kinase or a direct ROS scavenging/antioxidant effect of empagliflozin. Thus, these interesting data support an alternative mechanism whereby empagliflozin can activate intracellular mechanisms that reduce mitochondrial ROS generation, leading to consequent reductions in cytoplasmic ROS and enhanced NO bioavailability.

Although more work is needed to unravel the molecular mechanisms involved here, this study is quite timely, given the recent findings in both patients and an experimental model that HFpEF is associated with coronary microvascular endothelial dysfunction and oxidative stress, leading to a reduction of NO-dependent signaling from endothelial cells to cardiomyocytes (11). This study by Juni et al. (10) would have benefited from measures of soluble guanylate cyclase activity or cyclic guanosine monophosphate levels in the CM and inhibition of soluble guanylate cyclase to confirm NO-mediated effects on measures of contraction and relaxation. The addition of an experimental animal model of HF to support that the cellular measures of contraction and relaxation translate readily to measures of systolic and diastolic function would have strengthened the study. However, a recent study of nondiabetic mice treated with empagliflozin demonstrated preservation of systolic function relative to vehicle-treated mice in an aortic constriction model of pressure overload HF, supporting the findings of this cell-based system (8).

This new study also raises interesting questions as to whether the molecular mechanisms that govern the therapeutic effects of this emerging class of agents are specific to the inhibition of SGLT2. Though SGLT1 mRNA is abundantly expressed in the human heart and in other tissues, SGLT2, the selective target of empagliflozin, has been largely identified in skeletal muscle and kidney but not in heart (12,13). Some studies have indicated that SGLT2 may be expressed at low levels in endothelial cells (14,15), but the authors of the current investigation acknowledge that they and others have been unable to consistently detect SGLT2 from the CMEC. Improvements in the current forms of detection for SGLT2 RNA and protein may certainly be required. Ultimately, gene knockdown by small double-stranded interfering RNAs targeting SGLT2 in the CMEC or isolation of primary endothelial cells from SGLT2 knock-out mice may be helpful in confirming the specificity of the empagliflozin effect.

It is possible that empagliflozin has an effect, either directly or indirectly, on an alternative cation transport protein, the Na^+/H^+ exchanger-1 (NHE-1), leading to the reductions in mitochondrial ROS. Recent studies demonstrated that empagliflozin lowered cytosolic [Na^+] and [Ca^{2+}] while enhancing mitochondrial [Ca^{2+}], through impairment of NHE-1 (16,17). Prior studies have focused on cardiomyocytes, but it is possible empagliflozin may have similar effects on microvascular endothelial cells given that they also express NHE-1. Direct inhibition of NHE-1 by cariporide decreased ROS production, induced the regression of cardiac hypertrophy, and exerted beneficial effects in experimental HF (18,19). These actions may be cardioprotective, in part, because both increased cardiac intracellular Na+ and NHE activity have been linked to the occurrence of arrhythmias, myocardial hypertrophy, and aggravation of HF (20). Future studies involving conditional deletion systems of SGLT2 or NHE-1 in experimental models of HF are required to further dissect this new mechanism. Of note, targeting NHE-1 with cariporide clinically for the treatment of ischemia reperfusion injury was studied over a decade ago in the GAUARDIAN (Guard During Ischemia Against Necrosis) and EXPEDITION (The Na^+/H^+ Exchanger Inhibition to Prevent Coronary Events in Acute Cardiac Conditions) trials, and despite evidence of reduced myocardial injury, increased mortality caused by cerebrovascular events raised concerns about clinical safety (21–23). There may be something different about the study populations or the way empagliflozin is targeting mitochondrial NHE-1 to reduce mitochondrial ROS, but whatever the case, it is clear that more study is needed in this area.

In summary, the manuscript by Juni et al. (10) provides fascinating new insight into the impact of SGLT2 inhibitors on the cardiac microvascular and its protective role in cardiac mechanics. Empagliflozin counteracted inflammatory cytokine-induced impairment of CMEC-CM communication by reducing mitochondrial ROS and enhancing NO bioavailability for the preservation of CM contraction and relaxation. Results from EMPEROR-Preserved and EMPEROR-Reduced should provide additional clinical perspective on the potential protective effects of empagliflozin on the mechanics of the failing heart. Further research into the cellular and molecular mechanisms that determine these effects is required to help improve efficacy and reduce adverse events in this growing new class of pharmocotherapeutics.

ADDRESS FOR CORRESPONDENCE: Dr. Alan R. Morrison, Providence VA Medical Center, Research (151), 830 Chalkstone Avenue, Providence, Rhode Island 02908. E-mail: alan_morrison@brown.edu.

REFERENCES

1. Benjamin EJ, Virani SS, Callaway CW, et al. Heart disease and stroke statistics-2018 update: a report from the American Heart Association. Circulation 2018;137:e67–492.

2. Dunlay SM, Roger VL, Redfield MM. Epidemiology of heart failure with preserved ejection fraction. Nat Rev Cardiol 2017;14:591–602.

3. Zinman B, Wanner C, Lachin JM, et al. Empagliflozin, cardiovascular outcomes, and mortality in type 2 diabetes. N Engl J Med 2015;373:2117–28.

4. Fitchett D, Zinman B, Wanner C, et al. Heart failure outcomes with empagliflozin in patients with type 2 diabetes at high cardiovascular risk: results of the EMPA-REG OUTCOME(R) trial. Eur Heart J 2016;37:1526–34.

5. Boehringer Ingelheim, Eli Lilly Company. A Phase III Randomised, Double-blind Trial to Evaluate Efficacy and Safety of Once Daily Empagliflozin 10 mg Compared to Placebo, in Patients With Chronic Heart Failure With Preserved Ejection Fraction (HFpEF) (EMPEROR-Preserved). U.S. National Library of Medicine ClinicalTrials.gov. Feb 2017. Available at: https://clinicaltrials.gov/ct2/show/NCT03057951. Accessed August 1, 2019.

6. Boehringer Ingelheim, Eli Lilly Company. A Phase III Randomised, Double-blind Trial to Evaluate Efficacy and Safety of Once Daily Empagliflozin 10 mg Compared to Placebo, in Patients With Chronic Heart Failure With Reduced Ejection Fraction (HFrEF) (EMPEROR-Reduced). U.S. National Library of Medicine ClinicalTrials.gov. Feb 2017. Available at: https://clinicaltrials.gov/ct2/show/NCT03057977. Accessed August 1, 2019.

7. Zelniker TA, Braunwald E. Cardiac and renal effects of sodium-glucose co-transporter 2 inhibitors in diabetes: JACC state-of-the-art review. J Am Coll Cardiol 2018;72:1845–55.

8. Byrne NJ, Parajuli N, Levasseur JL, et al. Empagliflozin prevents worsening of cardiac function in an experimental model of pressure overload-induced heart failure. J Am Coll Cardiol Basic Trans Science 2017;2:347–54.

9. Neal B, Perkovic V, Mahaffey KW, et al. Canagliflozin and cardiovascular and renal events in type 2 diabetes. N Engl J Med 2017;377:644–57.

10. Juni RP, Kuster DWD, Goebel M, et al. Cardiac microvascular endothelial enhancement of cardiomyocyte function is impaired by inflammation and restored by empagliflozin. J Am Coll Cardiol Basic Trans Science 2019;4:575–91.

11. Franssen C, Chen S, Unger A, et al. Myocardial microvascular inflammatory endothelial activation in heart failure with preserved ejection fraction. J Am Coll Cardiol HF 2016;4:312–24.

12. Wright EM, Loo DD, Hirayama BA. Biology of human sodium glucose transporters. Physiol Rev 2011;91:733–94.

13. Zhou L, Cryan EV, D'Andrea MR, Belkowski S, Conway BR, Demarest KT. Human cardiomyocytes express high level of Na+/glucose cotransporter 1 (SGLT1). J Cell Biochem 2003;90:339–46.

14. El-Daly M, Pulakazhi Venu VK, Saifeddine M, et al. Hyperglycaemic impairment of PAR2-mediated vasodilation: prevention by inhibition of aortic endothelial sodium-glucose-co-transporter-2 and minimizing oxidative stress. Vascul Pharmacol 2018;109:56–71.

15. Mancini SJ, Boyd D, Katwan OJ, et al. Canagliflozin inhibits interleukin-1beta-stimulated cytokine and chemokine secretion in vascular endothelial cells by AMP-activated protein kinase-dependent and -independent mechanisms. Sci Rep 2018;8:5276.

16. Baartscheer A, Schumacher CA, Wust RC, et al. Empagliflozin decreases myocardial cytoplasmic Na(+) through inhibition of the cardiac Na(+)/H(+) exchanger in rats and rabbits. Diabetologia 2017;60:568–73.

17. Uthman L, Baartscheer A, Bleijlevens B, et al. Class effects of SGLT2 inhibitors in mouse cardiomyocytes and hearts: inhibition of Na(+)/H(+)

exchanger, lowering of cytosolic Na(+) and vasodilation. Diabetologia 2018;61:722–6.

18. Garciarena CD, Caldiz CI, Correa MV, et al. Na+/H+ exchanger-1 inhibitors decrease myocardial superoxide production via direct mitochondrial action. J Appl Physiol 2008;105:1706–13.

19. Cingolani HE, Ennis IL. Sodium-hydrogen exchanger, cardiac overload, and myocardial hypertrophy. Circulation 2007;115:1090–100.

20. Packer M, Anker SD, Butler J, Filippatos G, Zannad F. Effects of sodium-glucose cotransporter 2 inhibitors for the treatment of patients with heart failure: proposal of a novel mechanism of action. JAMA Cardiol 2017;2:1025–9.

21. Boyce SW, Bartels C, Bolli R, et al. Impact of sodium-hydrogen exchange inhibition by cariporide on death or myocardial infarction in high-risk CABG surgery patients: results of the CABG surgery cohort of the GUARDIAN study. J Thorac Cardiovasc Surg 2003;126:420–7.

22. Mentzer RM Jr., Bartels C, Bolli R, et al. Sodium-hydrogen exchange inhibition by cariporide to reduce the risk of ischemic cardiac events in patients undergoing coronary artery bypass grafting: results of the EXPEDITION study. Ann Thorac Surg 2008;85:1261–70.

23. Theroux P, Chaitman BR, Danchin N, et al. Inhibition of the sodium-hydrogen exchanger with cariporide to prevent myocardial infarction in high-risk ischemic situations. Main results of the GUARDIAN trial. Guard during ischemia against necrosis (GUARDIAN) Investigators. Circulation 2000;102:3032–8.

KEY WORDS cardiomyocyte, empagliflozin, endothelial cell, heart failure, microvasculature

JACC: BASIC TO TRANSLATIONAL SCIENCE VOL. 4, NO. 5, 2019

PRECLINICAL RESEARCH

Platelet Acetyl-CoA Carboxylase Phosphorylation

A Risk Stratification Marker That Reveals Platelet-Lipid Interplay in Coronary Artery Disease Patients

Shakeel Kautbally, MD,[a,*] Sophie Lepropre, PhD,[a,*] Marie-Blanche Onselaer, PhD,[a] Astrid Le Rigoleur, MD,[a] Audrey Ginion, MS,[a] Christophe De Meester de Ravenstein, PhD,[a] Jerome Ambroise, PhD,[b] Karim Z. Boudjeltia, PhD,[c] Marie Octave, MS,[a] Odile Wéra, MS,[d] Alexandre Hego, BSc,[d] Joël Pincemail, PhD,[e] Jean-Paul Cheramy-Bien,[e] Thierry Huby, PhD,[f] Martin Giera, PhD,[g] Bernhard Gerber, MD, PhD,[a,h] Anne-Catherine Pouleur, MD, PhD,[a,h] Bruno Guigas, PhD,[i,j] Jean-Louis Vanoverschelde, MD, PhD,[a,h] Joelle Kefer, MD, PhD,[a,h] Luc Bertrand, PhD,[a] Cécile Oury, PhD,[d] Sandrine Horman, PhD,[a,†] Christophe Beauloye, MD, PhD[a,h,†]

VISUAL ABSTRACT

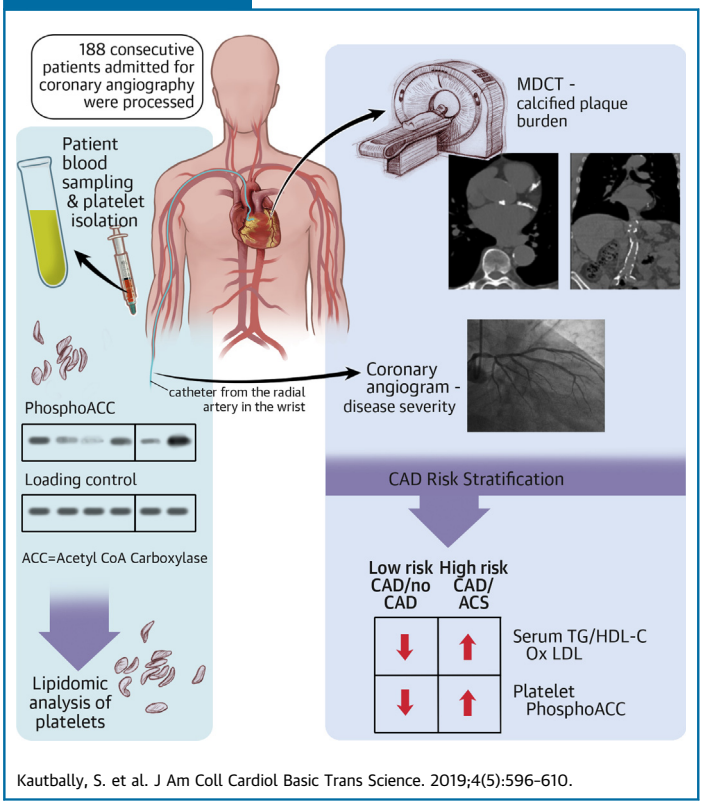

Kautbally, S. et al. J Am Coll Cardiol Basic Trans Science. 2019;4(5):596-610.

HIGHLIGHTS

- **Platelet phosphoACC is a marker for risk stratification in suspected CAD patients. It identifies high-risk CAD patients and correlates with severity of coronary artery calcification.**
- **The triglycerides/high-density lipoprotein cholesterol ratio is strongly associated with increased phosphoACC in circulating platelets. PhosphoACC is a metabolic signature of the platelet-proatherogenic lipid interplay in CAD patients.**
- **Phosphorylation and inhibition of acetyl-CoA carboxylase impacts platelet lipid content by down-regulating triglycerides lipid species.**

From the [a]Pôle de Recherche Cardiovasculaire, Institut de Recherche Expérimentale et Clinique, Université Catholique de Louvain, Brussels, Belgium; [b]Center for Applied Molecular Technologies, Institut de Recherche Expérimentale et Clinique, Université Catholique de Louvain, Brussels, Belgium; [c]Laboratory of Experimental Medecine (ULB 222 unit), Centre Hospitalier Universitaire de Charleroi, Université Libre de Bruxelles, Charleroi, Belgium; [d]Laboratory of Thrombosis and Hemostasis, GIGA-Cardiovascular Sciences, Department of Cardiology, Université de Liège, Liège, Belgium; [e]Department of Cardiovascular Surgery, Surgical Research

ISSN 2452-302X https://doi.org/10.1016/j.jacbts.2019.04.005

SUMMARY

Adenosine monophosphate–activated protein kinase (AMPK) acetyl-CoA carboxylase (ACC) signaling is activated in platelets by atherogenic lipids, particularly by oxidized low-density lipoproteins, through a CD36-dependent pathway. More interestingly, increased platelet AMPK-induced ACC phosphorylation is associated with the severity of coronary artery calcification as well as acute coronary events in coronary artery disease patients. Therefore, AMPK-induced ACC phosphorylation is a potential marker for risk stratification in suspected coronary artery disease patients. The inhibition of ACC resulting from its phosphorylation impacts platelet lipid content by down-regulating triglycerides, which in turn may affect platelet function.

ABBREVIATIONS AND ACRONYMS

ACC = acetyl-CoA carboxylase

AMPK = adenosine monophosphate–activated protein kinase

AoC = extra-coronary calcification score

AU = arbitrary units

CAC = coronary artery calcification

CAD = coronary artery disease

oxLDL = oxidized low-density lipoprotein

phosphoACC = acetyl-CoA carboxylase phosphorylation on serine 79

S-CAD = stable coronary artery disease

TG = triglyceride

Platelets are key players in atherothrombosis. In acute coronary syndrome (ACS), coagulation cascade activation upon plaque rupture leads to thrombin generation (ThG), a crucial platelet agonist enhancing the formation of platelet-rich thrombi (1). The association between increased ThG and ischemic risk in coronary artery disease (CAD) patients renders the coagulation cascade an interesting therapeutic target (2,3).

We previously established the adenosine monophosphate–activated protein kinase (AMPK) to be crucial for platelet activation. In human platelets, thrombin is the major agonist leading to AMPK activation through a calcium-dependent mechanism (4). Once activated, AMPK contributes to platelet secretion, platelet aggregation, and clot retraction by controlling the actin cytoskeleton. AMPK activation likewise leads to phosphorylation of acetyl-CoA carboxylase (ACC) on serine 79 (phosphoACC), its bona-fide substrate, typically used as a marker of AMPK activation in cells and tissues, including platelets (4). It is tempting to speculate that ThG affects platelet AMPK signaling, resulting in increased phosphoACC in CAD. However, although thrombin is crucial for thrombus formation at the plaque rupture site in ACS, its impact on circulating platelets remains unclear. In CAD patients, the atherogenic environment influences platelet biology and reactivity, mainly through CD36 (5,6). Oxidized low-density lipoprotein (oxLDL) binds to CD36, inducing platelet activation and shape changes via a calcium-dependent mechanism (7). Yet, other factors besides thrombin may affect AMPK-ACC signaling in circulating platelets of CAD patients.

ACC is the first committed enzyme of the fatty acid biosynthesis pathway, while its phosphorylation on serine 79 by AMPK inhibits its activity (8). We demonstrated that AMPK-ACC signaling is a key pathway in controlling platelet lipid content, thereby modulating platelet function and thrombus formation (9). However, ACC contribution to platelet lipid

Center and Plateform Nutrition Antioxydante et Santé, University Hospital of Liège, Liège, Belgium; [f]INSERM UMR_S 1166, Integrative Biology of Atherosclerosis Team, Université Pierre et Marie Curie-Paris 6 and Institute of Cardiometabolism and Nutrition, Pitié-Salpêtrière Hospital, Paris, France; [g]Center for Proteomics and Metabolomics, Leiden University Medical Center, Leiden, the Netherlands; [h]Division of Cardiology, Cliniques Universitaires Saint-Luc, Brussels, Belgium; [i]Department of Parasitology, Leiden University Medical Center, Leiden, the Netherlands; and the [j]Department of Cell and Chemical Biology, Leiden University Medical Center, Leiden, the Netherlands. *Drs. Kautbally and Lepropre contributed equally to this paper and are joint first authors. †Drs. Horman and Beauloye contributed equally to this paper and are joint senior authors. This work was supported by grants from the Fonds National de la Recherche Scientifique et Médicale (FNRS) (Belgium) and Louvain Foundation (Louvain-La-Neuve, Belgium), and by unrestricted grants from Bayer and AstraZeneca (Belgium). The Division of Cardiology at Cliniques universitaires Saint-Luc, Belgium, has received unrestricted research grants from AstraZeneca, Bayer Healthcare, and Daiichi-Sankyo (Belgium). Drs. Kautbally and Lepropre were supported by the FNRS (Belgium). Drs. Lepropre and Onselaer were supported by grants from the Salus Sanguinis Foundation (UCLouvain, Belgium). Drs. Octave and Wéra have FRIA fellowships from the FNRS (Belgium). Dr. Horman is a research associate, and Drs. Bertrand and Oury are senior research associates at the FNRS (Belgium). Dr. Pouleur is, and Dr. Beauloye was, a clinical master specialist at the FNRS (Belgium). All other authors have reported that they have no relationships relevant to the contents of this paper to disclose.

The authors attest they are in compliance with human studies committees and animal welfare regulations of the authors' institutions and Food and Drug Administration guidelines, including patient consent where appropriate. For more information, visit the *JACC: Basic to Translational Science* author instructions page.

Manuscript received November 29, 2018; revised manuscript received April 26, 2019, accepted April 27, 2019.

FIGURE 1 Flowchart of the Study Population

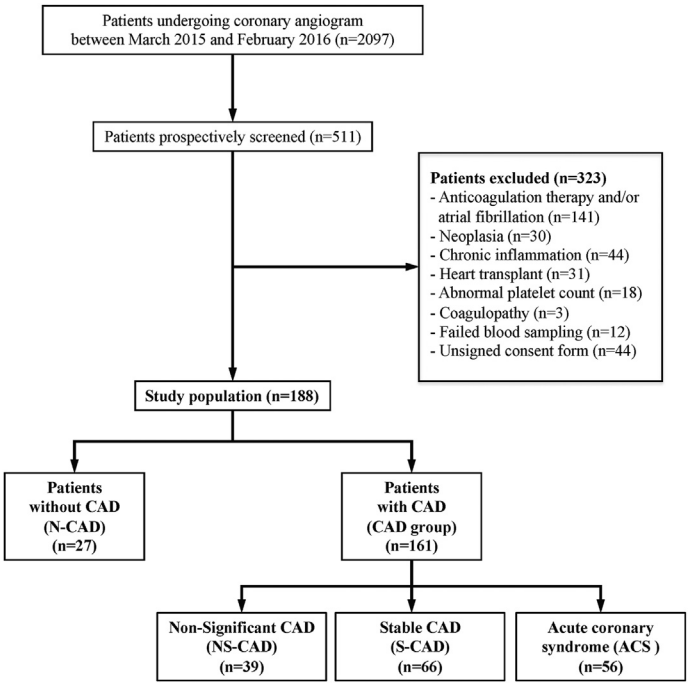

Patients included in the ACCTHEROMA study. Classification based on clinical presentation and angiographic data. ACCTHEROMA = prospective evaluation of Acetyl-CoA Carboxylase phosphorylation state in platelets as a marker of atherothrombotic coronary and extra-coronary artery disease; ACS = acute coronary syndrome; CAD = coronary artery disease; N-CAD = non-coronary artery disease; NS-CAD = nonsignificant coronary artery disease; S-CAD = significant coronary artery disease.

metabolism in CAD, in which atherogenic lipids interact with circulating platelets (10), remains unexplored.

Here, we report platelet phosphoACC as a potential risk stratification marker in suspected CAD patients. In consecutive patients admitted for coronary angiography, phosphoACC was significantly increased in circulating platelets of CAD patients and highly associated with acute coronary events. We identified an interplay between platelets and lipids, with oxLDL as a central contributor to increased platelet phosphoACC. Interestingly, the lipidomic data show that sustained phosphoACC regulates triglyceride (TG) lipids in circulating platelets of CAD patients.

METHODS

Methods (including experimental dataset) and reagents are described in the Supplemental Appendix.

CLINICAL COHORT. Study design. From March 2015 to February 2016, 188 consecutive patients admitted for coronary angiography were included in the ACCTHEROMA (prospective evaluation of Acetyl-CoA Carboxylase phosphorylation state in platelets as a marker of atherothrombotic coronary and extra-coronary artery disease) study (NCT03034148), with at least 2 patients prospectively screened per day, regardless of the indication for angiography. Based on indication and coronary angiography results analyzed by 2 experienced cardiologists, patients were classified into 4 groups. Patients undergoing angiography for chest pain or valvular disease investigation with normal coronary vessels were classed as non-CAD (N-CAD) (reference population). The presence of at least 1 plaque with <50% luminal stenosis was classed as nonsignificant CAD (NS-CAD). Patients presenting with stable disease with significant stenosis (>50%) were classed as stable CAD (S-CAD). ACS comprised unstable angina (n = 30), non-ST-segment elevation myocardial infarction (n = 22), and ST-segment elevation myocardial infarction (n = 4). Further details on patient classifications are provided in the Supplemental Appendix and study flowchart in Figure 1. The study was approved by the institutional ethics committee (2015/08JAN/010) and complied with the Declaration of Helsinki and good clinical practice guidelines. All participants provided written informed consent.

Blood sampling and phosphoACC analysis. All patients had been fasting for at least 6 h before angiography, except for 4 ST-segment elevation myocardial infarction patients. Blood samples drawn from the arterial sheath were collected in citrated tubes before any drug administration in the catheterization laboratory, including heparin. In a subgroup of patients (n = 8) undergoing right heart catheterization in addition to angiography, a venous blood sample was collected from the femoral access site to compare the level of ACC phosphorylation in arterial and venous blood simultaneously. All samples were immediately processed for platelet isolation. Using flow cytometry, we verified that platelet preparations did not contain any leukocytes (Supplemental Figure 1). Platelets were lysed in Laemmli buffer before phosphoACC analysis by Western blotting. A standard positive control for phosphoACC was prepared with washed platelets isolated from a healthy volunteer and stimulated with a high dose of thrombin (0.5 U/ml) for 2 min. This standard positive control was used for all the Western blots, placed 4 times on each gel to validate the signal reproducibility. For each patient, band intensities were normalized to corresponding loading controls (gelsolin) on the same gel. The normalized phosphoACC value was compared with the standard positive control. Western blot analyses were confirmed

by electrochemiluminescence immunoassay (Meso Scale Diagnostics, Rockville, Maryland).

Multidetector computed tomography. Thoracoabdominal multidetector computed tomography (MDCT) was performed in a subgroup of patients (n = 68) to assess calcified plaque burden. Arbitrarily, the first and third patient on the list for planned coronary angiogram underwent MDCT for calcium scoring. MDCT was done just before coronary angiogram. Scans were taken with a 256-slice multidetector-row CT scanner (Brilliance iCT 256, Philips Healthcare, Cleveland, Ohio) with 3.0-mm slice collimation, 120-kV tube voltage, and 100-mAs tube current using a prospectively gated "step and shoot" protocol. Coronary artery calcification (CAC) was expressed by means of the Agatston score using calcium scoring software (Philips Healthcare) with a threshold of 130 Hounsfield units. The degree of CAC was classified as mild (Agatston score <100), moderate (between 100 and 400), or severe (>400) (11). An extracoronary calcification score (aorta calcification [AoC]) was measured from the aortic root (excluding the aortic valve) to the common iliac artery in all patients. The AoC score was divided into tertiles for analysis.

Platelet lipidomics. To characterize the phosphoACC impact on regulating platelet lipid homeostasis, we performed a quantitative lipidomic study on 31 samples from patients with the lowest (n = 12) and highest (n = 19) platelet phosphoACC values. Lipids were extracted from a platelet pellet by the methyl-*tert*-butylether method and analyzed using Lipidyzer, a direct infusion-tandem mass spectrometry (DI-MS/MS)-based platform (Sciex, Redwood City, California).

STATISTICAL ANALYSIS. Clinical cohort. Analyses were conducted using SPSS version 24 (IBM Corporation, Armonk, New York). Continuous variables were expressed as mean ± SD or median (interquartile range [IQR]) depending on data distribution, and categorical variables were expressed as number and percentage. CAC and AoC scores, D-dimers, high-sensitivity C-reactive protein, and TG and high-density lipoprotein-cholesterol (HDL-C) ratio were normalized by log-10 transformation. Categorical variables were analyzed using the chi-square test or Fisher's exact test and continuous variables were analyzed using an unpaired Student's *t*-test or the Mann-Whitney *U* test, as appropriate. Data were subjected to the Kolmogorov-Smirnov normality test and Bartlett's test for homogeneity of variance. Group comparisons were made using either 1-way analysis of variance with the *F* test (Bonferroni correction) or Kruskal-Wallis test. Correlations were presented as Pearson (Rp) or Spearman (Rs) coefficients. Multivariable logistic regression analysis (backward elimination) included variables with p value < 0.05 on univariable analysis, with odds ratio (OR) and 95% confidence interval (CI) calculated to determine independent factors associated with ACS. With the receiver-operating characteristic curve, we determined a threshold phosphoACC value for CAD by maximizing sensitivity and specificity. C-statistics were used to describe diagnostic discrimination. The prognostic value of platelet phosphoACC for ischemic outcomes, including cardiovascular death and recurrent myocardial infarction/revascularization procedures, was assessed during patient follow-up. Multivariable Cox regression analysis was used to identify independent predictors for events. Hazard ratios with 95% CI are presented. Event-free survival according to platelet phosphoACC levels was computed using the Kaplan-Meier method.

Lipidomics. Lipid species concentrations obtained from DI-MS/MS (Lipidyzer) were analyzed using R software version 3.4.2 (R Foundation for Statistical Computing, Vienna, Austria) according to the following bioinformatics pipeline. Missing DI-MS/MS data were imputed using probabilistic principal component analysis from pcaMethods Bioconductor package (12). The data were normalized using total lipid abundance, with a log-2 transformation applied to normalized concentrations. The limma Bioconductor package was used to build a multivariable regression model for each lipid species with predictors including platelet phosphoACC, aspirin intake, diabetes, and plasma TG levels. Fold-change estimates and corresponding p values were derived from regression models for each lipid species and each predictor. To control for multiple testing, all p values were further adjusted for Benjamini-Hochberg false discovery rate, with a false discovery rate <0.05 considered statistically significant (13). Considering that 865 lipid species belong to 11 lipid classes, namely cholesterol ester, diacylglycerol, free fatty acid, lysophosphatidylcholine, lysophosphatidylethanolamine, phosphatidylcholine, phosphatidylethanolamine, plasmenyl phosphatidylethanolamine, plasmalogen phosphatidylethanolamine, sphingomyelin, and TG, lipid class enrichment analysis was performed using Fisher's exact tests to identify lipid classes with a high proportion of differentially regulated lipid species.

RESULTS

POPULATION BASELINE CHARACTERISTICS AND GLOBAL ATHEROSCLEROTIC CALCIFIED PLAQUE BURDEN. The study population comprised 188 individuals (70% men, 65 ± 12 years) admitted for

TABLE 1 Baseline Characteristics of the ACCTHEROMA Cohort

	Overall Population (N = 188)	NCAD (n = 27)	CAD			p Value
			NS-CAD (n = 39)	S-CAD (n = 66)	ACS (n = 56)	
Clinical characteristics						
Age, yrs	65 ± 12	59 ± 9	68 ± 11	66 ± 12	66 ± 14	0.029*
Male	131 (69.7)	15 (55.6)	23 (59.0)	48 (72.7)	45 (80.4)	0.046
BMI, kg/m^2	27.6 ± 4.9	27.4 ± 4.0	28.0 ± 5.3	27.4 ± 5.5	27.6 ± 4.2	0.94
Hypertension	119 (63.3)	8 (29.6)	21 (53.8)	52 (78.8)	38 (67.9)	<0.001
Smoking	104 (55.3)	12 (44.4)	17 (43.6)	39 (59.1)	36 (64.3)	0.13
Diabetes	43 (22.9)	1 (3.7)	9 (23.1)	14 (21.2)	19 (33.9)	0.022
Prior history of CAD	62 (33.0)	0 (0)	0 (0)	36 (54.5)	26 (46.4)	<0.001
MI	35 (18.6)	0 (0)	0 (0)	19 (28.8)	16 (28.6)	<0.001
PCI	47 (25.0)	0 (0)	0 (0)	26 (39.4)	21 (37.5)	<0.001
CABG	16 (8.5)	0 (0)	0 (0)	10 (15.2)	6 (10.7)	0.017
Aortic valvular disease	34 (18.1)	4 (14.8)	14 (35.9)	16 (24.2)	0 (0)	<0.001
Mitral valvular disease	12 (6.4)	7 (25.9)	3 (7.7)	2 (3.0)	0 (0)	<0.001
Biological						
Hemoglobin, g/dl	14.1 ± 1.6	13.7 ± 1.3	14.1 ± 1.5	14.2 ± 1.4	14.0 ± 1.9	0.62
Fasting glycemia, mg/dl	100 (92–114)	98 (92–105)	99 (91–123)	101 (93–108)	105 (95–134)	0.61
Creatinine, mg/dl	1.0 (0.8–1.1)	0.9 (0.8–1.1)	1.0 (0.8–1.0)	1.0 (0.9–1.2)	0.9 (0.8–1.1)	0.22
CRI	22 (11.7)	2 (7.4)	3 (7.7)	12 (18.2)	5 (8.9)	0.24
Non-HDL, mg/dl	120 ± 45	124 ± 49	123 ± 39	112 ± 45	127 ± 46	0.32
HDL, mg/dl	50.4 ± 15.3	53.8 ± 15.6	56.5 ± 17.8	50.2 ± 13.6	44.7 ± 13.4	0.002†
TG, mg/dl	102 (76–152)	84 (66–132)	95 (78–140)	95 (75–146)	126 (91–161)	0.017‡
hsCRP, mg/l	1.4 (0.6–3.4)	0.9 (0.5–2.1)	1.2 (0.6–3.0)	1.3 (0.5–3.6)	1.7 (0.8–5.6)	0.13
Platelet count (×10^3)/μl	244 ± 61	211 ± 38	268 ± 65	248 ± 66	240 ± 54	0.002*§
Multiplate analysis						
ASPI test, AU*min	515 ± 278	549 ± 319	631 ± 258	507 ± 287	427 ± 228	0.004†
ADP test, AU*min	638 ± 217	626 ± 163	692 ± 132	643 ± 243	601 ± 249	0.24
TRAP test, AU*min	1,101 ± 255	1,007 ± 258	1,177 ± 232	1,057 ± 226	1,146 ± 280	0.011*
D-dimers, ng/ml	407 (281–686)	282 (250–435)	398 (288–573)	407 (290–775)	443 (349–706)	0.018‡
Medication						
ACE inhibitor/ARB	86 (45.7)	6 (22.2)	16 (41.0)	43 (65.2)	21 (37.5)	<0.001
Beta-blockers	97 (51.6)	9 (33.3)	15 (38.5)	39 (59.1)	34 (60.7)	0.022
Lipid-lowering treatment	111 (59.0)	13 (48.1)	16 (41.0)	48 (72.7)	34 (60.7)	0.008
Aspirin	141 (75.0)	13 (48.1)	21 (53.8)	55 (83.3)	52 (92.9)	<0.001
Dual antiplatelet therapy	30 (16.0)	0 (0)	0 (0)	12 (18.2)	20 (35.7)	<0.001
Clopidogrel	15 (8.0)	0 (0)	0 (0)	6 (9.1)	9 (16.1)	0.013
Ticagrelor	13 (6.9)	0 (0)	0 (0)	3 (4.5)	10 (17.9)	<0.001
Prasugrel	4 (2.1)	0 (0)	0 (0)	3 (4.5)	1 (1.8)	0.35

Values are mean ± SD, n (%), or median (interquartile range). *Pairwise significant difference ($p < 0.05$) between NS-CAD and NCAD. †Pairwise significant difference ($p < 0.05$) between ACS and NS-CAD. ‡Pairwise significant difference ($p < 0.05$) between ACS and N-CAD. §Pairwise significant difference ($p < 0.05$) between S-CAD and NCAD.

ACCTHEROMA = prospective evaluation of Acetyl-CoA Carboxylase phosphorylation state in platelets as a marker of atherothrombotic coronary and extra-coronary artery disease; ACE = angiotensin-converting enzyme; ACS = acute coronary syndrome; ARB = angiotensin receptor blocker; ASPI = aspirin channel; AU = arbitrary units; BMI = body mass index; CABG = coronary artery bypass grafting; CAD = coronary artery disease; CRI = chronic renal insufficiency; hsCRP = high-sensitivity C-reactive protein; MI = myocardial infarction; NCAD = non-coronary artery disease; NS-CAD = nonsignificant coronary artery disease; PCI = percutaneous coronary intervention; S-CAD = significant coronary artery disease; TG = triglycerides; TRAP = thrombin receptor activating peptide.

coronary angiography. They were divided into 4 groups according to clinical presentation and coronary anatomy (Table 1). The N-CAD group included 27 (14.4%) patients with normal coronary arteries, with about 41% undergoing angiography for valvular disease. In the CAD group (n = 161), 122 (76%) patients had significant coronary stenosis above 50%, 46% of whom had ACS. Most ACS patients (93%) were taking aspirin at enrollment, with only 36% of them on dual antiplatelet therapy, as most unstable angina and non-ST-segment elevation myocardial infarction patients did not receive $P2Y_{12}$ inhibitors before angiography. Accordingly, mean platelet reactivity assessed using the Multiplate Analyzer (Roche Diagnostics International Ltd., Rotkreuz, Switzerland) showed decreased platelet aggregation in response to arachidonic acid in ACS patients. Laboratory parameters revealed significantly increased platelet counts in CAD patients, yet within the normal range. As previously reported (2), our data confirmed a significant

increase in ThG, assessed by D-dimer levels, in ACS patients.

Thoracoabdominal MDCT with prospective electrocardiography gating aimed to evaluate calcified plaque burden, including coronary (CAC Agatston) and extracoronary (AoC) calcification scores. We confirmed that N-CAD patient (reference population) classification based on angiographic data was consistent with low CAC Agatston scores (median 7.0 [interquartile range: 0.0 to 33.9]) (**Figure 2A**). Although N-CAD patients had low CAC Agatston scores, their AoC scores were fairly high (median 543 [interquartile range: 107 to 2,001]) (**Figure 2B**). Accordingly, we observed a modest correlation between CAC and AoC calcification scores (Rp = 0.42; $p < 0.001$), indicating a heterogeneous atherosclerotic development or arterial calcifications (**Figure 2C**).

IDENTIFICATION OF HIGH-RISK CAD PATIENTS BY PLATELET phosphoACC. Platelet phosphoACC was studied in consecutive patients by Western blotting (**Figure 3A**). Quantification of band intensities showed significant increased phosphoACC in circulating platelets of CAD compared with N-CAD patients (median 0.48 [IQR: 0.29 to 0.73] vs. 0.22 [IQR: 0.11 to 0.45]; $p < 0.001$) (**Figure 3B**). Platelet phosphoACC in N-CAD patients was almost never >0.5 arbitrary units (AU), a threshold value estimated from receiver-operating characteristic analysis (Supplemental Figure 2) with a 96% positive predictive value for CAD. PhosphoACC signal was fairly similar in arterial and central venous blood in a subset of patients, undergoing left and right heart catheterization (Supplemental Figure 3). Of note, phosphorylation of protein kinase C substrates, a readout of platelet activation, was nearly undetectable in the platelets of CAD patients (Supplemental Figure 4), suggesting that phosphoACC occurred independently of platelet activation.

These data were further confirmed by quantitative electrochemiluminescence analysis. Platelet phosphoACC was analyzed twice to test interexperiment reproducibility (intraclass correlation coefficient) and found to be high (0.90), with a bias of -0.03 (95% CI: -0.10 to 0.04) (Supplemental Figure 5A). Furthermore, phosphoACC correlated with Western blot results, confirming that it was significantly increased in circulating platelets of CAD patients (Supplemental Figures 5B and 5C).

Among the CAD subgroups, the highest platelet phosphoACC level was found in ACS patients (median 0.55 [IQR: 0.29 to 0.76]) (**Figure 3C**). Indeed, quartile analysis of platelet phosphoACC demonstrated that the fourth quartile included 98% of CAD patients, with

FIGURE 2 Assessment of Coronary and Aortic Calcified Plaque by Prospective Electrocardiography-Gated Multidetector Computed Tomography

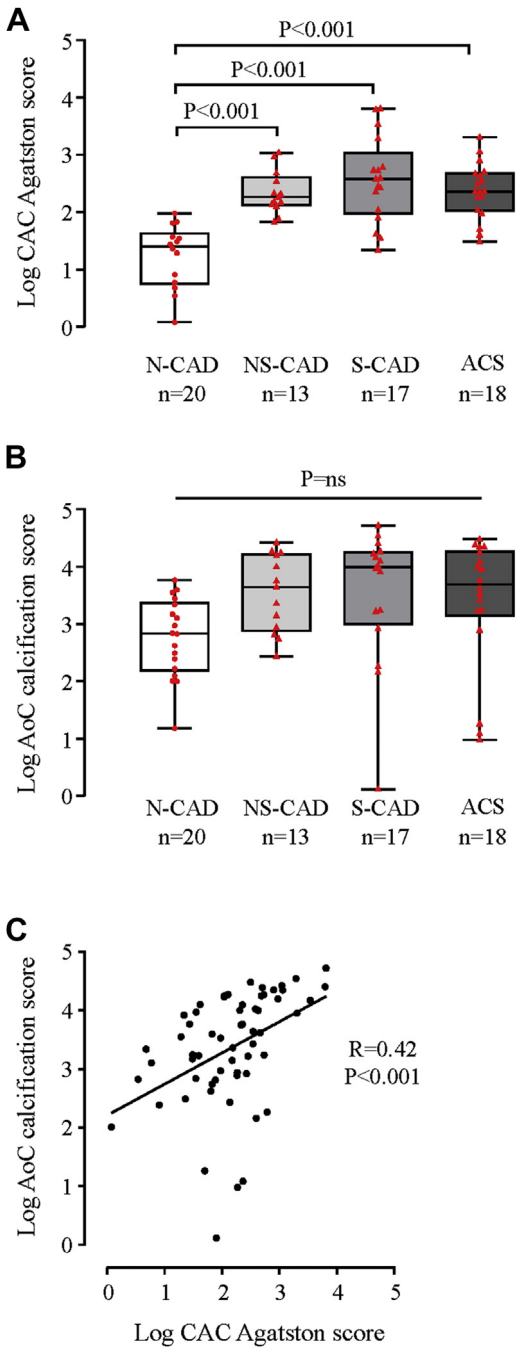

Box-plot representation of log-transformed **(A)** coronary artery calcification (CAC) Agatston and **(B)** aorta calcification (AoC) scores in the N-CAD and CAD subgroups of patients. **Red dots** (N-CAD, reference population) and **triangles** (CAD patients) represent individual values. Boxplots represent medians and corresponding whiskers represent extremes of the distribution. **(C)** Correlation between log-transformed CAC Agatston and AoC scores. Abbreviations as in **Figure 1**.

FIGURE 3 **PhosphoACC Correlates With Calcified Plaque Severity and Identifies High-Risk ACS Patients**

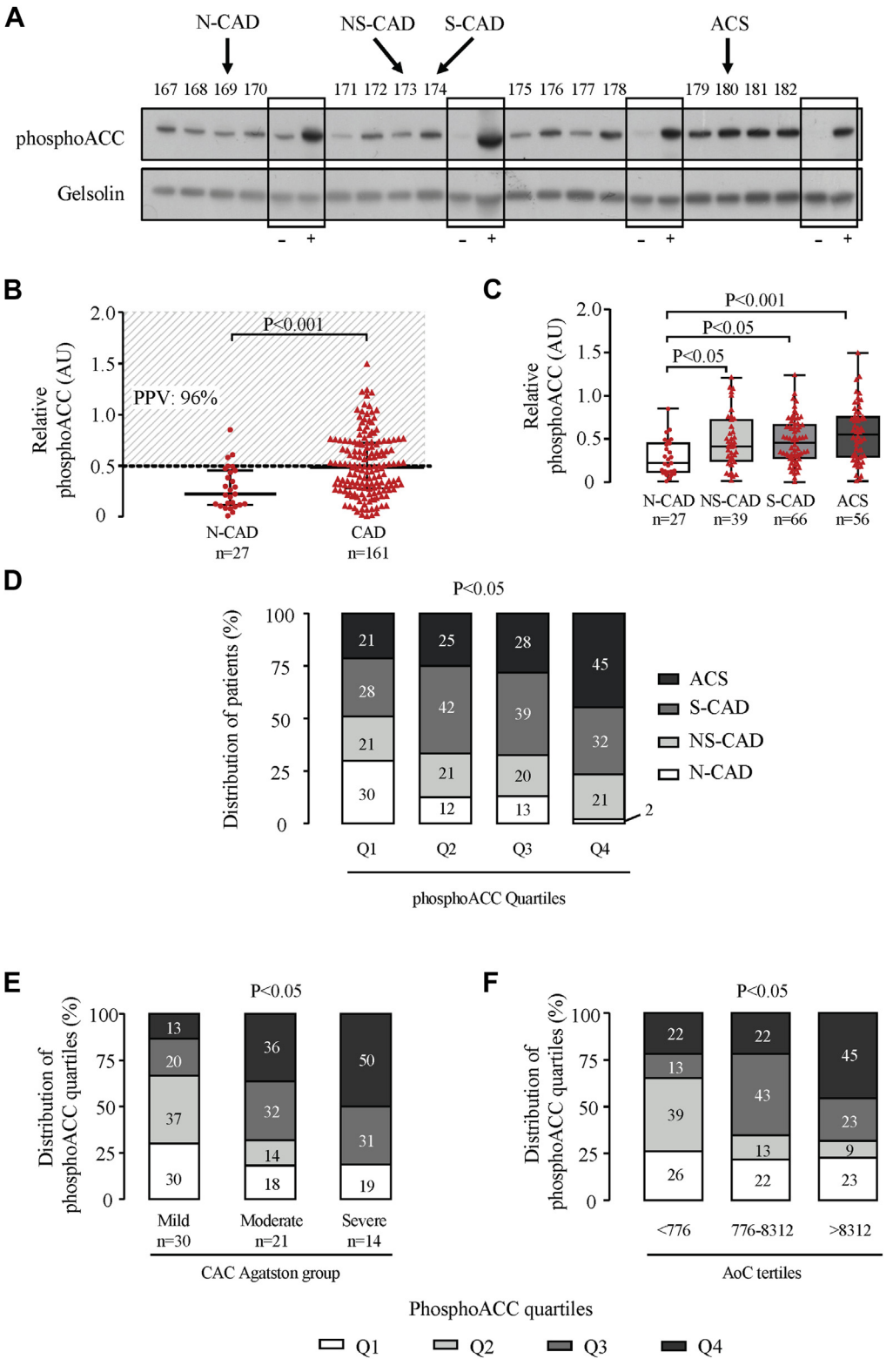

Continued on the next page

a large proportion of high-risk ACS patients (45%) (chi-square test; p = 0.020) (Figure 3D). Multivariable logistic regression results coincided with this, showing that, in addition to D-dimer levels (OR: 5.7; 95% CI: 1.8 to 17.8; p = 0.003) and the TG/HDL-C ratio (OR: 7.9; 95% CI: 2.1 to 29.9; p = 0.002), platelet phosphoACC (OR: 4.8; 95% CI: 1.5 to 15.8; p = 0.009) was independently associated to ACS (Table 2).

Prognostic value of platelet phosphoACC levels was assessed for ischemic events (cardiovascular death, recurrent myocardial infarction, and revascularization procedures) during a mean follow-up of 3.7 ± 0.4 years. In our cohort, 28 (14.8%) patients experienced with ischemic events. Multivariable Cox regression analysis identified increased platelet phosphoACC as an independent predictor of events (hazard ratio: 3.7; 95% CI: 1.1 to 12.1; p = 0.034), in addition to previous history of MI (hazard ratio: 3.2; 95% CI: 1.4 to 7.3; p = 0.006) and atherosclerotic cardiovascular disease score (hazard ratio: 10.1; 95% CI: 1.9 to 54.0; p = 0.007) (Supplemental Table 1). Kaplan-Meier event-free survival curves confirmed that patients with high phosphoACC levels (above 0.5 AU) had a higher events rate compared with low phosphoACC levels (log-rank test; p = 0.036) (Figure 4).

RELATIONSHIP BETWEEN PLATELET phosphoACC, CALCIFIED PLAQUE BURDEN, AND ThG MARKERS. In patients who underwent MDCT, platelet phosphoACC, in addition to age and D-dimer levels, was independently associated to coronary calcification severity (global R^2 = 0.47; p < 0.001) (Supplemental Table 2). Accordingly, as depicted in Figure 3E, 50% of patients with high phosphoACC (fourth quartile) exhibited severe CAC Agatston scores (chi-square test; p = 0.023). Similar results were obtained with the AoC score (Figure 3F). Altogether, these findings highlight the potential of platelet phosphoACC for identifying disease severity and high-risk CAD patients. We next confirmed such observations in an animal model developing spontaneous atherosclerosis, which is enhanced by a Western diet, the SR-B1$^{flox/flox}$/ApoE$^{-/-}$ hypercholesterolemic mice (Figures 5A and 5B). As in human platelets, phosphoACC levels drastically increased with the severity of atherosclerotic plaque burden (Figure 5C).

TABLE 2 Univariable and Multivariable Models of Factors Associated With ACS

	Univariable Analysis		Multivariable Analysis	
	OR (95% CI)	p Value	OR (95% CI)	p Value
ASCVD score	3.61 (0.80–16.24)	0.09		
hsCRP (log transformed)	1.99 (1.11–3.55)	0.020		
D-dimer (log transformed)	3.14 (1.16–8.51)	0.024*	5.69 (1.82–17.76)	0.003*
Non-HDL	1.00 (0.99–1.01)	0.23		
TG/HDL-C ratio (log transformed)	7.57 (2.32–24.72)	0.001*	7.95 (2.11–29.90)	0.002*
Platelet phosphoACC	4.02 (1.39–11.56)	0.010*	4.83 (1.48–15.81)	0.009*

*Statistical significance when p value < 0.05 in univariable and multivariable analysis.

ASCVD = atherosclerotic cardiovascular disease; CI = confidence interval; HDL-C = high-density lipoprotein cholesterol; OR = odds ratio; phosphoACC = acetyl-CoA carboxylase phosphorylation on Ser79; other abbreviations as in Table 1.

ThG markers correlated with the severity of calcified plaque, given that D-dimer levels (chi-square test; p = 0.014), thrombin antithrombin complexes (chi-square test; p = 0.036), or fragments 1.2 (chi-square test; p = 0.004) had a significant positive association with the severity of both CAC Agatston (Supplemental Figure 6A) and AoC score (Supplemental Figure 6B). However, we did not find any correlation between ThG markers (D-dimer levels) and platelet phosphoACC across the entire population (Supplemental Figure 6C), although thrombin is a major agonist leading to increased phosphoACC in platelets in vitro. Therefore, other factors besides thrombin should contribute to platelet phosphoACC in atherosclerosis.

CONTRIBUTION OF INFLAMMATION AND ATHEROGENIC oxLDL TO phosphoACC IN PLATELETS. As inflammatory cytokines may affect platelets (14) and are established circulating actors of atherosclerosis, we explored whether interleukin-1beta, interleukin-6, interleukin-10, interleukin-17A, and tumor necrosis

FIGURE 3 Continued

(A) Representative Western blot of platelet acetyl-CoA carboxylase phosphorylation on serine 79 (phosphoACC) in 16 consecutive patients from the ACCTHEROMA trial, with negative control (-) corresponding to washed unstimulated platelets from healthy volunteers and positive control (+) corresponding to washed platelets from healthy volunteers stimulated with thrombin (0.5 U/ml) for 2 min. Four different controls are shown on the Western blot. **(B)** PhosphoACC quantification in N-CAD and CAD patients. **Dotted line** represents the threshold value of 0.5 arbitrary units (AU) estimated from receiver-operating characteristic curve analysis for discriminating between N-CAD and CAD patients. Positive predictive values (PPVs) of this threshold for CAD are indicated on the graph. **Red dots** (N-CAD, reference population) and **triangles** (CAD patients) represent individual values. Medians with interquartile range are presented. **(C)** Boxplot representation of platelet phosphoACC quantifications in N-CAD and CAD subgroups. **(D)** Clinical and angiographic characteristics of patients across the different quartiles of platelet phosphoACC. Distribution of platelet phosphoACC quartiles across **(E)** CAC Agatston score groups and **(F)** AoC score tertiles. The statistical differences between the groups were determined using the Mann-Whitney *U* test in **B**, Kruskal-Wallis test in **C**, and chi-square test in **D to F**. ACCTHEROMA = prospective evaluation of Acetyl-CoA Carboxylase phosphorylation state in platelets as a marker of atherothrombotic coronary and extra-coronary artery disease; M = molecular weight marker; Q = quartile; other abbreviations as in Figures 1 and 2.

TABLE 3 Factors Associated With Increased Platelet phosphoACC in CAD Patients (>0.5 AU Threshold)

	OR (95% CI)	p Value
Aspirin treatment	1.16 (0.54–2.51)	0.70
DAPT	1.50 (0.68–3.34)	0.32
D-dimer (log transformed)	0.62 (0.20–1.94)	0.41
hsCRP (log transformed)	1.00 (0.58–1.71)	0.99
Non-HDL	1.00 (0.99–1.01)	0.53
TG	1.00 (1.00–1.01)	0.048*
HDL	0.97 (0.96–1.00)	0.043*
TG/HDL-C ratio (log transformed)	3.97 (1.25–12.61)	0.019*

*Statistical significance when p value <0.05.
DAPT = dual antiplatelet therapy; other abbreviations as in Tables 1 and 2.

factor-alpha impacted phosphoACC level in washed platelets from healthy volunteers. Although their respective receptors are present in human platelets (15), none of these cytokines affected platelet phosphoACC (Figure 6A).

We continued our analysis to identify biological mediators of increased platelet phosphoACC in the CAD group (above 0.5 AU) (Figure 3B). Whereas high-sensitivity C-reactive protein and ThG markers were not associated with increased phosphoACC, we identified a striking positive association between TG/HDL-C and platelet phosphoACC, suggesting atherogenic lipids to affect phosphoACC in circulating platelets (OR: 4.0; 95% CI: 1.3 to 12.6; p = 0.019) (Table 3). TG/HDL-C ratio, a well-known atherogenic marker, indicates LDL particle size (16), while TGs were shown to correlate with plasma oxLDL levels (17). In our cohort of patients, TG/HDL-C ratio correlated with oxLDL levels (Rp = 0.23; p = 0.002). We thus studied the effect of oxLDL on AMPK-ACC signaling. PhosphoACC was assessed in platelets from healthy volunteers treated with copper-oxidized LDL and myeloperoxidase-oxidized LDL. Both induced a time- and dose-dependent increase in platelet phosphoACC (Figures 6B to 6D, Supplemental Figure 7A). Myeloperoxidase-oxidized LDL-induced phosphoACC was prevented by preincubating platelets with a blocking anti-CD36 antibody (Figure 6E). Accordingly, oxidized choline glycerophospholipids ($OxPC^{CD36}$), a specific high-affinity ligand for CD36, increased platelet phosphoACC (Figure 6F).

FIGURE 4 Kaplan-Meier Curves for Ischemic Events According to Platelet PhosphoACC Levels

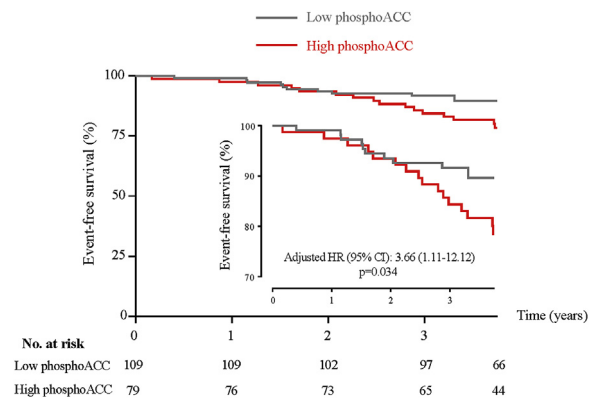

Ischemic events include cardiovascular death, recurrent myocardial infarction and revascularization procedures. Low and high phosphoACC defined according to threshold of 0.5 AU. CI = confidence interval; HR = hazard ratio; other abbreviations as in Figures 1 and 3.

LIPIDOMIC PROFILING OF CIRCULATING PLATELETS AND METABOLIC REGULATION OF INTRAPLATELET TG LEVELS BY phosphoACC IN CAD PATIENTS. We investigated the impact of ACC phosphorylation or inhibition on platelet lipid composition through unbiased lipidomic analysis. To this end, we selected platelet lysates from patients displaying the lowest and highest phosphoACC levels. Baseline characteristics of these patients are provided in Supplemental Table 3. Multivariable regression analysis first showed that diabetes and plasma TG levels were independently associated with up-regulation of intraplatelet TG lipid species. Of the 490 TG lipid species detected within platelets, 253 (52%) were significantly up-regulated (Figure 7A) when plasma TG levels increased. Contrarily, increased phosphoACC was independently associated with significant down-regulation of 66 (14%) intraplatelet TGs (Figure 7B, Supplemental Table 4). This was confirmed by lipid class enrichment analysis revealing a significant proportion of down-regulated lipid species belonging to TG class in platelets of patients with high phosphoACC levels (OR: 27.0; 95% CI: 7.1 to 228.3; p < 0.001) (Supplemental Figure 8). Furthermore, we characterized changes in fatty-acid-chain composition of TGs. Increased platelet phosphoACC was associated with down-regulation of TGs containing 14 carbons (C14:0, myristic acid) (Figure 7C). These findings support that circulating platelets interact with the hyperlipidemic environment in atherosclerosis and, more importantly, that ACC phosphorylation or inhibition affects endogenous platelet lipid content, by regulating TG lipid species and their fatty-acid-chain composition.

DISCUSSION

This study highlights that platelet phosphoACC is a risk marker in patients with suspected CAD and

FIGURE 5 Increased Platelet PhosphoACC in Atherosclerotic Mice

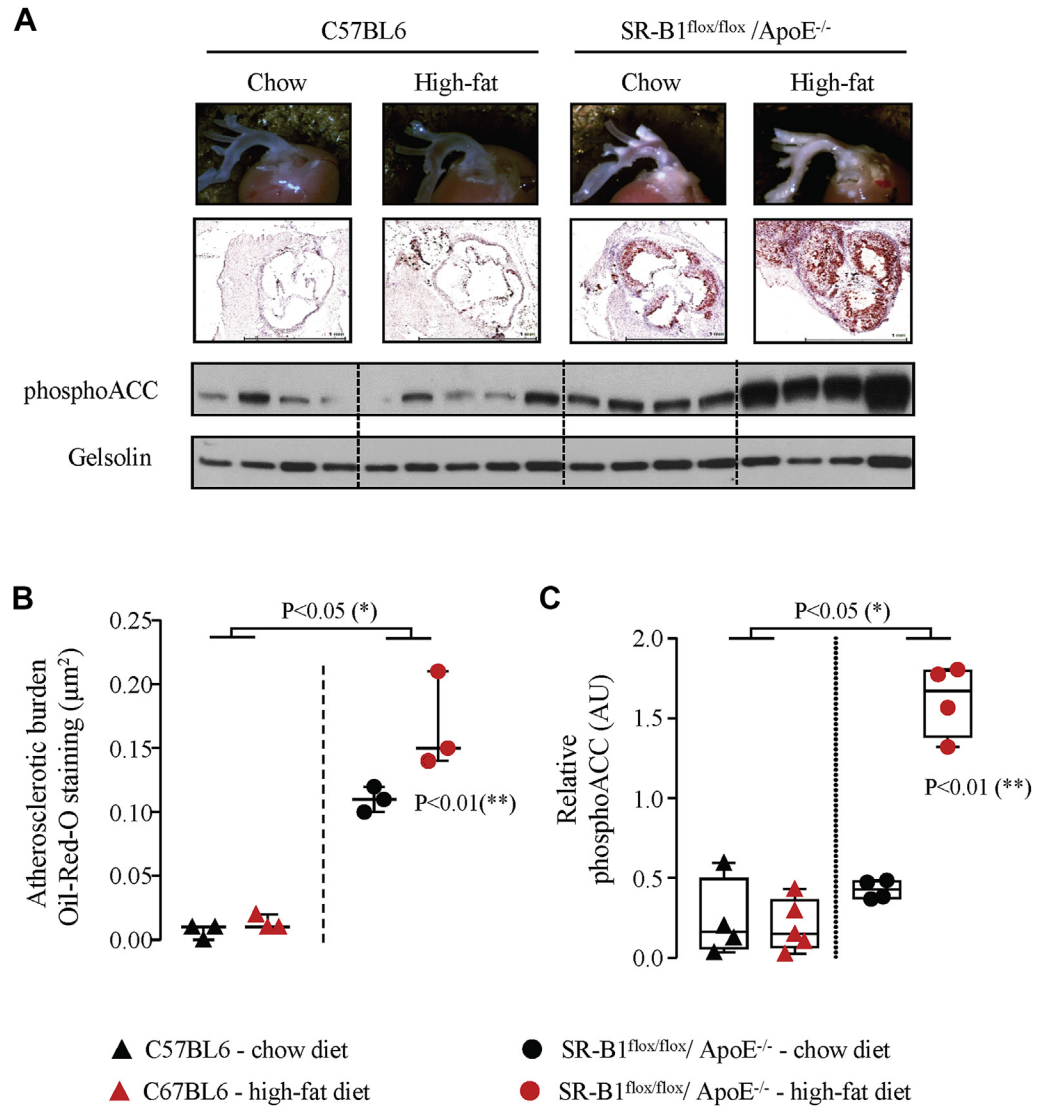

(A-C) Female SR-B1$^{flox/flox}$/ApoE$^{-/-}$ **(dot)** and control C57BL6 **(triangle)** mice received either chow diet for 24 weeks **(black symbols)** or 12 weeks chow diet followed by 12 weeks Western diet **(red symbols)** before sacrifice. Atherosclerotic burden was evaluated by **(A, B)** Oil-Red-O staining of the aortic root and **(A, C)** platelet phosphoACC by Western blot. **(A)** The **top 2 panels** show representative pictures of the aortic root **(top)** and of Oil-Red-O staining after cross section of the aortic root. Scale bar = 1 mm **(bottom).** The **bottom 2 panels** show representative Western blot of platelet phosphoACC. Gelsolin was used as loading control. Quantifications of **(B)** Oil-Red-O staining and **(C)** phosphoACC are shown. Data are represented as **(B)** medians with interquartile range or **(C)** boxplot. **Single asterisk** denotes statistical difference between C57BL6 and SR-B1$^{flox/flox}$/ApoE$^{-/-}$. **Double asterisk** denotes statistical differences between SR-B1$^{flox/flox}$/ApoE$^{-/-}$ under high-fat diet compared with all other groups. Abbreviations as in Figures 1 and 3.

provides additional evidence of an interplay between platelets and lipids in atherosclerosis. We demonstrate a clear relationship between platelet phosphoACC and CAC Agatston score severity, and acute coronary events in CAD. In a molecular point of view, oxLDL participates in increasing phosphoACC in circulating platelets via a CD36-dependent pathway. ACC phosphorylation/inhibition impacts endogenous platelet lipid synthesis by regulating TG lipid species.

PLATELET phosphoACC LEVELS AND RISK ASSESSMENT. Despite the LDL cholesterol-lowering drugs and platelet inhibitors currently available, substantial

FIGURE 6 Oxidized LDLs Induce Platelet phosphoACC in a CD36-Dependent Manner

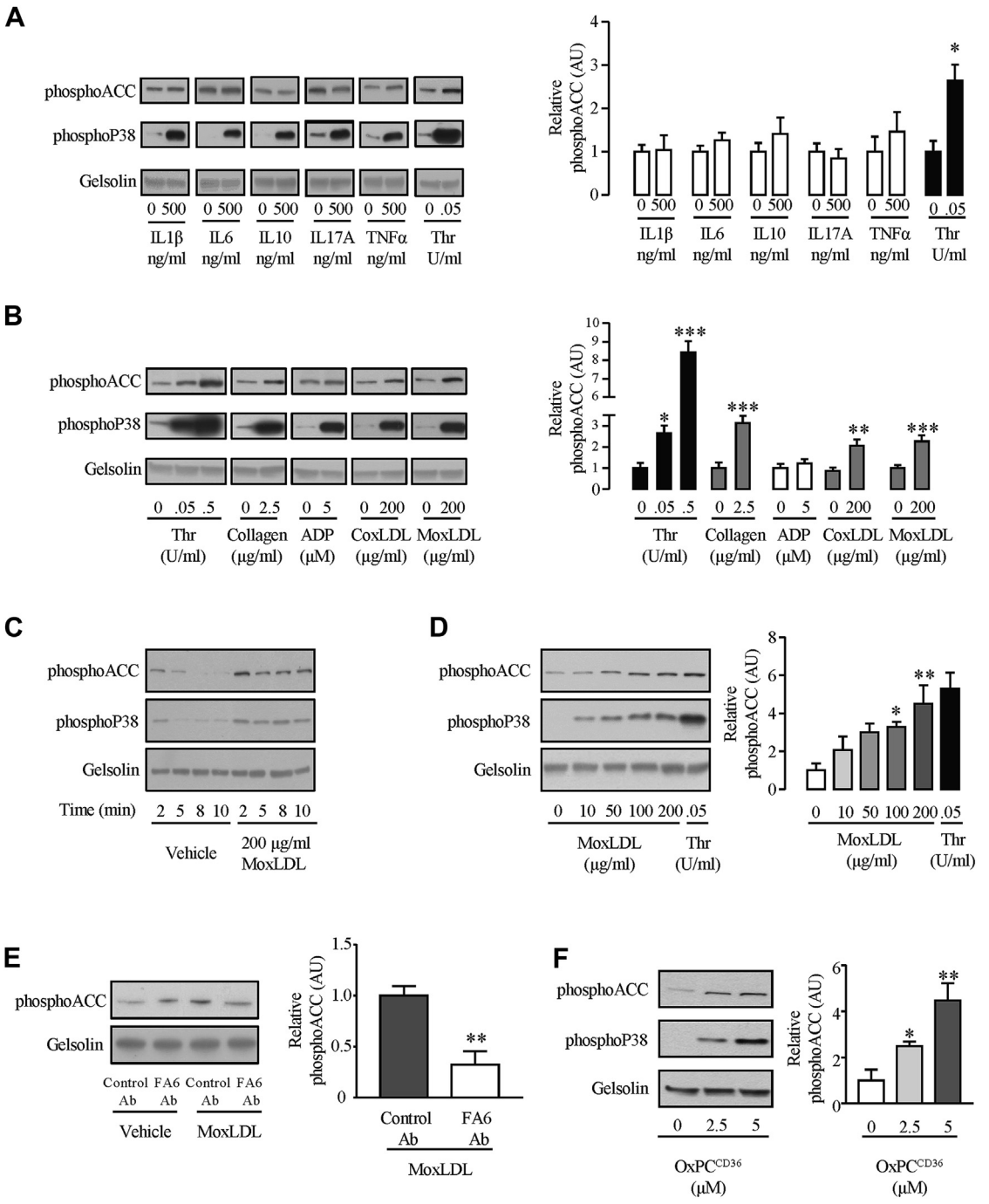

Washed platelets (4.0×10^8/ml) from healthy volunteers were **(A)** treated with the following selected cytokines (interleukin-1beta [IL1β], IL-6, IL-10, IL-17A, and tumor necrosis factor alpha [TNFα]) and **(B)** stimulated with thrombin (Thr), collagen, adenosine diphosphate (ADP), copper-oxidized low-density lipoprotein (coxLDL) or myeloperoxidase-oxidized low-density lipoprotein (moxLDL) before lysis. **(C)** Time course and **(D)** dose-response curve of effect of moxLDL on phosphoACC. **(E)** Platelets were pretreated with 0.2 U/ml anti-CD36 antibody (FA6-152) (FA6 Ab) or an isotype control (control Ab) for 15 min before stimulation with moxLDL. **(F)** Platelets were stimulated with varying concentrations of a specific CD36 ligand ($OxPC^{CD36}$) for 5 min before lysis. All experiments were carried out at least 4 times (biological replicates). Thr-stimulated platelets were used as a positive control. Gelsolin was the loading control. Representative Western blots are shown, with quantification of Western blots represented in the right-hand panels. Data are expressed as mean ± SEM. Significance was determined by **(A, B, E)** 2-tailed Student's *t*-test or (**B** [Thr], **D**, **F**) 1-way analysis of variance with Bonferroni post hoc analysis. *$p < 0.05$, **$p < 0.01$, ***$p < 0.001$ compared with unstimulated platelets. Ab = antibody; $OxPC^{CD36}$ = oxidized choline glycerophospholipids; other abbreviations as in Figure 3.

FIGURE 7 **PhosphoACC Regulates TG Lipid Species in Platelets of CAD Patients**

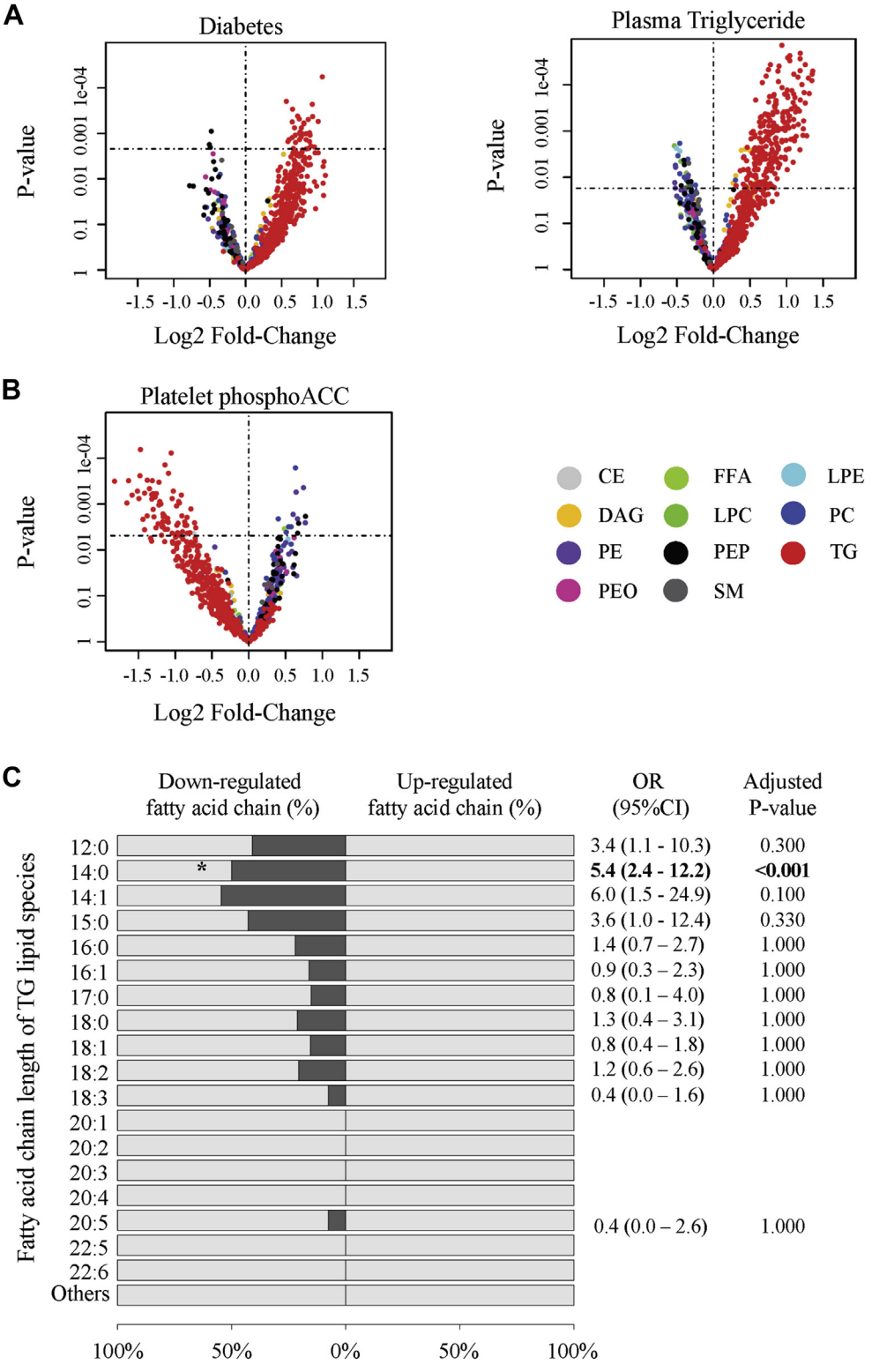

Continued on the next page

residual risk remains (18), and many patients should be given more aggressive treatment (3,19). These patients must be identified by measurable risk markers. Our study brings platelet phosphoACC to the fore as a marker for identifying high-risk patients. More importantly, higher phosphoACC states were detected in platelets of ACS patients, even if treated with aspirin, $P2Y_{12}$ inhibitors, or statins. The long-term influence of treatments on platelet phosphoACC remains to be determined in this high-risk population.

Numerous studies have reported that high on-treatment platelet reactivity and platelet activation indices reveal high-risk patients in CAD population (20). Particularly, increased circulating activated platelets, evidenced by monocyte- or neutrophil-platelet aggregates or P-selectin expression, can be detected in high-risk patients versus normal subjects. However, this increase is marginal and involves a small proportion of the total platelet pool (21–23). In our study, AMPK-ACC signaling activation was observed in circulating platelets. The absence of protein kinase C substrate phosphorylation, a sign of platelet activation (24), supports the theory that increased phosphoACC and platelet activation are unrelated. Even if thrombin is the principal agonist of platelet AMPK activation ex vivo (4), we found no association between ThG markers and phosphoACC. Therefore, platelet phosphoACC is not caused by thrombin-induced platelet activation in patients. Thus, our findings suggest that platelets of high-risk CAD patients exhibit altered metabolic phenotypes characterized by activation of AMPK-ACC signaling, independent of platelet activation state.

LIPID-PLATELET INTERACTION. Changes in LDL phenotypes, such as tendency to aggregate, oxidative status, or size and density, influence cardiovascular risk and can determine residual post-treatment risk (25,26). In line with previous studies (10), our work further supports that this atherogenic environment influences platelet phenotype in CAD. A novel finding of our study is the significant positive correlation between platelet phosphoACC and TG/HDL-C ratio, a marker of a proatherogenic lipid profile, including small LDL particles known to be more oxidizable (16,17). Based on our data, oxLDL mediates, at least in part, the phosphoACC increase in CAD patients. PhosphoACC in response to oxLDL occurs downstream of CD36. Numerous in vitro studies suggested that oxLDL binds to platelet CD36 promoting intracellular signals, including the recruitment of Src family kinases Fyn and Lyn (27), cytoskeleton rearrangement (7), and nicotinamide adenine dinucleotide phosphate oxidase activation (28). Interestingly, an increased binding of oxLDL on platelets has been reported in patients with ACS, in line with our observation (29). Additionally, CD36 is an established receptor for platelet interaction with atherogenic environments, and CD36 expression variability may determine platelet reactivity and thrombotic risk (5,6).

ACC AND PLATELET LIPID CONTENT. Given the central role of ACC in lipid biosynthesis, we performed lipidomic profiling to investigate the impact of its phosphorylation/inhibition on lipid content. Plasma TG levels were associated with an up-regulation of TG lipid species in platelets of CAD patients, highlighting the strong interaction between platelets and plasma lipids. Our results corroborate recent data revealing platelet lipid content to be altered in ACS patients (10). We further demonstrated that increased platelet phosphoACC in high-risk CAD patients is associated with platelet TG down-regulation, reflecting the inhibitory impact of phosphoACC on platelet lipid synthesis. Similar findings were reported in hepatocytes, where liver-specific pharmacological inhibition of ACC lowered lipogenesis and reduced liver TG (30). The down-regulation of fatty acid chains containing 14 carbons (C14:0, myristic acid) provides further evidence that endogenous platelet lipid synthesis is altered upon ACC phosphorylation. In line with our data, ACC inhibition in cancer cells decreases de novo fatty acid synthesis, leading to a reduction in fatty acids containing 14 to 18 carbons (31). To our knowledge, this is the first

FIGURE 7 Continued

(A, B) Volcano plot representations of the 865 lipid species detected in platelets by lipidomic profiling. Log fold-changes and p values were calculated from the multivariate regression model. Lipids above the horizontal dotted line were up- or down-regulated with significant adjusted p values. Relationship among **(A)** diabetic status and plasma triglyceride (TG) levels and **(B)** platelet phosphoACC and intraplatelet lipid species content. **(C)** Class enrichment analysis of fatty-acid-chain constituents of TG lipid species in platelets with respect to increased phosphoACC. **Bars (dark gray)** represent the percentage of down-regulated fatty acid-containing TG. Odds ratio (OR) and adjusted p values derived from Fisher's exact test are shown. CE = cholesterol ester; CI = confidence interval; DAG = diacylglycerol; FFA = free fatty acid; LPC = lysophosphatidylcholine; LPE = lysophosphatidylethanolamine; OR = odds ratio; PC = phosphatidylcholine; PE = phosphatidylethanolamine; PEO = plasmenyl phosphatidylethanolamine; PEP = plasmalogen phosphatidylethanolamine; SM = sphingomyelin; other abbreviations as in Figure 3.

study to report the impact of ACC phosphorylation/inhibition on the regulation of lipid content in circulating platelets of CAD patients.

STUDY LIMITATIONS. First, phosphoACC was determined using immunoblotting in whole platelet lysates. Given the circulating platelets' heterogeneity (32), it is still unclear whether increased phosphoACC occurs in the entire platelet population or in a subgroup only. Moreover, in this setting, platelets must be purified before phosphoACC is measured, and quantitative assessment of phosphoACC remains challenging. However, we employed a more quantitative method, electrochemiluminescence immunoassay, to confirm the phosphoACC increase. Second, the ACCTHEROMA trial was a single-center trial, with a limited patient number. This sample size allowed us to fully address our primary endpoint (i.e., increase in phosphoACC in CAD patients). However, despite this limited number of patients, we identified phosphoACC as an independent predictor for adverse cardiac events and more particularly ischemic events, during follow-up, reinforcing the link between phosphoACC and disease severity. Multicenter studies may be required to validate the prognostic impact of increased phosphoACC in peripheral blood and determine signal variability over time, as with LDL cholesterol (25).

CONCLUSIONS

Our study identifies platelet phosphoACC as a risk stratification marker that reflects the interaction between proatherogenic lipids and circulating platelets. In CAD patients, phosphoACC contributed to regulating endogenous lipid synthesis. We recently provided new insights into AMPK-ACC signaling's key role in regulating platelet lipid composition and function using a genetic mouse model. The absence of phosphoACC (and inhibition) by AMPK in platelets resulted in increased phospholipid content, with enhanced platelet reactivity and thrombus formation. It is tempting to speculate that increased phosphoACC is a counter-regulatory mechanism limiting lipogenesis and platelet reactivity in CAD patients within a proatherogenic environment.

ACKNOWLEDGMENTS The authors wish to thank professors Patrick Chenu, Olivier Gurné, and Jean Renkin for their support in collecting blood samples upon coronary angiography.

ADDRESS FOR CORRESPONDENCE: Dr. Christophe Beauloye, Division of Cardiology, Cliniques Universitaires Saint-Luc, Pôle de Recherche Cardiovasculaire, Institut de Recherche Expérimentale et Clinique (IREC), Université catholique de Louvain, Avenue Hippocrate, 55 (B1.55.05), 1200 Brussels, Belgium. E-mail: christophe.beauloye@uclouvain.be.

PERSPECTIVES

COMPETENCY IN MEDICAL KNOWLEDGE: The circulating platelets of high-risk CAD patients exhibit altered metabolic phenotypes characterized by phosphorylation and inhibition of ACC, the first committed enzyme of the fatty acid biosynthesis pathway. Platelet phosphoACC is thus a potential marker for risk stratification in suspected CAD patients, indicating an interplay between platelets and atherogenic lipids.

TRANSLATIONAL OUTLOOK 1: Additional studies are needed to further define the role of endogenous lipogenesis in the control of platelet function.

TRANSLATIONAL OUTLOOK 2: Large multicenter studies must investigate whether individual platelet phenotypes, including phosphoACC, influences major adverse outcomes in CAD.

REFERENCES

1. Mastenbroek TG, van Geffen JP, Heemskerk JW, Cosemans JM. Acute and persistent platelet and coagulant activities in atherothrombosis. J Thromb Haemost 2015;13 Suppl 1:S272–80.

2. Merlini PA, Bauer KA, Oltrona L, et al. Persistent activation of coagulation mechanism in unstable angina and myocardial infarction. Circulation 1994;90:61–8.

3. Eikelboom JW, Connolly SJ, Bosch J, et al. Rivaroxaban with or without aspirin in stable cardiovascular disease. N Engl J Med 2017;377:1319–30.

4. Onselaer MB, Oury C, Hunter RW, et al. The Ca(2+) /calmodulin-dependent kinase kinase beta-AMP-activated protein kinase-alpha1 pathway regulates phosphorylation of cytoskeletal targets in thrombin-stimulated human platelets. J Thromb Haemost 2014;12:973–86.

5. Podrez EA, Byzova TV, Febbraio M, et al. Platelet CD36 links hyperlipidemia, oxidant stress and a prothrombotic phenotype. Nat Med 2007;13:1086–95.

6. Ghosh A, Murugesan G, Chen K, et al. Platelet CD36 surface expression levels affect functional responses to oxidized LDL and are associated with inheritance of specific genetic polymorphisms. Blood 2011;117:6355–66.

7. Wraith KS, Magwenzi S, Aburima A, Wen Y, Leake D, Naseem KM. Oxidized low-density lipoproteins induce rapid platelet activation and shape change through tyrosine kinase and Rho kinase-signaling pathways. Blood 2013;122:580–9.

8. Dyck JR, Kudo N, Barr AJ, Davies SP, Hardie DG, Lopaschuk GD. Phosphorylation control of cardiac acetyl-CoA carboxylase by cAMP-dependent protein kinase and 5'-AMP activated protein kinase. Eur J Biochem 1999;262:184–90.

9. Lepropre S, Kautbally S, Octave M, et al. AMPK-ACC signaling modulates platelet phospholipids

content and potentiates platelet function and thrombus formation. Blood 2018;132:1180–92.

10. Chatterjee M, Rath D, Schlotterbeck J, et al. Regulation of oxidized platelet lipidome: implications for coronary artery disease. Eur Heart J 2017;38:1993–2005.

11. Greenland P, Blaha MJ, Budoff MJ, Erbel R, Watson KE. Coronary calcium score and cardiovascular risk. J Am Coll Cardiol 2018;72:434–47.

12. Stacklies W, Redestig H, Scholz M, Walther D, Selbig J. pcaMethods–a bioconductor package providing PCA methods for incomplete data. Bioinformatics 2007;23:1164–7.

13. Benjamini Y, Hochberg Y. Controlling the false discovery rate: a practical and powerful approach to multiple testing. J R Stat Soc Series B Stat Methodol 1995;57:289–300.

14. Beaulieu LM, Lin E, Mick E, et al. Interleukin 1 receptor 1 and interleukin 1beta regulate megakaryocyte maturation, platelet activation, and transcript profile during inflammation in mice and humans. Arterioscler Thromb Vasc Biol 2014;34:552–64.

15. Rowley JW, Oler AJ, Tolley ND, et al. Genome-wide RNA-seq analysis of human and mouse platelet transcriptomes. Blood 2011;118:e101–11.

16. Hanak V, Munoz J, Teague J, Stanley A Jr., Bittner V. Accuracy of the triglyceride to high-density lipoprotein cholesterol ratio for prediction of the low-density lipoprotein phenotype B. Am J Cardiol 2004;94:219–22.

17. Harmon ME, Campen MJ, Miller C, et al. Associations of circulating oxidized LDL and conventional biomarkers of cardiovascular disease in a cross-sectional study of the Navajo population. PLoS One 2016;11:e0143102.

18. Kaasenbrood L, Boekholdt SM, van der Graaf Y, et al. Distribution of estimated 10-year risk of recurrent vascular events and residual risk in a secondary prevention population. Circulation 2016;134:1419–29.

19. Sabatine MS, Giugliano RP, Keech AC, et al. Evolocumab and clinical outcomes in patients with cardiovascular disease. N Engl J Med 2017;376:1713–22.

20. Gurbel PA, Becker RC, Mann KG, Steinhubl SR, Michelson AD. Platelet function monitoring in patients with coronary artery disease. J Am Coll Cardiol 2007;50:1822–34.

21. Michelson AD, Barnard MR, Krueger LA, Valeri CR, Furman MI. Circulating monocyte-platelet aggregates are a more sensitive marker of in vivo platelet activation than platelet surface P-selectin: studies in baboons, human coronary intervention, and human acute myocardial infarction. Circulation 2001;104:1533–7.

22. Linden MD, Furman MI, Frelinger AL 3rd., et al. Indices of platelet activation and the stability of coronary artery disease. J Thromb Haemost 2007;5:761–5.

23. Stellos K, Bigalke B, Stakos D, Henkelmann N, Gawaz M. Platelet-bound P-selectin expression in patients with coronary artery disease: impact on clinical presentation and myocardial necrosis, and effect of diabetes mellitus and anti-platelet medication. J Thromb Haemost 2010;8:205–7.

24. Konopatskaya O, Gilio K, Harper MT, et al. PKCalpha regulates platelet granule secretion and thrombus formation in mice. J Clin Invest 2009;119:399–407.

25. Ruuth M, Nguyen SD, Vihervaara T, et al. Susceptibility of low-density lipoprotein particles to aggregate depends on particle lipidome, is modifiable, and associates with future cardiovascular deaths. Eur Heart J 2018;39:2562–73.

26. Laufs U, Weingartner O. Pathological phenotypes of LDL particles. Eur Heart J 2018;39:2574–6.

27. Chen K, Febbraio M, Li W, Silverstein RL. A specific CD36-dependent signaling pathway is required for platelet activation by oxidized low-density lipoprotein. Circ Res 2008;102:1512–9.

28. Magwenzi S, Woodward C, Wraith KS, et al. Oxidized LDL activates blood platelets through CD36/NOX2-mediated inhibition of the cGMP/protein kinase G signaling cascade. Blood 2015;125:2693–703.

29. Stellos K, Sauter R, Fahrleitner M, et al. Binding of oxidized low-density lipoprotein on circulating platelets is increased in patients with acute coronary syndromes and induces platelet adhesion to vascular wall in vivo-brief report. Arterioscler Thromb Vasc Biol 2012;32:2017–20.

30. Kim CW, Addy C, Kusunoki J, et al. Acetyl CoA carboxylase inhibition reduces hepatic steatosis but elevates plasma triglycerides in mice and humans: a bedside to bench investigation. Cell Metab 2017;26:394–406 e6.

31. Svensson RU, Parker SJ, Eichner LJ, et al. Inhibition of acetyl-CoA carboxylase suppresses fatty acid synthesis and tumor growth of non-small-cell lung cancer in preclinical models. Nat Med 2016;22:1108–19.

32. Ibrahim H, Nadipalli S, Usmani S, DeLao T, Green L, Kleiman NS. Detection and quantification of circulating immature platelets: agreement between flow cytometric and automated detection. J Thromb Thrombolysis 2016;42:77–83.

KEY WORDS AMPK, acetyl-CoA carboxylase, coronary artery disease, lipidomics, platelet

APPENDIX For expanded Methods and References sections as well as supplemental tables and figures, please see the online version of this paper.

JACC: BASIC TO TRANSLATIONAL SCIENCE VOL. 4, NO. 5, 2019

PRECLINICAL RESEARCH

Yes-Associated Protein (YAP) Facilitates Pressure Overload–Induced Dysfunction in the Diabetic Heart

Shohei Ikeda, MD, PhD,[a,b] Risa Mukai, MD, PhD,[a] Wataru Mizushima, MD, PhD,[a] Peiyong Zhai, MD, PhD,[a] Shin-ichi Oka, PhD,[a] Michinari Nakamura, MD, PhD,[a] Dominic P. Del Re, PhD,[a] Sebastiano Sciarretta, MD, PhD,[c,d] Chiao-Po Hsu, MD, PhD,[e] Hiroaki Shimokawa, MD, PhD,[b] Junichi Sadoshima, MD, PhD[a]

VISUAL ABSTRACT

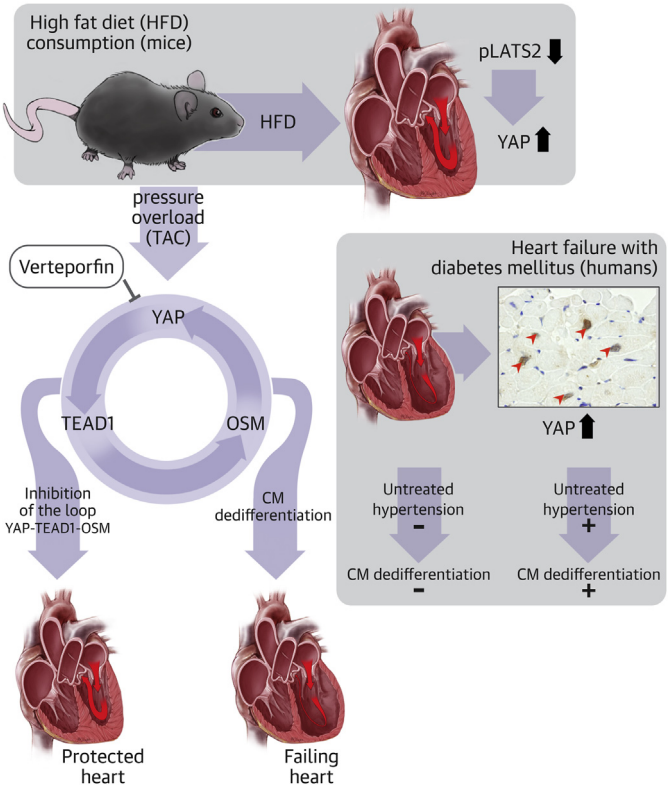

Ikeda, S. et al. J Am Coll Cardiol Basic Trans Science. 2019;4(5):611–22.

HIGHLIGHTS

- **YAP, a terminal effector of the Hippo signaling pathway, is activated in cardiomyocytes in response to high-fat diet consumption in mice and diabetes in patients.**
- **Long-term activation of YAP in response to high-fat diet consumption is detrimental for the heart in the presence of pressure overload.**
- **Detrimental effects of YAP during pressure overload are mediated through activation of a positive feedback loop, consisting of YAP, TEAD1, and OSM, and consequent dedifferentiation of cardiomyocytes.**
- **Chemical inhibitors of YAP, TEAD1, or OSM may be effective in treating patients who have diabetes, high blood pressure, and metabolic syndrome to prevent heart failure syndromes.**

From the [a]Department of Cell Biology and Molecular Medicine, Cardiovascular Research Institute, Rutgers New Jersey Medical School, Newark, New Jersey; [b]Department of Cardiovascular Medicine, Tohoku University Graduate School of Medicine, Sendai, Japan; [c]Department of Medico-Surgical Sciences and Biotechnologies, Sapienza University of Rome, Latina, Italy; [d]Istituto Di Ricovero e Cura a Carattere Scientifico Neuromed, Pozzilli, Italy; and the [e]Division of Cardiovascular Surgery, Department of Surgery, Taipei Veterans General Hospital, National Yang-Ming University School of Medicine, Taiwan. Dr. Sadoshima was supported in part by U.S. Public Health Service grants HL67724, HL91469, HL11233, HL132824, and AG23039, and by the Leducq Foundation Transatlantic Network of Excellence (15CBD04). Dr. Ikeda has been supported by a postdoctoral fellowship from the Japan Heart Foundation/Bayer Yakuhin Research Grant Abroad and grants-in-aid for scientific research (18K15876). All other authors have reported that they have no relationships relevant to the contents of this paper to disclose.

ISSN 2452-302X https://doi.org/10.1016/j.jacbts.2019.05.006

JACC: BASIC TO TRANSLATIONAL SCIENCE VOL. 4, NO. 5, 2019
SEPTEMBER 2019:611–22

ABBREVIATIONS AND ACRONYMS

HF = heart failure

HFD = high-fat diet

Lats2 = large tumor suppressor kinase 2

LV = left ventricular

Mst1 = mammalian sterile 20-like 1

ND = normal diet

OSM = oncostatin M

PO = pressure overload

Runx1 = runt-related transcription factor 1

TAC = transverse aortic constriction

TAZ = transcriptional coactivator with PDZ-binding motif

TEAD = transcriptional enhancer factor

YAP = Yes-associated protein

SUMMARY

Patients with diabetes are more prone to developing heart failure in the presence of high blood pressure than those without diabetes. Yes-associated protein (YAP), a key effector of the Hippo signaling pathway, is persistently activated in diabetic hearts, and YAP plays an essential role in mediating the exacerbation of heart failure in response to pressure overload in the hearts of mice fed a high-fat diet. YAP induced dedifferentiation of cardiomyocytes through activation of transcriptional enhancer factor 1 (TEAD1), a transcription factor. Thus, YAP and TEAD1 are promising therapeutic targets for diabetic patients with high blood pressure to prevent the development of heart failure. (J Am Coll Cardiol Basic Trans Science 2019;4:611–22)

Cardiovascular disease is a major cause of mortality in developed countries (1). Recently, the number of cases of cardiovascular disease associated with metabolic syndrome, such as obesity and diabetes mellitus, has been rapidly increasing worldwide (2). These patients often develop heart failure (HF) with either preserved left ventricular ejection fraction or reduced left ventricular ejection fraction, although metabolic derangements, such as insulin resistance, often favor development of HF with preserved left ventricular ejection fraction in obese patients with type 2 diabetes mellitus (3). Currently, the molecular mechanisms of cardiomyopathy associated with metabolic syndrome remain poorly understood, and thus, no specific treatment exists.

SEE PAGE 623

The Hippo signaling pathway is an evolutionarily conserved signaling pathway involved in organ size control, tissue regeneration, and tumorigenesis through regulation of apoptosis and cell proliferation (4). Major components of the Hippo pathway include upstream serine/threonine kinases, namely, Mst1/2 (mammalian sterile 20-like 1) and Lats1/2 (large tumor suppressor kinase 1 and 2), and downstream nuclear transcription factor cofactors YAP (Yes-associated protein) and TAZ (transcriptional coactivator with PDZ-binding motif), where Mst1/2 and Lats1/2 negatively regulate nuclear levels of YAP and TAZ (4). YAP and TAZ bind to transcription factors, such as TEAD (transcriptional enhancer factor) and FoxO1 (forkhead box O1), thereby regulating a variety of cellular functions, including cell proliferation and cell survival (5). Activation of the Hippo pathway is intimately involved in the pathogenesis of heart disease, including ischemia/reperfusion injury (6,7), cardiac remodeling, and HF (8,9). YAP is also involved in regeneration of the postnatal heart after myocardial infarction (10–12).

It has been proposed that either suppression of the upstream Hippo pathway components or stimulation of YAP can potentially be used as a therapeutic intervention to facilitate repair and regeneration of the heart after acute myocardial infarction (10–12); however, persistent inactivation of the Hippo pathway and consequent activation of YAP induces cardiac dysfunction in the presence of pressure overload (PO) through activation of cardiomyocyte dedifferentiation (13). This suggests that the function of YAP varies drastically depending on the type of stress. An important question remains as to whether persistent activation of YAP occurs in clinically relevant conditions and whether suppression of YAP improves such conditions.

YAP is up-regulated in liver cancer cells in response to high glucose (14) and in diabetic kidney epithelial cells (15). Patients with insulin resistance are more prone to developing hypertension, and the coexistence of diabetes and hypertension facilitates the development of HF (2,16). We asked: 1) whether YAP promotes cardiac dysfunction in response to PO in mice fed a high-fat diet (HFD), a mouse model of type 2 diabetes mellitus; 2) whether the exacerbation of cardiomyopathy in HFD-fed mice in the presence of PO is accompanied by cardiomyocyte dedifferentiation; and 3) whether YAP is up-regulated in the human diabetic heart.

The authors attest they are in compliance with human studies committees and animal welfare regulations of the authors' institutions and Food and Drug Administration guidelines, including patient consent where appropriate. For more information, visit the *JACC: Basic to Translational Science* author instructions page.

Manuscript received March 14, 2019; revised manuscript received April 19, 2019, accepted May 9, 2019.

METHODS

MOUSE MODELS. All animal experiments were conducted in accordance with protocols approved by the Rutgers University Animal Care and Use Committee. The background of all mice was C57BL/6J. Systemic TEAD1$^{+/-}$ mice have been described (13). Age- and sex-matched male littermate mice were used as controls. For HFD treatment, male mice were randomly divided into 2 groups and fed with either normal diet (ND) or HFD for 8 weeks (17). For verteporfin experiments, mice were randomly divided into 2 groups: verteporfin or DMSO control group. Twelve-week-old mice after sham operation or transverse aortic constriction (TAC) were injected intraperitoneally with verteporfin 100 mg/kg every other day for 10 days. To measure arterial pressure gradients, high-fidelity micromanometer catheters (1.4-F, Millar Instruments Inc., Houston, Texas) were used.

TRANSVERSE AORTIC CONSTRICTION. The methods used to impose PO in mice have been described (13). Male mice at 12 weeks of age were randomly divided into 2 groups: PO with TAC or sham operation. We focused on male mice in this study because previous studies of YAP loss of function in the heart conducted in this laboratory also focused on male mice (13). Mice were anesthetized with pentobarbital sodium (60 mg/kg) and mechanically ventilated. The number of animals used is described in each figure legend. Successful application of TAC was confirmed by a transverse aortic velocity above 4 m/s, evaluated by Doppler echocardiography. Mice that died of HF were included in the survival analysis but were excluded from the assessment of cardiac function and histology. There were no unexpected adverse events during the procedure. All operations and analyses were performed in a blinded manner with regard to the genotype of mice.

ECHOCARDIOGRAPHY. Mice were anesthetized using 12 μl/g body weight of 2.5% Avertin (Sigma-Aldrich, St. Louis, Missouri), and echocardiography was performed as described previously (13).

HUMAN SAMPLES FROM EXPLANTED HEARTS.
Samples for immunostaining. The study was approved by the Ethics Committee of Tohoku University Graduate School of Medicine. All patients provided written consent for the use of their heart tissues for research. Myocardial biopsy specimens were obtained from patients with HF in Tohoku University Hospital. Immunostaining was conducted using 66 consecutive observable biopsy specimens obtained from January 2016 to June 2017 (Supplemental Tables 1 and 2). Twenty-five patients were diagnosed with diabetes, and their average glycosylated hemoglobin level was 6.98 ± 0.68% (compared with 5.66 ± 0.32% in patients without diabetes; $p < 0.001$). Biopsy samples were fixed with 10% paraformaldehyde in phosphate-buffered saline (pH 7.4), paraffin embedded, and sectioned.

Samples for immunoblotting. The study was approved by the Ethics Committee of Taipei Veterans General Hospital, and all patients or their families expressed their willingness to participate through an informed consent form. The samples from the left atrial part of explanted hearts used in this study were obtained from patients who had received heart transplants and age-matched donors at the Taipei Veterans General Hospital. Patients with diabetes had their diabetes controlled with oral hypoglycemic agents. Immediately after tissue procurement, the samples for biochemical study were stored in liquid nitrogen and kept at −80°C.

ANTIBODIES AND REAGENTS. The following primary antibodies were used: YAP (Cell Signaling, #14074, Cell Sugnaling Technology, Danvers, Massachusetts), phospho-YAP (Ser127) (Cell Signaling, #4911), LATS2 (Bethyl Laboratories, #A300-479A, Bethyl Laboratories, Montgomery, Texas), phospho-LATS2 (Thr1041) (Cell Signaling, #8654), atrial natriuretic peptide (Abcam, #ab180649, Abcam, Cambridge, United Kingdom), TEAD1 (Sigma-Aldrich, #AV39521), MYH7 (Sigma-Aldrich, # M8421), ACTA2 (Sigma-Aldrich, #A5228), OSM (Santa Cruz, #sc374039, Santa Cruz Biotechnology, Dallas, Texas), OSMR (Santa Cruz, #sc30011), cardiac troponin T antibody (Abcam, #ab33589), sarcomeric actinin (Abcam, #ab68167), CD45 (Abcam, #ab10558), CD68 (Abcam, #ab31630), Ly6G (Abcam, #ab25377), and α-tubulin (Sigma-Aldrich, #T6199). Immunoblot analyses and histological analyses were conducted as described previously (13).

REAL-TIME QUANTITATIVE POLYMERASE CHAIN REACTION. Primers used have been described previously (13). Quantitative real-time polymerase chain reaction was performed on the CFX 96 Real-Time PCR Detection System (Bio-Rad Laboratories, Hercules, California). The cycle threshold (Ct) value determined with CFX Manager Software version 2.0 (Bio-Rad) for all samples was normalized to *Gapdh*, and the relative fold change was computed by the comparative Ct (ΔΔCt) method.

STATISTICAL ANALYSIS. Continuous data are presented as mean ± SEM or mean ± SD and visualized using bar graphs or box plots. In box plots, whiskers show minimum and maximum values, whereas bars represent the median and 25th and 75th percentiles. Sample sizes were determined using standard

FIGURE 1 HFD Induces Cardiac Activation of YAP in Mice

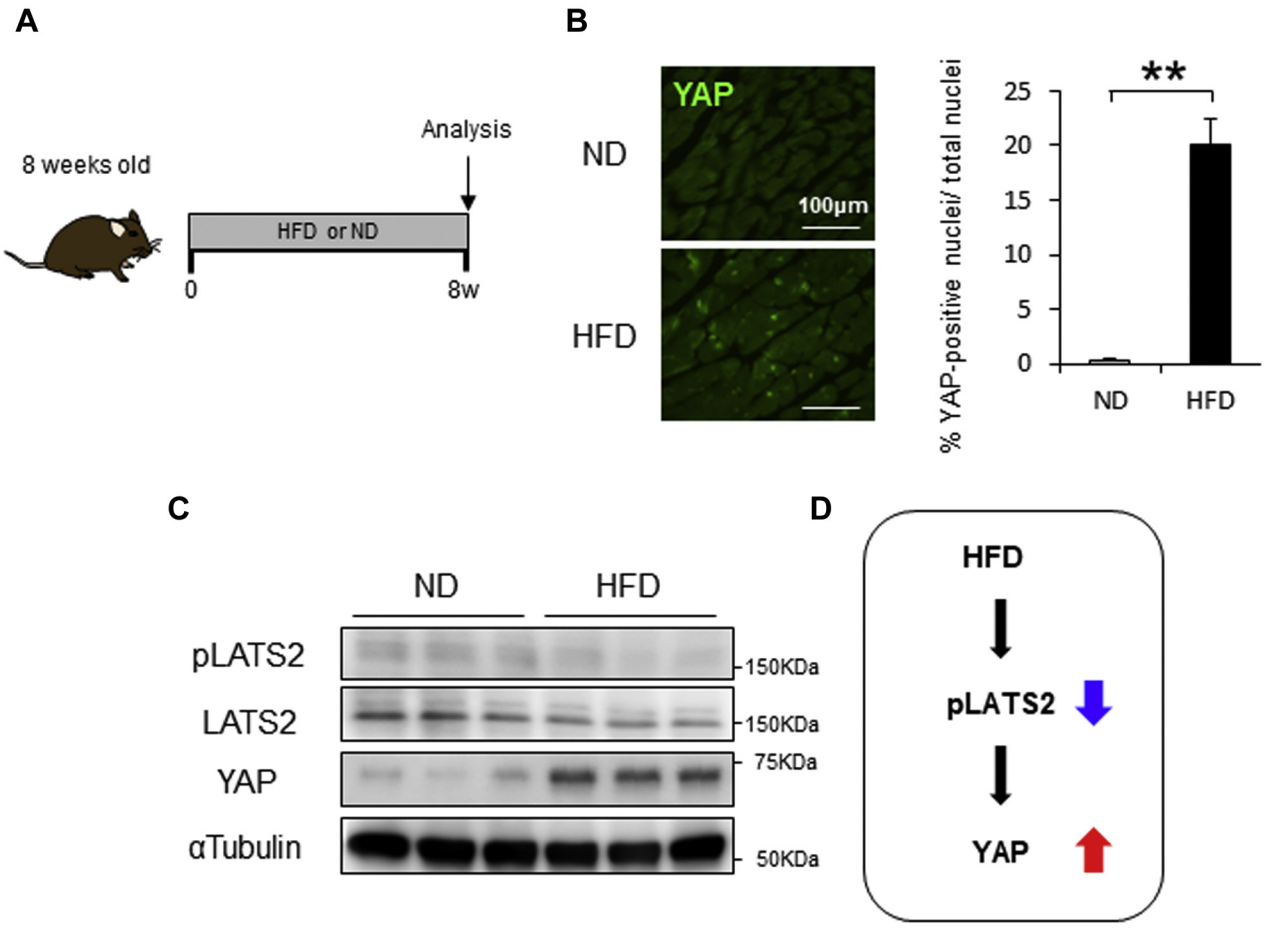

(A) Schematic representation of the experimental protocol. Mice were fed with either normal diet (ND) or high-fat diet (HFD) for 8 weeks. **(B)** Representative immunostaining of Yes-associated protein (YAP). Quantitative analysis is shown on the right (n = 6, each). **(C)** Representative gel pictures in the heart. **(D)** Effect of Hippo pathway by HFD feeding. All results are mean ± SEM. **p < 0.01 by analysis of variance.

power analysis (statistical power ≥0.8, and α <0.05). Indicated sample size (in Figure legends) always refers to biological replicates (independent animals). No data were excluded from statistical analyses. Unless otherwise stated, statistical testing was performed with statistical analysis software (Excel Tokei 2015, Social Survey Research Information Co., Ltd., Tokyo, Japan). Student's *t*-test (paired or unpaired, as appropriate) and analysis of variance followed by Tukey's honest significant difference tests were used for comparisons between 2 or multiple groups, respectively. Survival curves were analyzed by Kaplan-Meier log-rank test. In Supplemental Figure 4, Student's *t*-test and chi-square test were used to compare 2 quantitative variables. A p value of <0.05 was considered statistically significant.

RESULTS

YAP WAS ELEVATED IN THE HEARTS OF HFD-FED MICE. Consumption of a HFD by mice induces weight gain and insulin resistance, which in turn causes cardiac hypertrophy and diastolic dysfunction (17), mimicking diabetic cardiomyopathy in humans. HFD treatment for 8 weeks induced cardiac hypertrophy, as indicated by increases in heart weight/tibial length, cardiomyocyte cross-sectional area, and protein or mRNA expression of fetal-type genes, including ANP (atrial natriuretic peptide) and BNP (brain natriuretic peptide) (**Figure 1A**, Supplemental Figure 1). Immunostaining of heart sections showed that consumption of HFD significantly increased the number of cardiomyocytes with YAP-positive nuclei (**Figure 1B**). Immunoblot analyses confirmed that the

level of total YAP protein was also increased in the hearts of mice fed HFD (**Figure 1C**). Furthermore, consumption of HFD for 8 weeks significantly down-regulated the level of phospho-Lats2, which suggests that this model mimics Hippo deficiency (**Figure 1C**, Supplemental Figure 2). Echocardiographic measurements (Supplemental Table 3) and hemodynamic measurements (Supplemental Table 4) indicated that consumption of HFD for 8 weeks did not induce systolic cardiac dysfunction, consistent with our previous results (17).

PO INDUCED LEFT VENTRICULAR DYSFUNCTION WITH CARDIOMYOCYTE DE-DIFFERENTIATION IN HFD-FED MICE. Superimposition of high blood pressure on metabolic syndrome or diabetes mellitus dramatically facilitates the development of HF in humans (2,16,18). We have shown previously that up-regulation of YAP alone in mice with a loss of Hippo function exacerbates PO-induced cardiac dysfunction through a YAP-TEAD1-oncostatin M (OSM)-dependent mechanism, which is accompanied by induction of cardiomyocyte dedifferentiation (13). We therefore evaluated whether PO-induced cardiac dysfunction is exacerbated in mice fed an HFD. To this end, we fed mice an HFD or ND for 4 weeks, subjected the mice to either TAC or sham operation while being fed the same diet, and then conducted analyses at 8 weeks (**Figure 2A**).

TAC dramatically facilitated the progression of LV dysfunction, as indicated by decreases in fractional shortening and increases in LV end-diastolic dimension and death, in HFD-fed mice compared with mice that consumed an ND (**Figures 2B to 2D**). In HFD-fed mice, YAP was elevated with or without TAC, and expression of MYH7, ACTA2, and RUNX1, markers of cardiomyocyte dedifferentiation, was increased in the presence of TAC (**Figure 2E**, Supplemental Figure 3). Taken together, these observations suggest that dedifferentiation is facilitated by HFD consumption in the presence of PO, mimicking the cardiac phenotype of WW45cKO (homozygous knockout of WW45) mice in the presence of PO (13), in which both systolic dysfunction and cardiomyocyte dedifferentiation are exacerbated compared with in control mice.

VERTEPORFIN TREATMENT IMPROVED CARDIAC FUNCTION AND SURVIVAL RATE OF HFD-FED MICE AFTER PO. To evaluate the role of endogenous YAP in the development of cardiomyopathy in HFD-fed mice during PO, mice were treated with either verteporfin or vehicle (**Figure 3A**). Verteporfin is a benzoporphyrin derivative that is clinically available for photodynamic therapy. It disrupts the interaction between YAP and TEADs and is thus used as a specific inhibitor of YAP (13). We treated mice with verteporfin during the first 10 days after TAC. Verteporfin significantly improved the survival rate of HFD-fed mice after PO compared with vehicle treatment (**Figure 3B**). Furthermore, although verteporfin exacerbated TAC-induced LV dysfunction and dilation in ND-fed mice, as indicated by decreased fractional shortening, increased lung congestion, and increased LV end-diastolic dimension, it significantly normalized TAC-induced cardiac dysfunction and LV dilation (**Figures 3C to 3E**), as well as the increased expression of MYH7, ACTA2, and RUNX1 (**Figure 3F**, Supplemental Figure 4), in mice with HFD plus PO. These results suggest that YAP plays a crucial role in facilitating cardiac dysfunction in the presence of HFD consumption plus high blood pressure. Obesity induces low-grade systemic inflammation, which in turn promotes the development of cardiomyopathy (19). Thus, we evaluated the effect of verteporfin on inflammatory responses in the heart in the presence of HFD consumption with or without PO. Myocardial infiltration of CD45-positive cells (leukocytes), CD68-positive cells (macrophages), and Ly6G-positive cells (neutrophils) was enhanced by HFD plus PO, but the infiltration was significantly attenuated in the presence of verteporfin (Supplemental Figure 5).

TEAD1 HAPLOINSUFFICIENCY ATTENUATES PO-INDUCED CARDIAC DYSFUNCTION IN HFD-FED MICE. Because TEAD is a major transcription factor mediating the effect of YAP (5), we hypothesized that HFD-fed mice develop more severe HF in the presence of PO through a TEAD-dependent mechanism. To test this hypothesis, we investigated the effect of HFD consumption combined with TAC in TEAD1 heterozygous knockout mice (13). PO induced less severe LV dysfunction in HFD-fed TEAD1$^{+/-}$ mice than in HFD-fed control mice (**Figures 4A to 4D**, Supplemental Figures 6 and 7). The TAC-induced up-regulation of OSM and YAP in HFD-treated control hearts was attenuated in HFD-treated TEAD1$^{+/-}$ hearts, consistent with the notion that the YAP-TEAD1-OSM pathway forms a positive feedback mechanism (**Figure 4E**). HFD-fed TEAD1$^{+/-}$ mice exhibited lower expression of MYH7, ACTA2, and RUNX1, which indicates that PO-induced activation of TEAD1 in HFD-fed mice plays an important role in mediating cardiomyocyte dedifferentiation (**Figure 4E**).

YAP EXPRESSION WAS ELEVATED IN THE HEARTS OF PATIENTS WITH HF WITH DIABETIC CARDIOMYOPATHY. We investigated whether YAP is up-regulated in the hearts of HF patients with diabetes. Using myocardial biopsy specimens obtained from HF patients,

FIGURE 2 Up-Regulation of YAP Contributes to the Development of Cardiac Dysfunction in Response to Pressure Overload in the Presence of HFD

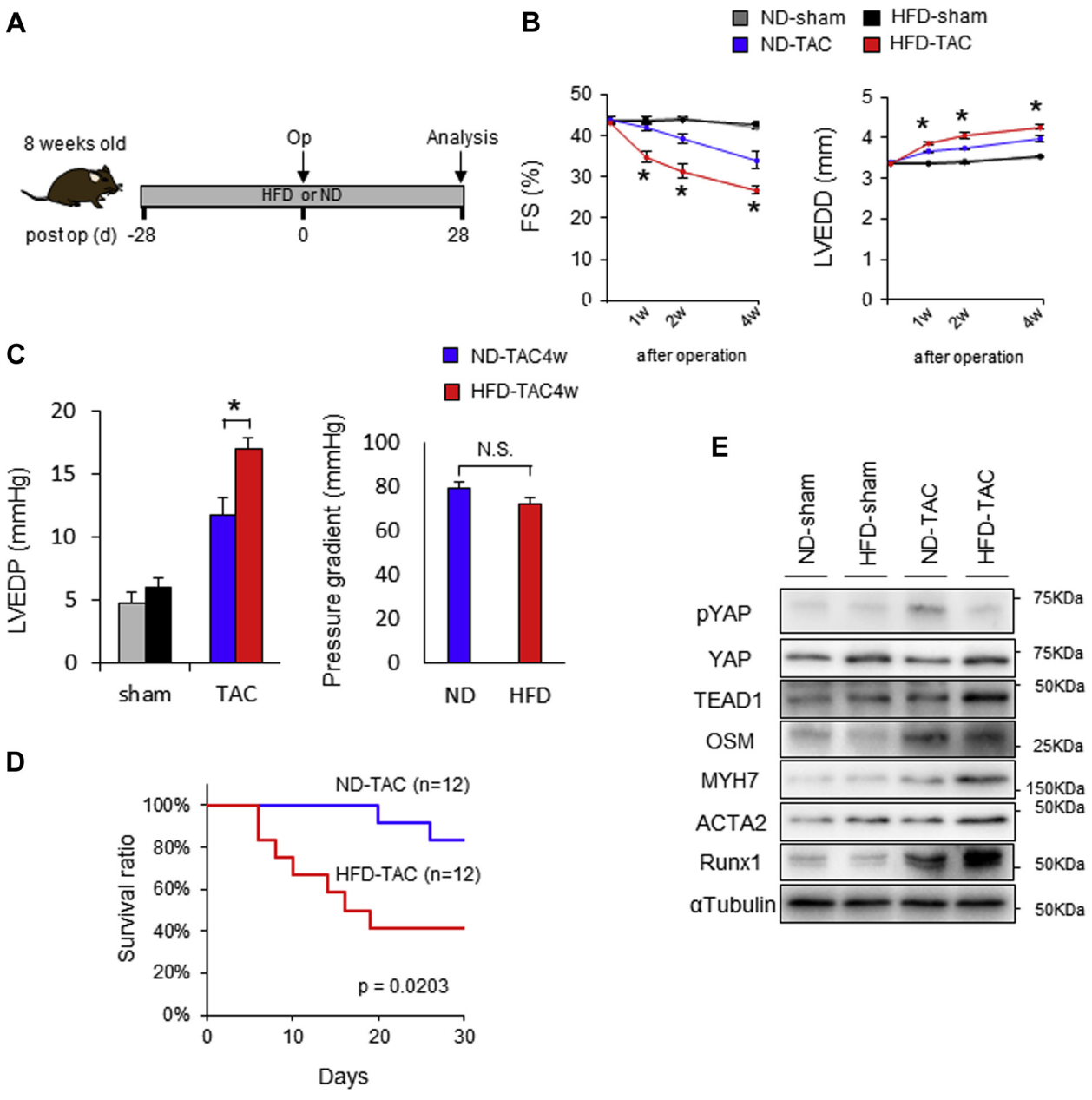

(A) Schematic representation of the experimental protocol. In **B–D**, mice were fed with either ND or HFD for 8 weeks. Four weeks after the start of ND or HFD, mice were subjected to either sham operation or transverse aortic constriction (TAC) for 4 weeks (4w). **(B)** Time course of percent fractional shortening (%FS) and left ventricular end-diastolic dimension (LVEDD) evaluated with echocardiography (n = 6, each). **(C)** Left ventricular end-diastolic pressure (LVEDP) and pressure gradient, evaluated by hemodynamic measurements (n = 6, each). **(D)** Kaplan-Meier survival curves after TAC. **(E)** Representative gel pictures of YAP, TEAD1, OSM, MYH7, ACTA2, RUNX1, and α-tubulin in the heart (n = 6, each). All results are mean ± SEM. *p < 0.05 by analysis of variance. Abbreviations as in Figure 1.

immunostaining and immunoblot analyses showed that both nuclear expression of YAP in cardiomyocytes and the level of YAP protein expression in the heart were significantly greater in patients with HF with diabetes than in HF patients without diabetes (Figures 5A and 5B, Supplemental Figure 8). The extent of nuclear positivity of YAP, as indicated by the proportion of YAP-positive nuclei divided by total nuclei, was greater in patients with higher glycosylated hemoglobin, which suggests that the level

FIGURE 3 **Verteporfin Improves Pressure Overload-Induced Cardiac Hypertrophy in the Presence of HFD**

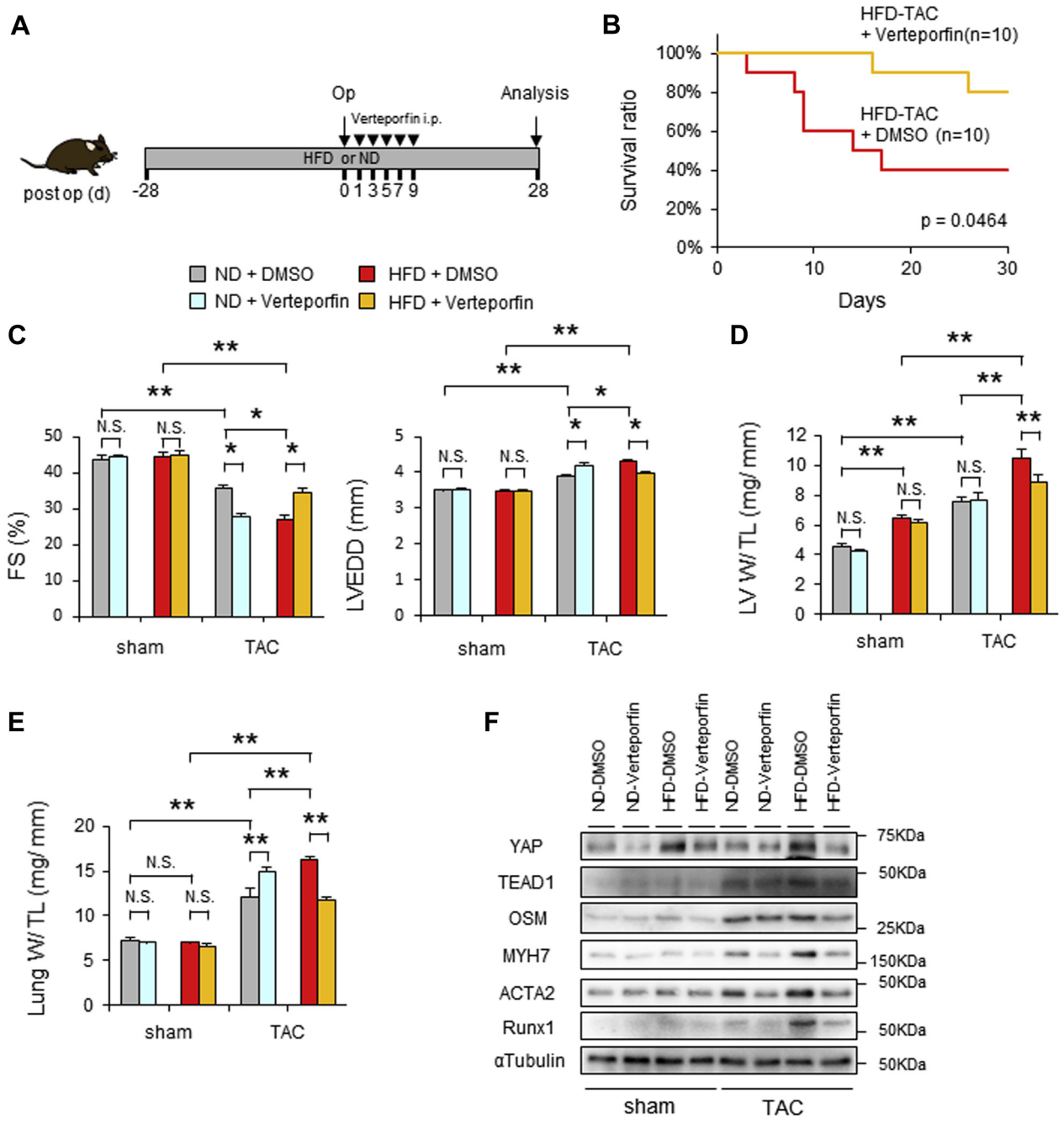

(A) Schematic representation of the experimental protocol. Mice were fed with either ND or HFD for 8 weeks. Four weeks after the start of ND or HFD, mice were subjected to either sham operation or TAC in the presence or absence of verteporfin for 4 weeks. **(B)** Kaplan-Meier survival curves for HFD-fed mice after TAC in the presence or absence of verteporfin. **(C)** %FS and LVEDD evaluated with echocardiography 4 weeks after TAC, with or without verteporfin treatment (n = 6, each). **(D)** Left ventricular weight to tibial length (LV W/ TL) ratio (n = 6, each). **(E)** Lung weight to tibial length (Lung W/ TL) ratio (n = 6, each). **(F)** Representative gel pictures of YAP, TEAD1, OSM, MYH7, ACTA2, RUNX1, and α-tubulin in the heart (n = 6, each). All results are mean ± SEM. *p < 0.05, **p < 0.01 by analysis of variance. i.p. = intraperitoneal; N.S. = not significant; Op = operation; post op = postoperative; other abbreviations as in Figures 1 and 2.

FIGURE 4 TEAD1 Deletion Attenuates Pressure Overload-Induced Cardiac Disfunction in the Presence of HFD

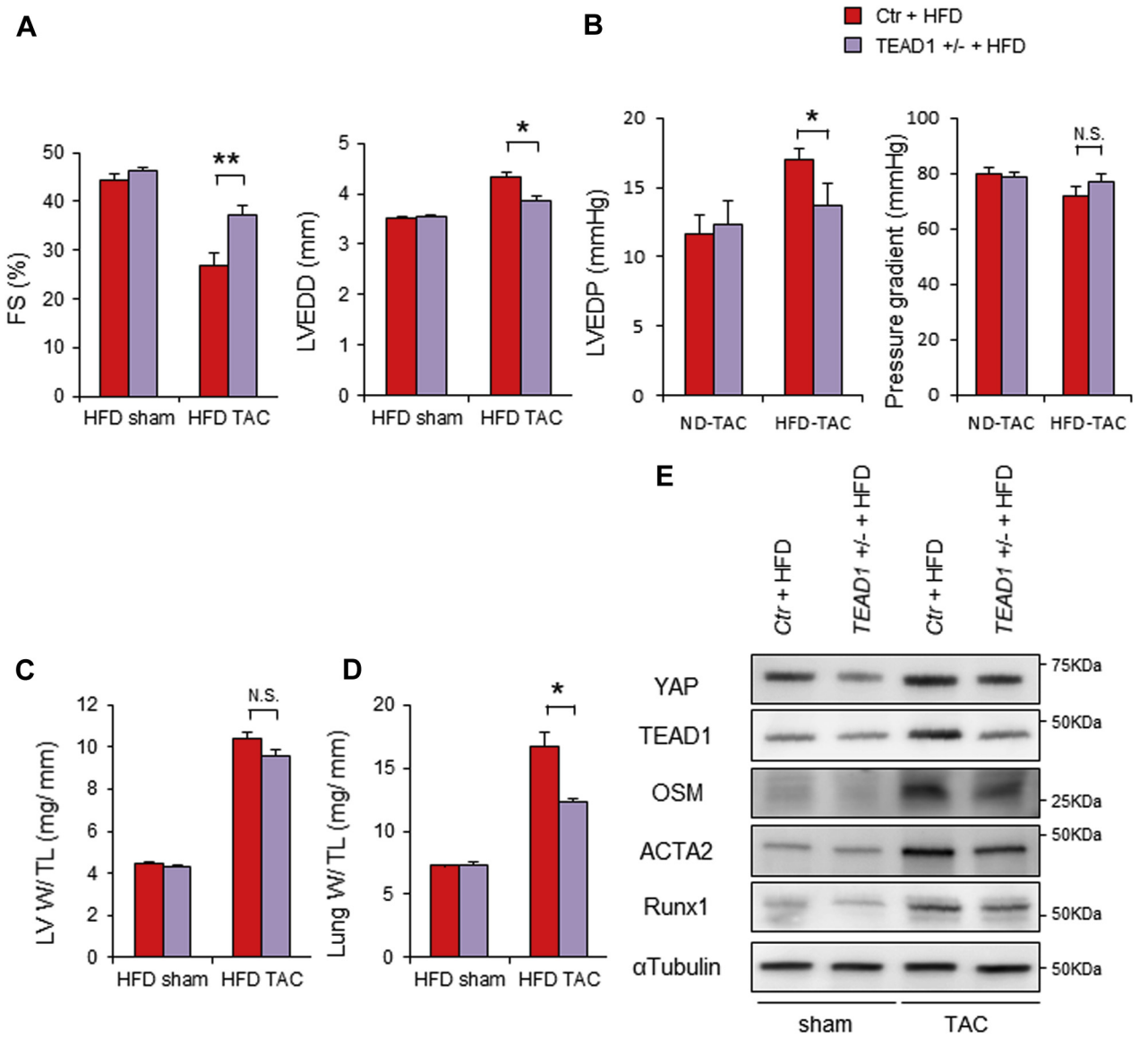

Control (Ctr) mice and TEAD1 heterozygous knockout (TEAD1$^{+/-}$) mice were fed with either ND or HFD for 8 weeks. Four weeks after the start of ND or HFD, mice were subjected to either sham operation or TAC. **(A)** %FS and LVEDD evaluated with echocardiography 4 weeks after TAC (n = 6, each). **(B)** LVEDP and pressure gradient, evaluated by hemodynamic measurements (n = 6, each). **(C)** LV W/ TL ratio (n = 6, each). **(D)** Lung W/ TL ratio (n = 6, each). **(E)** Representative gel pictures of YAP, TEAD1, OSM, ACTA2, RUNX1, and α-tubulin. All results are expressed as mean ± SEM. *p < 0.05, **p < 0.01 by analysis of variance. Abbreviations as in Figures 1 to 3.

of YAP may correlate with the severity of diabetes (Supplemental Figure 8B).

DISCUSSION

Here we have demonstrated that YAP is activated in the heart in response to HFD consumption, where persistent activation of YAP exacerbates cardiac dysfunction in the presence of PO. Importantly, both pharmacological and genetic interventions to inhibit the YAP-TEAD pathway attenuate the PO-induced exacerbation of HF in the heart in the presence of HFD consumption.

YAP IS ACTIVATED IN CARDIOMYOCYTES IN THE PRESENCE OF METABOLIC SYNDROME/DIABETES MELLITUS. HFD consumption by mice for 4 to 8 weeks induced activation of YAP in cardiomyocytes

FIGURE 5 Patients With HF With Diabetes Exhibit YAP Activation in Their Hearts

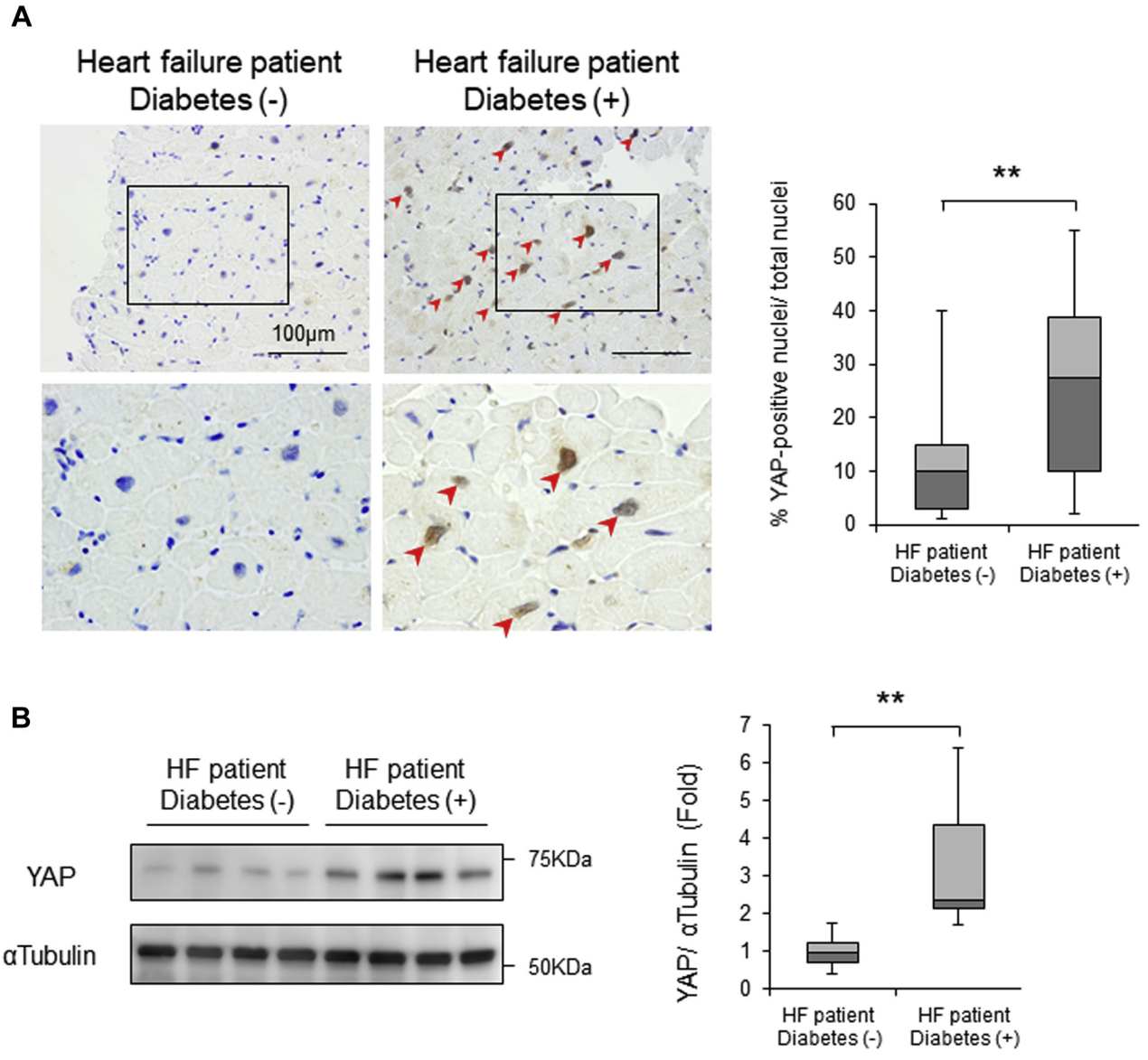

(A) Representative immunostaining of YAP in patients with heart failure (HF) with and without diabetes. Nuclear YAP accumulation is indicated by arrowheads. Quantitative analysis is shown on the right. **(B)** Representative gel pictures of YAP and α-tubulin in patients with HF with and without diabetes. Quantitative analysis is shown on the right (n = 7, each). **$p < 0.01$ by analysis of variance. The results are from 41 patients with HF without diabetes and 25 HF patients with diabetes. In box plots, whiskers show minimum and maximum values, while bars represent the median and 25th and 75th percentiles. YAP = Yes-associated protein. Abbreviations as in Figure 1.

in vivo. Our results show that HFD consumption down-regulated the activity of Lats2, an immediate upstream kinase of YAP, and decreased Ser127 phosphorylation of YAP. HFD also inhibited the activity of Lats2 in a mouse model of nonalcoholic steatohepatitis (20). Thus, a core component of the Hippo pathway seems to be inactivated in response to diabetes. Previous studies have suggested that O-GlcNAcylation may also be involved in the regulation of YAP in diabetic conditions in other cell types (21). However, it remains unclear whether these mechanisms up-regulate YAP through modulation of

Mst1 or Lats2. Both the nuclear localization of YAP in cardiomyocytes and the total YAP expression in the heart were also significantly up-regulated in patients with HF who had diabetes.

HFD CONSUMPTION EXACERBATES PO-INDUCED HF THROUGH THE YAP-TEAD PATHWAY. Activation of the upstream components of the Hippo pathway, including Mst1 and Lats2, generally promotes apoptosis and inhibits cell proliferation through suppression of YAP (4,5). Mst1 inhibits autophagy, thereby causing cellular dysfunction because of deficient protein quality control and eventual cell death (9). Thus, excessive activation of the Hippo pathway during myocardial ischemia and reperfusion, hemodynamic overload, and HF is generally detrimental for the heart (5). Interestingly, however, inactivation of the Hippo pathway below physiological levels through homozygous down-regulation of WW45, a scaffolding protein of the Hippo pathway, actually facilitates HF in the presence of PO (13). However, conditions in which the Hippo pathway is inactivated or the level of YAP is chronically elevated in the heart remained to be elucidated. We propose that metabolic syndrome and diabetes may fall into this category. Importantly, high blood pressure in the presence of metabolic syndrome or diabetes mellitus facilitates the development of HF in humans (2,16). Because inhibition of YAP attenuated the progression of PO-induced HF in WW45cKO mice and those that consumed HFD, pharmacological inhibition of YAP may be an appropriate intervention under clinical conditions in which YAP is chronically elevated in the presence of hypertension. Because inhibition of YAP suppressed PO-induced dedifferentiation of cardiomyocytes and inflammation in the heart in the presence of HFD, YAP may promote HF by stimulating cardiomyocyte dedifferentiation and inflammation in diabetic hearts in the presence of high blood pressure.

TEAD1 MEDIATES PO-INDUCED CARDIAC DYSFUNCTION IN DIABETIC HEARTS. YAP is a transcription factor cofactor that promotes downstream transcription factor activity through direct interaction (5). Although modest up-regulation of YAP alone may not induce a prominent phenotype in the heart at baseline, the superimposition of PO up-regulates TEAD1 in the nucleus, which in turn promotes transcription of genes involved in cell proliferation and dedifferentiation in the presence of YAP. Dedifferentiated cardiac muscle may not produce sufficient contractility against PO (13). The results of our loss-of-function experiments clearly show that endogenous TEAD1 is involved in the development of PO-induced HF in diabetic hearts. Furthermore, verteporfin is known to disrupt the interaction between YAP and TEADs (13). Thus, we propose that both YAP and TEAD may be effective targets to prevent the development of HF in diabetic patients with hypertension.

YAP INHIBITORS AS THERAPEUTIC OPTIONS IN CARDIAC DISEASE. In summary, persistent activation of YAP promotes PO-induced HF in the presence of HFD consumption in mice, mimicking the condition of obesity, metabolic syndrome, and insulin resistance in patients. Despite the generally protective roles of YAP in the heart, suppression of YAP may effectively improve some cardiovascular conditions. It is therefore important to identify additional conditions in which YAP and TEAD1 are coactivated and test the efficacy of YAP inhibitors in these conditions.

STUDY LIMITATIONS. The detailed molecular mechanisms by which diabetes inhibits LATS2 remain to be clarified.

We conducted this investigation with only male mice. Sex differences are noted in terms of responses to HFD consumption in mice (22). Whether high blood pressure exacerbates diabetic cardiomyopathy, and if so, whether the YAP-TEAD1 pathway is involved in the exacerbation in female mice as well remain to be elucidated. The HFD mouse model may not fully recapitulate type 2 diabetes. Thus, the role of the YAP-TEAD1 pathway should be confirmed in additional models of type 2 diabetes. Likewise, TAC may not faithfully mimic the condition of hypertension in humans, and multiple interventions that chronically impose PO on the LV need to be tested. Although our verteporfin treatment effectively inhibits the action of YAP-TEAD1 in vivo, the specificity of verteporfin should be further confirmed with cardiac-specific YAP knockout mice.

ACKNOWLEDGMENT The authors thank Daniela Zablocki (Rutgers New Jersey Medical School) for assistance with the manuscript.

ADDRESS FOR CORRESPONDENCE: Dr. Junichi Sadoshima, Department of Cell Biology and Molecular Medicine, Cardiovascular Research Institute, Rutgers New Jersey Medical School, 185 South Orange Avenue, MSB G609, Newark, New Jersey 07103. E-mail: sadoshju@njms.rutgers.edu.

PERSPECTIVES

COMPETENCY IN MEDICAL KNOWLEDGE 1: More than half of diabetic patients develop cardiac dysfunction, termed *diabetic cardiomyopathy*, a condition that is exacerbated in the presence of high blood pressure. The underlying molecular mechanism by which high blood pressure exacerbates cardiac dysfunction in diabetic patients is poorly understood.

COMPETENCY IN MEDICAL KNOWLEDGE 2: The Hippo signaling pathway is an evolutionarily conserved signaling mechanism that controls organ size through regulation of apoptosis and cell proliferation. We found that YAP, the key nuclear transcription cofactor of the Hippo signaling pathway, and its downstream target, TEAD1, a transcription factor, are involved in the exacerbation of cardiac dysfunction in mice that consume a high-fat diet, a model of type 2 diabetes, in the presence of high blood pressure. The exacerbation of heart failure in diabetic hearts in the presence of high blood pressure was alleviated in the presence of a chemical inhibitor of YAP or genetic down-regulation of TEAD1. Although high blood pressure induced dedifferentiation of cardiomyocytes in diabetic hearts, this effect was alleviated in the presence of the YAP inhibitor or down-regulation of TEAD1. YAP is activated in human heart samples obtained from heart failure patients with a history of diabetes compared with those without a history of diabetes.

COMPETENCY IN MEDICAL KNOWLEDGE 3: Our study provides clinician scientists with novel insights regarding the molecular mechanism by which the presence of high blood pressure exacerbates the progression of cardiac dysfunction in patients with diabetes.

TRANSLATIONAL OUTLOOK 1: YAP and TEAD1 are critically involved in the development of heart failure in the diabetic heart in the presence of high blood pressure. Although YAP is generally protective against cardiac stress, it can be detrimental under some conditions. Our results clearly show that YAP can be an important therapeutic target in diabetic patients with high blood pressure.

TRANSLATIONAL OUTLOOK 2: Our study suggests that chemical inhibitors of YAP or TEAD1 may be effective in treating patients who have diabetes, high blood pressure, and obesity (metabolic syndrome) to prevent heart failure syndromes.

REFERENCES

1. Roger VL. Epidemiology of heart failure. Circ Res 2013;113:646–59.

2. Perrone-Filardi P, Paolillo S, Costanzo P, Savarese G, Trimarco B, Bonow RO. The role of metabolic syndrome in heart failure. Eur Heart J 2015;36:2630–4.

3. Seferovic PM, Paulus WJ. Clinical diabetic cardiomyopathy: a two-faced disease with restrictive and dilated phenotypes. Eur Heart J 2015;36:1718–27. 1727a–c.

4. Ma S, Meng Z, Chen R, Guan KL. The Hippo pathway: biology and pathophysiology. Annu Rev Biochem 2019;88:577–604.

5. Wackerhage H, Del Re DP, Judson RN, Sudol M, Sadoshima J. The Hippo signal transduction network in skeletal and cardiac muscle. Sci Signal 2014;7:re4.

6. Yamamoto S, Yang G, Zablocki D, et al. Activation of Mst1 causes dilated cardiomyopathy by stimulating apoptosis without compensatory ventricular myocyte hypertrophy. J Clin Invest 2003;111:1463–74.

7. Del Re DP, Matsuda T, Zhai P, et al. Mst1 promotes cardiac myocyte apoptosis through phosphorylation and inhibition of Bcl-xL. Mol Cell 2014;54:639–50.

8. Del Re DP, Yang Y, Nakano N, et al. Yes-associated protein isoform 1 (Yap1) promotes cardiomyocyte survival and growth to protect against myocardial ischemic injury. J Biol Chem 2013;288:3977–88.

9. Maejima Y, Kyoi S, Zhai P, et al. Mst1 inhibits autophagy by promoting Beclin1-Bcl-2 interaction. Nat Med 2013;19:1478–88.

10. Leach JP, Heallen T, Zhang M, et al. Hippo pathway deficiency reverses systolic heart failure after infarction. Nature 2017;550:260–4.

11. Lin Z, von Gise A, Zhou P, et al. Cardiac-specific YAP activation improves cardiac function and survival in an experimental murine MI model. Circ Res 2014;115:354–63.

12. Xin M, Kim Y, Sutherland LB, et al. Hippo pathway effector Yap promotes cardiac regeneration. Proc Natl Acad Sci U S A 2013;110:13839–44.

13. Ikeda S, Mizushima W, Sciarretta S, et al. Hippo deficiency leads to cardiac dysfunction accompanied by cardiomyocyte dedifferentiation during pressure overload. Circ Res 2019;124:292–305.

14. Zhang X, Qiao Y, Wu Q, et al. The essential role of YAP O-GlcNAcylation in high-glucose-stimulated liver tumorigenesis. Nat Commun 2017;8:15280.

15. Chen J, Harris RC. Interaction of the EGF receptor and the Hippo pathway in the diabetic kidney. J Am Soc Nephrol 2016;27:1689–700.

16. Bozkurt B, Aguilar D, Deswal A, et al. Contributory risk and management of comorbidities of hypertension, obesity, diabetes mellitus, hyperlipidemia, and metabolic syndrome in chronic heart failure: a scientific statement from the American Heart Association. Circulation 2016;134:e535–78.

17. Nakamura M, Liu T, Husain S, et al. Glucogen synthase kinase-3α promotes fatty acid uptake and lipotoxic cardiomyopathy. Cell Metab 2019;29:1119–34.e12.

18. Page A, Dumesnil JG, Clavel MA, et al. Metabolic syndrome is associated with more pronounced impairment of left ventricle geometry and function in patients with calcific aortic stenosis: a substudy of the ASTRONOMER (Aortic Stenosis Progression Observation Measuring Effects of Rosuvastatin). J Am Coll Cardiol 2010;55:1867–74.

19. Frati G, Schirone L, Chimenti I, et al. An overview of the inflammatory signalling mechanisms in the myocardium underlying the development of diabetic cardiomyopathy. Cardiovasc Res 2017;113:378–88.

20. Aylon Y, Gershoni A, Rotkopf R, et al. The LATS2 tumor suppressor inhibits SREBP and suppresses hepatic cholesterol accumulation. Genes Dev 2016;30:786–97.

21. Peng C, Zhu Y, Zhang W, et al. Regulation of the Hippo-YAP pathway by glucose sensor O-GlcNAcylation. Mol Cell 2017;68:591–604.e5.

22. Lainez NM, Jonak CR, Nair MG, et al. Diet-induced obesity elicits macrophage infiltration and reduction in spine density in the hypothalami of male but not female mice. Front Immunol 2018;9:1992.

KEY WORDS diabetes, diabetic cardiomyopathy, Hippo pathway, pressure overload

APPENDIX For supplemental tables and figures, please see the online version of this paper.

JACC: BASIC TO TRANSLATIONAL SCIENCE VOL. 4, NO. 5, 2019

EDITORIAL COMMENT

The Hippo in the Clinic

An Ancient Signaling Pathway That Regulates Growth and Development Confronts a Modern Pandemic of Obesity, Diabetes, and Heart Failure*

Sheldon H. Gottlieb, MD

The relentless expansion of the worldwide waist (1,2) has led to accelerating rates of glycemic, liver, and heart failure, some cancers, and degenerative joint disease in persons around the globe (3). "Heart failure," a clinical syndrome that until the arrival of the obesity pandemic was typically categorized by cardiac enlargement with sodium and water overload, has become, in the modern era of ubiquitous obesity, a concatenation of multiple chronic conditions (4) that clinically present as a dysfunction of diastolic filling (5). The physiology of heart failure with preserved ejection fraction is strongly related to central obesity and diabetes (6); the clinical syndrome of heart failure with preserved ejection fraction (colloquially HEFPEF) can be defined by a point system (7). These operational definitions just hint at the clinical reality: that the phenotype of diastolic heart failure lies at the intersection of obesity (reflecting poor nutrition and associated high dietary sodium content), with type 2 diabetes, hypertension, social stress, and aging (8). The modern heart failure patients' internal milieu is unprecedented in evolutionary history.

It is curious that none of the recent reviews of diastolic dysfunction heart failure and its obesity phenotypes discuss an ancient signaling pathway that regulates growth and development central to every aspect of cardiovascular physiology, from apoptosis to Z-discs: the Hippo signaling pathway (Hippo) (9). The Hpo gene, which was discovered in the fruit fly, is homologous with the mammalian kinases Mst1 and Mst2 (10). Hippo regulates downstream levels of Yes Associated Protein (YAP), which interacts with transcriptional regulator TEAD1. Hippo is a highly conserved premetazoan kinase cascade; it possibly developed in response to selective pressure to facilitate communication between unicellular organisms (11). The nearly simultaneous discovery by 5 laboratories of the gene Hpo (its evocative name Hippo inspired by the overgrowth of the Drosophila eye imaginal disc with cellular disarray resembling the head of a hippopotamus) is reviewed (12,13). Hippo has been shown to regulate cell-to-cell contact, cell death and repair after myocardial infarction, dedifferentiation of cardiomyocytes to fibrocytes, and differentiation of stem cells to cardiomyocytes. It plays a regulatory role in the interaction of glucose and the heart (14).

SEE PAGE 611

In this issue of *JACC: Basic to Translational Science*, Ikeda et al. (15) present a proof of concept experiment of Hippo and its downstream effector YAP in a male mouse model of "metabolic syndrome" as defined by the intersection of obesity, type 2 diabetes, hypertension, and inflammation in their high fat diet (HFD), pressure overload (PO) via transverse aortic constriction (TAC) model. They have shown, in a series of publications (16,17), how YAP and associated transcriptional effector TEAD are modified. They investigated the interaction of these interventions with levels of YAP and associated pathways in their model, and after blockade of the pathways with verteporfin, which is a small-molecule specific inhibitor

*Editorials published in *JACC: Basic to Translational Science* reflect the views of the authors and do not necessarily represent the views of *JACC: Basic to Translational Science* or the American College of Cardiology.

From the Division of Cardiology, Johns Hopkins University School of Medicine, Johns Hopkins Bayview Medical Center, Baltimore, Maryland.
The author has reported that he has no relationships relevant to the contents of this paper to disclose.
The author attests they are in compliance with human studies committees and animal welfare regulations of the authors' institutions and Food and Drug Administration guidelines, including patient consent where appropriate. For more information, visit the *JACC: Basic to Translational Science* author instructions page.

ISSN 2452-302X https://doi.org/10.1016/j.jacbts.2019.08.004

of the YAP pathway (18). They also obtained interesting proof of concept data from myocardial biopsy specimens from human subjects with and without type 2 diabetes; they found that the concentration of YAP in the biopsy specimens was proportional to the patient's hemoglobin A_{1C} level.Based on these findings, they speculate that inhibitors of YAP or transcriptional effector TEAD1 may be effective in treating heart failure, as frequently seen in patients with type 2 diabetes and hypertension.

Of note in the Ikeda et al. (15) study is the possible interaction of glycemic dysregulation with PO in their HFD mouse model, where YAP overexpression, instead of protecting cardiomyocytes, may induce dedifferentiation and apoptosis. A model of metabolic syndrome in swine fed a high-fat diet and with PO with TAC has been published; an editorial expresses caution and support for animal models of metabolic syndrome (19).

Because of its role in regulating tissue growth, and its effect on tumorigenesis, there is interest in finding pharmacologic blockers and enhancers of Hippo; hundreds of compounds are currently being tested to block the central kinase of Hippo (20). Triastuti et al. (21) have used a blocker of the central Hippo kinase, to demonstrate that increase of the YAP-complex protects the mouse heart against PO. There are concerns regarding chronic treatment with small molecule kinase inhibitors because of the association of Hippo with tumorigenesis (20).

About a third of patients with aortic stenosis have type 2 diabetes (22). How the natural history of aortic stenosis could be modified by the interactions of type 2 diabetes with the central pressure and often volume overload of aortic stenosis, by manipulation of Hippo, is unstudied and speculative.

In summary, Hippo interacts with all levels of cardiovascular physiology. The mouse model used by Ikeda et al. (15) and others has provided important insights regarding Hippo and the heart, which may lead not only to treatment for diabetic pressure overload cardiomyopathy, but also for myocardial regeneration and prevention of heart failure after myocardial infarction (23). Hippo: it really is big.

ADDRESS FOR CORRESPONDENCE: Dr. Sheldon H. Gottlieb, Division of Cardiology, Johns Hopkins University School of Medicine, Johns Hopkins Bayview Medical Center, 4940 Eastern Avenue, Baltimore, Maryland 21224. E-mail: sgottli@jhmi.edu.

REFERENCES

1. Taylor C. World wide waist. Time 2001;157:82.

2. Centers for Disease Control and Prevention. National Center for Chronic Disease Prevention and Health Promotion, Division of Nutrition, Physical Activity, and Obesity. Data, trend and maps [online]. Available at: https://www.cdc.gov/nccdphp/dnpao/data-trends-maps/index.html. Accessed August 10, 2019.

3. GBD 2015 Obesity Collaborators. Health effects of overweight and obesity in 195 countries over 25 years. N Engl J Med 2017;377:13–27.

4. Triposkiadis F, Giamouzis G, Parissis J, et al. Reframing the association and significance of co-morbidities in heart failure. Eur J Heart Fail 2016;18:744–58.

5. Little WC. Heart failure with a normal left ventricular ejection fraction: diastolic heart failure. Trans Am Clin Clim Assoc 2008;119:93–101.

6. Selvaraj S, Martinez EE, Aguilar FG, et al. Association of central adiposity with adverse cardiac mechanics: findings from the Hypertension Genetic Epidemiology Network Study. Circ Cardiovasc Imaging 2016;9:e004396.

7. Reddy YNV, Carter RE, Obokata M, Redfield MM, Borlaug BA. A simple, evidence-based approach to help guide diagnosis of heart failure with preserved ejection fraction. Circulation 2018;138:861–70.

8. Tromp J, Shen L, Jhund PS, et al. Age-related characteristics and outcomes of patients with heart failure with preserved ejection fraction. J Am Coll Cardiol 2019;74:601–12.

9. Gabriel BM, Hamilton DL, Tremblay AM, Wackerhage H. The Hippo signal transduction network for exercise physiologists. J Appl Physiol 2016;120:1105–17.

10. Ardestani A, Lupse B, Maedler K. Hippo signaling: key emerging pathway in cellular and whole-body metabolism. Trends Endocrinol Metab 2018;29:492–509.

11. Sebé-Pedrós A, Zheng Y, Ruiz-Trillo I, Pan D. Premetazoan origin of the hippo signaling pathway. Cell Rep 2012;1:13–20.

12. Gokhale R, Pfleger CM. The power of *Drosophila* genetics: the discovery of the Hippo Pathway. Methods Mol Biol 2019;1893:3–26.

13. Badouel C, McNeill H. SnapShot: the Hippo signaling pathway. Cell 2011;145:484.

14. Koo JH, Guan K-L. Interplay between YAP/TAZ and metabolism. Cell Met Review 2018;28:196–206.

15. Ikeda S, Mukai R, Mizushima W, et al. Yes-associated protein (YAP) facilitates pressure-overload-induced dysfunction in the diabetic heart. J Am Coll Cardio Basic Trans Science 2019;4:611–22.

16. Byun J, Del Re DP, Zhai P, et al. Yes-associated protein (YAP) mediates adaptive cardiac hypertrophy in response to pressure overload. J Biol Chem 2019;294:3603–17.

17. Ikeda S, Mizushima W, Sciarretta S, et al. Hippo deficiency leads to cardiac dysfunction accompanied by cardiomyocyte dedifferentiation during pressure overload. Circ Res 2019;124:292–305.

18. Prins KW, Thenappan T, Weir EK, Kalra R, Pritzker M, Archer SL. Repurposing medications for treatment of pulmonary arterial hypertension: what's old is new again. J Am Heart Assoc 2019;8:e011343.

19. Sharp TE 3rd, Lefer DJ, Houser SR. Cardiometabolic heart failure and HFpEF: still chasing unicorns. J Am Coll Cardiol Basic Trans Science 2019;4:422–4.

20. Crawford JJ, Bronner SM, Zbieg JR. Hippo pathway inhibition by blocking the YAP/TAZ-TEAD interface: a patent review. Expert Opin Ther Patents 2018;28:867–73.

21. Triastuti E, Nugroho AB, Zi M, et al. Pharmacological inhibition of Hippo pathway using XMU-MP-1 protects the heart against adverse effects during pressure overload. Br J Pharmacol 2019 Jul 22 [E-pub ahead of print].

22. Banovic M, Athithan L, McCann GP. Aortic stenosis and diabetes mellitus: an ominous combination. Diab Vasc Dis Res 2019;16:310–23.

23. Heallen TR, Kadow ZA, Kim JH, Wang J, Martin JF. Stimulating cardiogenesis as a treatment for heart failure. Circ Res 2019;124:1647–57.

KEY WORDS diabetes, diastolic heart failure, Hippo pathway, mouse model metabolic syndrome, Yes-associated protein (YAP)

JACC: BASIC TO TRANSLATIONAL SCIENCE
PUBLISHED BY ELSEVIER ON BEHALF OF THE AMERICAN COLLEGE OF CARDIOLOGY FOUNDATION.

VOL. 4, NO. 5, 2019

PRECLINICAL RESEARCH

Alcohol Binge-Induced Cardiovascular Dysfunction Involves Endocannabinoid–CB1-R Signaling

Janos Paloczi, PhD,[a] Csaba Matyas, MD, PhD,[a] Resat Cinar, PhD,[b] Zoltan V. Varga, MD, PhD,[a] György Hasko, MD, PhD,[c] Thomas H. Schindler, MD,[d] George Kunos, MD, PhD,[b] Pal Pacher, MD, PhD[a]

VISUAL ABSTRACT

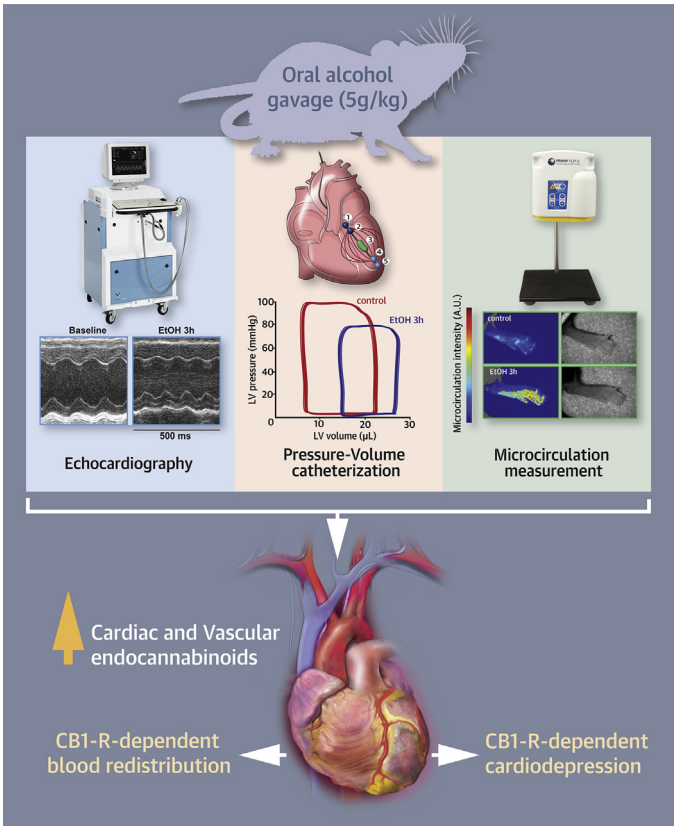

Paloczi, J. et al. J Am Coll Cardiol Basic Trans Science. 2019;4(5):625–37.

HIGHLIGHTS

- **Alcohol is one of the most frequently used intoxicants in the United States. Binge alcohol drinking is a major contributor of emergency department visits.**
- **Binge alcohol drinking may adversely affect cardiovascular function.**
- **Here we show that acute alcohol intoxication is associated with elevated levels of cardiac endocannabinoid anandamide and profound cardiovascular dysfunction and blood redistribution lasting for several hours.**
- **The adverse cardiovascular effects of acute alcohol intoxication are attenuated by CB1-R antagonist or in CB1-R knockout mice.**
- **A single alcohol binge has profound effect on the cardiovascular system, which involves endocannabinoid-CB1-R signaling.**

From the [a]Laboratory of Cardiovascular Physiology and Tissue Injury, National Institutes of Health/National Institute on Alcohol Abuse and Alcoholism (NIAAA), Bethesda, Maryland; [b]Laboratory of Physiological Studies, National Institutes of Health/National Institute on Alcohol Abuse and Alcoholism (NIAAA), Bethesda, Maryland; [c]Department of Anesthesiology, Columbia University, New York, New York; and the [d]Division of Nuclear Medicine, Washington University in St. Louis, St. Louis, Missouri. This study was supported by the Intramural Research Program of NIH/NIAAA to Dr. Pacher. The authors have reported that they have no relationships relevant to the contents of this paper to disclose.

ISSN 2452-302X https://doi.org/10.1016/j.jacbts.2019.05.007

ABBREVIATIONS AND ACRONYMS

2-AG = 2-arachidonyl glycerol

AEA = anandamide

CB1-R (CB1) = cannabinoid 1 receptor

CB2-R (CB2) = cannabinoid 2 receptor

dP/dtmax = maximal slope of pressure increment

EF = ejection fraction

LV = left ventricle

MAP = mean arterial pressure

PRSW = preload recruitable stroke work

P-V = pressure-volume

TPR = total peripheral resistance

SUMMARY

Excessive binge alcohol drinking may adversely affect cardiovascular function. In this study we characterize the detailed hemodynamic effects of an acute alcohol binge in mice using multiple approaches and investigate the role of the endocannabinoid–cannabinoid 1 receptor (CB1-R) signaling in these effects. Acute alcohol binge was associated with elevated levels of cardiac endocannabinoid anandamide and profound cardiovascular dysfunction lasting for several hours and redistribution of circulation. These changes were attenuated by CB1-R antagonist or in CB1-R knockout mice. Our results suggest that a single alcohol binge has profound effects on the cardiovascular system, which involve endocannabinoid–CB1-R signaling.

Alcohol remains one of the most frequently used intoxicants in the United States, especially among younger individuals (1,2). According to the National Epidemiologic Survey on alcoholism and related conditions, among 73% of human subjects aged 18 or older who drank, 46% consumed more than twice the number of drinks considered binge drinking at least once in the last year (1). Binge alcohol drinking, defined as having 4 or more drinks over 2 h on an occasion for women, or 5 or more drinks for men, is a major contributor of emergency department visits in the United States (1). There is also evidence that binge alcohol consumption can lead to development of life-threatening or fatal conditions (3). Apart from the severe indirect consequences, alcohol abuse has been shown to increase the risk of atrial fibrillation, acute myocardial infarction, and congestive heart failure to a similar degree as other well-known risk factors (4). Despite numerous studies investigating the effects of chronic moderate or excessive alcohol consumption on cardiovascular function and/or risk (4–10), relatively few reports have explored the cardiovascular effects of binge ethanol use and/or intoxication (11–17). Furthermore, these studies primarily focused on the determination of blood pressure or load- and/or heart rate-dependent indices of myocardial function measured by echocardiography (e.g., ejection fraction [EF]). Since alcohol is also known to time- and dose-dependently alter vascular function, heart rate, cardiac contractility, and peripheral resistance (10–18), reliance on load- and heart rate-dependent indices of contractile function may lead to inaccurate conclusions.

An increasing number of high school students and young adults have been reported to consume marijuana or synthetic cannabinoids [a mixture of potent cannabinoid 1 receptor (CB1-R) agonists (19,20)] for recreational purposes, which may induce deleterious cardiovascular effects via CB1-R-dependent mechanisms (21–23). Moreover, synthetic cannabinoids are often consumed together with alcoholic beverages, leading to more severe outcomes and longer hospital stays (24). In the cardiovascular system, CB1-R is expressed in cardiomyocytes, endothelial and smooth muscle cells, and fibroblasts (25–28), as well as in the peripheral and central autonomic nervous systems (29). The effects of synthetic cannabinoids acting via CB1-R have been well documented and may have robust impact on the cardiovascular system, leading to abnormalities in cardiac inotropy, chronotropy, conduction, and vascular tone (21,29,30) [for review see Montecucco et al. (21) and Pacher et al. (29)]. Endocannabinoids do not appear to play a significant role in normal cardiovascular regulation, but when overproduced in various pathologic conditions (e.g., various forms of shock, cardiomyopathies, or heart failure and atherosclerosis) may contribute to hypotension, decreased cardiac contractility, and/or vascular inflammation and cell death through cardiovascular and macrophage CB1-R [for review see Montecucco et al. (21) and Pacher et al. (29)].

In this study, using multiple approaches and a well-established animal model, we aimed to identify and characterize the effects of acute alcohol intoxication on the cardiovascular system and to explore the potential role of the endocannabinoid-CB1-R signaling in mediating these effects. These results

The authors attest they are in compliance with human studies committees and animal welfare regulations of the authors' institutions and Food and Drug Administration guidelines, including patient consent where appropriate. For more information, visit the *JACC: Basic to Translational Science* author instructions page.

Manuscript received March 20, 2019; revised manuscript received May 4, 2019, accepted May 13, 2019.

may have important implications for the management of the acute cardiovascular consequences of alcohol and mixed alcohol-synthetic cannabinoid intoxication.

SEE PAGE 638

METHODS

ANIMALS. Animal handling and usage were in accordance with the National Institutes of Health guidelines and experimental protocols were approved by our Institutional Animal Care and Use Committee of the National Institute on Alcohol Abuse and Alcoholism (Bethesda, Maryland). Eight- to 12-week-old male and female C57BL/6J mice were used (The Jackson Laboratory, Bar Harbor, Maine). NIAAA colony of male and female $Cnr1^{-/-}$ ($CB1^{-/-}$) and $Cnr2^{-/-}$ ($CB2^{-/-}$) mice on C57BL/6J background and their corresponding wild-type controls were also used in this study (31,32). A total number of 198 mice were used for the described experiments.

DRUGS. The CB1-R antagonist/inverse agonist rimonabant (SR141716) was purchased from Tocris (Tocris Bioscience, Bio-Techne, Minneapolis, Minnesota). Drugs were dissolved in dimethyl sulfoxide: Tocrisolve:saline solution at the ratio of 1:1:18 and vortexed to obtain a stable emulsion for bolus intravenous or intraperitoneal injections (26). Rimonabant was administered at the dose of 5 mg/kg.

EXPERIMENTAL DESIGN. In the first set of experiments, a single alcohol binge (31.5% vol/vol, given at the dose of 5 g/kg body weight) or isocaloric maltodextrin solution were given to mice following 12 h of fasting as previously described (33). Cardiac function and hemodynamics were assessed 3 or 12 h after alcohol binge.

In the second set of experiments, the CB1-R antagonist/inverse agonist rimonabant (5 mg/kg) or its vehicle were administered intravenously to both alcohol- and maltodextrin-binged mice 3 h after binge (peak of cardiovascular effects) and hemodynamics were assessed for at least 15 consecutive minutes until the drug response stabilized. In other cohorts, the acute hemodynamic effects of binge alcohol drinking in $CB1^{-/-}$ and $CB2^{-/-}$ mice or in their wild-type controls were also investigated 3 h after acute alcohol exposure.

PRESSURE-VOLUME CATHETERIZATION AND ECHOCARDIOGRAPHY. Left ventricular (LV) performance was assessed by using pressure-volume (P-V) approach (34). Briefly, a P-V catheter equipped with a 1-F size microtip (PVR-1045, Millar Instruments, Houston, Texas) was inserted into the right carotid artery and advanced into the LV. Polyethylene cannulas were also introduced into the right femoral artery and left jugular vein to measure mean arterial pressure (MAP) and to administer drugs, respectively. After stabilization, P-V signals were continuously recorded by using the PowerLab data acquisition system (ADInstruments Inc, Colorado Springs, Colorado). Multiple indices of load-dependent and load-independent LV function, MAP and total peripheral resistance (TPR) were calculated as previously described (35). Echocardiography was performed as previously reported (36).

ARTERIAL AND MICROVASCULAR BLOOD FLOW MEASUREMENTS. Blood flow in both renal and superior mesenteric arteries were measured by using Transonic flow probes (MA0.5PSB and MA0.7PSB perivascular flowprobes, Transonic Systems Inc., Ithaca, New York) and were recorded and evaluated by using Powerlab LabChart (ADInstruments Inc., Colorado Springs, Colorado). Acral microcirculation was also assessed by using the laser speckle contrast imager moorFLPI-2 (Moor Instruments, Wilmington, Delaware).

TISSUE ENDOCANNABINOID MEASUREMENT. Myocardial levels of anandamide (AEA), 2-arachidonyl glycerol (2-AG) were quantified by liquid chromatography/in-line mass spectrometry, as previously described (26). Values are expressed as femtomoles or picomoles per milligram of wet tissue.

STATISTICAL ANALYSIS. Results are expressed as mean ± SEM and plotted as bar graphs in all figures (see **Figures 1 to 8** and Supplemental Figures 1 to 6, except for Supplemental Figures 2B [pre-load recruitable stroke work or PRSW], Supplemental Figure 3A [maximal slope of pressure increment or dP/dt_{max}], and Supplemental Figure 4C [TPR], whereas data are presented as median ± 25th, 75th percentiles). Statistical significance between groups was determined by Student's *t* test or in case of multiple groups by 1-way analysis of variance followed by Dunnett's post hoc multiple comparison test to compare each group to control. Equality of variances was also examined by using either F-test of the equality of 2 variances or Brown-Forsythe test, respectively. If populations had different distribution, nonparametric tests (Mann-Whitney test for comparing 2 groups or Kruskal-Wallis test for multiple comparisons) were applied (Supplemental Figures 2B, 3A, and 4C) to analyze data. Statistical significance was assessed by using GraphPad Prism 7 software (San Diego, California). Probability values of $p < 0.05$ were considered significant.

RESULTS

A SINGLE ALCOHOL BINGE INDUCES CARDIAC DYSFUNCTION AND REDISTRIBUTION OF CIRCULATION. Alcohol binge or intoxication may adversely impact

FIGURE 1 Binge Alcohol Induces Left Ventricular Dysfunction

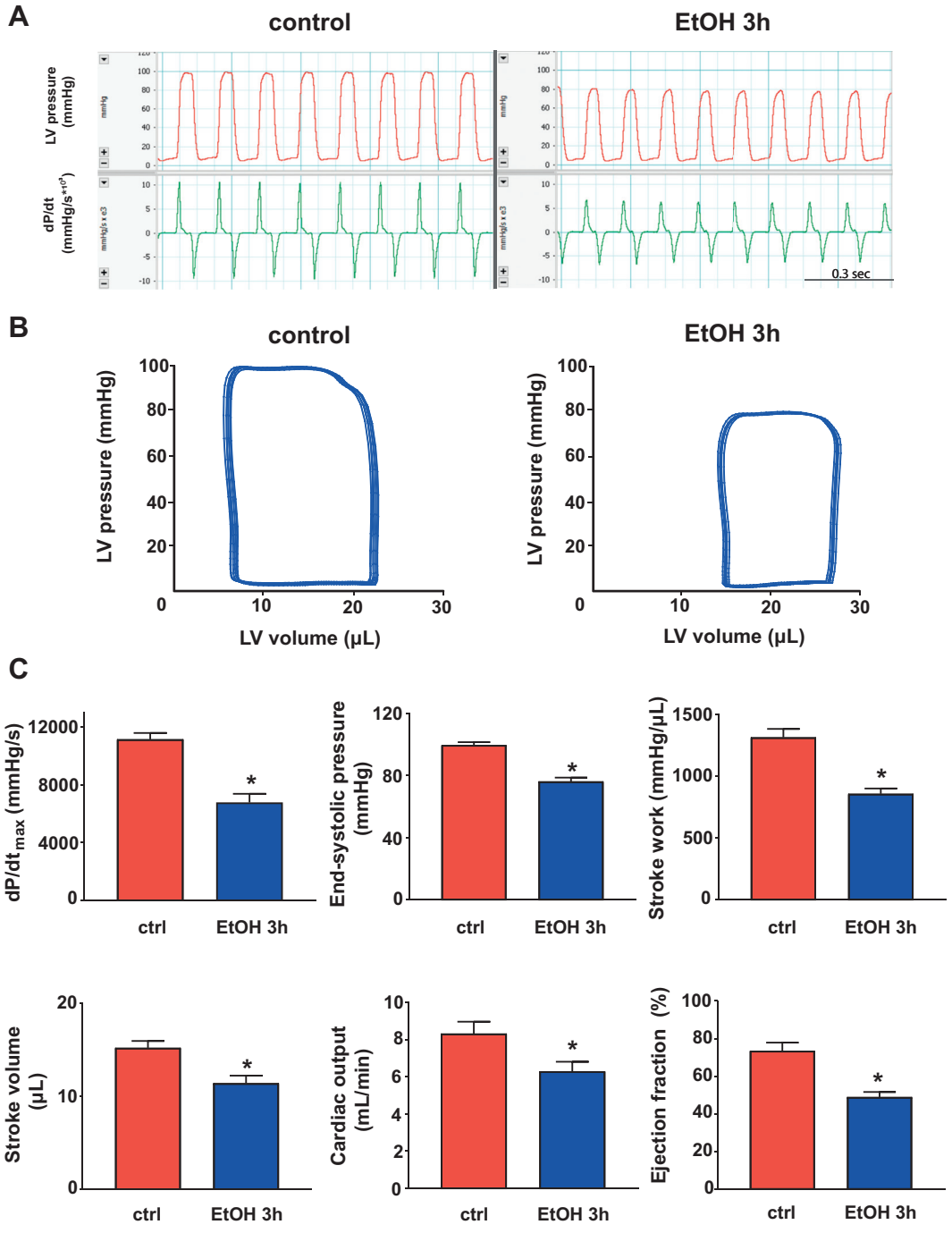

(A) Representative records of left ventricular (LV) pressure and its derivative (dP/dt) in control and alcohol-binged (EtOH 3h) mice, 3 h after maltodextrin or alcohol administration respectively. **(B)** Representative pressure-volume loops of control and alcohol-binged mice. **(C)** Systolic indices of LV performance [maximal slope of pressure increment (dP/dt_{max}), end-systolic pressure, stroke work, stroke volume, cardiac output and ejection fraction] in control (ctrl) and alcohol-binged (EtOH 3h) mice. Data are expressed as mean ± SEM, n = 7 to 8; *$p < 0.05$ vs. control group.

FIGURE 2 Binge Alcohol Decreases Load-Independent Indices of Left Ventricular Function

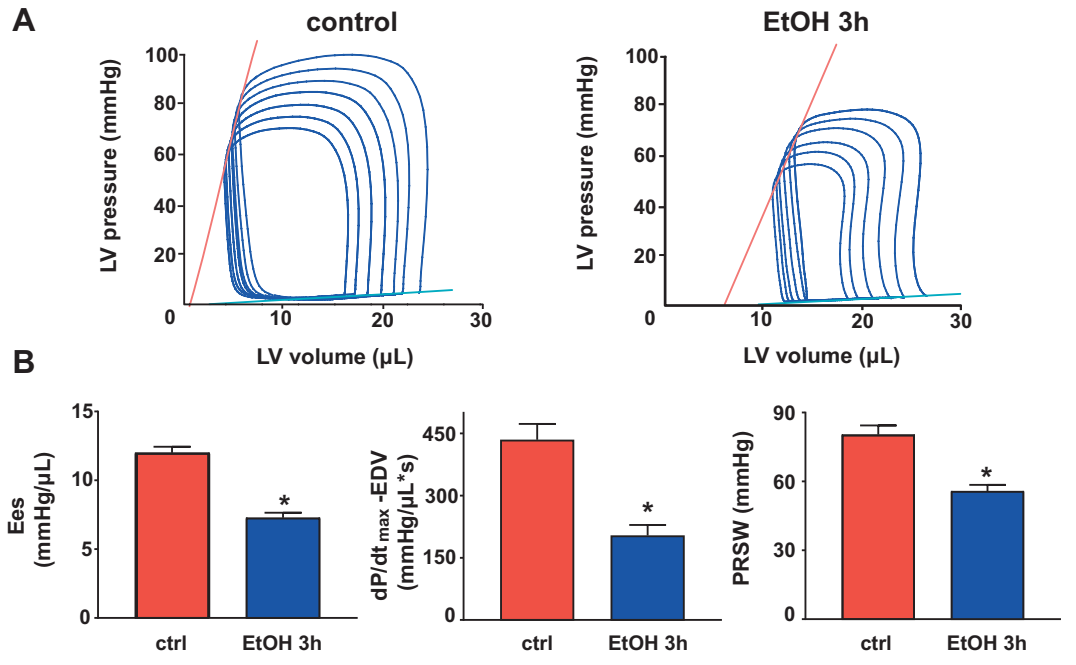

(A) Pressure-volume (P-V) loops of control and alcohol-binged mice after gradual preload reduction obtained by vena cava inferior occlusion. **Red lines** indicate the slope of end-systolic P-V relationship; **blue lines** display the slope of end-diastolic P-V relationship. **(B)** Load-independent indices of LV performance: end-systolic elastance (Ees), the dP/dt_{max}-end-diastolic volume (EDV) relation and preload recruitable stroke work (PRSW). Data are expressed as mean ± SEM, n = 7 to 8; *p < 0.05 vs. control group. Abbreviation as in Figure 1.

both cardiac and vascular function (see introduction); therefore, we investigated the acute effects of alcohol binge on both load-dependent and load-independent indices of cardiac contractility (using echocardiography and P-V approaches) as well as on vascular blood flow in mesenteric and renal arteries and on skin microcirculation (using Transonic flow probes and/or laser speckle analysis) in vivo in mice.

In the first set of experiments, we attempted to characterize the time course of the effect of an acute alcohol binge on cardiovascular function and blood redistribution (**Figures 1 to 3**; Supplemental Figures 1 to 3). First, we analyzed the effects of alcohol binge on cardiac function by echocardiography (Supplemental Figure 1). Alcohol-induced transient reduction of stroke volume and cardiac output peaked around 3 h following the binge and largely recovered after 12 h (Supplemental Figure 1). An acute binge had no significant effect on EF and fractional shortening measured by echocardiography. Since the latter parameters could be affected by loading conditions, which we hypothesized to change by alcohol binge, we further analyzed cardiac function using the P-V approach (35), allowing determination of load-independent indices of LV contractile function. In parallel, we also determined peripheral circulation by measuring blood flow in superior mesenteric and renal arteries of mice by using Transonic flow probes and acral area and hindlimb microcirculation by laser-speckle imaging; the MAP and TPR were also calculated.

P-V analysis revealed marked depression of both load-dependent (**Figure 1**) and load-independent (**Figure 2**) indices of LV contractile function 3 h following an acute alcohol binge, which largely recovered by 12 h (Supplemental Figure 2). Acute alcohol binge also induced decrease of the MAP and TPR (**Figure 3A**), a consequence of decreased cardiac function (**Figures 1 and 2**) and marked redistribution of circulation (acral area and hindlimb vasodilation) (**Figure 3B**), and decreased mesenteric and renal blood flow (**Figure 3C**). There was no difference in the hemodynamic response to acute alcohol binge in male and female mice (Supplemental Figure 3).

A SINGLE ALCOHOL BINGE INCREASES MYOCARDIAL ANANDAMIDE LEVELS. Because numerous previous studies have shown that tissue injury and associated

FIGURE 3 Binge Alcohol Induces Vascular Dysfunction, Blood Redistribution, and Increased Cardiac Anandamide Levels

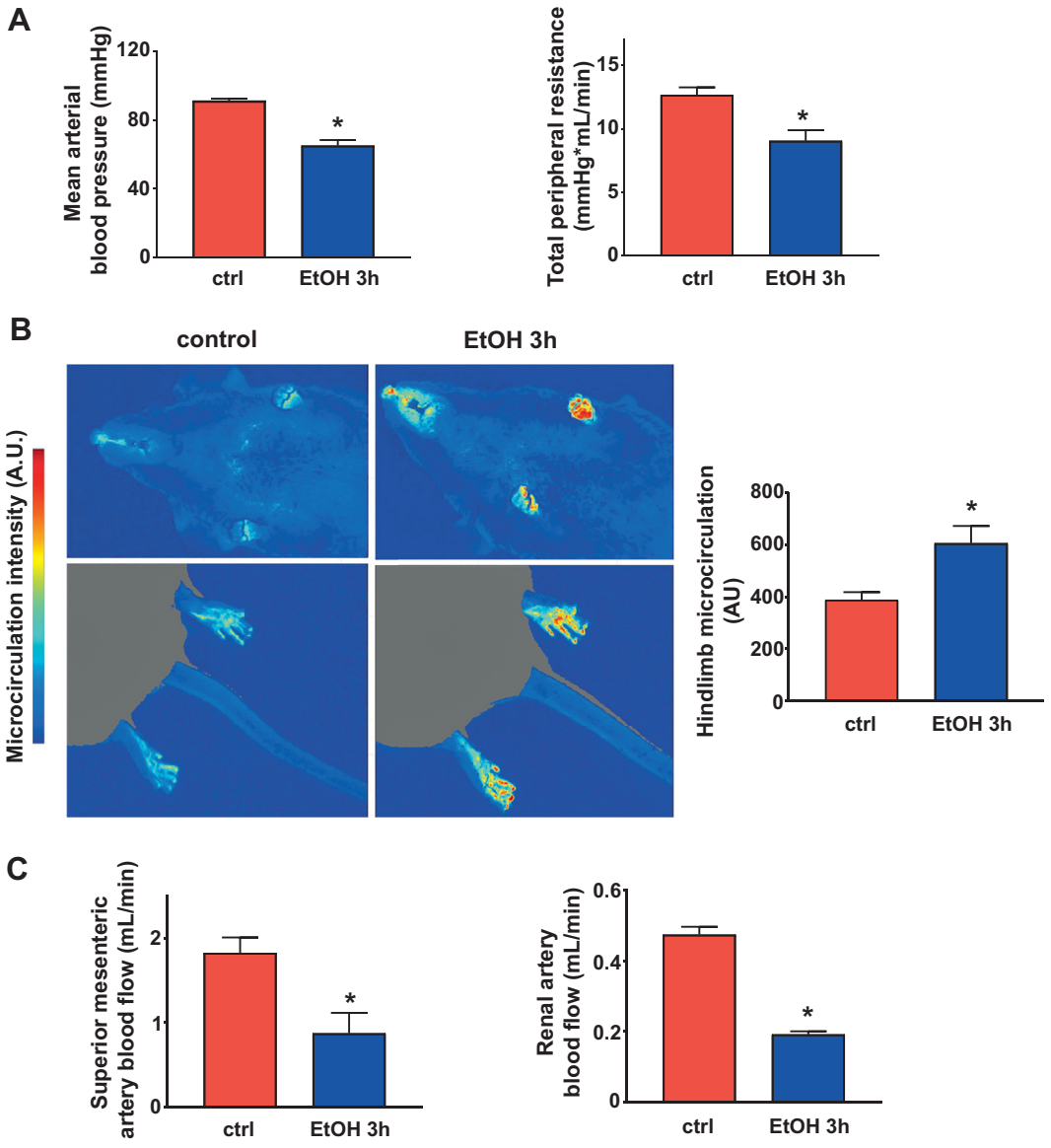

(A) Mean arterial blood pressure and total peripheral resistance measured in control and alcohol-binged (EtOH 3h) mice 3 h after maltodextrin or alcohol administration, respectively. **(B)** Representative images of the jowl and hindlimb microcirculation in control and alcohol-binged mice. **Red color** indicates more intense, whereas **blue color** represents lower microcirculation. **Right panel** shows data on hindlimb microcirculation in control and alcohol-binged mice. **(C)** Superior mesenteric artery and renal artery blood flow changes in control and alcohol-binged mice. Data are expressed as mean ± SEM, n = 6 to 8; *p < 0.05 vs. control group. Abbreviation as in Figure 1.

oxidative stress and inflammation can increase endocannabinoid levels in almost all organ systems and cell types (including myocardium, cardiomyocytes, activated endothelium, and inflammatory cells) and that endocannabinoid-CB1-R signaling promotes atherosclerosis and contributes to cardiovascular depressive state in various forms of shock, cardiomyopathies, heart failure, and liver cirrhosis (21,29), we hypothesized that this signaling may also contribute to the acute cardiovascular effects of alcohol. We found that acute alcohol binge exposure time-dependently increased myocardial endocannabinoid AEA, but not 2-AG levels, peaking 3 h following acute alcohol administration (Figure 4) when the cardiac and vascular effects of alcohol were the most pronounced (Figures 1 to 3). Myocardial AEA levels

FIGURE 4 Binge Alcohol Increases Cardiac Anandamide Level

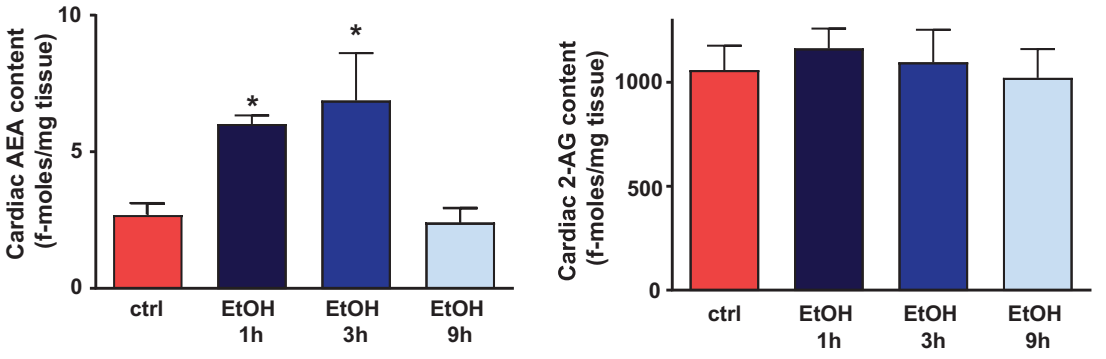

Cardiac levels of anandamide (AEA) and 2-arachidonyl glycerol (2-AG) measured in control and alcohol-binged mice. Data are expressed as mean ± SEM, n = 5 to 6; *p < 0.05 vs. control group. Abbreviations as in Figure 1.

returned to baseline 9 h after alcohol ingestion (Figure 3D) in parallel with the recovery of alcohol-induced cardiovascular dysfunction.

CB1-R SIGNALING CONTRIBUTES TO ALCOHOL-INDUCED ACUTE CARDIOVASCULAR EFFECTS. Because AEA is the endocannabinoid primarily exerting its effects on CB1-R, next we investigated the role of CB1-R signaling in the alcohol-induced cardiovascular effects by using a CB1-R antagonist/inverse agonist rimonabant and CB1-R knockout mice. Intravenous administration of rimonabant rapidly improved the 3-h alcohol intoxication-induced decrease of MAP, TPR, and superior mesenteric and renal artery blood flow, and attenuated the alcohol-induced peripheral vasodilation (hindlimb microcirculation) (Figures 5A to 5C). Rimonabant also markedly improved the alcohol binge-induced depression of load-dependent (Figures 6A to 6C) and load-independent (Figures 7A and 7B) indices of LV systolic function without exerting any effect in controls. The vehicle used had no hemodynamic effects in control or alcohol-binged groups (Supplemental Figure 4). The marked alcohol-induced depression of load-independent indices of LV systolic function 3 h following the alcohol binge were also largely attenuated in CB1-R knockout mice (Figure 8). CB1-R deletion was also associated with improved load-dependent indices of LV contractile function as well as better preservation of blood pressure and TPR 3 h following an acute alcohol binge (Supplemental Figure 5). In contrast, CB2-R deletion had no significant effects on the alcohol intoxication-induced cardiovascular effects (Supplemental Figure 6). These results indicated that endocannabinoid-CB1-R, but not CB2-R signaling contributes to the acute hemodynamic effects of alcohol binge.

DISCUSSION

In the present study, we characterized in detail the binge alcohol intoxication-induced hemodynamic alterations (cardiac and peripheral effects) in mice in vivo by using echocardiography, the state-of-the-art pressure-volume catheterization, ultrasound flow probes, and laser speckle contrast approach.

The results of the current investigation provide several unique findings worthy of consideration. At first, acute alcohol binge intoxication in mice induced a profound decrease in LV contractile function accompanied with marked redistribution of peripheral circulation leading to decreased TPR and MAP, which peaked around 3 h following acute alcohol exposure and recovered 12 h later. Secondly, these hemodynamic effects were paralleled by time-dependent increases in myocardial endocannabinoid AEA levels. Thirdly, the acute inhibition of CB1-R with rimonabant dramatically improved alcohol-induced cardiac dysfunction, whereas this effect was widely diminished in CB1-R, but not CB2-R, knockout mice. Such observations strongly suggest a critical role of CB1-R activation of the peripheral vessels and the myocardium in mediating a hypotensive and cardiodepressive response to acute alcohol binge intoxication.

Heavy episodic alcohol drinking (also known as binge drinking) is a serious health problem in the United States (2). According to the latest surveys (1) level I binge drinking is defined as 4 to 7 drinks for women, and 5 to 9 drinks for men; level II as 8 to 11 drinks for women and 10 to 14 drinks for men; and level III as 12 or more drinks for women and 15 or

FIGURE 5 Cannabinoid 1 receptor Antagonist Attenuates the Binge Alcohol-Induced Vascular Changes

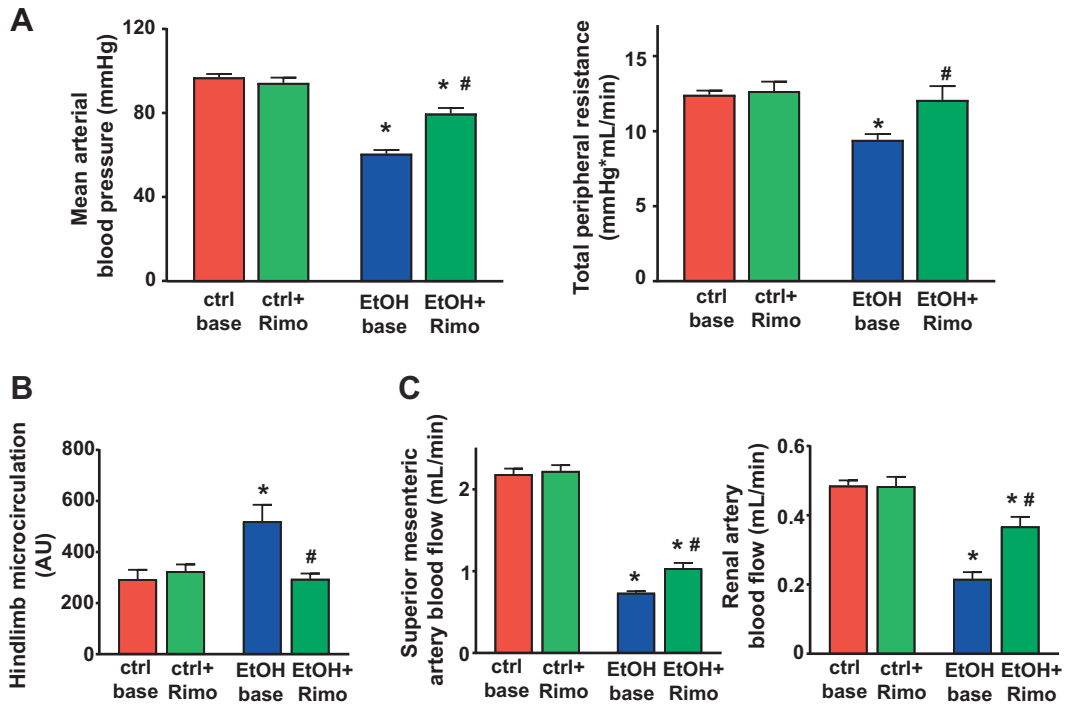

(A) Mean arterial blood pressure and total peripheral resistance measured after 3 h in control or in alcohol-binged mice before (ctrl base and EtOH base, respectively) and 15 min after intravenous rimonabant (Rimo) (ctlr + Rimo and EtOH + Rimo, respectively) administration. **(B)** Hindlimb microcirculation in control or in alcohol-binged mice before (ctrl base and EtOH base, respectively) and 15 min after intravenous Rimo. **(C)** Superior mesenteric artery and renal artery blood flow changes in control and in alcohol-binged mice before the treatment (ctrl base and EtOH base, respectively) and 15 min after intravenous Rimo (ctlr + Rimo and EtOH + Rimo, respectively) administration. Data are expressed as mean ± SEM, n = 5 to 7; *p < 0.05 vs. corresponding control group; #p < 0.05 vs. EtOH base group. CB1-R = cannabinoid 1 receptor; other abbreviations as in Figure 1.

more drinks for men on a single occasion. Alcohol drinking at levels II and III is considered extreme binge drinking and is associated with increased number of alcohol-related emergency department visits as compared to non-binge drinkers (1).

In this study, we used a single oral administration of an established dose of alcohol (5 g/kg) to mimic excessive human binge drinking (33). Consistent with previous reports using echocardiography, we found an alcohol-induced transient reduction of stroke volume and cardiac output with minimal effect on EF and fractional shortening (Supplemental Figure 1). However, under altered loading conditions, heart rate assessment of cardiac function by using echocardiography is challenging and may lead to a variety of interpretation of the results (35). We used multiple additional approaches including measurements of renal and superior mesenteric arterial flow and acral microcirculation by flow probes and/or laser speckle imaging combined with P-V analysis and found that excessive alcohol binge led to a profound redistribution of peripheral circulation (decreased mesenteric and renal blood flow and increased acral microcirculation) as well as a decrease in myocardial contractile function. The alcohol-induced decrease of mesenteric and renal blood flow can be the consequence of either the activation of compensatory mechanisms (e.g., activation of the sympathetic nervous system) to counteract the peripheral vasodilation, decrease in blood pressure, and cardiac output; however, this can also be the consequence of markedly reduced cardiac output. Based on our results, the vasodilation induced by binge alcohol exposure may ultimately lead to alteration of loading conditions affecting cardiac output and macrovascular function, at least in part, via CB1-R-dependent mechanism. Furthermore, the alcohol-induced activation of myocardial AEA-CB1-R signaling may also decrease LV intrinsic contractility (determined by evaluation of load- and heart rate-independent indices of LV function)

FIGURE 6 **CB1-R Blockade Attenuates the Binge Alcohol-Induced Contractile Dysfunction**

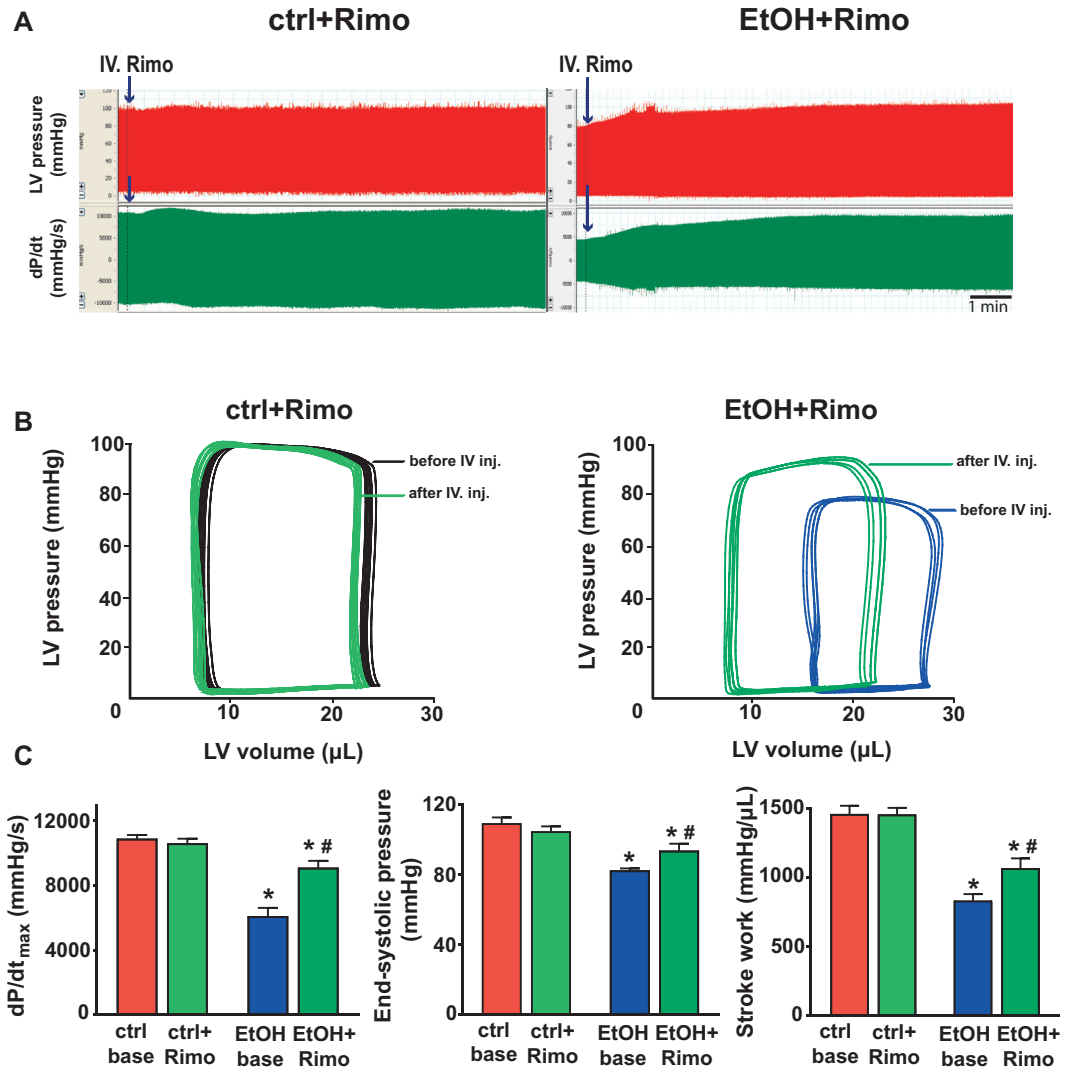

(A) Representative records of LV blood pressure changes and dP/dt in mice 3 h after either maltodextrin or alcohol binge alcohol binge following intravenous rimonabant (Rimo) (EtOH + Rimo) administration. **(B)** Representative pressure-volume (P-V) loops of maltodextrin and alcohol-binged mice before (**red and dark blue**, respectively) and 15 min after intravenous Rimo (ctrl + Rimo and EtOH + Rimo, **light green and dark green** loops, respectively) injection. **(C)** Systolic indices of LV performance [maximal slope of pressure increment (dP/dt_{max}), end-systolic pressure, stroke work] in control and in alcohol-binged mice before (ctrl base and EtOH base, respectively) and 15 min after intravenous Rimo (ctlr + Rimo and EtOH + Rimo, respectively) administration. Data are expressed as mean ± SEM, n = 6 to 8; *p < 0.05 vs. corresponding control group; #p < 0.05 vs. EtOH base group. Abbreviations as in Figures 1 and 5.

in vivo, further attenuating mean blood pressure and perhaps mesenteric and renal blood flow. These hemodynamic effects were peaking 3 h following the alcohol exposure (not different in male and female mice) and returned to baseline levels 12 h later. Similarly to our results, toxic doses of alcohol induced hypotension, decrease of TPR, and cardiac dysfunction in dogs (13). Human studies reported endothelial dysfunction and increases or biphasic effects on systolic blood pressure following binge alcohol consumption (14,16,37). In these studies, a relatively modest dose of alcohol was used.

Similar to the effects of binge alcohol drinking, increased endocannabinoid/CB1-R signaling has also been implicated in the impaired cardiac contractility associated with advanced liver cirrhosis (38,39). As liver cirrhosis often develops on a background of chronic alcoholism, the impairment of cardiac

FIGURE 7 CB1-R blockade attenuates the binge alcohol induced depression of load-independent indices of left ventricular contractile function

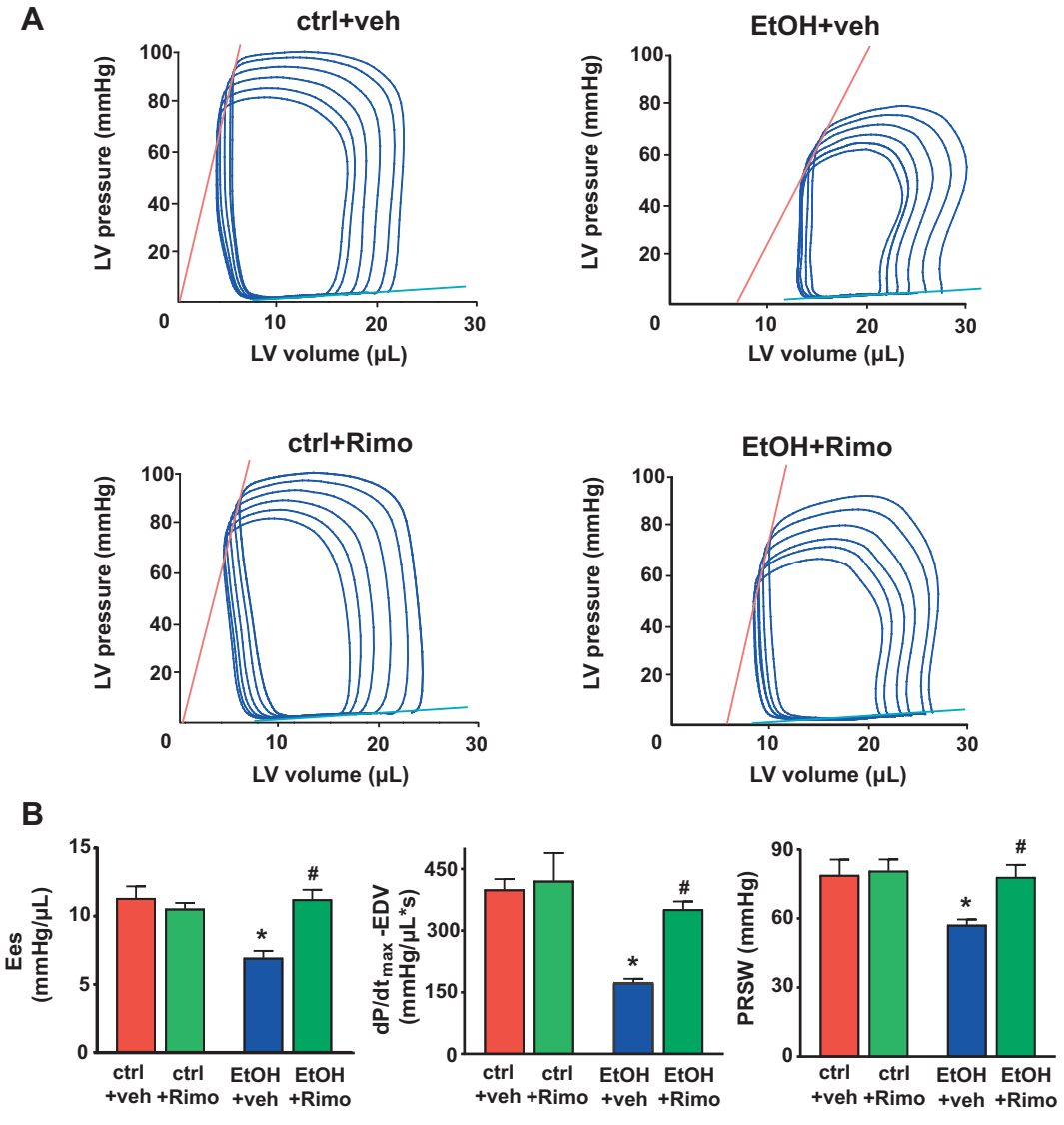

(A) Representative P-V loops obtained by gradual preload reduction obtained by vena cava occlusion of vehicle (veh) (ctrl + veh and EtOH + veh) or Rimo (ctrl + Rimo and EtOH + Rimo) treated mice 3 h after either oral alcohol or maltodextrin administration, respectively. **Red lines** indicate the slope of end-systolic P-V relationship, whereas **blue lines** depict the slope of end-diastolic P-V relationship **(B)** Load-independent indices of LV performance (Ees, the dP/dt_{max}–end-diastolic volume (EDV) relation, and PRSW) in vehicle-treated control or alcohol-binged mice (ctrl base, or EtOH base, respectively); or in rimonabant (Rimo)-treated control or alcohol-binged mice (ctlr + Rimo, or EtOH + Rimo, respectively). Data are expressed as mean ± SEM, n = 5 to 6; *$p < 0.05$ vs. corresponding control group; #$p < 0.05$ vs. EtOH base group. Abbreviations as in Figures 1, 2, 5, and 6.

contractility may be compounded in such cases. It has been also documented that binge alcohol drinking induces acute myocardial injury, and increases myocardial lipid peroxidation and protein carbonylation in mice (40). Oxidative stress has been implicated in triggering endocannabinoid production in parenchymal tissues (26,32) contributing to depression of cardiac function, vasodilation, or vasoconstriction (26,29,41). In this study we show that acute alcohol exposure is associated with time-dependent increases in myocardial endocannabinoid AEA levels, which correlate with cardiac dysfunction. We

FIGURE 8 CB1-R Deletion Attenuates the Binge Alcohol Intoxication-Induced Cardiac Dysfunction

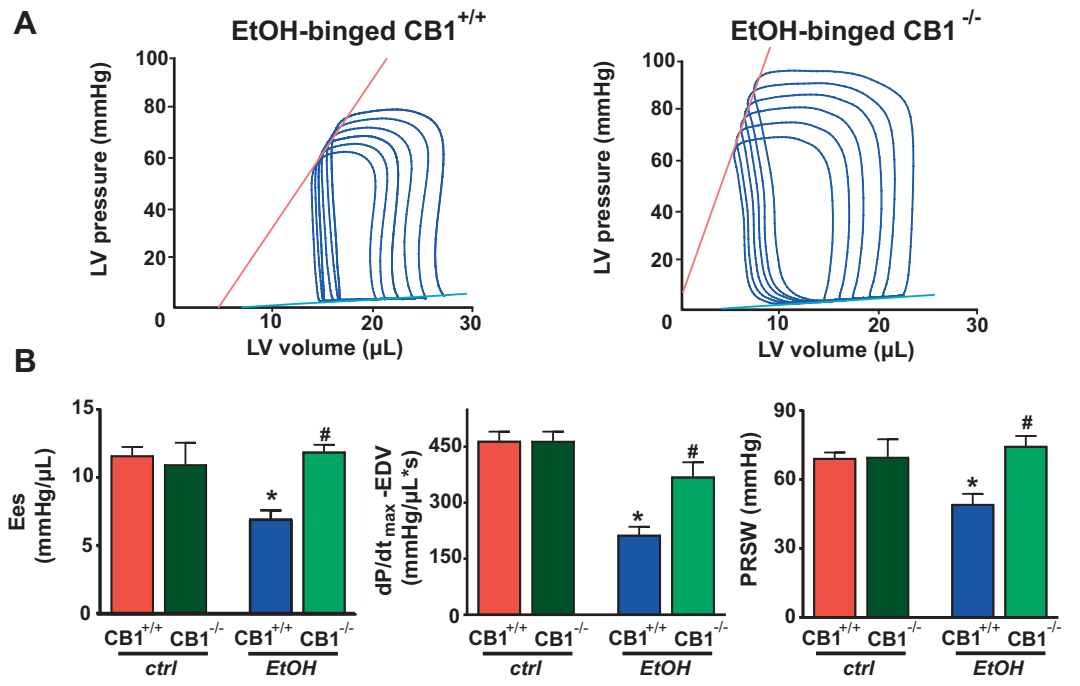

(A) Representative P-V loops of alcohol-binged $CB1^{+/+}$ and $CB1^{-/-}$ mice after gradual preload reduction obtained by vena cava occlusion. **Red lines** indicate the slope of end-systolic P-V relationship, whereas **blue lines** show the slope of end-diastolic P-V relationship. **(B)** Load-independent indices of LV performance (Ees, the dP/dt_{max} – EDV relation, and PRSW) in control or in alcohol-binged $CB1^{+/+}$ and $CB1^{-/-}$ mice. Data are expressed as mean ± SEM, n = 5 to 6; *p < 0.05 vs. corresponding control group; #p < 0.05 vs. alcohol-binged $CB1^{+/+}$ group. Abbreviations as in Figures 1, 2, 5, and 6.

also show that intravenous administration of CB1-R antagonist rimonabant 3 h after binge alcohol administration (at a peak of the cardiodepressive effects) significantly improves cardiac performance as well as redistribution of circulation, indicating an important role of the CB1-R signaling in these pathologic effects, whereas rimonabant had no effects in control mice (Figures 5 to 7). This is further substantiated by the resistance of $CB1^{-/-}$ mice to alcohol intoxication-induced hemodynamic effects (Figure 8).

Besides alcohol, synthetic cannabinoid abuse is an emerging risk for youth with documented severe adverse cardiovascular consequences mediated by cardiovascular CB1-R (29). Synthetic cannabinoids are often consumed together with alcoholic beverages for recreational use, leading to more severe outcomes (24,42).

STUDY LIMITATIONS. The in vivo study was performed in mice and mice known to metabolize alcohol faster and less sensitive to toxic effects of ethanol compared to dogs or humans. The hemodynamic effects of alcohol intoxication are complex and most likely also confounded by the time-dependent activation of various compensatory mechanism (e.g., sympathetic nervous system). In our study we performed detailed hemodynamic analysis only 3 and 12 h following the acute alcohol intoxication.

CONCLUSIONS

Collectively, we show that excessive alcohol binge exerts complex and profound cardiovascular effects with transient (lasting for several hours) marked depression of myocardial contractile function. This may represent a problem in individuals with pre-existing cardiovascular disease, chronic alcohol consumption, or regular cannabis use (29). We also show that these hemodynamic effects involve endocannabinoid-CB1-R signaling, suggesting that repurposing CB1-R antagonists for combined alcohol-synthetic cannabinoid intoxication may save lives.

ADDRESS FOR CORRESPONDENCE: Dr. Pal Pacher, Laboratory of Cardiovascular Physiology and Tissue Injury, 5625 Fishers Lane, Room 2N-17, Bethesda, Maryland 20892-9413. E-mail: pacher@mail.nih.gov.

PERSPECTIVES

COMPETENCY IN MEDICAL KNOWLEDGE: Excessive binge alcohol drinking has adverse effects on cardiovascular function. Activation of CB1-R signaling is a crucial step towards the development of acute alcohol intoxication-induced adverse cardiovascular events.

TRANSLATIONAL OUTLOOK: Since there is an increasing prevalence of alcohol ingestion alone, or in combination with synthetic cannabinoid use leading to adverse cardiovascular effects in adolescents, this emerging threat raises major health concerns, and targeting CB1-R signaling may evolve as an important therapeutic option in such conditions.

REFERENCES

1. Hingson RW, Zha W, White AM. Drinking beyond the binge threshold: predictors, consequences, and changes in the U.S. Am J Prev Med 2017;52:717–27.

2. Wechsler H, Nelson TF. What we have learned from the Harvard School Of Public Health College Alcohol Study: focusing attention on college student alcohol consumption and the environmental conditions that promote it. J Stud Alcohol Drugs 2008;69:481–90.

3. Hingson RW, Zha W, Weitzman ER. Magnitude of and trends in alcohol-related mortality and morbidity among U.S. college students ages 18-24, 1998–2005. J Stud Alcohol Drugs Suppl 2009:12–20.

4. Whitman IR, Agarwal V, Nah G, et al. Alcohol abuse and cardiac disease. J Am Coll Cardiol 2017;69:13–24.

5. Rodrigues P, Santos-Ribeiro S, Teodoro T, et al. Association between alcohol intake and cardiac remodeling. J Am Coll Cardiol 2018;72:1452–62.

6. Leifer ES. The risks and benefits of moderate alcohol consumption: there remains much to learn. J Am Coll Cardiol HF 2017;5:845–7.

7. Collaborators GBDA. Alcohol use and burden for 195 countries and territories, 1990–2016: a systematic analysis for the Global Burden of Disease Study 2016. Lancet 2018;392:1015–35.

8. Piano MR. Alcohol's effects on the cardiovascular system. Alcohol Res 2017;38:219–41.

9. Xi B, Veeranki SP, Zhao M, Ma C, Yan Y, Mi J. Relationship of alcohol consumption to all-cause, cardiovascular, and cancer-related mortality in U.S. adults. J Am Coll Cardiol 2017;70:913–22.

10. Voskoboinik A, Prabhu S, Ling LH, Kalman JM, Kistler PM. Alcohol and atrial fibrillation: a sobering review. J Am Coll Cardiol 2016;68:2567–76.

11. Bottoms GD, Fessler JF, Johnson M, Coatney RW, Voorhees W. Effects of acute alcohol intake on tolerance to hypotension. Alcohol Clin Exp Res 1990;14:776–80.

12. Kelbaek H, Gjorup T, Hartling OJ, Marving J, Christensen NJ, Godtfredsen J. Left ventricular function during alcohol intoxication and autonomic nervous blockade. Am J Cardiol 1987;59:685–8.

13. Webb WR, Degerli IU. Ethyl Alcohol and the cardiovascular system: effects on coronary blood flow. JAMA 1965;191:1055–8.

14. Rosito GA, Fuchs FD, Duncan BB. Dose-dependent biphasic effect of ethanol on 24-h blood pressure in normotensive subjects. Am J Hypert 1999;12:236–40.

15. Goslawski M, Piano MR, Bian JT, Church EC, Szczurek M, Phillips SA. Binge drinking impairs vascular function in young adults. J Am Coll Cardiol 2013;62:201–7.

16. Bau PF, Bau CH, Naujorks AA, Rosito GA. Early and late effects of alcohol ingestion on blood pressure and endothelial function. Alcohol 2005;37:53–8.

17. Gardner JD. Alcohol binge drinking: getting to the heart of it. Am J Physiol Heart Circ Physiol 2016;310:H1606–7.

18. Tsutsui M, Matsuguchi T, Tsutsui H, et al. Alcohol-induced sinus bradycardia and hypotension in patients with syncope. Jpn Heart J 1992;33:875–9.

19. Patrick ME, O'Malley PM, Kloska DD, et al. Novel psychoactive substance use by US adolescents: characteristics associated with use of synthetic cannabinoids and synthetic cathinones. Drug Alcohol Rev 2016;35:586–90.

20. McKeever RG, Vearrier D, Jacobs D, LaSala G, Okaneku J, Greenberg MI. K2—not the spice of life; synthetic cannabinoids and ST elevation myocardial infarction: a case report. J Med Toxicol 2015;11:129–31.

21. Montecucco F, Di Marzo V. At the heart of the matter: the endocannabinoid system in cardiovascular function and dysfunction. Trends Pharmacol Sci 2012;33:331–40.

22. Andonian DO, Seaman SR, Josephson EB. Profound hypotension and bradycardia in the setting of synthetic cannabinoid intoxication — a case series. Am J Emerg Med 2017;35:940 e5–6.

23. Kane EM, Hinson JS, Jordan CD, et al. Bradycardia and hypotension after synthetic cannabinoid use: a case series. Am J Emerg Med 2016;34.

24. Palamar JJ, Acosta P. Synthetic cannabinoid use in a nationally representative sample of US high school seniors. Drug Alcohol Depend 2015;149:194–202.

25. Batkai S, Pacher P, Osei-Hyiaman D, et al. Endocannabinoids acting at cannabinoid-1 receptors regulate cardiovascular function in hypertension. Circulation 2004;110:1996–2002.

26. Mukhopadhyay P, Batkai S, Rajesh M, et al. Pharmacological inhibition of CB1 cannabinoid receptor protects against doxorubicin-induced cardiotoxicity. J Am Coll Cardiol 2007;50:528–36.

27. Valenta I, Varga ZV, Valentine H, et al. Feasibility evaluation of myocardial cannabinoid type 1 receptor imaging in obesity: a translational approach. J Am Coll Cardiol Img 2018;11:320–32.

28. Rajesh M, Mukhopadhyay P, Hasko G, Liaudet L, Mackie K, Pacher P. Cannabinoid-1 receptor activation induces reactive oxygen species-dependent and -independent mitogen-activated protein kinase activation and cell death in human coronary artery endothelial cells. Br J Pharmacol 2010;160:688–700.

29. Pacher P, Steffens S, Haskó G, Schindler TH, Kunos G. Cardiovascular effects of marijuana and synthetic cannabinoids: the good, the bad, and the ugly. Nat Rev Cardiol 2017;15:151.

30. Pacher P, Batkai S, Kunos G. Cardiovascular pharmacology of cannabinoids. Handb Exp Pharmacol 2005:599–625.

31. Mukhopadhyay P, Rajesh M, Batkai S, et al. CB1 cannabinoid receptors promote oxidative stress and cell death in murine models of doxorubicin-induced cardiomyopathy and in human cardiomyocytes. Cardiovasc Res 2010;85:773–84.

32. Batkai S, Osei-Hyiaman D, Pan H, et al. Cannabinoid-2 receptor mediates protection against hepatic ischemia/reperfusion injury. FASEB J 2007;21:1788–800.

33. Bertola A, Mathews S, Ki SH, Wang H, Gao B. Mouse model of chronic and binge ethanol feeding (the NIAAA model). Nat Protoc 2013;8:627–37.

34. Pacher P, Batkai S, Osei-Hyiaman D, et al. Hemodynamic profile, responsiveness to anandamide, and baroreflex sensitivity of mice lacking fatty acid amide hydrolase. Am J Physiol Heart Circ Physiol 2005;289:H533–41.

35. Pacher P, Nagayama T, Mukhopadhyay P, Batkai S, Kass DA. Measurement of cardiac function using pressure-volume conductance catheter technique in mice and rats. Nat Protoc 2008;3:1422–34.

36. Matyas C, Varga ZV, Mukhopadhyay P, et al. Chronic plus binge ethanol feeding induces myocardial oxidative stress, mitochondrial and cardiovascular dysfunction, and steatosis. Am J Physiol Heart Circ Physiol 2016;310:H1658–70.

37. Hillbom M, Saloheimo P, Juvela S. Alcohol consumption, blood pressure, and the risk of stroke. Curr Hyperten Rep 2011;13:208–13.

38. Gaskari SA, Liu H, Moezi L, Li Y, Baik SK, Lee SS. Role of endocannabinoids in the pathogenesis of cirrhotic cardiomyopathy in bile duct-ligated rats. Br J Pharmacol 2005;146:315–23.

39. Batkai S, Mukhopadhyay P, Harvey-White J, Kechrid R, Pacher P, Kunos G. Endocannabinoids acting at CB1 receptors mediate the cardiac contractile dysfunction in vivo in cirrhotic rats. Am J Physiol Heart Circ Physiol 2007;293:H1689–95.

40. Kannan M, Wang L, Kang YJ. Myocardial oxidative stress and toxicity induced by acute ethanol exposure in mice. Exp Biol Med (Maywood) 2004;229:553–9.

41. Pacher P, Batkai S, Kunos G. The endocannabinoid system as an emerging target of pharmacotherapy. Pharmacol Rev 2006;58:389–462.

42. Castaneto MS, Gorelick DA, Desrosiers NA, Hartman RL, Pirard S, Huestis MA. Synthetic cannabinoids: epidemiology, pharmacodynamics, and clinical implications. Drug Alcohol Depend 2014;144:12–41.

KEY WORDS binge alcohol drinking, cannabinoids, contractility, endocannabinoids

APPENDIX For supplemental figures and tables, please see the online version of this article.

JACC: BASIC TO TRANSLATIONAL SCIENCE VOL. 4, NO. 5, 2019

EDITORIAL COMMENT

The Detrimental Effects of Alcohol and Cannabinoids on Cardiovascular Function*

Fabrizio Montecucco, MD, PhD,[a,b] Federico Carbone, MD, PhD[a,c]

People used to binging alcohol drinking or/and smoking marijuana to enjoy the weekend are likely not aware of their increased risk of developing acute cardiovascular (CV) dysfunction, cardiac arrhythmias, and other life-threatening conditions affecting the liver and brain (1). In their study in this issue of *JACC: Basic to Translational Science*, Paloczi et al. (2) described how exaggerated alcohol assumption, even in a single shot, may induce severe CV dysfunction in mice.

SEE PAGE 625

It is noteworthy that the authors recognized the up-regulation of the endogenous cannabinoid (also referred to as endocannabinoid) anandamide as a leading mechanism underlying alcohol-induced CV dysfunction (3). Such results strongly suggest how the concomitant assumption of alcohol and cannabinoids may synergistically determine CV dysfunction.

Although those observations raise a warning for public health, especially involving young people, any translation to human beings still remains highly speculative, and caution should be used. Our recommendation is justified by the following reasons already acknowledged by the authors in their article:

1) The study might suggest that both alcohol- and cannabinoid-mediated effects on CV dysfunction might trigger common pathways. Such evidence is limited to the animal model, whereas further data are needed to confirm a relevance for human beings. Indeed, mouse and human pathophysiology show several differences, especially concerning metabolism and the toxicity of exogenous compounds. Therefore, it often happens that intriguing evidence in mice is no longer confirmed in humans.
2) The mouse model might be distant from real life of human beings. Ethylic alcohol concentration may be correctly estimated in mice but not in humans. Indeed, wine, beer, and other alcoholic beverages combine ethylic alcohol with other "cardioprotective" compounds, such as polyphenols (3). Especially concerning moderate assumption of red wine, several studies in past decades investigated its antioxidant properties, which may partially balance alcohol toxicity. We need studies investigating whether this so-called "French paradox" might have a role in limiting the negative acute effects of binge alcohol drinking (3).
3) Concomitant administration of exogenous cannabinoids together with alcohol was not explored. Therefore, we cannot conclude about a potential synergistic toxicity of alcohol and cannabinoids on cardiac function.
4) Additional mechanisms, such as increased inflammation (elevated levels of macrophage migration inhibitory factor [MIF], interleukin 1β,

*Editorials published in *JACC: Basic to Translational Science* reflect the views of the authors and do not necessarily represent the views of *JACC: Basic to Translational Science* or the American College of Cardiology.

From the [a]IRCCS Ospedale Policlinico San Martino Genoa, Italian Cardiovascular Network, Genoa, Italy; [b]First Clinic of Internal Medicine, Department of Internal Medicine, and Centre of Excellence for Biomedical Research (CEBR), University of Genoa, Genoa, Italy; and the [c]First Clinic of Internal Medicine, Department of Internal Medicine, University of Genoa, Genoa, Italy. Both authors have reported that they have no relationships relevant to the contents of this paper to disclose.

The authors attest they are in compliance with human studies committees and animal welfare regulations of the authors' institutions and Food and Drug Administration guidelines, including patient consent where appropriate. For more information, visit the *JACC: Basic to Translational Science* author instructions page.

ISSN 2452-302X https://doi.org/10.1016/j.jacbts.2019.08.001

and interleukin-6), autophagy, and overt cardiac apoptosis, potentially impacting acute CV dysfunction were only partially explored, suggesting that further studies are needed to better clarify the relationship of alcohol and endocannabinoids on CV dysfunction.

Therefore, much remains to discover and clarify. Certainly, the authors might have identified an additional negative effect of excessive alcohol consumption that should further discourage people to abuse. In line with this, not only chronic alcohol abuse but also acute alcohol intoxication would have a detrimental role in triggering devastating complications (4).

Another strength of this study is the demonstration that alcohol-induced cardiac dysfunction is dependent on cannabinoid type 1 receptor (CB1) activation. Being ubiquitously expressed in several tissues (including brain, heart, vascular, and inflammatory cells), CB1 has been extensively studied in the last decade. Its activation has been associated with organ dysfunction in different CV disease models. A specific CB1 antagonist rimonabant was also proved to effectively reduce body weight and CV risk in humans in clinical trials, but the high rate of severe psychiatric adverse effects imposed withdrawal from the market (4).

The results provided by Paloczi et al. are in line with previous evidence indicating a pathophysiological role of CB1 in CV injury. This is an intriguing issue because beneficial effects of CB1 inhibition and/or CB2 activation were already demonstrated in other CV disease models, including atherosclerosis and related life-threatening complications (5). Ultimately, this study should stimulate further efforts in developing new CB1 pharmacological antagonists that do not pass the blood-brain barrier and therefore are better tolerated. Because CB2 was recently demonstrated to have anti-inflammatory activities circulating inflammatory cells, it would be of particular interest to develop compounds that simultaneously inhibit CB1 and activate CB2 at the same time (5).

Finally, we would stress future perspectives for endocannabinoids and their transmembrane receptors in CV research. The authors involved in this study are recognized as experts in this field of research and some of them (i.e., Pal Pacher, George Kunos, and Thomas Schindler) recently paved the way for analyzing the cannabinoid system by using cannabinoid tracers for cardiac nuclear imaging. We believe that this exciting route would be a very successful approach for translating mouse discoveries in human beings and for performing therapeutic strategies to limit alcohol-induced CV toxicity.

ADDRESS FOR CORRESPONDENCE: Dr. Fabrizio Montecucco, First Clinic of Internal Medicine, Department of Internal Medicine, University of Genoa, 6 Viale Benedetto XV, 16132 Genoa, Italy. E-mail: fabrizio.montecucco@unige.it.

REFERENCES

1. Lanthier N, Starkel P. Treatment of severe alcoholic hepatitis: past, present and future. Eur J Clin Invest 2017;47:531–9.

2. Paloczi J, Matyas C, Cinar R, et al. Alcohol binge-induced cardiovascular dysfunction involves endocannabinoid-CB1-R signaling. J Am Coll Cardiol Basic Trans Science 2019;4:625–37.

3. Liberale L, Bonaventura A, Montecucco F, Dallegri F, Carbone F. Impact of red wine consumption on cardiovascular health. Curr Med Chem 2017 May 17 [Epub ahead of print].

4. Mach F, Montecucco F, Steffens S. Effect of blockage of the endocannabinoid system by CB(1) antagonism on cardiovascular risk. Pharmacol Rep 2009;61:13–21.

5. Montecucco F, Di Marzo V. At the heart of the matter: the endocannabinoid system in cardiovascular function and dysfunction. Trends Pharmacol Sci 2012;33:331–40.

KEY WORDS alcohol, cardiovascular dysfunction, endocannabinoids

JACC: BASIC TO TRANSLATIONAL SCIENCE VOL. 4, NO. 5, 2019

STATE-OF-THE-ART REVIEW

Atrial Myopathy

Mark J. Shen, MD,[a,b] Rishi Arora, MD,[a] José Jalife, MD[c,d]

JACC: BASIC TO TRANSLATIONAL SCIENCE CME/MOC/ECME

This article has been selected as this month's *JACC: Basic to Translational Science* CME/MOC/ECME activity, available online at http://www.acc.org/jacc-journals-cme by selecting the *JACC* Journals CME/MOC/ECME tab.

Accreditation and Designation Statement

The American College of Cardiology Foundation (ACCF) is accredited by the Accreditation Council for Continuing Medical Education (ACCME) and the European Board for Accreditation in Cardiology (EBAC) to provide continuing medical education for physicians.

The ACCF designates this Journal-based CME/MOC/ECME activity for a maximum of 1 AMAPRA Category 1 Credit or 1 EBAC Credit. Physicians should only claim credit commensurate with the extent of their participation in the activity.

Successful completion of this CME activity, which includes participation in the evaluation component, enables the participant to earn up to 1 Medical Knowledge MOC point in the American Board of Internal Medicine's (ABIM) Maintenance of Certification (MOC) program. Participants will earn MOC points equivalent to the amount of CME credits claimed for the activity. It is the CME activity provider's responsibility to submit participant completion information to ACCME for the purpose of granting ABIM MOC credit.

Atrial Myopathy will be accredited by the European Board for Accreditation in Cardiology (EBAC) for 1 hour of External CME credits. Each participant should claim only those hours of credit that have actually been spent in the educational activity. The Accreditation Council for Continuing Medical Education (ACCME) and the European Board for Accreditation in Cardiology (EBAC) have recognized each other's accreditation systems as substantially equivalent. Apply for credit through the post-course evaluation.

Method of Participation and Receipt of CME/MOC/ECME Certificate

To obtain credit for *JACC: Basic to Translational Science* CME/MOC/ECME, you must:

1. Be an ACC member or JACBTS subscriber.
2. Carefully read the CME/MOC/ECME-designated article available online and in this issue of the *journal*.
3. Answer the post-test questions. At least 2 questions provided must be answered correctly to obtain credit.
4. Complete a brief evaluation.
5. Claim your CME/MOC/ECME credit and receive your certificate electronically by following the instructions given at the conclusion of the activity.

CME/MOC/ECME Objective for This Article: Upon completion of this activity, the learner should be able to: 1) select the factors contributing to stroke risk in atrial fibrillation; 2) recognize the indications and contraindications for treatment of atrial fibrillation with anti-arrhythmic medication and catheter ablation; and 3) identify the stages and characteristics of atrial myopathy.

CME/MOC/ECME Editor Disclosure: CME/MOC/ECME Editor L. Kristin Newby, MD, is supported by research grants from Amylin, Bristol-Myers Squibb Company, GlaxoSmithKline, Sanofi, Verily Life Sciences (formerly Google Life Sciences), the MURDOCK Study, NIH, and PCORI; receives consultant fees/honoraria from BioKier, DemeRx, MedScape/TheHeart.org, Metanomics, Philips Healthcare, Roche Diagnostics, CMAC Health Education & Research Institute; serves as an Officer, Director, Trustee, or other fiduciary role for the AstraZeneca HealthCare Foundation and the Society of Chest Pain Centers (now part of ACC); and serves in another role for the American Heart Association and is the Deputy Editor of *JACC: Basic to Translational Science*.

Author Disclosures: Dr. Arora is an owner of Rhythm Therapeutics, Inc. Dr. Jalife has received a research grant from Medtronic. Dr. Shen has reported that he has no relationships relevant to the contents of this paper to disclose.

Medium of Participation: Online (article and quiz).

CME/MOC/ECME Term of Approval

Issue Date: September 2019
Expiration Date: August 31, 2020

From the [a]Feinberg Cardiovascular and Renal Research Institute, Feinberg School of Medicine, Northwestern University, Chicago, Illinois; [b]Cardiac Electrophysiology, Prairie Heart Institute of Illinois, HSHS St. John's Hospital, Springfield, Illinois; [c]Center for Arrhythmia Research, University of Michigan, Ann Arbor, Michigan; and the [d]Centro Nacional de Investigaciones Cardiovasculares, Carlos III (CNIC), and CIBERCV, Madrid, Spain. Dr. Arora is an owner of Rhythm Therapeutics, Inc. Dr. Jalife has received a research grant from Medtronic. Dr. Shen has reported that he has no relationships relevant to the contents of this paper to disclose.

The authors attest they are in compliance with human studies committees and animal welfare regulations of the authors' institutions and Food and Drug Administration guidelines, including patient consent where appropriate. For more information, visit the *JACC: Basic to Translational Science* author instructions page.

Manuscript received December 12, 2018; revised manuscript received May 3, 2019, accepted May 5, 2019.

ISSN 2452-302X https://doi.org/10.1016/j.jacbts.2019.05.005

Atrial Myopathy

Mark J. Shen, MD,[a,b] Rishi Arora, MD,[a] José Jalife, MD[c,d]

HIGHLIGHTS

- **The authors discuss the concept of atrial myopathy; its relationship to aging, electrophysiological remodeling, and autonomic remodeling; the interplay between atrial myopathy, AF, and stroke; and suggest how to identify patients with atrial myopathy and how to incorporate atrial myopathy into decisions about anticoagulation.**
- **Atrial myopathy seen in animal models of AF and in patients with AF is the result of a combination of factors that lead to electrical and structural remodeling in the atrium. Although AF may lead to the initiation and/or progression of this myopathy, the presence of AF is by no means essential to the development or the maintenance of the atrial myopathic state.**
- **Methods to identify atrial myopathy include atrial electrograms, tissue biopsy, cardiac imaging, and certain serum biomarkers. A promising modality is 4-dimensional flow cardiac magnetic resonance. The concept of atrial myopathy may help guide oral anticoagulant therapy in selected groups of patients with AF, particularly those with low to intermediate risk of strokes and those who have undergone successful AF ablation. This review highlights the need for prospective randomized trials to test these hypotheses.**

SUMMARY

This paper discusses the evolving concept of atrial myopathy by presenting how it develops and how it affects the properties of the atria. It also reviews the complex relationships among atrial myopathy, atrial fibrillation (AF), and stroke. Finally, it discusses how to apply the concept of atrial myopathy in the clinical setting—to identify patients with atrial myopathy and to be more selective in anticoagulation in a subset of patients with AF. An apparent lack of a temporal relationship between episodes of paroxysmal AF and stroke in patients with cardiac implantable electronic devices has led investigators to search for additional factors that are responsible for AF-related strokes. Multiple animal models and human studies have revealed a close interplay of atrial myopathy, AF, and stroke via various mechanisms (e.g., aging, inflammation, oxidative stress, and stretch), which, in turn, lead to fibrosis, electrical and autonomic remodeling, and a pro-thrombotic state. The complex interplay among these mechanisms creates a vicious cycle of ever-worsening atrial myopathy and a higher risk of more sustained AF and strokes. By highlighting the importance of atrial myopathy and the risk of strokes independent of AF, this paper reviews the methods to identify patients with atrial myopathy and proposes a way to incorporate the concept of atrial myopathy to guide anticoagulation in patients with AF. (J Am Coll Cardiol Basic Trans Science 2019;4:640–54)

Atrial fibrillation (AF) is the most common arrhythmia in developed countries. Approximately 2.3 million people in the United States have been currently diagnosed with AF, and U.S. Census projections estimate that this count will more than double by 2050 (1). AF is associated with a 5-fold risk of stroke, and AF-related strokes are 2.5-fold likely to be fatal (2). AF-related strokes are usually attributed to clots forming in the left atrial appendage (LAA) due to local stasis, followed by dislodgement and embolization to the brain (particularly upon restoration of sinus rhythm). However, this classic concept has been challenged by observations from clinical trials of the past 2 decades. If local stasis during AF is the primary cause of stroke, maintenance of sinus rhythm should prevent embolism. This was not what early randomized clinical trials such as RACE (Rate Control versus Electrical Cardioversion for Persistent Atrial Fibrillation Study) and AFFIRM (Atrial Fibrillation Follow-up Investigation of Rhythm Management) demonstrated 16 years ago (3,4). Recently, several clinical studies in which patients' atrial rhythms were continuously monitored showed a temporal dissociation of the episodes of device-recorded subclinical AF and stroke (5–8). For instance, in the ASSERT (Asymptomatic Atrial Fibrillation and Stroke Evaluation in Pacemaker Patients and the Atrial Fibrillation Reduction Atrial Pacing) trial that enrolled 2,580 patients with cardiac implantable electronic devices, only 8% of patients with stroke had AF events detected within 30 days before stroke, and 16% of patients with stroke had

ABBREVIATIONS AND ACRONYMS

4D = 4 dimensional

AF = atrial fibrillation

APD = action potential duration

Ca^{2+} = calcium

CMR = cardiac magnetic resonance

CRP = C-reactive protein

Cx = connexin

GDF = growth differentiation factor

IL = interleukin

$K+$ = potassium

LA = left atrial

LAA = left atrial appendage

NADPH = nicotinamide adenine dinucleotide phosphate

NOX2 = catalytic, membrane-bound subunit of NADPH oxidase

NT-proBNP = N-terminal pro B-type natriuretic peptide

OAC = oral anticoagulant

ROS = reactive oxygen species

TGF = transforming growth factor

TNF = tumor necrosis factor

their first AF event after their strokes (5). The lack of a temporal relationship between the onset of AF and stroke suggests that additional factors may be important contributors to the occurrence of stroke and that the presence of AF is not necessary. The current paradigm of selecting individuals at elevated risk of stroke and who therefore warrant oral anticoagulation (OAC) therapy, as endorsed by major international societies (9,10), is by the CHA_2DS_2-VASc score (congestive heart failure, hypertension, age older than 75 years, diabetes mellitus, previous stroke, or transient ischemic attack or thromboembolism, vascular disease, age 65 to 74 years, sex category), but not the properties of AF per se (frequency, duration, ventricular rates, and so on). All these risk factors are known to cause atrial myopathy. There is mounting evidence that supports that atrial myopathy not only leads to stasis, but also to endothelial and/or endocardial dysfunction and the hypercoagulable state, which are 3 key factors in thrombogenesis described by Virchow (11). AF may not be the root cause of stroke, but rather, a marker that the atria are diseased. This review seeks to: 1) introduce the concept of atrial myopathy—whether in the absence or presence of AF—and highlight the recent translational and clinical studies that have investigated the relationship among atrial myopathy, AF, and stroke; 2) discuss how to identify patients with atrial myopathy, even in the absence of AF; and 3) discuss whether severity of atrial myopathy can help guide the decision to anticoagulate patients with AF.

ATRIAL MYOPATHY: THE CONCEPT

> *"… that the arrhythmia (AF) causes a tachycardia-induced atrial cardiomyopathy (myopathy) that results in electrophysiological and anatomic remodeling of the atria."* (12)

Most of our mechanistic understanding of the atrial myopathic state comes from research conducted either in animal models of AF or from examination of tissue removed from patients with a history of AF. In 1997, Zipes (12) first used the term "atrial myopathy" to describe that AF can lead to myopathy through atrial remodeling. The past 2 decades have seen the concept of atrial myopathy evolving. Several recent studies have demonstrated that the relationship between AF and atrial myopathy is more complex. For example, atrial myopathy may exist without AF and can facilitate the development of AF (13). Anatomical or structural changes, particularly fibrosis, play a major role in the pathogenesis of AF, by increasing the conduction heterogeneity in the atria, thereby providing the substrate for re-entry (14–17). Atrial interstitial fibrosis has been observed in patients with AF (18). In dogs with heart failure induced by rapid ventricular pacing, extensive atrial fibrosis underlies the mechanism by which AF is much easier to be induced and become sustained, despite unaltered atrial electrophysiological parameters (19). Fibroblast proliferation and extracellular matrix deposition in response to insults such as aging (20), atrial stretch (16), inflammation (21,22), and oxidative stress (21,23) may predispose to anisotropy and re-entry (24). The electrical derangement adds to a vicious cycle in which "AF begets AF" (25)—rapid atrial myocyte depolarization leads to intracellular calcium accumulation, triggering adaptive and inflammatory responses that potentiate myocyte apoptosis and accelerate atrial fibrosis (26).

Histologically, atrial fibrosis is characterized by cardiomyocytes exhibiting loss of sarcomeres as well as accumulation of glycogen storage granules, which are adaptive alterations in cellular metabolism not unlike those observed in response to ischemia (27). A principal mediator of AF-induced atrial cardiomyocyte apoptosis and necrosis is calpain (28), a protein concentrated in or near the nucleus, and intercalated discs, which are capable of both proteolysis and degradation of L-type calcium channels (29). Other potential mediators of structural remodeling include platelet-derived growth factor, atrial natriuretic peptide, and galectin-3 (30,31). In addition, the renin-angiotensin system appears to play a role, because angiotensin-converting enzyme inhibitors (or angiotensin-receptor blockers) blunt atrial fibrosis (32) and decrease the incidence of AF in heart failure in both animal (33,34) and clinical studies (35,36). Transforming growth factor-β (TGF-β) also has an important role. Mouse models that overexpress TGF-β1 have profound atrial fibrosis and AF (with normal ventricles) (15). In a canine model of heart failure with extensive atrial fibrosis, the drug pirfenidone significantly reduced atrial fibrotic remodeling and vulnerability, and was associated with a significant reduction in the expression of TGF-β1 (37). In a canine heart failure model, Kunamalla et al. (38) recently showed that targeted atrial expression of a plasmid expressing a dominant negative TGF-β1 receptor prevented atrial fibrosis, with a resulting homogenization of conduction and a decrease in inducible AF. To sum up, pathological

atrial remodeling leads to the development of AF: which worsens the atrial myopathic processes that then help to sustain more AF? The following sections help to further highlight the concept that although AF may lead to the initiation and/or progression of this myopathy, the presence of AF is by no means essential to the development or the maintenance of this myopathic state.

ATRIAL MYOPATHY AND THE AGING HEART

Aging leads to advancing decline in the structure and function of the heart, and is a leading risk factor for cardiovascular diseases (39), including AF. Although 50% of patients with AF are older than 80 years of age (40), the molecular mechanisms that relate aging to atrial deterioration remain partly elucidated, and it is unclear how aging promotes atrial remodeling. Aging is commonly associated with cardiovascular comorbidities, oxidative stress, calcium dysregulation, atrial myopathy with apoptosis, and fibrosis, all of which contribute to the initiation and/or maintenance of AF, but the mechanisms have been poorly explored (41). Chronic inflammation is associated with several age-related diseases such as atherosclerosis, Alzheimer's disease, sarcopenia, and arthritis (42). The genesis of chronic inflammation with aging is unclear, but inflammation could be an underlying mechanism that connects aging to atrial myopathy and AF (43). Clinical studies have connected various circulating inflammatory mediators, including C-reactive protein (CRP), interleukin (IL)-1β, IL-6, tumor necrosis factor (TNF)-α, and immune complement activation, with persistent AF (44). Epicardial fat is a major source of adipokines, inflammatory cytokines, and free fatty acids, which contributes to fibrotic remodeling within the atrial myocardium (45). Macrophages and neutrophils are key cellular mediators of inflammation that may contribute to AF by infiltrating the atria or epicardial fat (46), releasing reactive oxygen species (ROS), and producing inflammatory cytokines, chemokines, metalloproteinases, or myeloperoxidases (43). Inflammation is also critical for insulin resistance in experimental models of diet-induced obesity (47). Increasing adiposity leads to the recruitment of macrophages into fat depots. Macrophages, together with adipocytes, generate inflammatory mediators, including TNF-α, which may mediate insulin resistance. Thus, inflammation occurs in aging, obesity and AF, yet the inflammatory pathway linking obesity to AF has not been identified.

Comprehensive understanding of the molecular mechanisms of intrinsic cardiac aging, including atrial aging, will be required to improve understanding of the relationship among aging, inflammation, atrial myopathy, and AF. Such new understanding should guide the development and future translation of novel therapies to clinical application. Mechanistic insights may also identify other more specific therapeutic targets and provide guidance toward interventions for AF-related comorbidities.

ATRIAL MYOPATHY AND ELECTROPHYSIOLOGICAL REMODELING

Besides structural changes, atrial myopathy is associated with alterations in calcium cycling (excitation–contraction coupling), ion channels, and gap junctions that, in turn, lead to electrophysiological remodeling in the atrium.

Oxidative stress associated with atrial myopathy leads to intracellular calcium overload, promoting triggered activity and apoptosis. However, during AF, the exceedingly high frequency of excitation of the atria is expected to lead to ryanodine receptor type 2 refractoriness (48), as well as down-regulation of calcium (Ca^{2+}) handling proteins (49), which act to prevent triggered activity. Nevertheless, $[Ca^{2+}]_i$ overload, together with atrial dilatation, mitochondrial ROS, and activation of inflammatory and pro-fibrotic pathways, progressively alters gene expression, with consequent myocyte hypertrophy, interstitial fibrosis, and ion channel remodeling, all of which occur slowly but reach critical levels when AF becomes persistent (49).

The spatial distribution of ion channel functional expression is heterogeneous throughout the atria (50–52). In addition, the amount of remodeling ion channels undergo with time in AF is also heterogeneous (53). Such heterogeneities are responsible for the different electrophysiological properties of different regions of the atria in terms of conduction velocity, action potential duration (APD), and the refractory period, all of which condition the ability of each region to harbor re-entrant circuits at different frequencies in response to the remodeling process. Cellular electrophysiological studies in atrial myocytes from patients in persistent or permanent AF have revealed marked reductions in the densities of the L-type voltage-gated Ca_{2+} current, the transient outward potassium (K+) current, and the ultra-rapid delayed rectifier K+ current (54). Sustained high-frequency excitation in a sheep model of long-term atrial tachypacing led to APD abbreviation secondary to ion channel gene expression changes (the main cardiac sodium channel, L-type calcium channel, and voltage gated potassium channel decrease; and stria

specific inward rectifying potassium channel increase) (49). A study using specimens of human atrium demonstrated that chronic AF reduced the transient outward current and the ultrarapid delayed rectifier potassium channel (I_{Kur}) (55). In addition, the slow component of the delayed rectifier K^+ current is increased, which results in significant APD abbreviation. Importantly, such changes are quantitatively different between right and left atria, which may explain the propensity of 1 atrium to sustain more stable re-entry at a higher frequency than the other.

Gap junctions are essential in atrial conduction, and gap junction remodeling, such as changes in distribution, intercellular orientation, and expression of gap junction proteins, is associated with electrophysiological and structural changes that result in sustained AF (56,57). Two major gap junction proteins, connexin (Cx) 40 and Cx43, mediate cardiomyocyte-to-cardiomyocyte electrical coupling. Abnormal expression and heterogeneous distributions of Cxs have a strong association with AF in patients (58) and rapid pacing animal models (59,60). In a dilated left atrium (LA) with chronic pressure overload and left ventricular hypertrophy, reduced expression and lateral distribution of Cx43, as well as interstitial fibrosis, lead to conduction abnormality, which increases the susceptibility to AF (61). Moreover, the laterally redistributed Cx43 does not form gap junction channels (62). Together with the significant reduction in sodium current associated with atrial remodeling (49), reduced Cx function should significantly reduce atrial conduction velocity. In patients with hypertension and left ventricular hypertrophy but no history of AF, global conduction slowing, focal conduction delay, and increased vulnerability to AF have been noted (63). In a subgroup of 485 patients from the ASSERT cohort (5), serial noninvasive programmed atrial stimulation showed those who went on to develop atrial tachyarrhythmias had P-wave prolongation and increased vulnerability to AF induction at baseline but no difference in atrial refractoriness (64).

ATRIAL MYOPATHY AND AUTONOMIC REMODELING

In addition to alterations in ion channels, gap junctions, and excitation–contraction coupling, the autonomic nervous system is another contributor to electrical remodeling in the fibrillating atrium. Animal studies have shown that atrial myopathy or LA distention caused by obesity and obstructive sleep apnea (65) can lead to remodeling of the autonomic nervous system, which is instrumental in pathogenesis of cardiac arrhythmias (66), including that of AF (67). Patterson et al. (68,69) described "calcium transient triggering," in that sympathetic activation causes an increasing calcium transient (70), whereas vagal activation can reduce the atrial effective refractory period (71). The discrepancy between APD and the intracellular calcium transient, which are normally tightly coupled, leads to an increased forward sodium/Ca exchanger current, which contributes to generation of early afterdepolarizations and triggered activity (68). This is particularly evident in the muscle sleeves of the pulmonary veins, of which focal activities are critically important in the initiation of AF in humans (72). Histologically, the pulmonary vein muscle sleeves are particularly richly innervated with both sympathetic and parasympathetic nerves (73,74). With direct nerve recordings, the intrinsic cardiac nerve activities recorded from the fat pad next to the left superior pulmonary vein and LA junction were found to be in close temporal relationships, with nerve activities recorded from extracardiac nerve structures (e.g., the left stellate ganglion and the thoracic vagus nerve). Intrinsic cardiac nerve activities invariably preceded spontaneously occurring atrial tachyarrhythmias in a canine model of pacing-induced AF (75). In patients recovering from open heart surgery, these fat pad intrinsic cardiac nerve activities were associated with an increased burden of premature atrial complexes and might predict the development of post-operative AF (76).

ATRIAL MYOPATHY: ITS INTERPLAY BETWEEN AF AND STROKE

One major link between atrial myopathy, AF, and stroke is inflammation (77). Inflammatory markers, such as CRP, TNF-α, and IL-2, -6, and -8, increase in patients with AF (78). Several prospective epidemiological studies confirmed that inflammation confers an increased risk of AF. For example, in a large cohort that involved 25,883 participants of the Women's Health Study, inflammatory biomarkers, including CRP, soluble intercellular adhesion molecule-1, and fibrinogen, were independently associated with increased incidence of AF in initially healthy, middle-aged women during a median follow-up of 14.4 years, after controlling for traditional risk factors (79). In another large cohort study of 47,000 subjects, elevated plasma CRP levels were robustly associated with increased incidence of AF (80). In the absence of AF, it is possible that the pro-inflammatory state can contribute to the development of atrial myopathy, which, in turn, leads to endothelial dysfunction or other structural changes, and thereby more pro-

CENTRAL ILLUSTRATION **Atrial Myopathy: Its Relationship Between Atrial Fibrillation and Strokes**

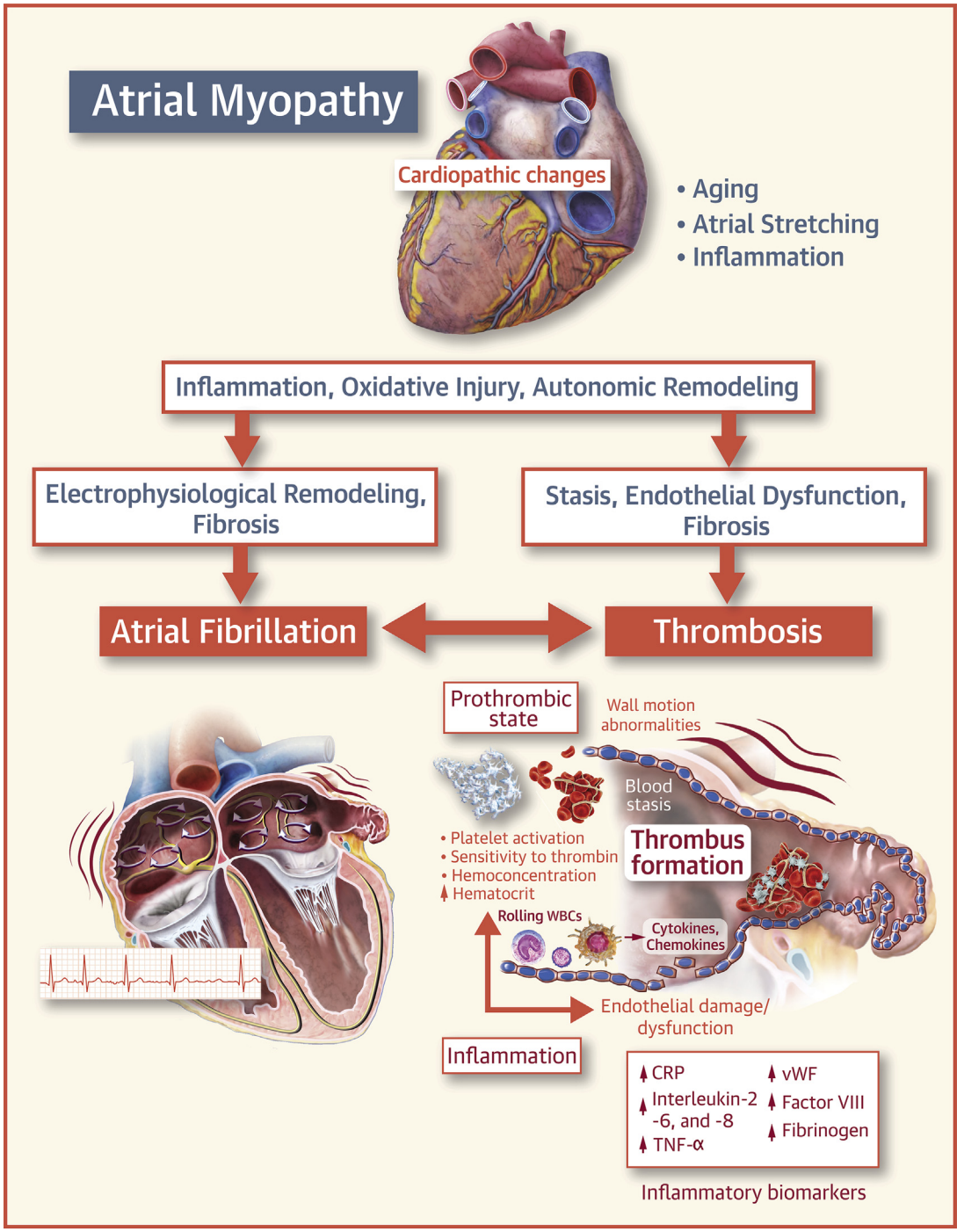

Shen, M.J. et al. J Am Coll Cardiol Basic Trans Science. 2019;4(5):640–54.

Atrial myopathy is typically caused by insults such as aging, inflammation, oxidative stress, and stretching of the atria. These myopathic changes alter the properties of myocardial electrophysiology and cardiac autonomic nervous system. They can also lead to architectural structural changes characterized by fibrosis. Furthermore, atrial myopathy results in endothelial dysfunction and stasis, thereby a prothrombotic state. Electrophysiological remodeling and fibrosis facilitate the development of atrial fibrillation, which leads to more inflammation, fibrosis and autonomic remodeling, all of which contribute to a worsening prothrombotic environment, mediated by circulating inflammatory cytokines, chemokines and other molecules such as C-reactive protein (CRP), interleukin (IL)- 2, -6 and -8, tumor necrosis factor (TNF)-α, etc. Atrial fibrillation and thrombosis can develop separately and interact closely to further aggravate the underlying atrial myopathic processes. CRP = C-reactive protein; vWF = von Willebrand's Factor; WBC = white blood cell.

FIGURE 1 Stages of Atrial Myopathy

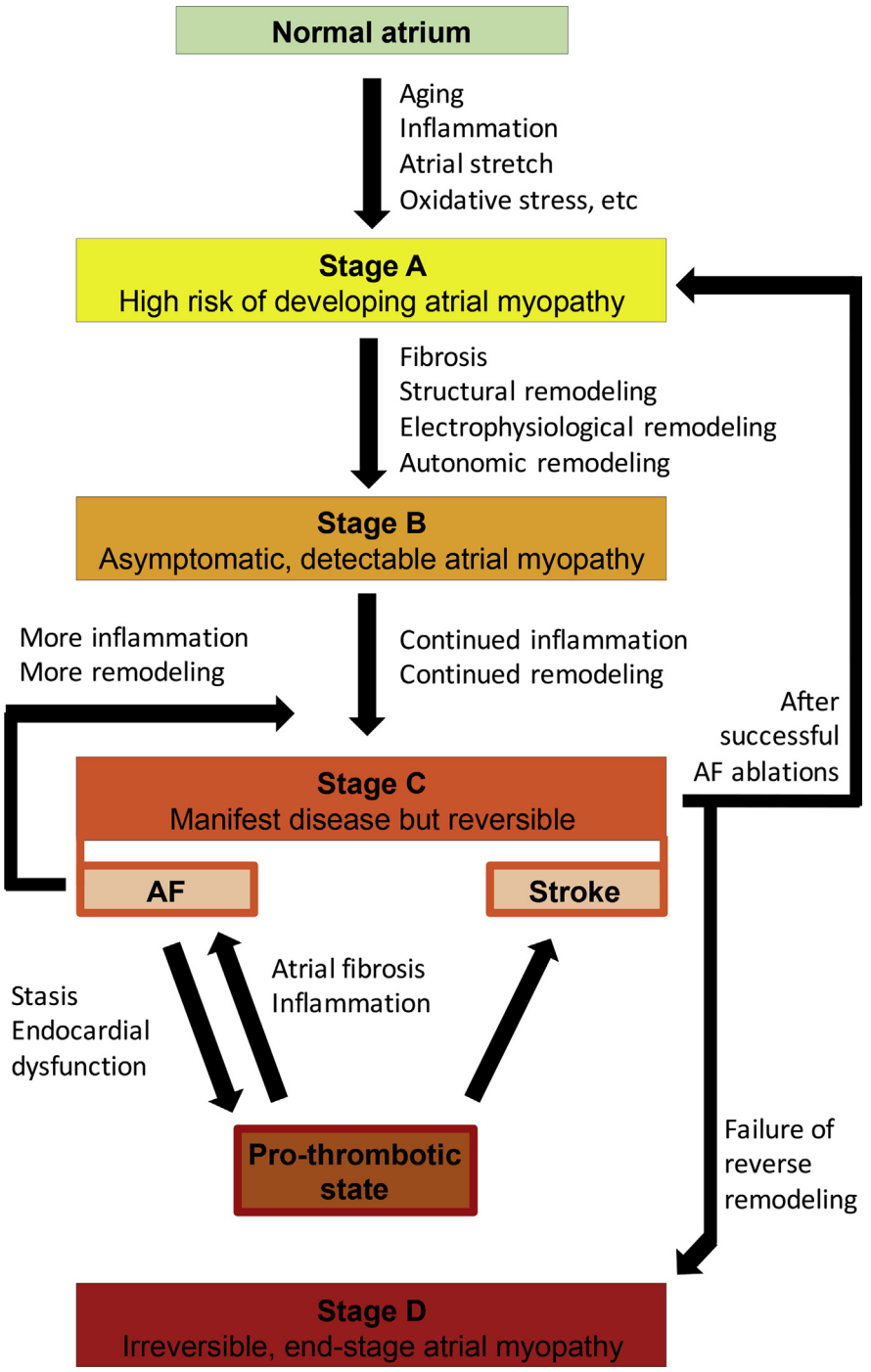

AF = atrial fibrillation.

inflammatory (81). Once AF occurs, the inflammatory state may help perpetuate AF, as evident by the observation that CRP levels are higher in patients who remained in AF, compared with those of patients who converted to sinus rhythm (82). Inflammation might also be involved in the creation of a pro-thrombotic state during AF (83). In a cohort of 880 patients with AF, CRP levels were correlated with risk of stroke and all-cause mortality (84).

Inflammatory cells such as monocytes, macrophages, and lymphocytes produce cytokines and chemokines and can trigger thrombosis in AF. One such cytokine, IL-6, induces the expression of tissue factor, fibrinogen, factor VIII, and von Willebrand factor, mediating a pro-thrombotic state. It may also cause endothelial activation and endothelial cell damage, which leads to platelet aggregation and sensitivity to thrombin (78). Activated platelets in patients with AF could, in turn, promote and sustain the pro-thrombotic state and increase inflammatory biomarkers. Altered endothelial function also contributes to inflammation and thrombosis in AF (85,86). Upon endothelial activation, substances such as von Willebrand factor and soluble P-selectin are rapidly released onto the endothelial surface, promoting the attachment of rolling white blood cells to the endothelium and subsequently contributing to the development of a pro-inflammatory and pro-thrombotic environment. A recent interesting discovery was that not only AF could promote thrombosis, the hypercoagulable state itself promoted atrial fibrosis and thereby facilitated AF, at least in mouse models (87). OAC therapy might not only prevent strokes but inhibit the development of a substrate for AF. Another mechanism invoked in the creation of atrial myopathy that is closely related to inflammation is oxidative stress, in which ROS are believed to modify the function of key ion channels and Ca^{2+} cycling proteins (88–90), as well as activating pro-fibrotic signaling (91,92). The major source of atrial ROS in patients with AF is NOX2, a membrane-bound protein containing nicotinamide adenine dinucleotide phosphate (NADPH) oxidase (93). Reilly et al. (94) showed that NADPH oxidase is elevated early in AF (e.g., with post-operative AF), with mitochondrial oxidases and uncoupled NO syntheses being noted in long-standing AF. Yoo et al. (95) recently showed that ROS are preferentially elevated in the posterior LA in a heart failure model of AF, with a resulting increase in the substrate for both triggered activity (by Ca^{2+}/calmodulin-dependent protein kinase II phosphorylation of ryanodine receptor type 2) and re-entry (via Ca^{2+}/calmodulin-dependent protein kinase II phosphorylation of the main cardiac sodium channel). In response to oxidative stress, the expression of growth differentiation factor 15 (GDF-15) was shown to increase significantly (96). GDF-15 emerged as a novel biomarker to provide prognostic information regarding cardiovascular events, beyond traditional risk factors and other biomarkers, in patients with myocardial infarction (97) or heart failure (98). Moreover, GDF-15 was also shown to be an independent risk factor for stroke in patients with AF (99). After adjusting for potential clinical risk factors, GDF-15 was associated with LAA thrombus in patients with nonvalvular AF (100) (**Central Illustration**).

Figure 1 shows the proposed stages of atrial myopathy (staging in line with 2013 American College of Cardiology Foundation/American Heart Association guidelines for heart failure [101]). With aging, inflammation, atrial stretch from volume and/or pressure overload, and oxidative stress, atria may be at risk of developing atrial myopathy (stage A). At this stage, clinical atrial myopathy is not detectable (see the paragraph "How to identify patients with atrial myopathy"). Once fibrosis and various ways of atrial remodeling, including structural, electrophysiological, and autonomic remodeling have taken place, atrial myopathy is established and becomes detectable (stage B). At this stage, the individual remains asymptomatic. Nevertheless, with ongoing inflammation and remodeling, the myopathic atria become manifest in the form of AF and stroke that typically draw clinical attention. AF leads to a pro-thrombotic state that feeds back to cause more AF by facilitating atrial fibrosis and inflammation. At stage C, the manifest atrial myopathy can be reversed by aggressive interventions such as lifestyle modification and a successful AF ablation. If failure to reverse occurs, the disease progresses to stage D, or end-stage atrial myopathy. This illustration does not account for AF being the initiating stimulus underlying the development of the atrial myopathy. However, once paroxysmal or chronic AF has led to the development of some electrical and/or structural remodeling, several of the paradigms suggested in **Figure 1** would again come into play to help perpetuate these myopathic changes, potentially even in the absence of the initiating stimulus (i.e., AF).

ATRIAL MYOPATHY: A LOGICAL EXPLANATION TO THE LACK OF TEMPORAL RELATIONSHIPS BETWEEN AF AND STROKE

Key observations, including the apparent inability of AF rhythm control strategies to lower stroke risk (3,4), and the lack of a strong temporal association between paroxysmal AF and stroke in patients with prolonged

FIGURE 2 Atrial 4D Flow CMR in Patients With AF

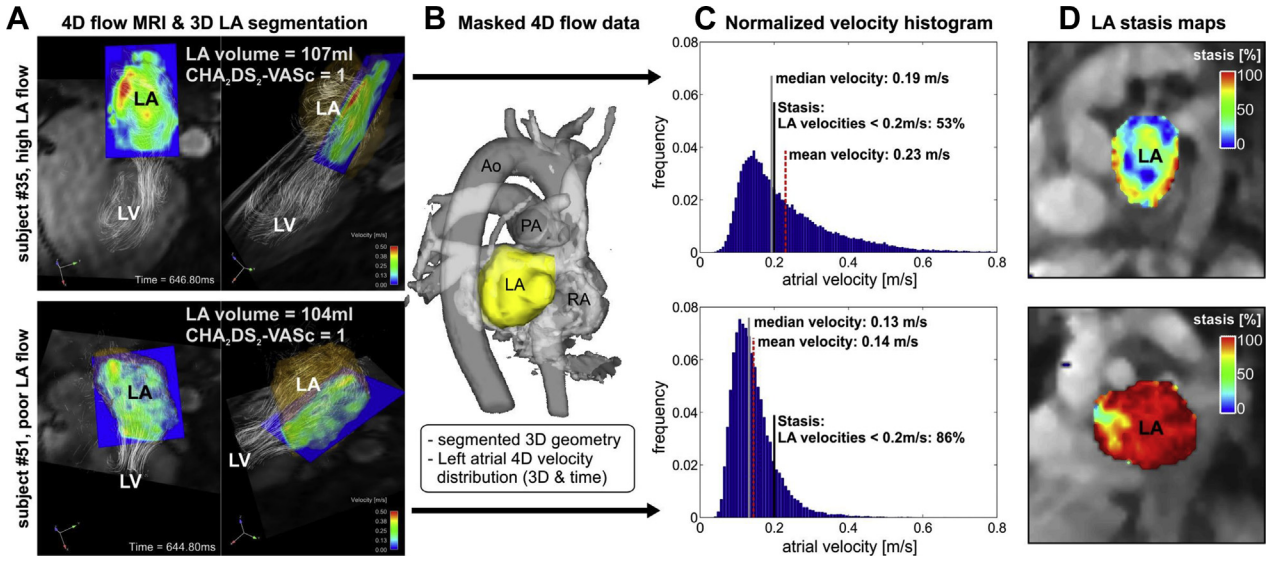

(A) Atrial 4-dimensional (4D) flow cardiac magnetic resonance (CMR) for 2 patients with AF with comparable left atrial (LA) volume and identical CHA_2DS_2-VASc scores = 1 indicating low thromboembolic risk. Velocity histograms **(C)** quantify the LA velocity distribution inside the **(B)** LA. **(D)** LA stasis maps depict the relative amount of low LA flow velocities (<0.2 m/s). Note the substantially increased flow stasis **(red)** in subject #51 compared with subject #35 despite identical CHA_2DS_2-VASc scores. Ao = aorta; LV = left ventricle; PA = pulmonary artery; RA = right atrium; other abbreviation as in Figure 1.

rhythm monitoring via cardiac implantable electronic devices (8,102,103) have heightened the search for additional factors that could account for AF-related strokes beyond the rhythm disturbance itself. Although strokes may occur in the absence of AF itself, AF burden is positively correlated with risk of stroke (104). Furthermore, it has been recently reported that patients with persistent or permanent AF have much more thromboembolic events compared with those with paroxysmal AF (105). If stroke can occur independently of AF, how could more AF be associated with more strokes? One possibility is that these strokes observed in clinical trials were not cardioembolic strokes but rather strokes related to aortic, carotid. or intracerebral atherosclerosis (106). A more likely explanation is that the presence of atrial myopathy, and its associated atrial remodeling (structural, electrical, and autonomic), endocardial dysfunction and pro-thrombotic state, may lead to cardioembolic strokes without the necessity of fibrillating atria. Higher AF burden (or persistent and/or permanent AF) may merely reflect underlying more severe atrial myopathy. In other words, the most logical explanation to all these clinical observations is that atrial myopathy facilitates the development of both AF and stroke (in parallel, not in series). Atrial myopathy may manifest periodically as AF but is always present and continually thrombogenic (107). Recent reviews and editorials have suggested the importance of atrial myopathy and have called for additional studies of its role in AF and AF-associated complications (106,108–110). The following section will discuss how to identify patients with atrial myopathy and how to apply the concept of atrial myopathy in guiding OAC therapy in patients with AF.

ATRIAL MYOPATHY: TRANSLATING THE CONCEPT INTO CLINICAL PRACTICE

HOW TO IDENTIFY PATIENTS WITH ATRIAL MYOPATHY. Macroscopically, atrial myopathy may manifest as AF or non-AF atrial arrhythmias, atrial dilatation, impaired atrial systole, or abnormal cardiac imaging findings (111). Therefore, several methods have been reported to identify patients with atrial myopathy and who are at risk of developing AF and AF-related complications, particularly strokes.

Non-AF atrial arrhythmias, such as frequent atrial premature beats or paroxysmal atrial tachycardia, might indicate an abnormal atrial substrate and a predisposition to AF, and have been associated with increased risk of stroke in long-term follow-up, independent of diagnosed AF (112,113). Atrial electrograms acquired either noninvasively or invasively

may shed some light on underlying atrial myopathy or potentially elevated thromboembolic risk, even in the absence of AF. In a case–cohort analysis of the Northern Manhattan Study, which was a prospective cohort study of stroke risk factors, P-wave terminal force in lead V_1 in sinus rhythm (a marker of LA abnormality) was associated with an increased risk of cardioembolic stroke independently of the presence of AF (114). Invasively, with high-density patch electrodes in the LA in canines with healthy hearts and pacing-induced heart failure with atrial fibrosis, the atrial electrograms during induced AF were markedly different: the overall AF electrograms in dogs with heart failure (and extensive atrial fibrosis) were slower and paradoxically more organized (115). However, in the autonomic nerve-rich posterior LA, the regional electrograms in dogs with heart failure exhibited more spatial heterogeneity and were less organized. Clinical and animal studies suggested that regions of complex fractionated atrial electrograms during AF might represent sites of high autonomic innervation (75,116).

Imaging can be a useful tool in detecting patients with atrial myopathy. Echocardiography (2 dimensional, pulsed-wave Doppler, speckle-tracking echo, strain and strain rate imaging) and cardiac computed tomography are both useful in providing volumetric and functional assessment of the LA (117,118). Larger LA size, assessed by echocardiography, is associated with a higher recurrence rate of AF after AF ablation (119), and with an increased risk of recurrent stroke in patients with nonvalvular AF and ischemic stroke (120).

In recent years, cardiac magnetic resonance (CMR) has become the gold standard of assessment of chamber structure and function, mainly because of its superiority in tissue characterization, particularly in fibrosis. Delayed-enhanced CMR has been applied to assess the extent of LA fibrosis and was found to be correlated with surgical biopsy results and with AF recurrence after catheter ablation (121,122). Furthermore, delayed-enhanced CMR–detected LA fibrosis was found to be an independent risk factor of stroke, after adjusting for other clinical risk factors, in patients with AF (123). Complimentary to this, a novel noninvasive approach is atrial 4-dimensional (4D) flow CMR, which provides a comprehensive characterization of atrial flow dynamics that can overcome limitations of transesophageal echocardiography. It measures 3-D blood flow velocities with full coverage of the LA and LAA, deriving stasis maps (124) that provide intuitive visualizations and quantification of stasis in the LA and LAA, the typical site of thrombus formation (124–127). Moreover, 4-D flow CMR can detect physiological changes in LA hemodynamics in AF and reveal an increased predisposition to atrial thrombogenesis that is not discernible by the CHA_2DS_2-VASc score (124,125,128,129). **Figure 2** shows data from 2 patients with AF and with identically low CHA_2DS_2-VASc scores of 1 but substantially different LA blood flow velocity histograms (**Figure 2C**) and blood stasis maps (**Figure 2D**, color coded for an intuitive visualization of stasis, where the red color corresponds to a heightened risk for thrombogenesis). Therefore, 4-D flow CMR-derived atrial stasis may serve as an important new metric that measures predisposition to atrial thrombogenesis that is not captured with current clinical risk predictors and may provide guidance in anticoagulation therapy in selected groups of patients with AF.

Despite the promising data, several challenges limit routine application for patients with AF. Beyond the costs, a high level of expertise is required for image acquisition and the time required for image processing. Accurate 3-D imaging of the LA involves manual segmentation from other images and careful intensity threshold calibration to differentiate normal from fibrotic tissue (130). Anatomic variability and imaging artifacts may confound image processing. Among the relevant patient factors are body size and habitus that allow optimum image quality and adequate heart rate control to facilitate gating.

HOW TO INCORPORATE THE CONCEPT OF ATRIAL MYOPATHY IN GUIDING ANTICOAGULATION THERAPY. Current guidelines endorsed the use of the CHA_2DS_2-VASc score to guide anticoagulation therapy in patients with AF. Because stroke, as discussed earlier, might occur independently of AF, individuals with an elevated risk of stroke and no history of AF might be identified and be protected by OAC therapy. The CHA_2DS_2-VASc score was found to be valuable in predicting stroke risk in the absence of AF. In patients with heart failure and sinus rhythm, the CHA_2DS_2-VASc score was found to provide prognostic information on future stroke risk (131). Similarly, the CHA_2DS_2-VASc score was associated with spontaneous echo contrast in the LA in patients with rheumatic mitral stenosis and no history of AF, who are at risk of LA thrombus formation and thromboembolism, despite being in sinus rhythm (132). On the other end of the spectrum, with AF, the lack of key atrial myopathic features might be helpful in identifying individuals who do not require OAC therapy, thereby sparing them the unnecessary risk of bleeding. The current guidelines recommend no need for anticoagulation if the CHA_2DS_2-VASc score is 0 or 1, if female. A logical integration of the concept of atrial myopathy to the present paradigm would be to

examine the features of atrial myopathy in 2 groups of patients: male with a CHA_2DS_2-VASc score of 1 and female with a CHA_2DS_2-VASc score of 2. A review article by Calenda et al. (107) proposed that in these 2 groups of individuals with AF, the lack of atrial myopathic features might spare them of unnecessary OAC therapy. Conversely, individuals with a low CHA_2DS_2-VASc score but who have evidence of atrial myopathy might benefit from OAC therapy. A prospective, randomized clinical trial, ARCADIA (Atrial Cardiopathy and Antithrombotic Drugs In Prevention After Cryptogenic Stroke) sought to answer if OAC therapy compared with daily baby aspirin would prevent recurrent ischemic stroke in patients with cryptogenic stroke who possess at least 1 marker of atrial myopathy: an abnormal P wave, N-terminal pro B-type natriuretic peptide (NT-proBNP) level, and dilated LA on echocardiography (133).

Finally, observational studies showed that after a successful AF ablation, the stroke risk might be substantially reduced and cessation of anticoagulation might be safe in many patients (134,135). It is possible that reverse remodeling can take place after a successful AF ablation. Therefore, the assessment of atrial myopathy after an AF ablation might aid in the identification of individuals who no longer require anticoagulation therapy. Conversely, failure of reverse remodeling after an AF ablation might support a need for indefinite OAC therapy despite the absence of AF recurrence. After AF ablation, elevated circulating fibrocytes were found to serve as a marker of LA fibrosis and predict the recurrence of AF (136). It is possible that persistently elevated serum fibrocytes may indicate the failure of reverse remodeling of an underlying atrial myopathic process, which may be continuously thrombogenic. Cessation of OAC therapy in this group of patients might not be safe. This hypothesis needs to be tested in prospective, randomized trials.

Serum biomarkers can further improve risk stratification for strokes beyond traditional risk factors. Although generally not specific to atrial myocardial disease, a growing body of evidence suggests that serum biomarkers might be useful to quantify stroke risk in patients with AF, in addition to clinical risk factors. Various biomarkers correlated with myocyte injury, oxidative stress, inflammation, and fibrosis (BNP, NT-proBNP, troponins, CRP, IL-6, among others) have been reported to be elevated in AF or predictive of development of AF (137) and linked to outcomes in AF, including strokes (138). Using troponins and NT-proBNP, the novel biomarker-based ABC (age, biomarkers, clinical history of stroke or transient ischemic attack) stroke risk score system has been shown to outperform the classic CHA_2DS_2-VASc score system in both the derivation cohort (c-statistic: 0.68 vs. 0.62) and in the validation cohort (c-statistic: 0.66 vs. 0.58) (139).

CONCLUSIONS

Atrial myopathy characterized atrial fibrotic remodeling, together with electrical and autonomic remodeling, facilitates the development of both AF and stroke. Various animal models of atrial myopathy, such as a canine model of pacing-induced heart failure and extensive atrial fibrosis (19), a mouse model that overexpresses TGF-β1 (15), and a rat model of obesity and artificially induced obstructive apnea (65), have helped demystify the complex interplay between atrial myopathy and AF. However, most animal studies do not have long enough follow-up to further determine a causal relationship between atrial myopathy and strokes. The chronicity of human clinical trial data allows bridging of this gap, showing that individuals with markers of atrial myopathy have an elevated risk of developing both AF and strokes (84,99,112-114,123,140,141). Methods to identify atrial myopathy include atrial electrograms, tissue biopsy, cardiac imaging, and certain serum biomarkers. A promising modality is 4-D flow CMR. The concept of atrial myopathy may help guide OAC therapy in selected groups of patients with AF, particularly those with low-intermediate risk of strokes (male with a CHA_2DS_2-VASc score of 1 and female with a CHA_2DS_2-VASc score of 2) and those who have undergone a successful AF ablation. Prospective randomized trials are needed to test these hypotheses.

ADDRESS FOR CORRESPONDENCE: Dr. José Jalife, Center for Arrhythmia Research, University of Michigan, 2800 Plymouth Road, Ann Arbor, Michigan 48109. E-mail: jjalife@med.umich.edu.

REFERENCES

1. Benjamin EJ, Chen PS, Bild DE, et al. Prevention of atrial fibrillation: report from a National Heart, Lung, and Blood Institute workshop. Circulation 2009;119:606-18.

2. McGrath ER, Kapral MK, Fang J, et al. Association of atrial fibrillation with mortality and disability after ischemic stroke. Neurology 2013; 81:825-32.

3. Van Gelder IC, Hagens VE, Bosker HA, et al. A comparison of rate control and rhythm control in patients with recurrent persistent atrial fibrillation. N Engl J Med 2002;347:1834-40.

4. Wyse DG, Waldo AL, DiMarco JP, et al. A comparison of rate control and rhythm control in patients with atrial fibrillation. N Engl J Med 2002;347:1825–33.

5. Brambatti M, Connolly SJ, Gold MR, et al. Temporal relationship between subclinical atrial fibrillation and embolic events. Circulation 2014; 129:2094–9.

6. Glotzer TV, Daoud EG, Wyse DG, et al. The relationship between daily atrial tachyarrhythmia burden from implantable device diagnostics and stroke risk: the TRENDS study. Circ Arrhythm Electrophysiol 2009;2:474–80.

7. Ip J, Waldo AL, Lip GY, et al. Multicenter randomized study of anticoagulation guided by remote rhythm monitoring in patients with implantable cardioverter-defibrillator and CRT-D devices: rationale, design, and clinical characteristics of the initially enrolled cohort The IMPACT study. Am Heart J 2009;158:364–370 e1.

8. Martin DT, Bersohn MM, Waldo AL, et al. Randomized trial of atrial arrhythmia monitoring to guide anticoagulation in patients with implanted defibrillator and cardiac resynchronization devices. Eur Heart J 2015;36:1660–8.

9. January CT, Wann LS, Alpert JS, et al. 2014 AHA/ACC/HRS guideline for the management of patients with atrial fibrillation: executive summary: a report of the American College of Cardiology/American Heart Association Task Force on practice guidelines and the Heart Rhythm Society. Circulation 2014;130:2071–104.

10. Kirchhof P, Benussi S, Kotecha D, et al. 2016 ESC Guidelines for the management of atrial fibrillation developed in collaboration with EACTS. Eur Heart J 2016;37:2893–962.

11. Watson T, Shantsila E, Lip GY. Mechanisms of thrombogenesis in atrial fibrillation: Virchow's triad revisited. Lancet 2009;373:155–66.

12. Zipes DP. Atrial fibrillation. A tachycardia-induced atrial cardiomyopathy. Circulation 1997; 95:562–4.

13. Kottkamp H. Fibrotic atrial cardiomyopathy: a specific disease/syndrome supplying substrates for atrial fibrillation, atrial tachycardia, sinus node disease, AV node disease, and thromboembolic complications. J Cardiovasc Electrophysiol 2012; 23:797–9.

14. Boldt A, Wetzel U, Lauschke J, et al. Fibrosis in left atrial tissue of patients with atrial fibrillation with and without underlying mitral valve disease. Heart 2004;90:400–5.

15. Everett THt, Olgin JE. Atrial fibrosis and the mechanisms of atrial fibrillation. Heart Rhythm 2007;4:S24–7.

16. Burstein B, Nattel S. Atrial structural remodeling as an antiarrhythmic target. J Cardiovasc Pharmacol 2008;52:4–10.

17. Hirsh BJ, Copeland-Halperin RS, Halperin JL. Fibrotic atrial cardiomyopathy, atrial fibrillation, and thromboembolism: mechanistic links and clinical inferences. J Am Coll Cardiol 2015;65: 2239–51.

18. Kostin S, Klein G, Szalay Z, Hein S, Bauer EP, Schaper J. Structural correlate of atrial fibrillation in human patients. Cardiovasc Res 2002;54:361–79.

19. Li D, Fareh S, Leung TK, Nattel S. Promotion of atrial fibrillation by heart failure in dogs: atrial remodeling of a different sort. Circulation 1999; 100:87–95.

20. Luo T, Chang CX, Zhou X, Gu SK, Jiang TM, Li YM. Characterization of atrial histopathological and electrophysiological changes in a mouse model of aging. Int J Mol Med 2013;31:138–46.

21. Van Wagoner DR. Oxidative stress and inflammation in atrial fibrillation: role in pathogenesis and potential as a therapeutic target. J Cardiovasc Pharmacol 2008;52:306–13.

22. Korantzopoulos P, Letsas KP, Tse G, Fragakis N, Goudis CA, Liu T. Inflammation and atrial fibrillation: a comprehensive review. J Arrhythm 2018;34:394–401.

23. Youn JY, Zhang J, Zhang Y, et al. Oxidative stress in atrial fibrillation: an emerging role of NADPH oxidase. J Mol Cell Cardiol 2013;62:72–9.

24. Eckstein J, Verheule S, de Groot NM, Allessie M, Schotten U. Mechanisms of perpetuation of atrial fibrillation in chronically dilated atria. Prog Biophys Mol Biol 2008;97:435–51.

25. Nattel S, Harada M. Atrial remodeling and atrial fibrillation: recent advances and translational perspectives. J Am Coll Cardiol 2014;63: 2335–45.

26. Schotten U, Neuberger HR, Allessie MA. The role of atrial dilatation in the domestication of atrial fibrillation. Prog Biophys Mol Biol 2003;82: 151–62.

27. Corradi D. Atrial fibrillation from the pathologist's perspective. Cardiovasc Pathol 2014;23: 71–84.

28. Bukowska A, Lendeckel U, Bode-Boger SM, Goette A. Physiologic and pathophysiologic role of calpain: implications for the occurrence of atrial fibrillation. Cardiovasc Ther 2012;30:e115–27.

29. Suzuki K, Imajoh S, Emori Y, Kawasaki H, Minami Y, Ohno S. Calcium-activated neutral protease and its endogenous inhibitor. Activation at the cell membrane and biological function. FEBS Lett 1987;220:271–7.

30. Jalife J. Mechanisms of persistent atrial fibrillation. Curr Opin Cardiol 2014;29:20–7.

31. Takemoto Y, Ramirez RJ, Yokokawa M, et al. Galectin-3 regulates atrial fibrillation remodeling and predicts catheter ablation outcomes. J Am Coll Cardiol Basic Trans Science 2016;1:143–54.

32. Takemoto Y, Ramirez RJ, Kaur K, et al. Eplerenone reduces atrial fibrillation burden without preventing atrial electrical remodeling. J Am Coll Cardiol 2017;70:2893–905.

33. Shi Y, Li D, Tardif JC, Nattel S. Enalapril effects on atrial remodeling and atrial fibrillation in experimental congestive heart failure. Cardiovasc Res 2002;54:456–61.

34. Li D, Shinagawa K, Pang L, et al. Effects of angiotensin-converting enzyme inhibition on the development of the atrial fibrillation substrate in dogs with ventricular tachypacing-induced congestive heart failure. Circulation 2001;104: 2608–14.

35. Boldt A, Scholl A, Garbade J, et al. ACE-inhibitor treatment attenuates atrial structural remodeling in patients with lone chronic atrial fibrillation. Basic Res Cardiol 2006;101:261–7.

36. Healey JS, Baranchuk A, Crystal E, et al. Prevention of atrial fibrillation with angiotensin-converting enzyme inhibitors and angiotensin receptor blockers: a meta-analysis. J Am Coll Cardiol 2005;45:1832–9.

37. Lee KW, Everett THT, Rahmutula D, et al. Pirfenidone prevents the development of a vulnerable substrate for atrial fibrillation in a canine model of heart failure. Circulation 2006; 114:1703–12.

38. Kunamalla A, Ng J, Parini V, et al. Constitutive expression of a dominant-negative TGF-beta type II receptor in the posterior left atrium leads to beneficial remodeling of atrial fibrillation substrate. Circ Res 2016;119:69–82.

39. Chiao YA, Rabinovitch PS. The aging heart. Cold Spring Harb Perspect Med 2015;5:a025148.

40. Zoni-Berisso M, Lercari F, Carazza T, Domenicucci S. Epidemiology of atrial fibrillation: European perspective. Clin Epidemiol 2014;6: 213–20.

41. Lin YK, Chen YA, Lee TI, Chen YC, Chen SA, Chen YJ. Aging modulates the substrate and triggers remodeling in atrial fibrillation. Circ J 2018; 82:1237–44.

42. Chung HY, Cesari M, Anton S, et al. Molecular inflammation: underpinnings of aging and age-related diseases. Ageing Res Rev 2009;8:18–30.

43. Anumonwo JM, Jalife J, Goldstein DR. Triple threat: adiposity, aging, atrial fibrillation. Aging (Albany NY) 2017;9:2235–6.

44. Kourliouros A, Savelieva I, Kiotsekoglou A, Jahangiri M, Camm J. Current concepts in the pathogenesis of atrial fibrillation. Am Heart J 2009;157:243–52.

45. Pandit SV, Anumonwo J, Jalife J. Atrial fibrillation susceptibility in obesity: an excess adiposity and fibrosis complicity? Circ Res 2016;118: 1468–71.

46. Haemers P, Hamdi H, Guedj K, et al. Atrial fibrillation is associated with the fibrotic remodelling of adipose tissue in the subepicardium of human and sheep atria. Eur Heart J 2017;38:53–61.

47. Wong CX, Brooks AG, Leong DP, Roberts-Thomson KC, Sanders P. The increasing burden of atrial fibrillation compared with heart failure and myocardial infarction: a 15-year study of all hospitalizations in Australia. Arch Intern Med 2012; 172:739–41.

48. Wang L, Myles RC, De Jesus NM, Ohlendorf AK, Bers DM, Ripplinger CM. Optical mapping of sarcoplasmic reticulum $Ca2+$ in the intact heart: ryanodine receptor refractoriness during alternans and fibrillation. Circ Res 2014; 114:1410–21.

49. Martins RP, Kaur K, Hwang E, et al. Dominant frequency increase rate predicts transition from paroxysmal to long-term persistent atrial fibrillation. Circulation 2014;129:1472–82.

50. Vaquero M, Calvo D, Jalife J. Cardiac fibrillation: from ion channels to rotors in the human heart. Heart Rhythm 2008;5:872–9.

51. Voigt N, Trausch A, Knaut M, et al. Left-to-right atrial inward rectifier potassium current gradients in patients with paroxysmal versus chronic atrial fibrillation. Circ Arrhythm Electrophysiol 2010;3:472–80.

52. Swartz MF, Fink GW, Lutz CJ, et al. Left versus right atrial difference in dominant frequency, K(+) channel transcripts, and fibrosis in patients developing atrial fibrillation after cardiac surgery. Heart Rhythm 2009;6:1415–22.

53. Nattel S, Maguy A, Le Bouter S, Yeh YH. Arrhythmogenic ion-channel remodeling in the heart: heart failure, myocardial infarction, and atrial fibrillation. Physiol Rev 2007;87:425–56.

54. Van Wagoner DR. Basic mechanisms of atrial fibrillation. Cleve Clin J Med 2003;70 Suppl 3: S2–5.

55. Caballero R, de la Fuente MG, Gomez R, et al. In humans, chronic atrial fibrillation decreases the transient outward current and ultrarapid component of the delayed rectifier current differentially on each atria and increases the slow component of the delayed rectifier current in both. J Am Coll Cardiol 2010;55:2346–54.

56. Chaldoupi SM, Loh P, Hauer RN, de Bakker JM, van Rijen HV. The role of connexin40 in atrial fibrillation. Cardiovasc Res 2009;84:15–23.

57. Severs NJ, Coppen SR, Dupont E, Yeh HI, Ko YS, Matsushita T. Gap junction alterations in human cardiac disease. Cardiovasc Res 2004;62: 368–77.

58. Polontchouk L, Haefliger JA, Ebelt B, et al. Effects of chronic atrial fibrillation on gap junction distribution in human and rat atria. J Am Coll Cardiol 2001;38:883–91.

59. Elvan A, Huang XD, Pressler ML, Zipes DP. Radiofrequency catheter ablation of the atria eliminates pacing-induced sustained atrial fibrillation and reduces connexin 43 in dogs. Circulation 1997;96:1675–85.

60. van der Velden HM, Ausma J, Rook MB, et al. Gap junctional remodeling in relation to stabilization of atrial fibrillation in the goat. Cardiovasc Res 2000;46:476–86.

61. Shin SY, Jo WM, Min TJ, et al. Gap junction remodelling by chronic pressure overload is related to the increased susceptibility to atrial fibrillation in rat heart. Europace 2015;17:655–63.

62. Rucker-Martin C, Milliez P, Tan S, et al. Chronic hemodynamic overload of the atria is an important factor for gap junction remodeling in human and rat hearts. Cardiovasc Res 2006;72:69–79.

63. Medi C, Kalman JM, Spence SJ, et al. Atrial electrical and structural changes associated with longstanding hypertension in humans: implications for the substrate for atrial fibrillation. J Cardiovasc Electrophysiol 2011;22:1317–24.

64. Healey JS, Israel CW, Connolly SJ, et al. Relevance of electrical remodeling in human atrial fibrillation: results of the Asymptomatic Atrial Fibrillation and Stroke Evaluation in Pacemaker Patients and the Atrial Fibrillation Reduction Atrial Pacing Trial mechanisms of atrial fibrillation study. Circ Arrhythm Electrophysiol 2012;5:626–31.

65. Iwasaki YK, Shi Y, Benito B, et al. Determinants of atrial fibrillation in an animal model of obesity and acute obstructive sleep apnea. Heart Rhythm 2012;9:1409–16 e1.

66. Shen MJ, Zipes DP. Role of the autonomic nervous system in modulating cardiac arrhythmias. Circ Res 2014;114:1004–21.

67. Shen MJ, Choi EK, Tan AY, et al. Neural mechanisms of atrial arrhythmias. Nat Rev Cardiol 2011;9:30–9.

68. Patterson E, Lazzara R, Szabo B, et al. Sodium-calcium exchange initiated by the Ca2+ transient: an arrhythmia trigger within pulmonary veins. J Am Coll Cardiol 2006;47:1196–206.

69. Patterson E, Jackman WM, Beckman KJ, et al. Spontaneous pulmonary vein firing in man: relationship to tachycardia-pause early afterdepolarizations and triggered arrhythmia in canine pulmonary veins in vitro. J Cardiovasc Electrophysiol 2007;18:1067–75.

70. Bers DM. Cardiac excitation-contraction coupling. Nature 2002;415:198–205.

71. Wijffels MC, Kirchhof CJ, Dorland R, Allessie MA. Atrial fibrillation begets atrial fibrillation. A study in awake chronically instrumented goats. Circulation 1995;92:1954–68.

72. Haissaguerre M, Jais P, Shah DC, et al. Spontaneous initiation of atrial fibrillation by ectopic beats originating in the pulmonary veins. N Engl J Med 1998;339:659–66.

73. Tan AY, Li H, Wachsmann-Hogiu S, Chen LS, Chen PS, Fishbein MC. Autonomic innervation and segmental muscular disconnections at the human pulmonary vein-atrial junction: implications for catheter ablation of atrial-pulmonary vein junction. J Am Coll Cardiol 2006;48:132–43.

74. Chou CC, Nihei M, Zhou S, et al. Intracellular calcium dynamics and anisotropic re-entry in isolated canine pulmonary veins and left atrium. Circulation 2005;111:2889–97.

75. Choi EK, Shen MJ, Han S, et al. Intrinsic cardiac nerve activity and paroxysmal atrial tachyarrhythmia in ambulatory dogs. Circulation 2010; 121:2615–23.

76. Shen MJ, Coffey AC, Straka S, et al. Simultaneous recordings of intrinsic cardiac nerve activity and skin sympathetic nerve activity from human patients during the postoperative period. Heart Rhythm 2017;14:1587–93.

77. Aviles RJ, Martin DO, Apperson-Hansen C, et al. Inflammation as a risk factor for atrial fibrillation. Circulation 2003;108:3006–10.

78. Guo Y, Lip GY, Apostolakis S. Inflammation in atrial fibrillation. J Am Coll Cardiol 2012;60: 2263–70.

79. Conen D, Ridker PM, Everett BM, et al. A multimarker approach to assess the influence of inflammation on the incidence of atrial fibrillation in women. Eur Heart J 2010;31:1730–6.

80. Marott SC, Nordestgaard BG, Zacho J, et al. Does elevated C-reactive protein increase atrial fibrillation risk? A Mendelian randomization of 47, 000 individuals from the general population. J Am Coll Cardiol 2010;56:789–95.

81. Tousoulis D, Zisimos K, Antoniades C, et al. Oxidative stress and inflammatory process in patients with atrial fibrillation: the role of left atrium distension. Int J Cardiol 2009;136:258–62.

82. Acevedo M, Corbalan R, Braun S, Pereira J, Gonzalez I, Navarrete C. Biochemical predictors of cardiac rhythm at 1 year follow-up in patients with non-valvular atrial fibrillation. J Thromb Thrombolysis 2012;33:383–8.

83. Conway DS, Buggins P, Hughes E, Lip GY. Relationship of interleukin-6 and C-reactive protein to the prothrombotic state in chronic atrial fibrillation. J Am Coll Cardiol 2004;43:2075–82.

84. Lip GY, Patel JV, Hughes E, Hart RG. High-sensitivity C-reactive protein and soluble CD40 ligand as indices of inflammation and platelet activation in 880 patients with nonvalvular atrial fibrillation: relationship to stroke risk factors, stroke risk stratification schema, and prognosis. Stroke 2007;38:1229–37.

85. Yacoub D, Hachem A, Theoret JF, Gillis MA, Mourad W, Merhi Y. Enhanced levels of soluble CD40 ligand exacerbate platelet aggregation and thrombus formation through a CD40-dependent tumor necrosis factor receptor-associated factor-2/Rac1/p38 mitogen-activated protein kinase signaling pathway. Arterioscler Thromb Vasc Biol 2010;30:2424–33.

86. Raviele A, Ronco F. Endothelial dysfunction and atrial fibrillation: what is the relationship? J Cardiovasc Electrophysiol 2011;22:383–4.

87. Spronk HM, De Jong AM, Verheule S, et al. Hypercoagulability causes atrial fibrosis and promotes atrial fibrillation. Eur Heart J 2017;38: 38–50.

88. Hool LC. Reactive oxygen species in cardiac signalling: from mitochondria to plasma membrane ion channels. Clin Exp Pharmacol Physiol 2006;33:146–51.

89. Zima AV, Blatter LA. Redox regulation of cardiac calcium channels and transporters. Cardiovasc Res 2006;71:310–21.

90. Nediani C, Raimondi L, Borchi E, Cerbai E. Nitric oxide/reactive oxygen species generation and nitroso/redox imbalance in heart failure: from molecular mechanisms to therapeutic implications. Antioxidants Redox Signaling 2011;14: 289–331.

91. Lijnen PJ, van Pelt JF, Fagard RH. Stimulation of reactive oxygen species and collagen synthesis by angiotensin II in cardiac fibroblasts. Cardiovasc Ther 2012;30:e1–8.

92. Nabeebaccus A, Zhang M, Shah AM. NADPH oxidases and cardiac remodelling. Heart Fail Rev 2011;16:5–12.

93. Kim YM, Guzik TJ, Zhang YH, et al. A myocardial Nox2 containing NAD(P)H oxidase contributes to oxidative stress in human atrial fibrillation. Circ Res 2005;97:629–36.

94. Reilly SN, Jayaram R, Nahar K, et al. Atrial sources of reactive oxygen species vary with the duration and substrate of atrial fibrillation: implications for the antiarrhythmic effect of statins. Circulation 2011;124:1107–17.

95. Yoo S, Aistrup G, Shiferaw Y, et al. Oxidative stress creates a unique, CaMKII-mediated substrate for atrial fibrillation in heart failure. JCI Insight 2018;3.

96. Schlittenhardt D, Schober A, Strelau J, et al. Involvement of growth differentiation factor-15/macrophage inhibitory cytokine-1 (GDF-15/MIC-1) in oxLDL-induced apoptosis of human macrophages in vitro and in arteriosclerotic lesions. Cell Tissue Res 2004;318:325–33.

97. Wollert KC, Kempf T, Peter T, et al. Prognostic value of growth-differentiation factor-15 in patients with non-ST-elevation acute coronary syndrome. Circulation 2007;115:962–71.

98. Kempf T, von Haehling S, Peter T, et al. Prognostic utility of growth differentiation factor-15 in patients with chronic heart failure. J Am Coll Cardiol 2007;50:1054–60.

99. Wallentin L, Hijazi Z, Andersson U, et al. Growth differentiation factor 15, a marker of oxidative stress and inflammation, for risk assessment in patients with atrial fibrillation: insights from the Apixaban for Reduction in Stroke and Other Thromboembolic Events in Atrial Fibrillation (ARISTOTLE) trial. Circulation 2014;130:1847–58.

100. Hu XF, Zhan R, Xu S, et al. Growth differentiation factor 15 is associated with left atrial/left atrial appendage thrombus in patients with nonvalvular atrial fibrillation. Clin Cardiol 2018;41:34–8.

101. Yancy CW, Jessup M, Bozkurt B, et al. 2013 ACCF/AHA guideline for the management of heart failure: a report of the American College of Cardiology Foundation/American Heart Association Task Force on Practice Guidelines. J Am Coll Cardiol 2013;62:e147–239.

102. Al-Khatib SM, Allen LaPointe NM, Chatterjee R, et al. Rate- and rhythm-control therapies in patients with atrial fibrillation: a systematic review. Ann Intern Med 2014;160:760–73.

103. Healey JS, Connolly SJ, Gold MR, et al. Subclinical atrial fibrillation and the risk of stroke. N Engl J Med 2012;366:120–9.

104. Botto GL, Padeletti L, Santini M, et al. Presence and duration of atrial fibrillation detected by continuous monitoring: crucial implications for the risk of thromboembolic events. J Cardiovasc Electrophysiol 2009;20:241–8.

105. Link MS, Giugliano RP, Ruff CT, et al. Stroke and mortality risk in patients with various patterns of atrial fibrillation: results from the ENGAGE AF-TIMI 48 Trial (Effective Anticoagulation With Factor Xa Next Generation in Atrial Fibrillation-Thrombolysis in Myocardial Infarction 48). Circ Arrhythm Electrophysiol 2017;10:pii:e004267.

106. Piccini JP, Daubert JP. Atrial fibrillation and stroke: it's not necessarily all about the rhythm. Heart Rhythm 2011;8:1424–5.

107. Calenda BW, Fuster V, Halperin JL, Granger CB. Stroke risk assessment in atrial fibrillation: risk factors and markers of atrial myopathy. Nat Rev Cardiol 2016;13:549–59.

108. Goldberger JJ, Arora R, Green D, et al. Evaluating the atrial myopathy underlying atrial fibrillation: identifying the arrhythmogenic and thrombogenic substrate. Circulation 2015;132:278–91.

109. Kamel H, Okin PM, Elkind MS, Iadecola C. Atrial fibrillation and mechanisms of stroke: time for a new model. Stroke 2016;47:895–900.

110. Guichard JB, Nattel S. Atrial cardiomyopathy: a useful notion in cardiac disease management or a passing fad? J Am Coll Cardiol 2017;70:756–65.

111. Kuppahally SS, Akoum N, Burgon NS, et al. Left atrial strain and strain rate in patients with paroxysmal and persistent atrial fibrillation: relationship to left atrial structural remodeling detected by delayed-enhancement MRI. Circ Cardiovasc Imaging 2010;3:231–9.

112. Binici Z, Intzilakis T, Nielsen OW, Kober L, Sajadieh A. Excessive supraventricular ectopic activity and increased risk of atrial fibrillation and stroke. Circulation 2010;121:1904–11.

113. Larsen BS, Kumarathurai P, Falkenberg J, Nielsen OW, Sajadieh A. Excessive atrial ectopy and short atrial runs increase the risk of stroke beyond incident atrial fibrillation. J Am Coll Cardiol 2015;66:232–41.

114. Kamel H, Hunter M, Moon YP, et al. Electrocardiographic left atrial abnormality and risk of stroke: Northern Manhattan Study. Stroke 2015;46:3208–12.

115. Koduri H, Ng J, Cokic I, et al. Contribution of fibrosis and the autonomic nervous system to atrial fibrillation electrograms in heart failure. Circ Arrhythm Electrophysiol 2012;5:640–9.

116. Katritsis D, Giazitzoglou E, Sougiannis D, Voridis E, Po SS. Complex fractionated atrial electrograms at anatomic sites of ganglionated plexi in atrial fibrillation. Europace 2009;11:308–15.

117. Todaro MC, Choudhuri I, Belohlavek M, et al. New echocardiographic techniques for evaluation of left atrial mechanics. Eur Heart J Cardiovasc Imaging 2012;13:973–84.

118. Rohner A, Brinkert M, Kawel N, et al. Functional assessment of the left atrium by real-time three-dimensional echocardiography using a novel dedicated analysis tool: initial validation studies in comparison with computed tomography. Eur J Echocardiogr 2011;12:497–505.

119. Njoku A, Kannabhiran M, Arora R, et al. Left atrial volume predicts atrial fibrillation recurrence after radiofrequency ablation: a meta-analysis. Europace 2018;20:33–42.

120. Ogata T, Matsuo R, Kiyuna F, et al. Left atrial size and long-term risk of recurrent stroke after acute ischemic stroke in patients with nonvalvular atrial fibrillation. J Am Heart Assoc 2017;6:pii:e006402.

121. McGann C, Akoum N, Patel A, et al. Atrial fibrillation ablation outcome is predicted by left atrial remodeling on CMR. Circ Arrhythm Electrophysiol 2014;7:23–30.

122. Marrouche NF, Wilber D, Hindricks G, et al. Association of atrial tissue fibrosis identified by delayed enhancement MRI and atrial fibrillation catheter ablation: the DECAAF study. JAMA 2014;311:498–506.

123. Daccarett M, Badger TJ, Akoum N, et al. Association of left atrial fibrosis detected by delayed-enhancement magnetic resonance imaging and the risk of stroke in patients with atrial fibrillation. J Am Coll Cardiol 2011;57:831–8.

124. Markl M, Lee DC, Ng J, Carr M, Carr J, Goldberger JJ. Left atrial 4-dimensional flow magnetic resonance imaging: stasis and velocity mapping in patients with atrial fibrillation. Invest Radiol 2016;51:147–54.

125. Fluckiger JU, Goldberger JJ, Lee DC, et al. Left atrial flow velocity distribution and flow coherence using four-dimensional FLOW MRI: a pilot study investigating the impact of age and pre- and postintervention atrial fibrillation on atrial hemodynamics. J Magn Reson Imaging 2013;38:580–7.

126. Foll D, Taeger S, Bode C, Jung B, Markl M. Age, gender, blood pressure, and ventricular geometry influence normal 3D blood flow characteristics in the left heart. Eur Heart J Cardiovasc Imaging 2013;14:366–73.

127. Lee DC, Markl M, Ng J, et al. Three-dimensional left atrial blood flow characteristics in patients with atrial fibrillation assessed by 4D flow MRI. Eur Heart J Cardiovasc Imaging 2016;17:1259–68.

128. Markl M, Lee DC, Furiasse N, et al. Left Atrial and left atrial appendage 4d blood flow dynamics in atrial fibrillation. Circ Cardiovasc Imaging 2016;9:e004984.

129. Lee DC, Markl M, Ng J, et al. Three-dimensional left atrial blood flow characteristics in patients with atrial fibrillation assessed by 4D flow MRI. Eur Heart J Cardiovasc Imaging 2016;17:1259–68.

130. Appelbaum E, Manning WJ. Left atrial fibrosis by late gadolinium enhancement cardiovascular magnetic resonance predicts recurrence of atrial fibrillation after pulmonary vein isolation: do you see what I see? Circ Arrhythm Electrophysiol 2014;7:2–4.

131. Wolsk E, Lamberts M, Hansen ML, et al. Thromboembolic risk stratification of patients hospitalized with heart failure in sinus rhythm: a nationwide cohort study. Eur J Heart Fail 2015;17:828–36.

132. Belen E, Ozal E, Pusuroglu H. Association of the CHA2DS2-VASc score with left atrial spontaneous echo contrast: a cross-sectional study of patients with rheumatic mitral stenosis in sinus rhythm. Heart Vessels 2016;31:1537–43.

133. Kamel H, Longstreth WT Jr., Tirschwell DL, et al. The AtRial Cardiopathy and Antithrombotic Drugs In prevention After cryptogenic stroke randomized trial: rationale and methods. Int J Stroke 2019;14:207–14.

134. Ha AC, Hindricks G, Birnie DH, Verma A. Long-term oral anticoagulation for patients after successful catheter ablation of atrial fibrillation: is it necessary? Curr Opin Cardiol 2015;30:1–7.

135. Deng L, Xiao Y, Hong H. Withdrawal of oral anticoagulants 3 months after successful radiofrequency catheter ablation in patients with atrial fibrillation: a meta-analysis. Pacing Clin Electrophysiol 2018;41:1391–400.

136. Liu Y, Niu XH, Yin X, et al. Elevated circulating fibrocytes is a marker of left atrial fibrosis and recurrence of persistent atrial fibrillation. J Am Heart Assoc 2018;7:pii:e008083.

137. Smith JG, Newton-Cheh C, Almgren P, et al. Assessment of conventional cardiovascular risk factors and multiple biomarkers for the prediction of incident heart failure and atrial fibrillation. J Am Coll Cardiol 2010;56:1712–9.

138. Hijazi Z, Oldgren J, Siegbahn A, Granger CB, Wallentin L. Biomarkers in atrial fibrillation: a clinical review. Eur Heart J 2013;34:1475–80.

139. Hijazi Z, Lindback J, Alexander JH, et al. The ABC (age, biomarkers, clinical history) stroke risk score: a biomarker-based risk score for predicting stroke in atrial fibrillation. Eur Heart J 2016;37:1582–90.

140. Hijazi Z, Siegbahn A, Andersson U, et al. High-sensitivity troponin I for risk assessment in patients with atrial fibrillation: insights from the Apixaban for Reduction in Stroke and other Thromboembolic Events in Atrial Fibrillation (ARISTOTLE) trial. Circulation 2014;129:625–34.

141. Hijazi Z, Wallentin L, Siegbahn A, et al. N-terminal pro-B-type natriuretic peptide for risk assessment in patients with atrial fibrillation: insights from the ARISTOTLE Trial (Apixaban for the Prevention of Stroke in Subjects With Atrial Fibrillation). J Am Coll Cardiol 2013;61:2274–84.

KEY WORDS atrial fibrillation, atrial myopathy, electrophysiology, thrombosis

Go to http://www.acc.org/jacc-journals-cme to take the CME/MOC/ECME quiz for this article.

JACC: BASIC TO TRANSLATIONAL SCIENCE VOL. 4, NO. 5, 2019

EDITOR'S PAGE

Current Education of Physicians: Lost in Translation?

Andrew I. Schafer, MD,[a] Douglas L. Mann, MD[b]

The first warning about the endangered future of physician-scientist careers was articulated by James Wyngaarden in 1979, later director of the National Institutes of Health (NIH). He noted that the number of MD applicants for research grants from the NIH was decreasing while that of PhD applicants was rapidly rising (1). Deep concern about this problem has intensified over the past decade, resulting in a call for action by the current NIH director, Francis Collins, who in 2014 convened and charged the Physician-Scientist Workforce Working Group to examine the roots of the problem and recommend potential solutions. Its report concluded that "analysis of AMA [American Medical Association] and NIH data demonstrate continued aging over the past decade of physicians engaged in research, which presage a significant decline in the physician-scientist workforce, especially as the current cohort of senior physician-scientists retires" (2).

Many plausible causes have been proposed for the loss of interest among young physicians (MDs and MD-PhDs) in serious research careers (3). However, it now appears that the number entering that career path is less of a problem than the number dropping out. Early attrition from this career pathway has been referred to as the "leaky pipeline." Other critically important factors that have been discussed include the increasing length of training required to start an independent clinical research career (with the mean age of physicians securing a first independent NIH grant now approaching the mid-40s); the increasing indebtedness of medical school graduates (with the average for medical students graduating in 2018 ballooning to $197,000 in student loans); changes in generational priorities for work-life balance and controllable lifestyles; the continued discouragement of women from entering the physician-scientist career path, even though their potential for productive careers is at least as great as that of men (with women now representing 50% of matriculating medical students); and the increasing perception of insecurity in those jobs.

In our opinion, 1 major factor that has not been discussed is the number of consecutive years of required training of physicians that are virtually devoid of exposure to scientific thinking. Take for example the typical training path of a cardiologist. With medical school curricular reform, the period of teaching foundational sciences has been reduced from 24 months to 12 to 18 months in most schools. The rationale for this is commendable: instead of rigidly bisecting medical education into the foundational sciences years and the clinical years, as the traditional curriculum dictated for the past century, these 2 facets of education can be now fully integrated seamlessly (4). This curricular change entails early exposure of medical students to meaningful clinical experiences while they are studying basic sciences (which has been accomplished successfully), and substantively inserting the foundational sciences into the clinical years. Theoretically, this would justify shortening of the basic science curriculum by 6 to 12 months. Unfortunately, the second part of the plan has not been possible to achieve. The most recent (2019) annual surveys administered by the Association of American Medical Colleges to all medical students in the United States at the times of their matriculation and graduation now show an approximately 10% drop over the course of 4 years of medical school in the likelihood of including research during their careers (https://www.aamc.org/data/student-surveys/). In good faith, the U.S. Medical

From the [a]Division of Hematology/Medical Oncology, Weill Cornell Medicine, New York, New York; and the [b]Center for Cardiovascular Research, Cardiovascular Division, Washington University School of Medicine, St. Louis, Missouri. Both authors have reported that they have no relationships relevant to the contents of this paper to disclose.

ISSN 2452-302X https://doi.org/10.1016/j.jacbts.2019.08.002

JACC: BASIC TO TRANSLATIONAL SCIENCE VOL. 4, NO. 5, 2019
SEPTEMBER 2019:655–7

Licensing Examination did introduce foundational science questions into the Step 2 board examinations (which are taken at the end of medical school). Step 2 has 2 components, a clinical skills examination (which is purely that) and a clinical knowledge examination. However, at the time of this writing, the latter portion of the test includes only 1% to 3% of questions under "general principles of foundational science." This example of the failure to integrate the science of medicine into clinical training is 1 of several examples of ineffective curricular reform and is emblematic of the recurring cyclic problem of recommending but not effecting meaningful integration. Many professional educators who make recommendations about curriculum are not regularly exposed to the practical realities of clinical practice today, with its breakneck pace, intensity, and complexity, all of which are further pressurized by restricted work duty hours. Thus it is understandable that the architects of curricular reform may not have fully appreciated the impossibility of inserting meaningful scientific thinking into a busy clinical environment.

After medical school, a future cardiologist undergoes 3 years of residency in internal medicine. The practical challenges of introducing medical science into those whirlwind years are even greater than those of students in clerkships. The problem is compounded today by the virtual disappearance of physician-scientist role models from both the inpatient and outpatient arenas. In the hospital, physician-scientists have been replaced by hospitalists, who are often outstanding clinicians who provide excellent and much needed continuity of care and supervision but whose main responsibilities are ensuring efficiency and cost-effectiveness of care and teaching mostly the technical aspects of medicine to residents. Time pressures require discussions of "what" and "how" rather than "why." Following this comes a period of 2 to 3 continuous years of clinical training in a fellowship, with the same constraints on time for scientific thinking before the next opportunity research opportunity reappears. This means typically about 7 to 8 uninterrupted years of pure clinical training. As critical as this prolonged training is to develop excellent clinical specialists, it also means the current generation of trainees will not be exposed to scientific thinking during the most formative years of their careers. This problem is particularly pernicious for training the next generation of translational physician-scientists, who will no longer have a sufficient scientific background to begin to ask meaningful questions about the pathophysiology of disease, let alone understand how to identify therapeutic targets within disease-causing pathways. Moreover, it is unrealistic to expect young physicians to ever become reinspired by the excitement of a career as a physician-scientist when they have not had any exposure during their most formative years.

Thorough and intensive clinical training cannot be replaced, even for future physicians who aspire to predominantly research careers. So what can be done to keep the pilot light of interest in a research career burning during this period of intensive clinical training? First, dedicated research time during undergraduate and graduate medical education requires extramural financial support, which is conspicuously absent today. Given the massive commitment to biomedical research in the United States that is supported by industry, philanthropy, and public tax dollars (5), it is ironic that we are failing to invest in the durable cultivation of the very workforce that will be required to sustain this country's biomedical research enterprise. A notable exception has been the longstanding and highly successful support by the NIH for MD-PhD combined degree programs. Another possibility for fostering the development of translational physician-scientists during clinical training would be to incorporate elements of the NIH Intramural Translational Science Training Program into medical school and post-graduate medical training programs. The Translational Science Training Program is currently a 2-day boot camp–style course that intertwines multidisciplinary scientific content, understanding of the drug development process, clinical trial terminology, and career exploration (https://www.training.nih.gov/tstp). A similar type of approach could be adopted to research electives in medical school, residency, and fellowship to provide ongoing exposure to scientific thinking. For medical students, a meaningful period of protected time for original research under the guidance of a good faculty mentor can be introduced into the curriculum late in the third year or during the fourth year. An example of this is the required 6-month block of "protected" research time toward the end of medical school, named the Areas of Concentration program, that has been successfully implemented at Weill Cornell Medical College. Another example is the Duke medical school curriculum, wherein students learn the core basic sciences in the first year and complete core clinical clerkships in the second year. The students then devote 10 to 12 months to scholarly investigation and fulfill elective rotations in the third and fourth years. Thus, by condensing the traditionally structured training from 4 years into 3 years, the Duke medical school curriculum provides students with ample opportunity to pursue their own independent research interests. Finally, active physician-scientists

must be brought back onto inpatient services for attending and teaching rounds in partnership with hospitalists, who should maintain responsibility for supervision and oversight. Not only would this kind of arrangement permit continued exposure of clerkship students and residents to the scientific underpinnings of medical practice, but it would also provide the hospitalists with the same and the physician-scientists with much needed exposure to the current realities of clinical practice. As always, we welcome your thoughts about how to train the next generation of translational scientists, either through social media (#JACC:BTS) or by e-mail (jaccbts@acc.org).

ADDRESS FOR CORRESPONDENCE: Dr. Andrew I. Schafer, Weill Cornell Medicine, Division of Hematology/Medical Oncology, 1305 York Avenue, 8th Floor, Box 403, New York, New York 10021. E-mail: ais2007@med.cornell.edu.

REFERENCES

1. Wyngaarden JB. The clinical investigator as an endangered species. N Engl J Med 1979;301:1254–9.

2. National Institutes of Health. Physician-Scientist Workforce Working Group report. Available at: https://acd.od.nih.gov/documents/reports/PSW_Report_ACD_06042014.pdf. Accessed August 14, 2019.

3. Schafer AI, ed. 2009. The Vanishing Physician-Scientist? Ithaca, NY: Cornell University Press.

4. Hopkins R, Pratt D, Bowen JL, Regehr G. Integrating basic science without integrating basic scientists: reconsidering the place of individual teachers in curriculum reform. Acad Med 2015;90:149–53.

5. Asch DA, Weinstein DF. Innovation in medical education. N Engl J Med 2014;371:794–5.